
Impact of new pharmacological strategies for the treatment of acute myocardial infarction: study of the effects and synergy of sacubitril/valsartan and empagliflozin.

Doctoral thesis presented by

DAINA MARTÍNEZ FALGUERA

to apply for the doctoral degree at the University of Barcelona.

This thesis was directed by

Dr. Carolina Gálvez Montón and Prof. Antoni Bayés Genís

*Institut de Recerca Germans Trias i Pujol i Institut del cor (Icor), Hospital
Universitari Germans Trias i Pujol*

And tutored by

Dr. Eduard Guasch Casany

Institut Cardiovascular, Hospital Clínic (IDIBAPS), Universitat de Barcelona

Doctoral Program in Medicine and Translational Research

Faculty of Medicine and Health Science, University of Barcelona



**UNIVERSITAT DE
BARCELONA**



January 2025

Agraïments

M'agradaria agrair a totes les persones que, d'alguna forma o altra, han fet que aquest camí d'aprenentatge, que ha estat la tesi, sigui més enriquidor, divertit i amè. Gràcies, de tot cor, a cadascuna de vosaltres.

En primer lloc, m'agradaria agrair als meus directors de tesi. **Carol...** per on començar! Gràcies per la confiança que has tingut en mi des del primer dia fins l'últim. Per donar-me l'oportunitat de formar part d'aquest projecte tan bonic i de tots els que han vingut després. Per ensenyar-me i ajudar-me a convertir-me en una investigadora més polivalent, independent, crítica i resolutive. Per corregir-me i guiar-me amb saviesa. En definitiva, moltes gràcies per la teva dedicació diària i per tot el que m'has ensenyat durant aquesta etapa. **Toni**, gràcies per haver-me donat l'oportunitat de formar part d'aquest gran equip que és l'iCOR. T'estic molt agraïda pel teu suport i confiança al llarg d'aquest projecte i per estar sempre disponible quan t'he necessitat. Per aportar la teva mirada crítica i constructiva per millorar el nostre treball i també per valorar la feina ben feta.

També m'agradaria tenir unes paraules d'agraïment cap al meu tutor. **Edu**, gràcies pels teus consells, la teva disposició i facilitat. Ha sigut un plaer tenir-te com a tutor.

Continuaré pel "*Piggy Dream Team*". Gràcies, **Júlia, Felipe, Edgar, Oriol i Teis**. Al vostre costat he après moltíssim. M'heu endinsat en l'interessantíssim i a vegades complicat món de l'electrofisiologia, l'hemodinàmica i la imatge cardíaca. Gràcies per tot el que m'heu ensenyat i per tots els moments que hem compartit junts. En especial, voldria dedicar unes paraules a la **Júlia**.

Gràcies per les nostres converses, tant de resultats com les més personals. Per les petites empentes que ens hem donat mútuament quan les necessitem i per les alegries compartides que aquest projecte ens ha donat.

A tots els membres del laboratori. Gràcies a tots i cadascun de vosaltres. Soc la investigadora que soc gràcies a les vostres ensenyances i consells.

Carol S, no podria tenir millor companya de despatx. Gràcies pels teus consells, tan metodològics com més personals, per la teva calma, el teu suport i pel dia a dia. **Gemma**, gràcies per estar sempre disposada a ajudar-me, escoltar-me i discutir el que faci falta. **Paloma**, gracias por el día a día y por tener siempre la puerta abierta para resolver cualquier duda clínica que he tenido. **Elena**, gracias por todas las risas y experiencias vividas durante este tiempo, y por estar siempre dispuesta a ayudarme cuando lo he necesitado. **Santi**, gràcies pels consells, les bromes i els riures. **Uri**, gràcies per les ensenyances i xerrades compartides. **Yvan**, gracias por todas las charlas y momentos compartidos. ¡Ánimo, que ya te queda menos! **Marta**, gràcies per ensenyar-me tantíssimes coses i per ser una referent per mi. Treballar amb tu és un luxe i et trobo molt a faltar! **Pol**, gràcies per les converses, els riures i els consells sempre encertats. **Cris**, no podia oblidar-me de tu! Vas estar en els meus inicis i em vas ensenyar la millor forma de treballar: amb alegria i humor. **Georgina**, des que has arribat, t'has convertit en un pilar fonamental per mi dintre del laboratori. Gràcies per tots els moments compartits i pels que vindran! **Esther**, des de la teva arribada tot funciona millor. Gràcies pels consells sempre encertats i per guiar-me amb la saviesa de la teva experiència. **Maria**, aquest viatge comença per tu, però ja veuràs que, malgrat les dificultats, ens ho passarem molt bé! **Sheila**, simplement gràcies

per tot. Per estar sempre disposada a ajudar-me i posar les coses fàcils. **Leonie**, muchas gracias por estar siempre abierta a ayudar y por resolverme todas mis dudas acerca de la tesis, que no han sido pocas. **Fran i Borja**, gràcies per tots els experiments i moments compartits junts.

També voldria dedicar unes paraules a totes les persones que he conegut i que han compartit amb mi part d'aquesta etapa tan especial.

Raquel, amb tu vaig descobrir el fascinant món del mapejos. Gràcies pels moments i fites compartides juntes. **Idoia**, mil gracias por todo. Trabajar contigo y aprender de ti fue un verdadero lujo. **JuanRi**, gracias a ti, los días de cirugía fueron mucho más divertidos y amenos. **Marco**, me iniciaste en el interesante mundo de la citometría, y quería decirte que fué un placer aprender del mejor. **Pilar**, gràcies per estar sempre disposada a ajudar i a ensenyar amb tanta paciència i dedicació. **Adriana**, contigo hice los primeros experimentos y pasos en el mundo de las tinciones. Gracias por todos los momentos compartidos juntas. **Alèxia**, gràcies per totes les converses, riures i el suport constant. Ets genial! **Marteta**, gràcies pels moments viscuts juntes, tant dintre com fora l'IGTP. M'ha agradat conèixer-te i compartir aquesta etapa amb tu! Gràcies també a la **Roser, Marc, Carme**, membres del PhD committe (**Sara, Laure**)... i a la resta de persones amb qui he compartit bons moments.

Per últim, m'agradaria agrair a les persones que esteu al meu costat sempre i incondicionalment.

A la meua família. Gràcies, **Mama, Papa, Edgard i Anna**. Sé que sempre esteu al meu costat i celebren totes les meves fites com si fossin vostres. Gràcies pel vostre suport incondicional, per escoltar-me, per la vostra immensa generositat i per l'estima que sempre em demostreu. En definitiva, gràcies per recolzar-me sempre i acompanyar-me en totes les aventures de la meua vida.

Gràcies, **JuanMi**. Per ser-hi sempre. Per acompanyar-me al llarg d'aquesta etapa, per escoltar-me, pels teus consells i, sobretot, pel teu suport i ajuda incondicionals. Gràcies també per tot l'amor, els riures i la calidesa que em dones. Compartir amb tu les dificultats i alegries que he anat trobat durant aquest camí l'ha fet molt més fàcil i divertit!

Gràcies a les amigues i amics de sempre, les de Tarragona i els de Prades. En especial, **Sandra, Mariona, Ona, Sutil, Marina, Berta, Esther, Aurora, Jordina...** Heu viscut, gaudit i patit aquesta etapa amb mi. Gràcies per tots els riures, aventures i moments de confessions. Amb vosaltres, a la fi del món!

I per acabar, no vull oblidar-me de totes aquelles persones que, d'una manera o altra, van despertar en mi la curiositat per l'apassionant món de la ciència. En especial, als professors i professores de la universitat i del màster, de qui vaig aprendre tantes coses.

A tots vosaltres i als que no he mencionat, però que també hem compartit moments al llarg d'aquest camí, **MOLTES GRÀCIES!!!**

Table of Content

<i>Agraïments</i>	<i>I</i>
<i>Table of Figures</i>	<i>IX</i>
<i>List of Tables</i>	<i>XI</i>
<i>Abbreviations</i>	<i>XIII</i>
<i>List of Articles</i>	<i>XVII</i>
<i>Resum tesi doctoral</i>	<i>XIX</i>
<i>Thesis summary</i>	<i>XXIII</i>
Introduction	1
1. Myocardial Infarction	3
2. Post-MI Healing and Repair: From Inflammation to Fibrosis	7
2.1. Inflammatory Response After MI	8
2.1.1. Inflammatory Phase.....	8
2.1.2. Proliferative Phase.....	13
2.1.3. Maturation Phase	16
2.2. Fibrosis After MI: Replacement and Reactive Fibrosis	18
2.2.1 Post-MI Arrhythmias	19
3. Myocardial Infarction Management	21
3.1. Fourth Universal Definition of Myocardial Infarction.....	21
3.2. Diagnosis	22
3.2.1. Clinical Symptoms Evaluation, Physical Examination and Clinical History....	22
3.2.2. Diagnostic Tools.....	22
3.3. Acute Management of Patients with MI	27
3.3.1. Strategies of Reperfusion	29
3.3.2. Antithrombotic Therapy	31
3.4. Long Term MI Treatment	34
3.4.1. Cardiac Rehabilitation.....	34

3.4.2. Lifestyle Management	34
3.4.3. Pharmacological Treatment.....	36
3.5. Complications from MI to HF	37
4. New Era of HF Drugs	39
4.1. Angiotensin Receptor/Neprilysin Inhibitor.....	39
4.1.1. Mechanism of Action	40
4.1.2. Cardiovascular Effects.....	42
4.2. Sodium-Glucose Co-Transporter 2 Inhibitors	47
4.2.1. Mechanism of Action	48
4.2.2. Cardiovascular Effects.....	50
4.3. Safety and Synergistic Effects of ARNi and SGLT2 Inhibitors.....	57
4.4. Early Initiation of Sacubitril/Valsartan and Empagliflozin After MI	58
<i>Hypothesis & Objectives.....</i>	61
<i>Material, Methods & Results.....</i>	65
<i>Discussion</i>	167
<i>Conclusions</i>	187
<i>References</i>	191

Table of Figures

Figure 1. Top 10 leading causes of death globally	4
Figure 2. Different phases of the healing process after MI	8
Figure 3. Innate immune response after MI	11
Figure 4. Inflammatory phase after MI.....	12
Figure 5. Proliferative phase after MI	16
Figure 6. Maturation phase after MI	17
Figure 7. Types of cardiac fibrosis after MI.....	19
Figure 8. Classification of patients presenting with suspected acute coronary syndrome (ACS): from working to final diagnosis.....	24
Figure 9. An overview of the initial triage, management and examination of patients who present signs and symptoms potentially consistent with acute coronary syndrome (ACS)	28
Figure 10. Antithrombotic treatments in acute coronary syndrome (ACS) and pharmacological targets	33
Figure 11. Long-term management after acute coronary syndrome (ACS): comprehensive cardiac rehabilitation and its core components.....	35
Figure 12. Mechanism of action and cardiovascular effects of sacubitril/valsartan	41
Figure 13. Mechanism of action and cardiovascular effects of sodium glucose co-transporter 2 inhibitors.....	49
Figure 14. Graphical summary of results: effects of early initiation of sacubitril/valsartan and/or empagliflozin after MI.....	185

List of Tables

Table 1. Cardiovascular effects of sacubitril/valsartan42

Table 2. Cardiovascular effects of empagliflozin50

Abbreviations

A

ACE	Angiotensin-converting enzyme
ACEi	Angiotensin-converting enzyme inhibitor
ACS	Acute coronary syndrome
AF	Atrial fibrillation
AMI	Acute myocardial infarction
AMPK	5' adenosine monophosphate-activated protein kinase
APC	Antigen-presenting cell
ARA+EPA	Arachidonic acid + eicosapentaenoic acid
ARB	Angiotensin II receptor blocker
ARNi	Angiotensin receptor/neprilysin inhibitor
ATP	Adenosine triphosphate

B

BB	Beta-blocker
BP	Blood pressure
BZ	Border zone

C

C1M	Fragment of type I collagen
C3M	Fragment of type III collagen
CABG	Coronary artery bypass grafting

CAD	Coronary artery disease
cGMP	Cyclic guanosine monophosphate
CCL2	Chemokine ligand 2
CCR2	C-C chemokine receptor type 2
CCTA	Cardiac computed tomography angiography
CKD	Chronic kidney disease
CK-MB	Creatine kinase myoglobin isoform
CMR	Cardiac magnetic resonance
Col I	Collagen type I
Col III	Collagen type III
CR	Cardiac rehabilitation
CRP	C-reactive protein
cTn	Cardiac troponin
cTnI	Cardiac troponin I
cTnT	Cardiac troponin T
CV	Cardiovascular
CVD	Cardiovascular disease
CVF	Collagen volume fraction
CXCL	Cytokine-induced neutrophil chemoattractant

D

DAMPs	Damage-associated molecular patterns
DHA	Docosahexaenoic acid
DNA	Deoxyribonucleic acid
DZ	Deceleration zone

E

EC Endothelial cell
ECG Electrocardiogram
ECM Extracellular matrix
EDA-FN Extra domain A fibronectin
EMA European Medicines Agency
eNOS Endothelial nitric oxide synthase

F

FDA Food and Drug Administration
FFA Free fatty acid
FN Fibronectin

G

GLUT4 Glucose transporter type 4
GP Glycoprotein
GRACE Global Registry of Acute Coronary Events

H

HF Heart failure
HFpEF Heart failure with preserved ejection fraction
HFrEF Heart failure with reduced ejection fraction
HMGB1 High-mobility group box-1

I

ICAM Intracellular adhesion molecule
ICD Implantable cardioverter defibrillator
IFN- γ Interferon- γ

XIV

IHD Ischemic heart disease
IL Interleukin

K

KB Ketone bodies

L

LGE-CMR Late gadolinium enhancement cardiac magnetic resonance
LV Left ventricular
LVEDV Left ventricular end diastolic volume
LVEF Left ventricular ejection fraction
LVESV Left ventricular end systolic volume
LVSV Left ventricular stroke volume

M

MCP-1 Monocyte chemoattractant protein-1
MDA Malondialdehyde
MI Myocardial infarction
MMP Matrix metalloproteinase
MRA Mineralocorticoid receptor antagonist
MRI Magnetic resonance imaging

N

NLRP3 Nucleotide binding domain leucine rich repeat and pyrin domain containing 3
NMR Nuclear magnetic resonance
NO Nitric oxide

NP	Natriuretic peptide	SGLT2	Sodium glucose cotransporter 2
NSTEMI	Non-ST-elevation myocardial infarction	SOD	Superoxide dismutase
NT-proBNP	N-terminal pro B-type natriuretic peptide	sST2	Soluble ST2
P		STEMI	ST-elevation myocardial infarction
PCI	Percutaneous coronary intervention	α -SMA	α -Smooth muscle actin
PCr/ATP	Phosphocreatine-to-ATP	T	
PDK4	Pyruvate dehydrogenase kinase 4	T2DM	Type II diabetes mellitus
PICP	Procollagen type I carboxy-terminal propeptide	TGF- β	Transforming growth factor β
PIIINP	N-terminal propeptide of collagen III	Th1	T-helper type 1 cell
PINP	N-terminal propeptide of collagen I	Th2	T-helper type 2 cell
PRR	Pattern recognition receptor	TIMP	Tissue inhibitor of metalloproteinase
PVB	Premature ventricular beat	TNF- α	Tumour necrosis factor- α
PVC	Premature ventricular contraction	Treg	Regulatory T-cell
R		TSP	Thrombospondin
RAAS	Renin-angiotensin-aldosterone system	TXA ₂	Thromboxane A ₂
RNA	Ribonucleic acid	U	
ROS	Reactive oxygen species	URL	Upper reference limit
S		V	
SGLT	Sodium glucose cotransporter	VA	Ventricular arrhythmia
SGLT1	Sodium glucose cotransporter 1	VCAM-1	Vascular cell adhesion molecule-1
		VEGF	Vascular endothelial growth factor
		VF	Ventricular fibrillation
		VLA-4	Very late antigen-4
		VT	Ventricular tachycardia

List of Articles

Thesis in the form of collection (compendium) of published articles. This thesis comprises of three objectives and three articles:

ARTICLE 1: This article is related to objective 1.

Authors: **Martínez-Falguera D**, Fadeuilhe E, Teis A, Aranyo J, Adeliño R, Bisbal F, Rodríguez-Leor O, Gálvez-Montón C.

Title: **Myocardial Infarction by Percutaneous Embolization Coil Deployment in a Swine Model.**

Published in the *Journal of Visualized Experiments* 2021 Nov 4;(177). doi: 10.3791/63172.

Impact factor (Journal Citation Reports): **1.424**

Quartil (Journal Citation Reports): **Q3 MULTIDISCIPLINARY SCIENCES**

ARTICLE 2: This article is related to objective 2.

Authors: **Martínez-Falguera D**, Aranyó J, Teis A, Ferrer-Curriu G, Monguió-Tortajada M, Fadeuilhe E, Rodríguez-Leor O, Díaz-Güemes I, Roura S, Villuendas R, Sarrias A, Bazan V, Delgado V, Bayes-Genis A, Bisbal F, Gálvez-Montón C.

Title: **Antiarrhythmic and Anti-Inflammatory Effects of Sacubitril/Valsartan on Post-Myocardial Infarction Scar.**

Published in the *Circulation: Arrhythmia and Electrophysiology*. 2024 May;17(5):e012517. doi: 10.1161/CIRCEP.123.012517. Epub 2024 Apr 26. PMID: 38666379.

Impact factor (Journal Citation Reports): **9.1**

Quartil (Journal Citation Reports): **Q1 (D1) CARDIAC & CARDIOVASCULAR SYSTEMS**

ARTICLE 3: This article is related to objectives 2 and 3.

Authors: **Martínez-Falguera D**, Aranyó J, Ferrer-Curriu G, Teis A, Revuelta-López E, Díaz-Güemes I, Monguió-Tortajada M, Fadeuilhe E, Rodríguez-Leor O, Poblador F, Montejo B, Roura S, Villuendas R, Sarrias A, Bazan V, Jorge E, Delgado V, Jimenez Trinidad FR, Rigol M, Martinez-Micaelo N, Amigó N, Bayes-Genis A, Bisbal F, Gálvez-Montón C.

Title: **Initiating Empagliflozin and Sacubitril/Valsartan Early Post-Myocardial Infarction: Mechanistic Study.**

Status: Under review.

Resum tesi doctoral

Impacte de noves estratègies farmacològiques per al tractament de l'infart agut de miocardi: estudi dels efectes i la sinergia de sacubitril/valsartan i empagliflozina.

Introducció: La introducció de nous fàrmacs com el sacubitril/valsartan i l'empagliflozina ha millorat significativament els resultats clínics en pacients amb insuficiència cardíaca (IC). El seu paper en la IC està ben establert; no obstant, la seva eficiència després d'un infart agut de miocardi (IAM) roman en gran mesura inexplorada. Existeix poca evidència sobre la seguretat i els possibles efectes sinèrgics quan es combinen aquests dos fàrmacs després d'un IAM.

Hipòtesi: L'administració primerenca d'empagliflozina i/o sacubitril/valsartan després d'un IAM pot exercir un paper protector contra la lesió post-isquèmica mitjançant la reducció de la inflamació i l'estrès oxidatiu, la millora del metabolisme cardíac i/o la provisió d'efectes protectors sobre el remodelat estructural i elèctric cardíac. La combinació d'ambdós fàrmacs podria ser segura i exercir un efecte sinèrgic.

Objectius: Avaluar l'impacte de la iniciació primerenca de l'empagliflozina i/o el sacubitril/valsartan sobre la inflamació, l'estrès oxidatiu, el metabolisme, la fibrosi, la funció cardíaca, les propietats electrofisiològiques i histològiques de la cicatriu, i la inducibilitat de taquicàrdia ventricular (TV) en un model porcí d'IAM.

Mètodes: Trenta-tres porcs (55% femelles) amb IAM van ser assignats aleatòriament a rebre tractament amb beta-bloquejants (BB) (grup Control-IAM; n=8), BB+sacubitril/valsartan (grup Sac/Val; n=9), BB+empagliflozina (grup Empa; n=8) o BB+empagliflozina+sacubitril/valsartan (grup Empa+Sac/Val; n=8) durant 30 dies. Es va fer un seguiment longitudinal de la resposta immune, el perfil metabòlic i la funció cardíaca dels animals. A 30 dies post-IAM, es va utilitzar l'estimulació elèctrica programada i la cartografia d'alta densitat per avaluar les propietats electrofisiològiques del miocardi i la inducibilitat de TV. Posteriorment, es van recollir mostres de teixit per a l'anàlisi de la inflamació cardíaca, l'estrès oxidatiu i del perfil metabòlic.

Resultats principals: El grup tractat amb sacubitril/valsartan va mostrar una reducció dels leucòcits circulants aguts ($p=0.009$) i dels nivells d'interleucina-12 a 2 dies post-IAM ($p=0.024$), va disminuir l'expressió del receptor CCR2 en la superfície de monòcits a 15 dies post-IAM ($p=0.047$), i va reduir el contingut de col·lagen I (Col I) a la cicatriu miocardiàcia ($p=0.049$), la relació col·lagen I/III ($p=0.040$), la massa total de la cicatriu ($p=0.046$) i la massa de la zona fronterera (BZ) ($p=0.043$). També va reduir el nombre i la massa dels corredors de la BZ ($p=0.009$ i $p=0.026$, respectivament) i el nombre de zones de desacceleració ($p=0.016$), cosa que va conduir a una reducció relativa del 55% de la inducibilitat de TV ($p=0.034$). No es van detectar efectes significatius en els paràmetres de la funció cardíaca. El grup tractat amb empagliflozina presentà una disminució en el nombre de leucòcits circulants aguts a 2 i 15 dies post-IAM ($p=0.010$, $p=0.050$, respectivament) i en el nombre de monòcits circulants CCR2⁺ 15 dies post-IAM ($p=0.049$). També va augmentar la biodisponibilitat de l'òxid nítric (NO) al miocardi sa ($p=0.059$),

els nivells de lípids omega cardioprotectors al fetge, i el contingut de col·lagen III a la cicatriu miocardiàca ($P=0.023$). No es van observar efectes sobre la funció cardíaca ni la inducibilitat de TV a 30 dies post-IAM. El tractament combinat amb empagliflozina i sacubitril/valsartan va reduir el contingut de Col I a la cicatriu ($p=0.082$), va millorar la distensibilitat ventricular esquerra (increment del volum telediastòlic indexat, $P=0.029$; i del volum sistòlic, $P=0.044$), el remodelat electrofisiològic (reducció de corredors de BZ i zones de desacceleració; $p=0.008$ i $p=0.006$, respectivament), i va reduir el criteri compost de mort cardiovascular o inducibilitat de TV ($p=0.025$) a 30 dies post-IAM.

Conclusions: La iniciació primerenca de sacubitril/valsartan després d'un IAM reduí la resposta inflamatòria aguda, disminuí el contingut de Col I a la cicatriu miocardiàca, reduí la massa total de la cicatriu i de la BZ, i mitigà les propietats proarrítmiques del cor, disminuint finalment la inducibilitat de TV. El tractament amb empagliflozina reduí la inflamació i l'estrès oxidatiu, augmentà els lípids amb perfil cardioprotector a nivell hepàtic, i alterà el contingut de col·lagen de la cicatriu sense afectar la funció cardíaca ni la inducibilitat de TV. La combinació d'empagliflozina i sacubitril/valsartan reduí el contingut de Col I a la cicatriu, millorà el remodelat del ventricle esquerre i disminuí la inducibilitat de TV, malgrat que no es va detectar un efecte sinèrgic.

Thesis summary

Impact of new pharmacological strategies for the treatment of acute myocardial infarction: study of the effects and synergy of sacubitril/valsartan and empagliflozin.

Introduction: The introduction of new drugs such as sacubitril/valsartan and empagliflozin has markedly improved clinical outcomes in patients with heart failure (HF). The role of these drugs in HF is well-established; however, their efficacy on post-acute myocardial infarction (AMI) remains largely unexplored. Limited evidence exists on the safety and the potential synergistic effects when combining empagliflozin with sacubitril/valsartan post-AMI.

Hypothesis: The early administration of empagliflozin and/or sacubitril/valsartan after MI may exert a protective role against post-ischemic injury by reducing inflammation and oxidative stress, enhancing cardiac metabolism, and/or providing protective effects on post-AMI structural and electrical remodelling. The combination of both drugs could be safe and may have a synergistic effect.

Objectives: To evaluate the cardiac impact of early initiation of empagliflozin and/or sacubitril/valsartan on inflammation, oxidative stress, metabolism, myocardial fibrosis, cardiac function, electrophysiological and histological scar properties, and ventricular tachycardia (VT) inducibility in an AMI pig model.

Methods: Thirty-three pigs (55% females) with MI were randomly assigned to receive beta-blocker (BB) treatment alone (Control-MI group; n=8), BB+sacubitril/valsartan (Sac/Val group; n=9), BB+empagliflozin (Empa group; n=8) or BB+empagliflozin+sacubitril/valsartan (Empa+Sac/Val group; n=8) during 30 days. The immune response, metabolic profile, and cardiac function were longitudinally monitored. At 30 days post-MI, programmed electrical stimulation and high-density mapping were employed to evaluate myocardial electrophysiological properties and the inducibility of VT. Subsequently, tissue samples were collected for the analysis of cardiac inflammation, oxidative stress, and metabolic profiles.

Main results: Sacubitril/valsartan reduced acute circulating leukocytes ($p=0.009$) and interleukin-12 ($p=0.024$) levels at 2-days post-MI, decreased C-chemokine receptor type 2 (CCR2) expression in monocyte surface at 15-day post-MI ($p=0.047$), and reduced myocardial scar collagen I (Col I) content ($p=0.049$), collagen I/III ratio ($p=0.040$), total scar mass ($p=0.046$) and border zone (BZ) mass ($p=0.043$). It also lowered the number and mass of BZ corridors ($p=0.009$ and $p=0.026$, respectively) and the number of deceleration zones ($p=0.016$), leading to a relative reduction risk of 55% in VT inducibility ($p=0.034$). No effect on cardiac function parameters were detected. Empagliflozin decreased acute circulating leukocytes count at 2- and 15-days post-MI ($p=0.010$, $p=0.050$, respectively) and activated CCR2⁺ monocytes at 15 days post-MI ($p=0.049$). It also increased the bioavailability of nitric oxide (NO) in the healthy myocardium ($p=0.059$), the cardioprotective omega lipid levels in the liver, and the collagen III (Col III) content in the myocardial scar ($p=0.023$). No effect on cardiac function and

VT inducibility was observed at 30 days. The combined treatment with empagliflozin and sacubitril/valsartan reduced scar Col I deposition ($p=0.082$), enhanced left ventricular (LV) compliance (increased iLVEDV, $P=0.029$; and LVS_V, $P=0.044$), improved electrophysiological remodelling (reduced BZ corridors and deceleration zones; $p=0.008$ and $p=0.006$, respectively), and reduced the composite endpoint of cardiovascular death or VT inducibility ($p=0.025$) 30 days after MI.

Conclusions: Early initiation of sacubitril/valsartan after MI reduced the acute inflammatory response, decreased myocardial scar Col I content, reduced total scar and BZ mass, and mitigated proarrhythmogenic properties, ultimately lowering VT inducibility. Empagliflozin treatment reduced inflammation and oxidative stress, increased cardioprotective liver lipids, and modified scar collagen without affecting cardiac function or VT inducibility. Empagliflozin combined with sacubitril/valsartan decreased scar Col I, enhanced LV remodelling and reduced VT inducibility, although no synergistic effect was observed.

Chapter One

Introduction

1. Myocardial Infarction

Cardiovascular diseases (CVDs) are a group of disorders that affect the heart or blood vessels. The subgroups of CVDs include: coronary heart disease, cerebrovascular disease, peripheral arterial disease, rheumatic heart disease, congenital heart disease, deep vein thrombosis, and pulmonary embolism. Despite current advancements in prevention, detection, treatment, and control, CVDs remain the leading cause of death globally. In 2019, CVDs caused an estimated 17.9 million deaths worldwide, representing 32% of all deaths (1). CVDs also significantly contribute to premature deaths (occurring before the age of 70) representing more than 38% of all premature deaths in 2019, as well as disability, imposing a substantial burden on communities and healthcare systems worldwide (1–3).

In terms of total deaths, ischemic heart disease (IHD) is the world's leading cause, accounting for 16% of all deaths, followed by stroke and chronic obstructive pulmonary disease, accounting for 11% and 6% of total deaths, respectively. The global burden of CVDs is increasing as life expectation rises and population ages. Notably, deaths due to IHD have seen the greatest increase since 2000, rising by 1.6 million to 8.9 million in 2019 (**Figure 1**) (4). Similarly, in Europe, CVDs remain the most common cause of death, resulting in 4 million deaths annually in the region (44% of all deaths), with IHD and stroke accounting for nearly 44% and 25% of these CVD-related deaths, respectively (5).

IHD refers to cardiac problems caused by inadequate blood supply to the myocardium due to partial or complete blockage of coronary arteries. This obstruction results in decreased coronary blood flow, leading to inadequate oxygen and nutrient supply to the heart. When blood flow is completely

blocked, it results in a myocardial infarction (MI), colloquially referred to as a heart attack. Artery narrowing is predominantly caused by an atheromatous plaque, a build-up of lipids (cholesterol), calcium, and inflammatory cells, that progressively accumulates within the coronary artery wall, reducing the arterial lumen (stenosis) (6). When an atheromatous plaque ruptures, its contents become exposed to the arterial lumen, rapidly activating the coagulation cascade and resulting in thrombus formation. This thrombus may partially or completely occlude the coronary artery, significantly reducing or completely obstructing blood flow. Plaque rupture is the most common cause of MI (7).

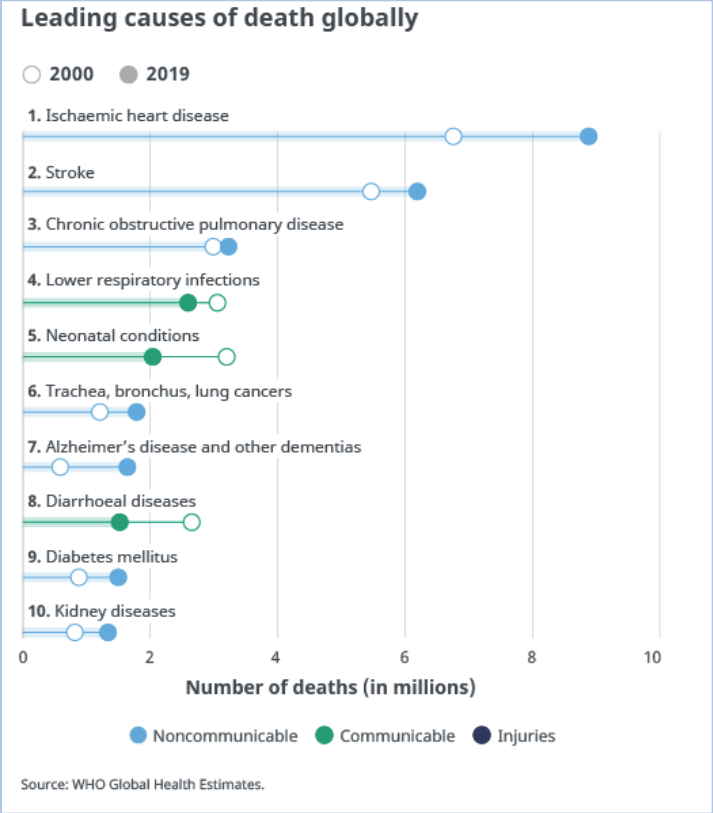


Figure 1. Top 10 leading causes of death globally. Comparison between 2000 and 2019. Font: WHO webpage.

Even though IHD remains a significant contributor to mortality and morbidity, it is preventable. The primary goal of health system programs is to prevent the progression of the atherosclerosis disease via controlling the modifiable cardiovascular (CV) risks factors. This includes promoting healthy lifestyle habits, such as maintaining a balanced diet, engaging in regular exercise, limiting alcohol consumption, avoiding smoking, and effectively managing conditions such as hypertension, dyslipidaemia, diabetes, and obesity as needed (8). However, when preventive measures prove ineffective and coronary obstruction occurs, the MI pathology begins. The myocardium distal to the occlusion site becomes ischemic, leading to the necrosis of cardiomyocytes. Damage-associated molecular patterns (DAMPs) and chemokines released from resident injured cardiac cells, trigger an acute inflammatory response, resulting in the infiltration of immune cells into the injured part of the myocardium (9). This immune response facilitates the clearance of dead cells and prepares the tissue for repair, the replacement of the necrotic tissue with a collagen scar (10). The abrupt loss of viable cardiomyocytes, along with their replacement by non-contractile scar tissue, activates neurohumoral compensatory mechanisms intended to preserve cardiac function – the ability of the heart to pump blood in order to meet the metabolic demand of the body. However, this maladaptive response after MI results in molecular and cellular changes in the infarcted, border and the non-infarcted myocardial tissue —a process known as adverse cardiac remodelling. These changes alter the structure and function of the heart, resulting in modifications to wall stress and stiffness, which lead to progressive cardiac dilatation and thinning of the heart muscle, ultimately causing cardiac dysfunction and heart failure (HF) —the inability of the heart to pump enough blood to meet the body's needs. Additionally, the sudden

massive loss of contractile cardiomyocytes triggers an electrophysiological cardiac remodelling, potentially leading to fatal ventricular arrhythmias (VAs), and, eventually, sudden cardiac death in the post-MI period (11).

Currently, the acute management of MI focuses on the rapid restoration and maintenance of proper blood circulation to minimize cardiac damage. This typically involves 1) pharmacological treatment, including antiplatelet agents, fibrinolytic agents, anticoagulants, and nitrates; and 2) surgical interventions, such as percutaneous coronary intervention (PCI), and/or, occasionally, coronary artery bypass grafting (CABG) (12,13). The following steps in the secondary prevention of MI include antithrombotic therapy, the minimization of CV risk factors, and the comorbidities management (12). These secondary measures can mitigate the risk of future heart attacks and other CV complications; however, they fail to address issues stemming from unresolved tissue damage – the initiation of the adverse remodelling and subsequent cardiac dysfunction. Currently, different treatments have shown promising results in managing HF symptoms (14), including drugs that inhibit the renin-angiotensin-aldosterone system (RAAS), combinations of medicines such as angiotensin receptor/neprilysin inhibitor (ARNi) and sodium glucose cotransporter 2 (SGLT2) inhibitors. However, there is still the need to explore new approaches to prevent the progression from MI to HF, rather than treat the HF symptoms. Therefore, the aim of the present study is to evaluate new therapeutic interventions that may limit myocardial ischemic injury following MI, mitigate the progression of adverse remodelling, and reduce the risk of developing HF and fatal VAs.

2. Post-MI Healing and Repair: From Inflammation to Fibrosis

Ischemic injury causes myocardial cell necrosis, which triggers molecular signals of damage and the activation of an intense inflammatory response necessary for the clearance of damaged tissue and the preparation of the infarct zone for the healing process. However, timely and appropriate resolution of inflammation is essential in determining the quality of wound healing and minimizing post-MI remodelling and HF (15).

The healing process after MI comprises three successive phases that overlap (**Figure 2**): 1) the inflammatory phase: orchestrated by cells from the innate immune response, critical for the removal of extracellular matrix (ECM) debris and dead cells; 2) the proliferative/reparative phase: during this phase, pro-inflammatory signals are down-regulated while pro-reparative and pro-fibrotic factors are up-regulated. Myofibroblasts become activated to initiate the cardiac healing process, the formation of the collagen-scar; and 3) the maturation phase: this final stage is marked by the apoptosis of the majority of inflammatory and reparative cells, along with the cross-linking of the collagen fibers.

Timely progression and resolution of both the inflammatory and reparative phases are necessary for proper MI healing. An overactive or incompletely resolved inflammatory phase can cause sustained tissue damage and poor healing, promoting scar expansion, unfavourable remodelling, chamber dilatation, and contractile dysfunction (10,16), as well as adverse electrophysiological remodelling, VAs, and sudden cardiac arrest (17). Therefore, appropriately managing the initial inflammatory phase and

promoting its progression to the reparative stage would protect the myocardium from excessive inflammatory damage.

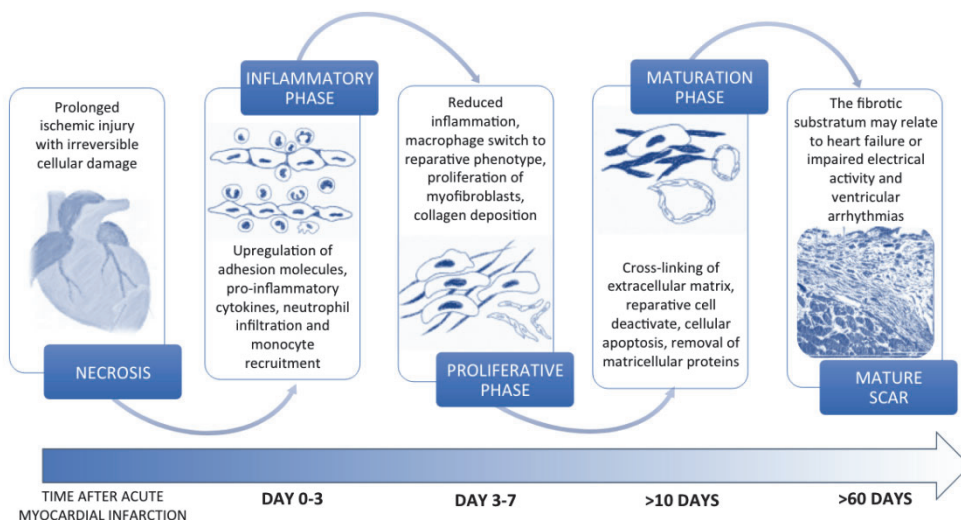


Figure 2. Different phases of the healing process after MI. Figure adjusted from Scalise RFM *et al.*, 2021 (18).

2.1. Inflammatory Response After MI

2.1.1. Inflammatory Phase

After ischemic injury, necrotic cells release endogenous signals (alarmins) known as danger-associated molecular patterns (DAMPs) into the extracellular space (19). Following MI, common DAMPs include high-mobility group box-1 (HMGB1), heat shock proteins, adenosine triphosphate (ATP), nuclear factors, deoxyribonucleic acid (DNA), ribonucleic acid (RNA), reactive oxygen species (ROS), free radicals and components of degraded ECM, among others. These molecules alert the body to the myocardial injury and activate the innate immune system. Surrounding immune cells recognize DAMPs through pattern recognition receptors (PRRs), triggering downstream pro-inflammatory cascades. This activation leads to the release of

pro-inflammatory mediators such as interleukin (IL)-1 β , IL-6, IL-18 and tumour necrosis factor- α (TNF- α) (16). Another significant contributor to the early post-MI inflammatory response is the activation of inflammasomes. Inflammasomes are large cytoplasmic protein complexes that are activated in response to DAMPs and trigger the conversion of pro-caspase-1 into its active form, caspase-1. Active caspase-1 subsequently mediates the activation and release of pro-inflammatory cytokines, specifically IL-1 β and IL-18, in cardiac fibroblasts and endothelial cells (ECs). Furthermore, caspase-1 promotes a highly inflammatory form of cellular death called pyroptosis in cardiac fibroblasts, ECs, and cardiomyocytes (20). Pyroptosis is characterized by the rupture of the plasma membrane, resulting in cellular swelling and subsequent lysis. This process results in nuclear condensation and the release of inflammatory cytokines, as well as intracellular DAMPs. Altogether, this initiates a powerful pro-inflammatory response that promotes the leukocytes recruitment to the infarct zone.

Neutrophils

Circulating neutrophils are the first immune cells recruited to the injured myocardium in response to elevated levels of chemotactic factors, such as cytokine-induced neutrophil chemoattractant 1 (CXCL1) and IL-8/CXCL8 (21,22). Once in the necrotic myocardium, neutrophil adherence is promoted by their adhesion into molecules that are overexpressed on activated epithelial cells (L- and P-selectin and intracellular adhesion molecule (ICAM)-1) (**Figure 3**) (22). Neutrophils develop multiple roles, including the phagocytosis of cellular debris, degradation of ECM through the release of proteolytic granules that contain matrix metalloproteinases (MMPs), ROS

generation, and the secretion of factors to attract chemotactic monocytes (21).

Monocytes/macrophages

Shortly after neutrophils (2-3 days post-MI), circulating monocytes are recruited to the infarct zone primarily in response to the secretion of monocyte chemoattractant protein-1 (MCP-1)/chemokine ligand 2 (CCL2) (23). This chemokine is rapidly upregulated in the infarcted tissue and acts as a strong attractant for positive C-C chemokine receptor type 2 (CCR2) monocytes (15,16,24), activated monocytes that predominate in the first inflammatory phase. Monocyte binding to the tissue is facilitated by the interaction between the very late antigen-4 (VLA-4) integrin on monocytes and the vascular cell adhesion molecule-1 (VCAM-1) on ECs, both of which are upregulated following MI (**Figure 3**) (22). Once in the tissue, monocytes differentiated into macrophages. The CCR2⁺ monocyte/macrophage subpopulation promotes the recruitment of leukocytes to the infarcted heart, whereas CCR2⁻ macrophages limit this recruitment (25). Monocytes/macrophages dominate the cellular infiltration of the infarct zone for the first 2 weeks after MI, playing essential roles in both the inflammatory and reparative phases. They exhibit two primary phenotypes: M1 (CD14⁺CD16⁻), which has pro-inflammatory features, and M2 (CD14⁺CD16⁺), which possesses anti-inflammatory and pro-fibrotic characteristics (18,26,27). During the acute inflammatory phase, M1 macrophages are responsible for phagocytosing dead cells, recruiting other leukocytes to the infarcted area, and producing proteases, including MMP-1, MMP-2, MMP-3, MMP-7, MMP-9, and MMP-12 (17,23). These proteases contribute to clear cellular and ECM debris, thus preparing the ground for the granulation tissue

(18). In contrast, the anti-inflammatory M2 macrophages become predominant in the subsequent proliferative phase.

Innate immune response after MI

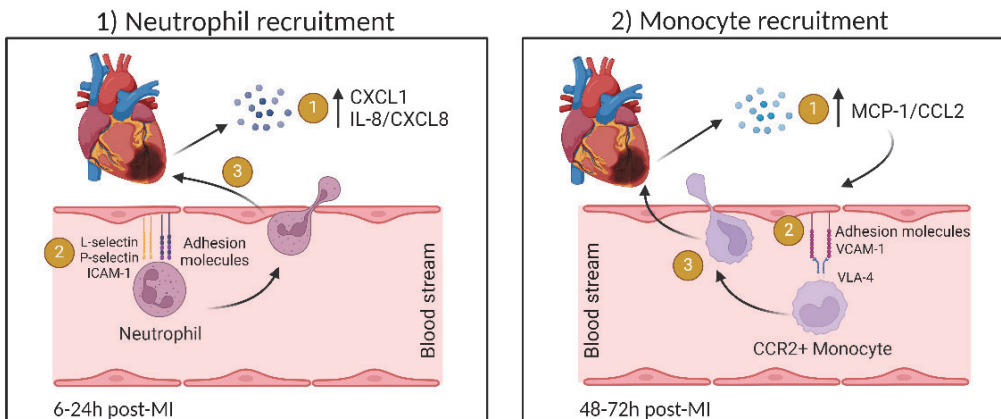


Figure 3. Innate immune response after MI. Neutrophils are first recruited into injured tissue in response to increased levels of CXCL1, IL-8/CXCL8 chemotactic factors. Their adhesion and subsequent transmigration (extravasation) through the endothelium are facilitated by the up-regulation of adhesion molecules, including L-/P-selectin and ICAM-1. Shortly after them (48-72h post-MI), monocytes are recruited primarily in response to elevated levels of MCP-1/CCL2. Their extravasation is facilitated by their interaction with adhesion molecules such as VCAM-1. Both, neutrophils and monocytes play essential functions in the early phase after MI, including the phagocytosis of cellular debris, degradation of ECM through the release of proteolytic proteins, and promotion of the inflammatory response. *Original figure created by Biorender.com.*

T cells

Finally, T cells from the adaptive immune response also play a crucial role in both the inflammatory and reparative phases after MI. Upon activation by antigen-presenting cells (APCs), T cells differentiate into various phenotypes. During the acute inflammatory phase, cytotoxic T cells (CD8+) and T-helper 1 cells (Th1) predominate, driving cytotoxic effects and promoting the release of the pro-inflammatory cytokine interferon- γ (IFN- γ), respectively. In contrast, in the reparative and chronic phases, T-helper 2 cells (Th2) and regulatory T cells (Tregs) predominate, facilitating tissue repair and

modulating the immune response (18,28). The prolonged presence of M1 macrophages and sustained T cell response can prolong the initial inflammatory phase, exacerbating infarct expansion, adverse remodelling, and contributing to the progression of HF in later chronic stages.

Inflammatory phase

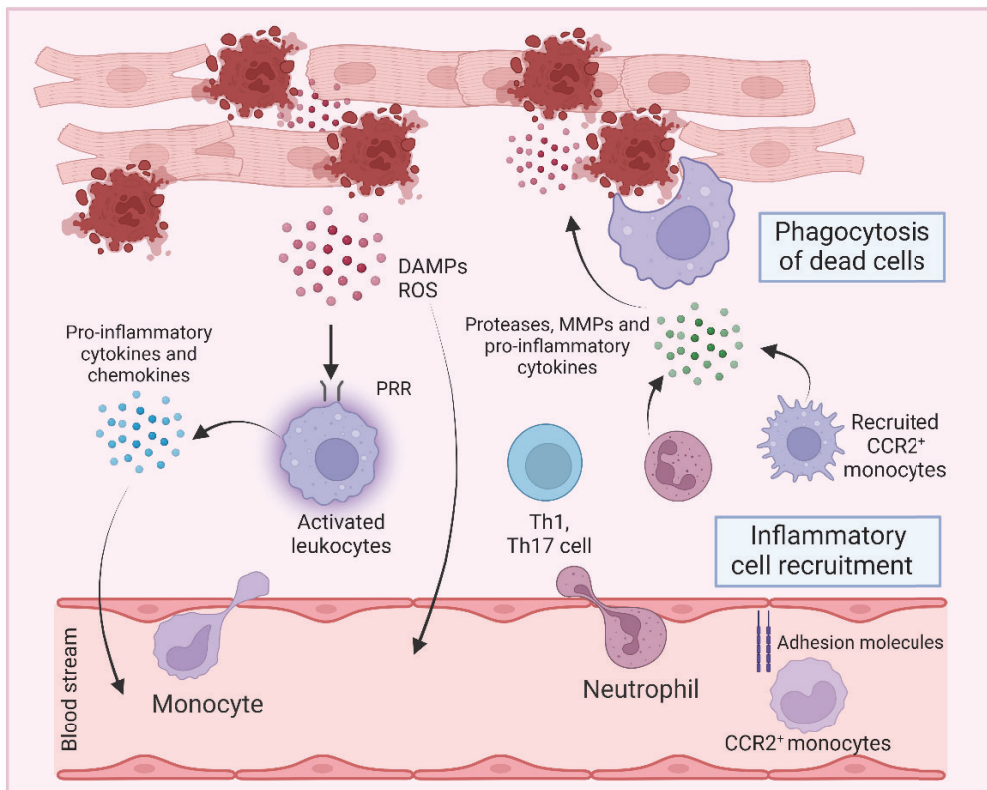


Figure 4. Inflammatory phase after MI. Ischemic injury-induced cell death releases damage-associated molecular patterns (DAMPs) and reactive oxygen species (ROS), which triggers inflammation by being recognized by pattern recognition receptors (PRRs) on surrounding cells. This process stimulates the secretion of pro-inflammatory cytokines and chemokines, leading to an intense influx of neutrophils and inflammatory monocytes into the ischemic cardiac area. These cells are responsible for the phagocytosis and clearance of necrotic tissue. Additionally, Th1 and Th17 cells from the adaptive immune response are also implicated. *Original figure created with Biorender.com.*

2.1.2. Proliferative Phase

The proliferative/repairative phase of healing begins around 3–5 days after MI, when pro-inflammatory signals start to decrease as a result of innate immune cell death and the upregulation of anti-inflammatory, pro-fibrotic and pro-angiogenic signals. This phase is marked by the activation of myofibroblasts, which are the primary cells responsible for collagen scar formation (**Figure 5**).

Fibroblasts and Myofibroblasts

Fibroblasts become the predominant cell type in the infarcted area and adopt a proliferative, migratory, and secretory myofibroblast phenotype (29). Different stimulus are implicated in the induction of fibroblasts proliferation, migration to the injured area, and differentiation into myofibroblasts, including mechanical stress, specific hormones, growth factors, and cytokines (30).

Myofibroblasts are specialized cells that exhibit characteristics of both fibroblasts and smooth muscle cells, and are typically absent in healthy myocardium. Their defining feature is a migratory and contractile nature, which is driven by the production of contractile proteins such as α -smooth muscle actin (α -SMA) and non-muscle myosin (31). Myofibroblasts synthesize large quantities of ECM proteins, including collagen type I (Col I) and III (Col III), which contribute to the formation of the cardiac scar that strengthens myocardial tissue and prevents ventricular wall rupture. Additionally, myofibroblasts secrete fibronectin (FN), particularly extra domain A (EDA)-FN, along with other matricellular proteins like thrombospondins (TSPs) and

tenascin C. These secreted factors further promote myofibroblast migration and play a regulatory role in the healing process (32).

In addition to local fibroblasts, myofibroblasts can also originate from other cell types, such as bone marrow-derived progenitor cells, pericytes, and certain epithelial and ECs.

Macrophages

During the reparative phase, macrophages transition from the pro-inflammatory M1 phenotype to the anti-inflammatory M2 phenotype. This shift is influenced by different factors, including the engagement of PRRs, the cytokine profile—particularly IL-4, IL-10, and IL-13, which promote M2 polarization—and the phagocytosis of apoptotic and necrotic cells. M2 macrophages play a crucial role in the secretion of mediators that promote the suppression of inflammation and the activation of the reparative phase: transforming growth factor β (TGF- β), IL-10 and vascular endothelial growth factor (VEGF) (16).

TGF- β

TGF- β stimulates the differentiation of fibroblasts into activated myofibroblasts and enhances ECM protein synthesis. Additionally, TGF- β suppresses the activity of proteases that degrade ECM by inhibiting the expression of MMPs and upregulating the synthesis of tissue inhibitor of MMPs (TIMPs) and other proteases inhibitors. Activation of the Smad3 signalling pathway appears to be important in mediating TGF- β -induced ECM protein synthesis and TIMP upregulation (33).

A properly regulated balance between MMPs and TIMPs is essential for maintaining ECM homeostasis. However, overactivation of TGF- β has been associated with an exacerbate fibrotic process and is a negative predictor factor for HF (18).

IL-10

The anti-inflammatory mediator IL-10 is also upregulated during the reparative phase. IL-10 is involved in promoting the shift from M1 to M2 in macrophages, reducing the secretion of proteinases, and enhancing fibroblast migration and proliferation (18,34). Additionally, IL-10 influences fibroblast activity by reducing the Col I/III ratio, which enhances tissue compliance and improves myocardial function (18).

VEGF

An increase in the angiogenic factor VEGF is also observed during the proliferative phase. VEGF promotes the formation of a new vascular network in the infarcted area by inducing ECs migration and tube formation (16). This process ensures a sufficient oxygen and nutrients supply to the healing tissue.

T cells

Th2 and Treg cell phenotypes are predominant in the reparative phase. Th2 cells secrete IL-4 and IL-13, which are pro-fibrotic factors that significantly enhance collagen synthesis and facilitate the transition from M1 to M2 macrophages (35,36). Tregs also contribute to cardiac fibrosis by stimulating the production of TGF- β and IL-10 (37,38), and also aid in promoting M2 macrophage polarization (39).

Proliferative phase

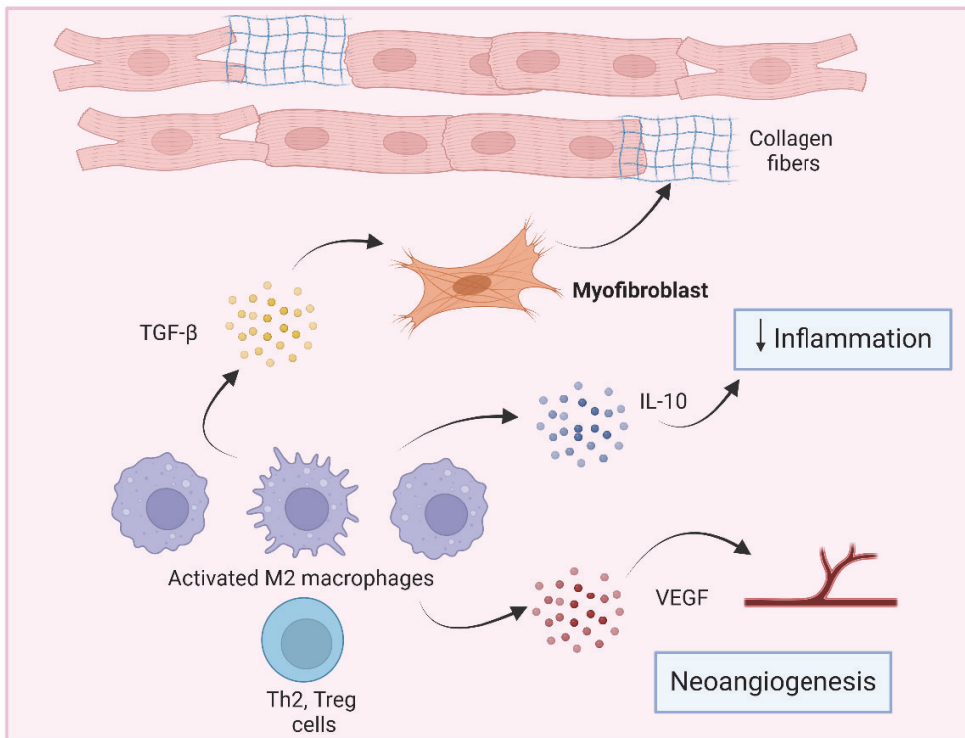


Figure 5. Proliferative phase after MI. The inflammatory phase transitions into the proliferative phase, which is characterized by the resolution of inflammation and the formation of a collagen scar. Tissue macrophages, whether resident or derived from recruited monocytes, shift to an M2 anti-inflammatory phenotype and produce TGF- β , IL-10, and VEGF. Additionally, Th2 and Treg cells from the adaptive immune response contribute to this anti-inflammatory and pro-fibrotic response. These processes collectively promote collagen deposition by myofibroblasts, attenuation of inflammation, and the formation of new blood vessels (neoangiogenesis). *Original figure created with Biorender.com.*

2.1.3. Maturation Phase

The proliferative phase of cardiac repair is followed by the scar maturation phase, during which ECM structures undergo cross-linking to stabilize the collagen scar tissue, and cells involved in the reparative phase are deactivated and undergo apoptosis (**Figure 6**). While still not fully elucidated, different factors are believed to influence the transition from the proliferative/reparative phase to the maturation phase. These include STOP

signals that terminate TGF- β signalling and the clearance of matricellular proteins, which may suppress proliferation and reduce the matrix synthetic activity of myofibroblasts. Additionally, the induction and secretion of anti-fibrotic mediators may also contribute to the conclusion of the matrix production response (16).

Maturation phase

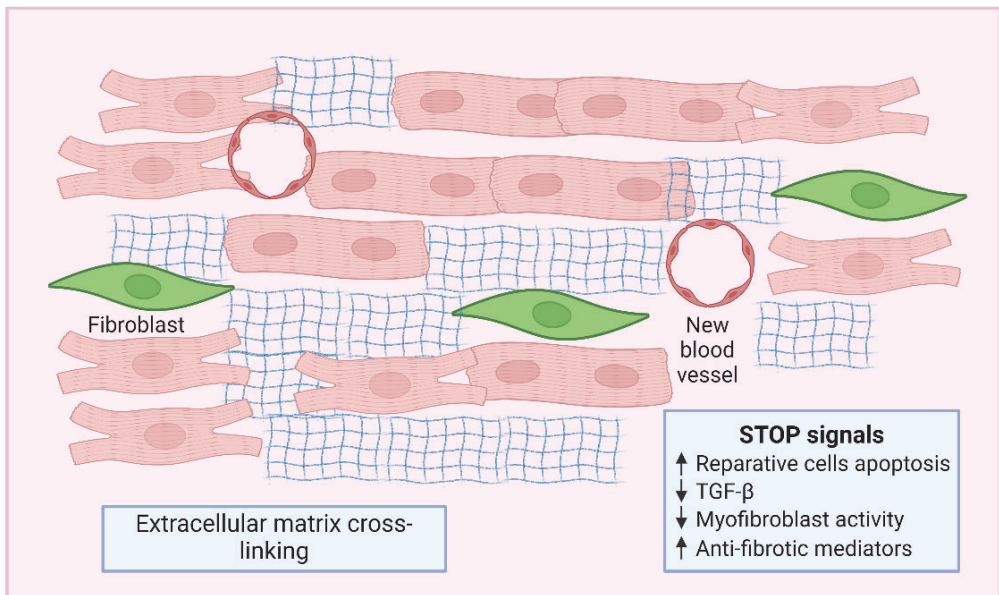


Figure 6. Maturation phase after MI. During this phase, the scar matures via ECM cross-linking. The cellular activity and signaling pathways involved in the reparative phase are gradually resolved. *Original figure created with Biorender.com.*

The complex mechanisms involved in controlling the inflammatory and reparative phases must be strictly well regulated to achieve optimal healing (18). Inappropriate collagen deposition and excessive fibrotic tissue contraction can affect cardiac compliance, diastolic and systolic function, scar stiffness, and lead to VAs. Conversely, insufficient collagen deposition and cross-linking are associated with a weak scar that could lead to dilatation and wall rupture.

2.2. Fibrosis After MI: Replacement and Reactive Fibrosis

Fibrosis is one of the primary mechanisms in the cardiac repair process following an MI and may manifest as either replacement and/or reactive fibrosis (**Figure 7**), both of which are produced by fibroblasts and myofibroblasts (31). Replacement fibrosis involves the substitution of necrotic cardiac tissue with fibrotic compact scar tissue, thereby preventing ventricular wall rupture.

Reactive fibrosis, on the other hand, results in interstitial fibrosis within the infarct border zone (BZ) and the surrounding myocardium, arising as a consequence of an incomplete resolution of inflammation or an excessive pro-fibrotic response, which leads to local fibroblasts activation and increased collagen deposition in the interstitial compartment (interstitial fibrosis) and in the adventitia of coronary vessels (perivascular fibrosis) (40). Both types of fibrosis may alter ventricular structure and systolic-diastolic function, contributing to the development of HF (31). The composition of the fibrosis is also important. The major components of the cardiac ECM are fibrillar collagens, specifically Col I and Col III (41). The quantity and distribution of these collagen fibres in the myocardium are crucial for global cardiac function, and elevated Col I/III ratio can negatively affect myocardial compliance and diastolic function of both the left and right ventricles (42,43).

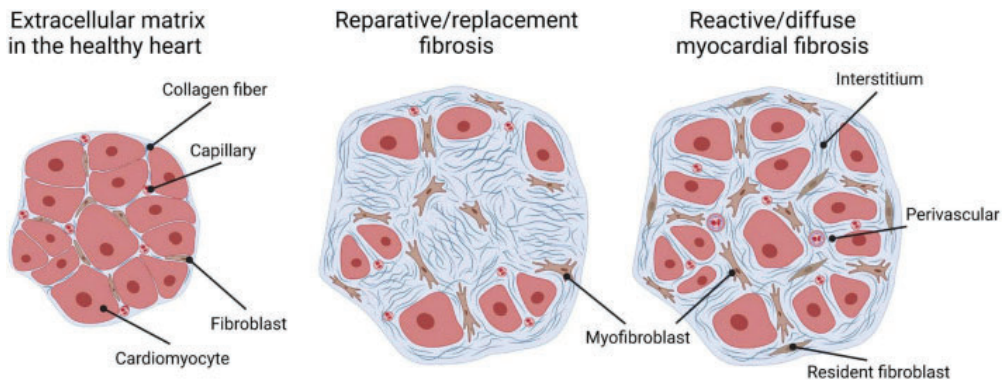


Figure 7. Types of cardiac fibrosis after MI. In the healthy heart (left), the extracellular matrix (ECM) consists of a 3D collagen fiber network that provides structural support to cardiac cells. After MI, two types of fibrosis are generated: 1) Reparative/replacement fibrosis (middle), which refers to collagen-based scar formation that replaces death cardiomyocytes following ischemic injury; and 2) Reactive/diffuse myocardial fibrosis (right), which occurs in HF due to pressure overload and is characterized by widespread collagen deposition in interstitial and perivascular regions. *Figure adjusted from K. Schimmel et al., 2022 (44).*

2.2.1 Post-MI Arrhythmias

Both replacement and reactive fibrosis interfere with the propagation of electrical impulses, producing areas of electric heterogeneity and slow conduction, facilitating the formation of re-entry circuits, the basic mechanism of VAs (45,46). The association between fibrosis and increased risk for VAs has been documented in practically every cardiac pathologic condition (47). The compact fibrotic scar following MI is mainly acellular and electrically inactive, but it can provide a site for re-entrant arrhythmias, potentially leading to sustained ventricular tachycardia (VT) (48), a wide complex tachycardia defined as three or more consecutive beats at a rate of more than 100 per minute, arising from the ventricle (49). However, interstitial fibrosis is often more arrhythmogenic. By separating myocytes with non-conductive collagenous septa, it can facilitate focal (ectopic) activity, slow electrical conduction, and create unidirectional conduction

blocks, all of which contribute to the development of re-entrant VT (50). Moreover, interstitial fibrosis can impact conduction by causing wave fronts to follow a 'zig-zag' pattern, slowing down conduction and increasing repolarization dispersion, which further supports re-entrant arrhythmias. Surviving cardiomyocytes in the infarct BZ, on the other hand, undergo significant electrophysiological remodelling, also contributing to the development of VAs. Electrophysiological changes in the infarct BZ include a reduction in repolarizing potassium currents, leading to prolonged action potential duration (51), decreased expression of connexin 43 which slows conduction (52), and mishandling of intracellular calcium that can trigger abnormal activity (53). These alterations collectively set the stage for malignant VAs. Although post-MI electrophysiological remodelling has been extensively studied, the precise upstream mechanisms driving these changes remain elusive. Elevated levels of pro-inflammatory cytokines and proteases, such as TNF- α , IL-1 β , IL-6, and MMPs, observed in the myocardium following MI, induce changes in cardiomyocytes that resemble those occurring in the infarct BZ. This suggests that inflammation plays a pivotal role in driving electrophysiological remodelling and the subsequent risk of arrhythmias. Clinical evidence supports this, showing that post-MI patients with arrhythmias have higher levels of inflammatory cytokines compared to those without arrhythmias (54). Additionally, systemic inflammation, even without MI or structural heart disease, is associated with a higher risk of VAs (55).

3. Myocardial Infarction Management

Timely and accurate diagnosis of MI is crucial for effective treatment and management of the condition. MI diagnostic process involves a combination of symptoms evaluation, clinical history, and conducting several diagnostic tests. Once MI is diagnosed, the preferred treatment is the rapid reperfusion to restore blood flow in the occluded artery. After acute management and patient stabilization, additional measures are taken to prevent recurring events and reduce CV risk. These include pharmacological therapy, lifestyle changes and addressing psychosocial factors.

This section contains the most relevant information regarding the management of acute coronary syndromes (ACS) described in the latest guidelines of the European Society of Cardiology (56).

3.1. Fourth Universal Definition of Myocardial Infarction

According to the last universal definition of MI (57), acute MI (AMI) is clinically present when there is acute myocardial injury detected by a rise and/or fall in cardiac biomarker values, preferably cardiac troponin (cTn), with at least one value above the 99th percentile upper reference limit (URL), and at least one of the following conditions:

- Symptoms of myocardial ischemia
- New ischemic changes on electrocardiogram (ECG)
- Presence of pathological Q waves on ECG
- Imaging evidence of new loss of viable myocardium or new regional wall motion abnormality in a pattern consistent with an ischemic aetiology

- Identification of a coronary thrombus by angiography or autopsy

3.2. Diagnosis

3.2.1. Clinical Symptoms Evaluation, Physical Examination and Clinical History

Myocardial ischemic symptoms commonly include chest pain, described as discomfort, pressure, tightness, or burning in the chest area, which may extend to the upper extremities, mandible, or epigastric area. It is also common to experience general ischemic symptoms such as fatigue or dyspnoea (56). Other less common signs include palpitations, cardiac arrest, or even no symptoms at all (58). A prompt assessment of vital signs and a physical examination are required during the evaluation, including checking all major pulses, measuring blood pressure in both arms, auscultating the heart and lungs, and assessing signs of HF or circulatory compromise. This evaluation is crucial for stratifying CV risk and ruling out other pathologies. Furthermore, it is essential to review the patient's medical history to gather important information about their risk factors and any previous CV events.

3.2.2. Diagnostic Tools

The diagnosis of MI is confirmed through different tests. The primary diagnostic tool is an ECG, which records the electrical activity of the heart and can identify specific patterns indicative of an MI event. Blood tests also play a crucial role in diagnosing MI by measuring levels of specific proteins that are released into the bloodstream in response to heart muscle injury. Furthermore, complementary imaging techniques may be employed to help in diagnosis and assess the extent of myocardial damage.

Electrocardiogram

ECG is the first required diagnostic test. If MI is suspected, an 12-lead ECG has to be acquired and interpreted as soon as possible, within 10 min (59,60). It should be repeated as necessary. Based on ECG result, patients are initially categorized into one of the two working diagnosis (**Figure 8**):

- ST-elevation MI patients (STEMI patients): patients with acute pain and an ECG consistent with persistent ST-segment elevation or equivalent ECG patterns. Most of these individuals will have elevated cTn serum levels and myocardial necrosis, fulfilling MI criteria and receiving a final diagnosis of STEMI.
- Non-ST-elevation MI patients (NSTEMI patients): patients with acute pain but without persistent ST-segment elevation on ECG. They may exhibit other ECG abnormalities, such as transient ST-segment elevation, persistent or transient ST-segment depression, and/or T wave abnormalities. A normal ECG may also be an option. Patients who also show a rise and/or fall in cTn levels (meeting MI criteria) will receive a final diagnosis of NSTEMI. Otherwise, cTn levels below the 99th centile indicate unstable angina.

The treatment route adopted will differ depending on the initial diagnosis derived from the ECG and cTn levels.

The ACS spectrum

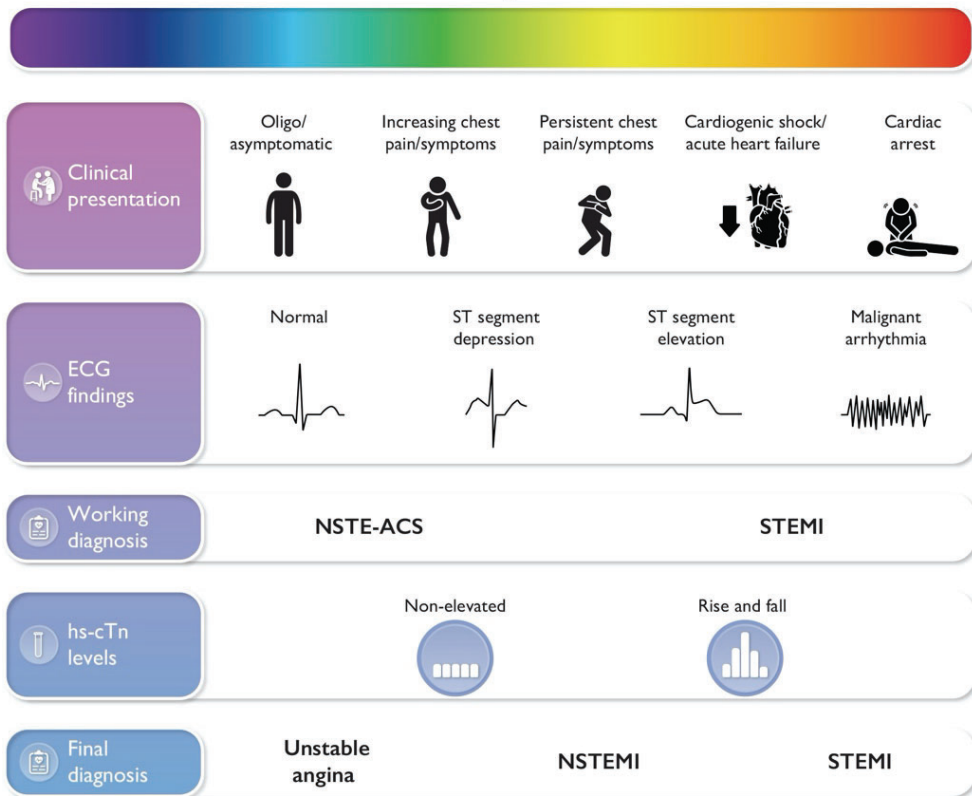


Figure 8. Classification of patients presenting with suspected acute coronary syndrome (ACS): from working to final diagnosis. ACS, acute coronary syndrome; ECG, electrocardiogram; hs-cTn, high-sensitivity cardiac troponin; NSTEMI-ACS, non-ST-elevation acute coronary syndrome; NSTEMI, non-ST-elevation myocardial infarction; STEMI, ST-elevation myocardial infarction. *Figure adjusted from Byrne RA et al., 2023 (56).*

Biomarkers

When MI is suspected, measuring a biomarker of cardiomyocyte damage, preferably cTn, is essential. cardiac troponin I (cTnI) and cardiac troponin T (cTnT) are components of the contractile apparatus of myocardial cells and are almost exclusively present in heart tissue (61,62). Upon onset of MI symptoms, circulating levels of cTn increase rapidly, often within an hour, and remain elevated for a period, typically several days (57,63). cTnI and cTnT are

the preferred biomarkers for assessing myocardial injury, and high-sensitivity-cTn assays are recommended for routine clinical use (**Figure 8**) (62). Other cardiac biomarkers, such as creatine kinase myoglobin isoform (CK-MB), can also be assessed but are less sensitive and specific (64).

Non-invasive imaging

Transthoracic echocardiography

A transthoracic echocardiography is a real-time test that uses ultrasound waves to create visual representations of cardiac chambers, valves and blood vessels. In case of suspected MI with diagnostic uncertainty, transthoracic echocardiography is valuable for identifying signs of ongoing myocardial ischemia, such as wall-motion abnormalities, and for ruling out other causes associated with chest pain (e.g., acute aortic disease or right ventricular signs in pulmonary embolism).

Cardiac computed tomography angiography

Cardiac computed tomography angiography (CCTA) uses computed tomography scanning technology to create 3D images of the heart and coronary arteries. This imaging technique helps determine the overall function and structure of the heart and evaluate the degree of stenosis in coronary arteries. During the procedure, contrast dye is injected intravenously to enhance visibility of blood vessels. The patient is then positioned on a computed tomography scanner that uses X-rays to capture detailed images. CCTA is commonly employed as an initial diagnostic test to exclude other potentially life-threatening conditions like pulmonary embolism or aortic dissection.

Cardiac magnetic resonance imaging

Cardiac magnetic resonance (CMR) imaging is the gold standard for evaluating cardiac structure and function, including the assessment of volumes, mass, and contractility. The incorporation of delayed contrast enhancement in CMR facilitates direct visualization of infarcted regions, which provides crucial information on healing. Therefore, CMR enables differentiation between MI scars and other types of myocardial injury, such as myocarditis. CMR is preferred over echocardiography when poor echocardiographic windows hinder diagnostic examination.

Invasive imaging

Coronary angiography

Coronary angiography is the preferred imaging technique used to identify blockages within the coronary arteries, essential for subsequent reperfusion procedures. It is a minimally invasive procedure conducted in a catheterization laboratory using X-ray equipment. During the procedure, a catheter is inserted through the radial or femoral artery to access the coronary arteries. Contrast dye is then injected through the catheter to enhance visibility of the coronary arteries, while live X-ray capture the movement of the dye, allowing the detection of any coronary blockages.

3.3. Acute Management of Patients with MI

Patients with suspected ACS are categorized based on the preliminary ECG examination, the clinical context, and hemodynamic stability into (**Figure 9**):

- Patients with a working diagnosis of STEMI: these patients should be evaluated for immediate reperfusion therapy, either via an invasive strategy (PCI) or a non-invasive strategy (fibrinolysis treatment), if an emergent primary percutaneous intervention (PPCI) cannot be performed within 120 minutes of diagnosis.
- Patients with a working diagnosis of NSTEMI: depending on the stability and the features of the patient:
 - Very high-risk patients, characterized by haemodynamic instability, chest pain resistant to medical treatment, acute HF, fatal arrhythmias, cardiac arrest or intermittent ST-segment elevation, are recommended for an immediate coronary angiography and PCI as necessary.
 - High-risk patients, displaying dynamic ST-segment or T wave changes, transient ST-segment elevation or a Global Registry of Acute Coronary Events (GRACE) risk score exceeding 140, should undergo an early PCI within 24 hours. GRACE risk score is a stratification tool used to estimate the likelihood of mortality or major adverse cardiac events in patients with ACS, based on clinical parameters such as age, heart rate, blood pressure, and renal function (65).
 - Patients lacking very high risk or high-risk criteria may receive personalized management based on clinical suspicion.

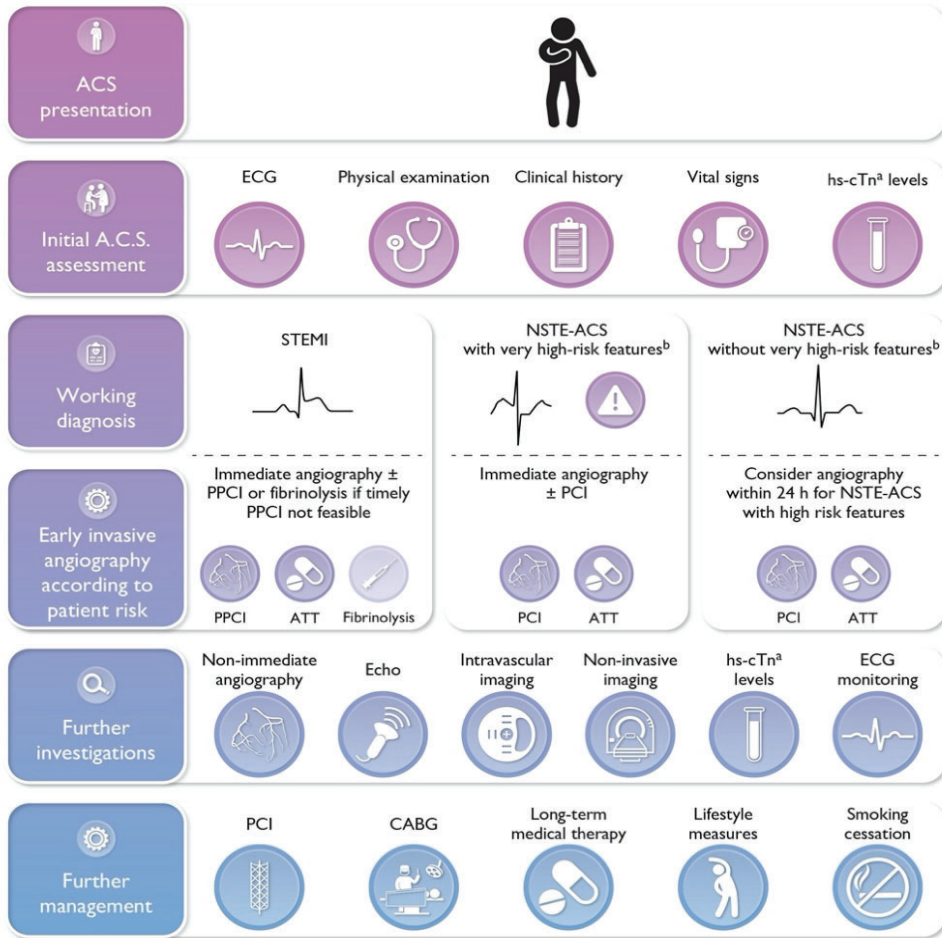


Figure 9. An overview of the initial triage, management and examination of patients who present signs and symptoms potentially consistent with acute coronary syndrome (ACS). ACS, acute coronary syndrome; ATT, antithrombotic therapy; CABG, coronary artery bypass grafting; ECG, electrocardiogram; hs-cTn, high-sensitivity cardiac troponin; NSTE-ACS, non-ST-elevation acute coronary syndrome; PPCI, primary percutaneous coronary intervention; STEMI, ST-elevation myocardial infarction. *Figure adjusted from Byrne RA et al., 2023 (56).*

3.3.1. Strategies of Reperfusion

3.3.1.1. Invasive Strategies

Percutaneous coronary intervention

PCI is a minimally invasive, non-surgical procedure performed by an interventional cardiologist to diagnose and treat narrowed or blocked coronary arteries. The procedure begins with a coronary angiography to assess the extent of the blockage, followed by the insertion of a catheter with a balloon at the site of the narrowing. The balloon is then inflated to reopen the artery, a process known as balloon angioplasty. In most cases, a stent (a mesh tube) is placed to keep the artery open. Stents are often coated with drugs to prevent restenosis – the recurrence of artery narrowing. In cases of suspected MI, emergent PCI, referred to as primary PCI (PPCI), is typically recommended.

Coronary artery bypass grafting surgery

CABG surgery is a surgical intervention in which a patient's artery or vein is grafted onto the coronary artery, bypassing the blocked section and creating a new pathway for blood flow. The most commonly used vessels in CABG include the internal thoracic artery, saphenous vein, radial artery and right gastroepiploic artery (66). Emergency CABG may be considered for MI patients with unsuitable anatomy for PCI and a large myocardial ischemic area. However, CABG involves a delay in reperfusion and is associated with a relatively low probability of myocardial salvage.

3.3.1.2. Non-invasive Strategies of Reperfusion

In most cases, MI is triggered by a thrombus formation, typically resulting from the rupture or erosion of an atheroma plaque within a coronary artery. This event initiates platelet adhesion, activation, and aggregation at the site of injury. Concurrently, activation of clotting factors from the coagulation cascade leads to the formation of a fibrin network, which stabilizes the platelet plug and contributes to the development of a mature thrombus. Therefore, treatments that directly dissolve the thrombus (lytic agents) or prevent new atherothrombotic events (antithrombotic agents) are widely used in MI management.

Fibrinolysis treatment

Fibrinolytic therapy is another reperfusion strategy for STEMI patients presenting within 12 hours of symptom onset when emergent PCI cannot be performed in a timely manner (<120min from symptoms start). Fibrinolytic agents convert the inactive proenzyme plasminogen into its active form, plasmin, which degrades fibrin and dissolves the thrombus. Examples of fibrinolytic agents include tissue plasminogen activators such as tenecteplase, alteplase and reteplase, as well as other options like urokinase or streptokinase (67). When fibrinolytic therapy is indicated, it should be initiated within 10 min of STEMI diagnosis, in the pre-hospital setting, as needed (68,69), without waiting for cardiac biomarker testing results. After initiating fibrinolytic therapy, patients should be immediately transferred to a PCI centre. Subsequent management steps depend on the response to fibrinolysis and the patient's clinical presentation:

- Patients who have experienced failed fibrinolysis or present with hemodynamic instability: they should be rapid transfer to PCI centre for urgent angiography and PCI as necessary.
- Patients with successful fibrinolysis: characterized by ST-segment resolution >50% at 60–90 min, typical reperfusion arrhythmia, and resolution of chest pain, may benefit from routine early angiography, ideally performed within 2-24 hours.

3.3.2. Antithrombotic Therapy

Advanced age, female sex, chronic kidney disease (CKD), diabetes mellitus, prior HF/revascularization, history of cancer, and frailty or unsuitable anatomy for revascularization are some common reasons for not performing diagnostic angiography on MI patients (56). Although coronary angiography is generally considered a relatively low-risk, when some of these clinical or anatomical factors coincide, the risk associated with the revascularization procedure outweighs the benefits. Additionally, approximately 30% of eligible patients for revascularization do not receive timely intervention or experience failed reperfusion strategies (70). MI patients who do not undergo reperfusion or experiencing failed reperfusion should receive antithrombotic treatment.

Antithrombotic treatment is crucial in managing MI since coronary thrombosis is the primary trigger for MI. Antithrombotic therapy is initiated in the acute management of all forms of ACS, including both STEMI and NSTEMI patients, and is typically continued as part of long-term treatment (56). Antithrombotic treatments are classified into two main groups based on their mechanism of action:

Antiplatelet drugs: therapeutic agents that block platelet activation pathway in different points to inhibit their stimulation and aggregation, thereby preventing atherothrombotic progression (**Figure 10**):

- **Aspirin (acetylsalicylic acid):** selectively blocks cyclo-oxygenase and the formation of thromboxane A₂ (TXA₂), a potent platelet aggregator. Consequently, aspirin drastically reduces platelet aggregation capacity. Additionally, aspirin has a vasodilator effect.
- **P2Y₁₂ receptor inhibitors:** P2Y₁₂ receptor is located on the surface of platelets and plays a crucial role in platelet activation. By inhibiting this receptor, these medications prevent platelet aggregation and reduce the formation of blood clots. This group of drugs includes clopidogrel, prasugrel, ticagrelor, and cangrelor, which vary in their efficacy in platelet inhibition, with prasugrel and ticagrelor being the most potent inhibitors (56,71,72) .
- **Glycoprotein (GP) IIb/IIIa receptor inhibitors:** GP IIb/IIIa receptors are found on the surface of platelets and serve as binding sites for fibrinogen and von Willebrand factor, both involved in platelet cross-linking and aggregation. Proper inhibition of these receptors limits platelet aggregation and thrombus progression. Available GP IIb/IIIa inhibitors include tirofiban and eptifibatide.

Anticoagulant drugs: these drugs act at distinct points within the coagulation cascade, thereby reducing the risk of thrombosis. Primarily, they inhibit thrombin synthesis, which converts soluble fibrinogen into insoluble fibrin strands. Additionally, thrombin inhibition attenuates other clot-related processes, such as platelet activation and aggregation. Some of these agents

work directly by inhibiting the enzyme, while others exert their effects indirectly by binding to antithrombin or preventing its synthesis in the liver. Examples of these agents included heparin and low molecular weight heparin agents, direct thrombin inhibitors like bivalirudin, and direct factor Xa inhibitors such as fondaparinux.

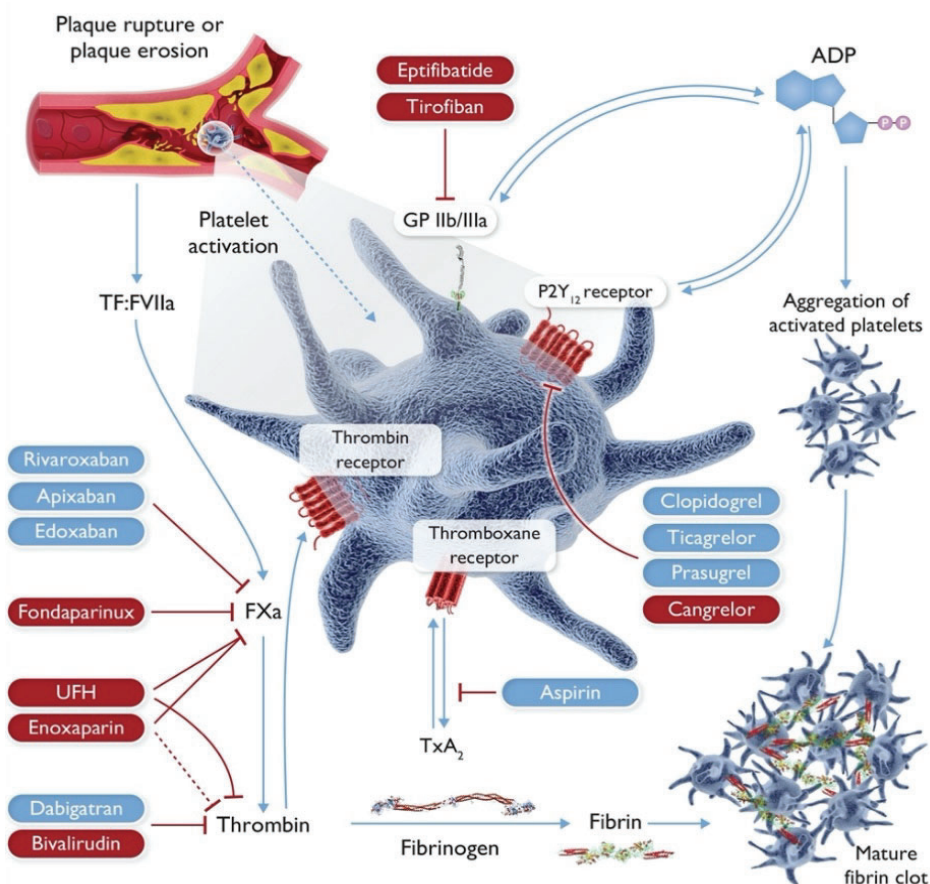


Figure 10. Antithrombotic treatments in acute coronary syndrome (ACS) and pharmacological targets. ADP, adenosine diphosphate; FVIIa, Factor VIIa; FXa, Factor Xa; GP, glycoprotein; TF, tissue factor; TxA₂, thromboxane A₂; UFH, unfractionated heparin. Medications for oral administration are indicated in blue, while those with preferred parenteral administration are highlighted in red. *Figure adjusted from Byrne RA et al., 2023 (56).*

3.4. Long Term MI Treatment

Following the acute phase of MI, it is essential to implement measures to prevent recurrent events and optimize CV risk, a process known as secondary prevention. This involves a combination of lifestyle modifications and medical therapy, effectively implemented via structured cardiac rehabilitation (CR) programs. Secondary prevention after MI is crucial for improving quality of life and reducing both morbidity and mortality, and it should be initiated as early as possible (73).

3.4.1. Cardiac Rehabilitation

CR is a comprehensive and multidisciplinary intervention designed for patients with diverse CV conditions, including MI. CR programs aim to educate patients on managing and controlling CV risk factors through lifestyle modifications and the implementation of pharmacological therapies (**Figure 11**). One of the main benefits of CR is its ability to improve patient adherence and persistence to prescribed treatments and lifestyle recommendations. CR programs have been shown to significantly reduce CV hospitalizations, recurrent MI, CV mortality and, even all-cause mortality (74,75).

3.4.2. Lifestyle Management

Management of lifestyle habits is one of the cornerstones of CR programs (**Figure 11**). It includes:

- *Smoking cessation*: after ACS, abstinence from tobacco reduces the risk of re-infarction by 30–40% and death by 35–45% (76).

- *Healthy diet and restriction in alcohol consumption*: it is recommended to adopt a healthy diet, such as the Mediterranean diet (77), and limit alcohol consumption to a maximum of 100g per week (78).
- *Physical activity promotion*: it is recommended to engage in physical activity of any intensity, including light intensity (79). A combination of regular aerobic exercise and resistance training is considered the most effective approach.
- *Psychological management*: psychological and pharmacological interventions should be considered for MI patients with depression, anxiety, and stress, as they are associated with worse outcomes.

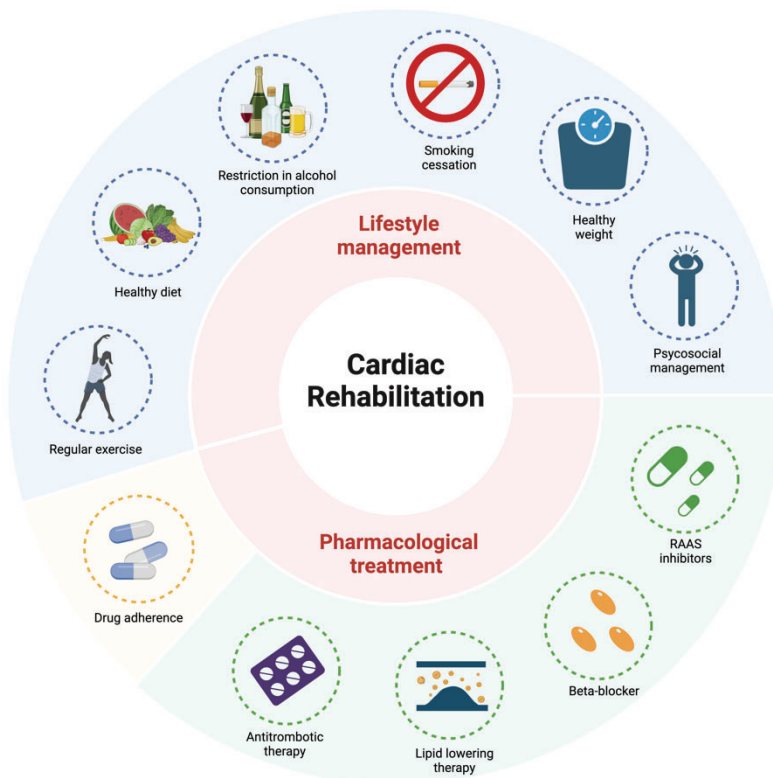


Figure 11. Long-term management after acute coronary syndrome (ACS): comprehensive cardiac rehabilitation and its core components. RAAS, renin angiotensin aldosterone system. *Original figure created with Biorender.com.*

3.4.3. Pharmacological Treatment

Long-term treatment for MI typically involves the following classes of drugs (**Figure 11**):

Antithrombotic therapy

Antithrombotic treatment is a cornerstone in the management of MI, both during the acute phase and in the long term. It significantly reduces the risk of recurrent ischemic events, such as MI and stent thrombosis, while also lowering mortality rates. Although anticoagulation therapy after PCI is typically not required, continued antiplatelet therapy is crucial for effective long-term management of MI. Standard treatment typically involves a potent P2Y₁₂ receptor inhibitor (prasugrel or ticagrelor) combined with aspirin, known as dual antiplatelet therapy, for a duration of 12 months. After the first year, aspirin monotherapy is usually sufficient for most patients.

Lipid-lowering therapy

Patients with dyslipidaemia—characterized by abnormal levels of blood lipids such as cholesterol, triglycerides, and lipoproteins—face a heightened risk of CV events due to lipid accumulation in blood vessels, which can result in atherosclerosis. Lipid-lowering therapy is designed to prevent atherosclerosis progression, reduce the risk of recurrent MI, and enhance overall CV health. Commonly used medications in this treatment include statins, fibrates, bile acid sequestrants, and cholesterol absorption inhibitors.

Beta-blockers

Beta-blockers (BBs) work by blocking adrenergic stimulation, leading to a reduction in heart rate and blood pressure while also providing vasodilatory

and antiarrhythmic effects. Their long-term use is strongly recommended for MI patients with reduced left ventricular ejection fraction (LVEF) < 40% (80,81). The evidence for prescribing BBs in MI patients with LVEF > 40% is less robust.

Renin–angiotensin–aldosterone system inhibitors

RAAS inhibitors are a class of drugs used to manage various CV conditions, including hypertension, HF and MI. These drugs act on different components of the RAAS pathway, which plays a key role in regulating blood pressure and fluid balance. This class includes angiotensin-converting enzyme inhibitors (ACEis), angiotensin II receptor blockers (ARBs), and aldosterone antagonists. ACEis work by blocking the conversion of angiotensin I to angiotensin II, a potent vasoconstrictor, thereby promoting vasodilation and reducing blood pressure. Their use is recommended for MI patients with comorbid conditions such as HF and/or LVEF \leq 40%, diabetes, CKD, and/or hypertension (82–84). Examples of ACEis include enalapril and ramipril. For patients who are intolerant to ACEis, ARBs can be prescribed as an alternative treatment.

3.5. Complications from MI to HF

In summary, the current management of MI focuses on two primary objectives: 1) the rapid restoration and maintenance of proper blood circulation to minimize myocardial damage, and 2) the implementation of long-term measures to reduce the CV risk (secondary prevention). While current interventions effectively reduce mortality, recurrent MI, and death, they do not entirely prevent complications arising from the injury/death of myocardial tissue affected by the ischemia. As detailed in Section 2, post-MI

injury or unresolved ischemic tissue triggers different cardiac modifications, leading to adverse ventricular remodelling. Initially serving as a compensatory mechanism, ventricular remodelling can eventually impair cardiac function, increase the risk of VAs, and contribute to HF development. In fact, IHD and MI remain the leading causes of HF (85). Acute HF resulting from an MI significantly increases mortality, morbidity, and re-hospitalization rates and is associated with other in-hospital complications, such as renal dysfunction, respiratory failure, and pneumonia (86). These patients require effective management of both MI and HF conditions.

In recent years, the introduction of new medications, such as angiotensin receptor–neprilysin inhibitor (ARNi) and sodium-glucose cotransporter 2 (SGLT2) inhibitors, has significantly improved clinical outcomes for HF patients and generated considerable research interest. However, rather than treating HF symptoms, cardiologists aim to prevent the progression from MI to HF. This involves strategies to limit ischemic injury post-MI, mitigate adverse remodelling, and preserve myocardial function to reduce the risk of HF development. While the efficacy of these novel drugs in HF management is well-established, their potential benefits in the post-MI scenario remain largely unexplored, highlighting the need for further research in this area.

4. New Era of HF Drugs

The introduction of new medications such as ARNi and SGLT2 inhibitors has significantly improved HF treatment by reducing re-hospitalization rates and CV mortality. This advancement represents an important shift in HF management, providing promising outcomes for these patients. While the role of these drugs in HF is well established, their efficacy in the post-AMI scenario remains largely unexplored.

4.1. Angiotensin Receptor/Neprilysin Inhibitor

Sacubitril/valsartan is the first approved agent in a new class of drugs known as ARNi. It has received approval from both the U.S. Food and Drug Administration (FDA) and the European Medicines Agency (EMA) for the treatment of chronic heart failure with reduced ejection fraction (HFrEF; LVEF < 40%). Interest in sacubitril/valsartan has significantly increased following the results published from the PARADIGM-HF trial (87). The trial evaluated the efficacy of sacubitril/valsartan compared with enalapril (ACEi) in patients with HFrEF. Sacubitril/valsartan significantly reduced the risk of CV death and hospitalization for HF. Similar results were achieved in a paediatric study of HFrEF, the PANORAMA-HF trial (88). These outcomes highlighted the superiority of sacubitril/valsartan over traditional HF therapies. However, in the case of heart failure with preserved ejection fraction (HFpEF; LVEF > 45%), sacubitril/valsartan did not significantly reduce the composite endpoint of total hospitalizations for HF and CV death compared to valsartan (ARB), as evaluated in the PARAGON-HF trial (89). Currently, sacubitril/valsartan is recommended as an alternative to ACEi or ARBs for the treatment of HFrEF

and is typically prescribed alongside other standard HF treatments, such as BBs and aldosterone antagonists.

4.1.1. Mechanism of Action

HF pathophysiology involves the activation of different compensatory mechanisms, including the RAAS. In response to different triggers, the RAAS is activated in the kidneys, leading to renin secretion. Renin initiates a cascade by acting on angiotensinogen to produce angiotensin I, which is subsequently converted into angiotensin II by the angiotensin-converting enzyme (ACE). Angiotensin II promotes vasoconstriction and aldosterone secretion, leading to sodium and water retention, which in turn increases blood volume and pressure (90). While the RAAS is essential for maintaining CV balance, its dysregulation can result in vasoconstriction, hypertension, increased sympathetic tone, and cardiac remodelling, thereby exacerbating HF. The activation of RAAS is widely recognized as a significant driver of ventricular remodelling and HF progression following MI. Medications such as ACEis, ARBs, and aldosterone antagonists target different points in the RAAS pathway to manage HF progression.

Another compensatory mechanism activated in HF is the natriuretic peptide system, which functions antagonistically to the RAAS and exerts protective effects against HF progression. Activation of this system results in elevated levels of beneficial natriuretic peptides (NPs), including B-type natriuretic peptide and N-terminal pro B-type natriuretic peptide (NT-proBNP). Through the generation of cyclic guanosine monophosphate (cGMP) (91), these peptides promote vasodilation, natriuresis, and diuresis, while also decreasing blood pressure, sympathetic tone, renin, and aldosterone levels,

and exerting anti-fibrotic effects. Natriuretic peptides are degraded by the enzyme neprilysin (92).

Sacubitril/valsartan is a combination medication consisting of a neprilysin inhibitor prodrug (sacubitril) and an ARB (valsartan). By inhibiting NP catabolism and the RAAS, this combination drug provides multiple benefits, including the induction of vasodilation, natriuresis, inhibition of the renin-angiotensin and sympathetic systems, and reductions in cardiac inflammation, cell death, fibrosis, and reverse left ventricular (LV) remodelling (93) (**Figure 12**).

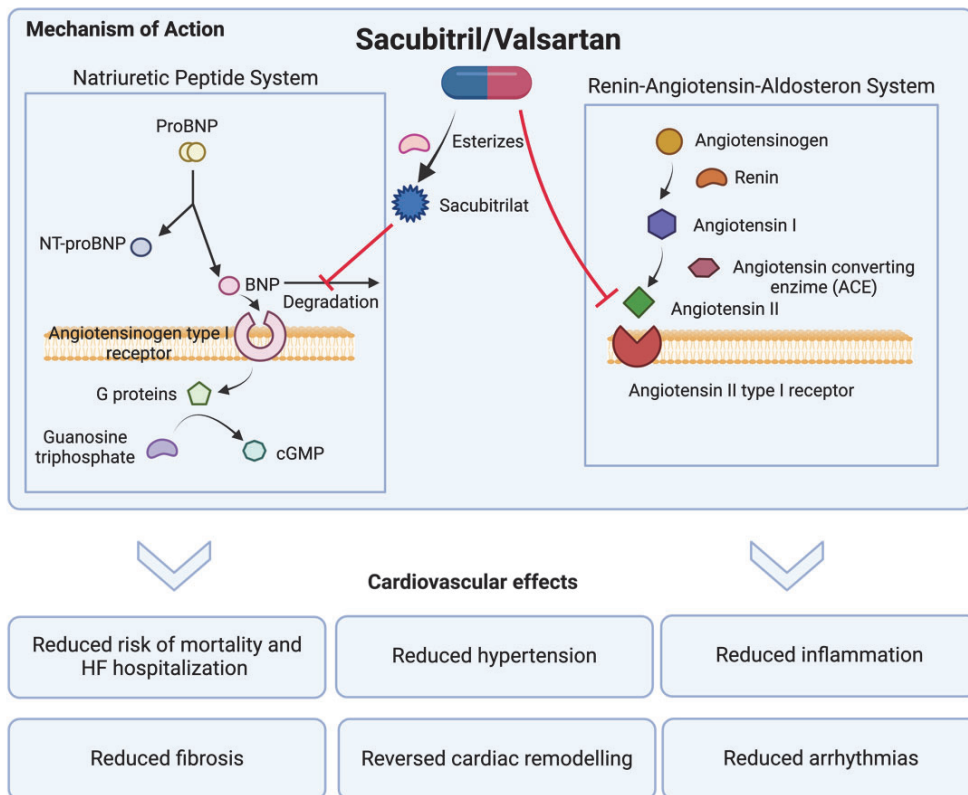


Figure 12. Mechanism of action and cardiovascular effects of sacubitril/valsartan. The active form of sacubitril (sacubitrilat) inhibits the catabolism of natriuretic peptides, while valsartan blocks the RAAS by antagonizing the angiotensin II receptor. ProBNP, pro B type natriuretic peptide; NT-proBNP, N-terminal pro B-type natriuretic peptide; cGMP, cyclic guanosine monophosphate. *Original figure created with Biorender.com.*

4.1.2. Cardiovascular Effects

In the following section, we described the reported effects of sacubitril/valsartan (**Table 1**):

Table 1. Cardiovascular effects of sacubitril/valsartan

Cardiovascular effects of sacubitril/valsartan			
On	Effect	Pathology	Ref
Blood pressure	Reduced systolic and diastolic BP values	Human hypertension	(94–98)
Inflammation	Reduced levels of TNF- α , IL-18, IL-6, and CRP	Human HFrEF	(99–101)
	Reduced levels of TNF- α , IL-6, IL-1 β and CRP; Reduced expression of ICAM-1 and VCAM-1	HF rodent preclinical model	(102,103)
	Reduced levels of IL-1 β , IL-6 and TNF- α	MI rodent preclinical model	(104,105)
	Increased levels of IL-10	MI and diabetic kidney disease rodent preclinical model	(105,106)
	Reduced oxidative stress: reduced intracellular ROS and MDA; increased levels of antioxidant enzymes	MI rat preclinical model	(107)
Fibrosis	Reduced plasma pro-fibrotic biomarkers (aldosterone, MMP-9, sST2, TIMP-1, PINP, PIIINP)	Human HFrEF and HFpEF	(108,109)
	Reduced fibrosis area and pro-fibrotic biomarkers Col I and Col III	HF rat preclinical model	(103,110,111)
	Reduced fibrosis area and pro-fibrotic biomarkers Col I and Col III	MI rodent preclinical model	(112–117)
	Reduced expression of TGF- β 1	MI, HF and diabetic rodent preclinical models	(114,118)
Cardiac function	Increased LVEF, reduced LVEDV, LVESV, left atrial volume and/or LV mass	Human HFrEF	(119–124)

	Improved LVEF, LVEDD or LVEDV, LVESD and/or LV Mass	Human MI	(125–127)
	Improved LVEF and reduced LVEDD	MI rodent preclinical model	(112,117,118)
Arrhythmias	Reduced ICD shocks, occurrences of VF, VT, PVCs, cardiac arrest or sudden cardiac death	Human HFrEF	(87,128–131)
	Reduced VA inducibility	MI rodent preclinical model	(132,133)

BP, blood pressure; TNF- α , tumour necrosis factor alpha; IL, interleukin, CRP, C-reactive protein, HFrEF, heart failure reduced ejection fraction; HFpEF, heart failure preserved ejection fraction; ICAM-1, intercellular adhesion molecules; VCAM-1, vascular cell adhesion molecule 1; MI, myocardial infarction; ROS, reactive oxygen species; MDA, malondialdehyde; MMP, metalloproteinase; sST2, soluble ST2; TIMP-1, tissue inhibitor of metalloproteinase-1; PINP, N-terminal propeptide of collagen I; PIIINP, N-terminal propeptide of collagen III; Col, collagen; TGF- β 1, transforming growth factor β 1; LV, left ventricle; LVEF, left ventricular ejection fraction; LVEDV, left ventricular end diastolic volume; LVESV, left ventricular end systolic volume; LVEDD, left ventricular end diastolic diameter; LVESD, left ventricular end systolic diameter; ICD, implantable cardioverter-defibrillator; VF, ventricular fibrillation; VT, ventricular tachycardia; PVC, premature ventricular contraction; VA, ventricular arrhythmia.

Blood pressure

Sacubitril/valsartan is an effective and safe antihypertensive agent (**Table 1**). Numerous clinical trials have consistently shown that sacubitril/valsartan reduces both diastolic and systolic blood pressure values compared to placebo (94). Impressively, these reductions are evident within 24 hours of its initiation (95). Furthermore, sacubitril/valsartan has demonstrated greater efficacy in lowering blood pressure compared to monotherapy with ARBs in both young and elderly hypertensive patients (96–98). Additionally, emerging research suggests that sacubitril/valsartan may also be beneficial in managing blood pressure in patients with resistant hypertension (134).

Inflammation

Recent studies indicate that sacubitril/valsartan therapy has anti-inflammatory effects in patients with both chronic and acute HFrEF (**Table 1**). Clinical trials have shown that sacubitril/valsartan reduces levels of pro-inflammatory cytokines, including TNF- α , IL-18, IL-6, and c-reactive protein (CRP) (99–101). These findings are further supported by preclinical models of HF, where sacubitril/valsartan has been demonstrated to reduce systemic and local myocardial inflammation, including decreased expression of adhesion molecules such as ICAM-1 and VCAM-1 (103). Additionally, sacubitril/valsartan has shown promising results in lowering pro-inflammatory cytokines (IL-1 β , IL-6 and TNF- α) across various preclinical models, including diabetic (106,135), atherosclerotic (136), cardiotoxic (137,138) and MI (104,105) models. Some of these studies also reported an increase in levels of the anti-inflammatory cytokine IL-10 (105,106). Furthermore, sacubitril/valsartan exhibits the potential to reduce intracellular ROS and oxidative products, such as malondialdehyde (MDA), while restoring antioxidant enzyme levels in the myocardium of MI rat model (107).

Fibrosis

Patients with HFrEF and HFpEF treated with sacubitril/valsartan experienced a significant reduction in plasma pro-fibrotic biomarkers, such as aldosterone, metalloproteinase-9 (MMP-9), soluble ST2 (sST2), tissue inhibitor of metalloproteinase-1 (TIMP-1), N-terminal propeptide of collagen I (PINP), and N-terminal propeptide of collagen III (PIIINP) after 8 and 12 months of treatment (**Table 1**). Compared to valsartan (ARB) or enalapril

(ACEi), sacubitril/valsartan demonstrated superior efficacy in modifying these biomarkers (108,109). In patients with HF with a mildly reduced ejection fraction (HFmrEF; LVEF 41% - 49%), a reduction in diffuse myocardial fibrosis content was observed after 12 months of sacubitril/valsartan treatment, as assessed by magnetic resonance imaging (MRI) (139). Similarly, in various preclinical models, including HF (103,110,111), hypertensive (140,141), diabetic (118,142), and MI (112–117), sacubitril/valsartan significantly reduced fibrosis area and downregulated key pro-fibrotic markers, such as Col I and Col III. The antifibrotic effects of sacubitril/valsartan are believed to be mediated through the inhibition of two key signalling pathways: TGF- β 1/Smad and Wnt/ β -catenin. In animal models of HFpEF (103) and MI (114,118), the drug reduced the expression of TGF- β 1, Smad proteins such as Smad2, Smad3, and Smad4, and components of Wnt/ β -catenin pathway, including β -catenin and Dvl-1, while upregulating the pathway inhibitor sFRP-1 (115). These molecular changes resulted in decreased collagen synthesis and reduced fibrotic areas in cardiac tissue, underscoring sacubitril/valsartan's role in mitigating cardiac remodelling and fibrosis.

Cardiac function

Global LV systolic performance is reflected by LV volumes and LVEF, which are generally impaired in patients with HF. Sacubitril/valsartan therapy has shown promising results in reversing adverse LV remodelling, leading to improvements in ventricular volume overload and enhanced LVEF in HF patients (121–124) (**Table 1**). Treatment with sacubitril/valsartan has been shown to reduce left ventricular end-diastolic volume (LVEDV), left ventricular end-systolic volume (LVESV), left atrial volume index, and/or LV

mass, with greater efficacy compared to ACEi drugs (127). In preclinical MI models, sacubitril/valsartan significantly improved cardiac function, including better LVEF, reduced LV end-diastolic diameter, improved diastolic wall strain, and decreased interventricular septal thickness (112,117,118). In AMI patients, the initiation of sacubitril/valsartan has generally shown promising results in cardiac function, with improvements observed as early as one week (125) or at 6 months following treatment initiation (126). However, in some other trials, such as PARADISE-MI, sacubitril/valsartan did not significantly improve LVEF compared to ramipril (ACEi) after 8 months, although it resulted in smaller increase in LVEDV and a greater decline in LV mass (127).

Arrhythmias

Sacubitril/valsartan has demonstrated promising potential in preventing malignant ventricular arrhythmic events in HFrEF patients compared to ARB and ACEi agents. These benefits include fewer implantable cardioverter defibrillator (ICD) shocks, reduced occurrences of ventricular fibrillation (VF) and VT, fewer premature ventricular contractions (PVCs), and lower rates of cardiac arrest or sudden cardiac death (87,128–131) (**Table 1**). However, sacubitril/valsartan does not appear to affect atrial fibrillation (128,131). While sacubitril/valsartan's antiarrhythmic effects in HF are well-established, rare cases of VAs have been reported in a small subset of high-risk patients, particularly shortly after the therapy's initiation (143–145). In such cases, discontinuing sacubitril/valsartan and switching to conventional medications may help mitigate VAs (143). There is limited research on the arrhythmogenic effects of sacubitril/valsartan following MI. To date, only two primary studies have demonstrated a reduction in VA inducibility in rat and rabbit MI models

(132,133); however, more studies are needed to elucidate the potential antiarrhythmic benefits of early initiation of sacubitril/valsartan after MI.

4.2. Sodium-Glucose Co-Transporter 2 Inhibitors

SGLT2 inhibitors are a new class of anti-hyperglycaemic drugs used to control blood glucose levels in adults with type II diabetes mellitus (T2DM). These drugs work by blocking the SGLT2 receptor in the kidneys, which is responsible for approximately 90% of glucose reabsorption into the bloodstream. Currently, there are six SGLT2 inhibitors available, approved by the U.S. FDA and the European EMA: canagliflozin, dapagliflozin, empagliflozin, ertugliflozin, sotagliflozin, and bexagliflozin. While initially developed for T2DM management, SGLT2 inhibitors have demonstrated significant additional benefits, particularly in CV and renal protection. Numerous clinical trials, including EMPA-REG (146), DECLARE-TIMI 58 (147), EMPEROR-Reduced (148), EMPEROR-Preserved (149), DAPA-HF (150), and DELIVER (151), have shown that empagliflozin and dapagliflozin effectively reduce the risk of CV death and/or HF hospitalization. These benefits extend across the full spectrum of ejection fraction categories (HFrEF, HFmrEF, and HFpEF). Additionally, the EMPA-KIDNEY (152) and DAPA-CKD (153) trials have demonstrated the efficacy of these medications in slowing the decline in kidney function in CKD patients, regardless of their diabetes status. Consequently, empagliflozin and dapagliflozin are now recommended with a class IA designation as part of the standard treatment regimen for HF patients, alongside other medications such as ACEi/ARB, ARNi, BBs, and mineralocorticoid receptor antagonists (MRAs) (154,155).

4.2.1. Mechanism of Action

The primary mechanism of action of SGLT2 inhibitors is the inhibition of the SGLT2 cotransporter, a membrane protein responsible for glucose reabsorption in the kidneys. In healthy individuals, more than 99% of plasma glucose filtered through the renal glomerulus is reabsorbed. SGLT2 cotransporters, which are almost exclusively expressed in the kidney, handle 90% of this reabsorption in the proximal renal tubule. The remaining 10% is reabsorbed in more distal parts of the tubule by SGLT1 cotransporters (156). Glucose enters renal tubular cells through SGLT2 or SGLT1 by coupling with sodium and exits across the basolateral membrane via GLUT2 (for SGLT2-expressing cells) and GLUT1 (for SGLT1-expressing cells) transporters, returning to the bloodstream. This unidirectional transport of glucose and sodium is maintained by a Na-K-ATPase pump located on the basolateral membrane (157) (**Figure 13**). By inhibiting SGLT2, these drugs block glucose reabsorption in the proximal tubule, resulting in increased glucose excretion in the urine (glycosuria). This action lowers blood glucose levels while also contributing to blood pressure reduction. Furthermore, SGLT2 inhibition promotes sodium excretion (natriuresis), further contributing to their therapeutic benefits, particularly in managing T2DM. However, these medications induce greater glycosuria and consequently osmotic diuresis in individuals with diabetes compared to those without (158). Therefore, their role in primary HF prevention in non-diabetic patients remains unclear. Beyond glucose management, multiple mechanisms have been proposed as major drivers for the direct cardiac benefits of SGLT2 inhibitors (159–162) (**Figure 13**), including: (1) improved myocardial contractility through the inhibition of the cardiac Na⁺/H⁺ exchanger (NHE), which is overexpressed in

HF, helps normalize sodium and calcium imbalances; (2) enhanced metabolic function in the failing heart; (3) reduction of oxidative stress; (4) energy production optimization by promoting autophagy in dysfunctional mitochondria; (5) anti-inflammatory effects through activation of 5' adenosine monophosphate-activated protein kinase (AMPK) and suppression of inflammasome pathways; (6) reduction of apoptosis by inhibiting caspase activity; (7) anti-fibrotic and anti-remodelling effects due to decreased inflammation, oxidative stress and apoptosis; and (8) improved cardiac function.

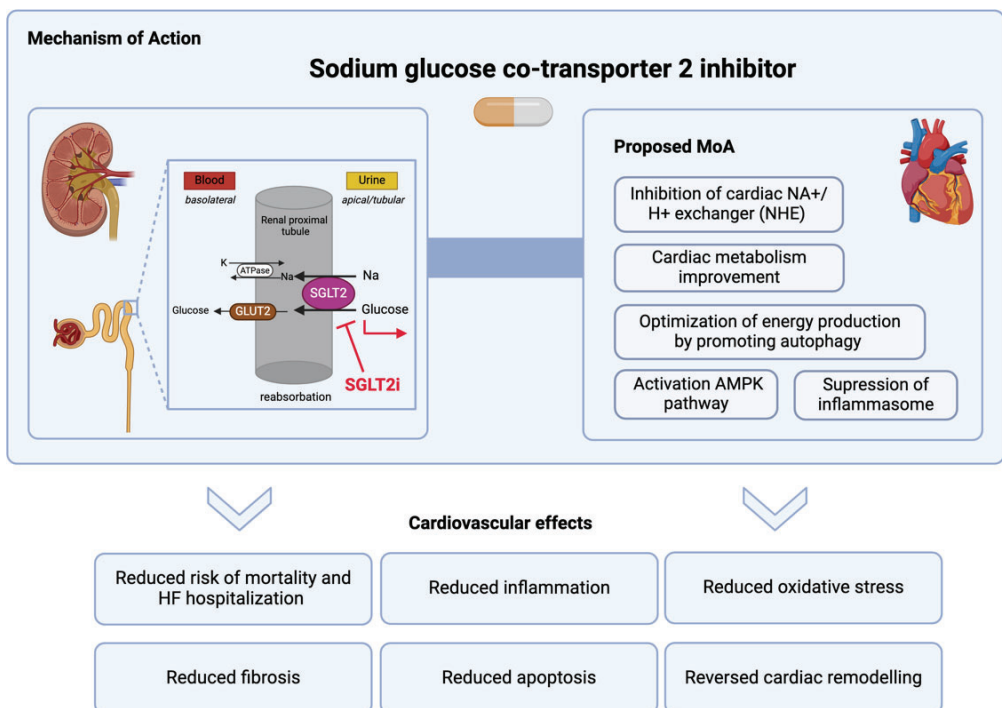


Figure 13. Mechanism of action and cardiovascular effects of sodium glucose co-transporter 2 inhibitors. These drugs function by blocking the sodium glucose co-transporter 2 (SGLT2) receptor in the proximal renal tubule (left), which is responsible for the majority of glucose reabsorption into the bloodstream. The right panel illustrates the principal proposed direct cardiac mechanisms of action of these drugs, while the section below outlines their cardiovascular effects. *Original figure created with Biorender.com*

Although all above-mentioned SGLT2 inhibitors have a shared primary mechanism of action in the kidneys, their CV effects vary significantly. Therefore, this thesis focuses on the CV effects of empagliflozin, with the subsequent section dedicated specifically to this compound.

4.2.2. Cardiovascular Effects

In the following section, we described the reported effects of empagliflozin (Table 2):

Table 2. Cardiovascular effects of empagliflozin

Cardiovascular effects of empagliflozin			
On	Effect	Pathology	Ref
Blood pressure	Reduced systolic and/or diastolic BP values	Human T2DM and/or HF w/wo hypertension	(149,163–166)
Inflammation	Reduced levels of IL-6, TNF- α , CRP	Human HFREF, HFpEF, T2DM+CAD	(167–169)
	Reduced NLRP3 inflammasome activation	Human HFpEF and T2DM at high CV risk	(162,170)
	Reduced levels of TNF- α , IL-6, IL-1 β , CRP and/or MCP-1	T2DM, HF, diabetic nephropathy and cardiotoxicity rodent preclinical models	(171–173)
	Reduced NLRP3 inflammasome activation	HF and cardiotoxicity rodent preclinical models	(171,174)
	Prevention of M1 monocyte accumulation and promotion of their polarization towards M2 phenotype	Obese and/or diabetic rodent preclinical models	(175,176)
	Reduced oxidative stress: reduced MDA, lipid peroxidation and increased levels of antioxidant enzymes	Cardiotoxicity and diabetic nephropathy rodent preclinical models	(171,177,178)
Cardiac metabolism	Improved PCr/ATP and/or circulating levels of FFA and KB	Human T2DM w/wo HF	(179–181)

	Improved myocardial energetics; reduced myocardial glucose uptake and increased utilization of FFA and KB	MI porcine and rodent preclinical models	(182–185)
Fibrosis	Reduced plasma pro-fibrotic biomarkers (PICP, PRO-C3)	Human HFrEF and HFpEF	(186)
	Reduced interstitial fibrosis	Human HFrEF and T2DM+CAD	(187,188)
	Reduced myocardial fibrosis	HF and MI porcine and rodent preclinical models	(183,184,189–191)
	Reduced expression of MMP9, TGF- β 1, Col I and Col III	MI, cardiotoxicity and diabetic porcine and murine preclinical models	(171,189,192)
Cardiac function	Reduced LVEDV, LVESV, and/or LV mass w/wo improved LVEF	Human HFrEF w/woT2DM	(189,193–197)
	Improved LVEDV, LVESV and LVEF	Human MI	(198)
Arrhythmias	Reduced atrial arrhythmic risk; reduced AF, AF/atrial flutter	Human T2DM, HF and CKD	(199–202)
	Reduced PVB, VF inducibility and sudden death preclinical model	MI rodent preclinical model	(203,204)

BP, blood pressure; T2DM, type 2 diabetes mellitus; HF, heart failure; HFrEF, heart failure reduced ejection fraction; HFpEF, heart failure preserved ejection fraction; CAD, coronary artery disease; MI, myocardial infarction; IL, interleukin; TNF- α , tumour necrosis factor alpha; CRP, C-reactive protein, MCP-1, monocyte chemoattractant protein 1; MDA, malondialdehyde; PCr/ATP, phosphocreatine (PCr)/adenosine triphosphate (ATP) ratio; FFA, free fatty acids; KB, ketone bodies; PICP, Procollagen type I carboxy-terminal propeptide; PRO-C3, N-terminal type III collagen; MMP, metalloproteinase; TGF- β 1, transforming growth factor β 1; Col, collagen; LV, left ventricle; LVEDV, left ventricular end diastolic volume; LVESV, left ventricular end systolic volume; LVEF, left ventricular ejection fraction; AF, atrial fibrillation; PVB, premature ventricular beat; VF, ventricular fibrillation; w/wo, with or without.

Blood pressure

Empagliflozin has been shown to lower both systolic and diastolic blood pressure in patients with T2DM, regardless of the presence of hypertension

or the concurrent use of other antihypertensive medications, such as diuretics or ACEis/ARBs (163,164,205) (**Table 2**). Regardless of diabetes status, empagliflozin reduces blood pressure, particularly systolic blood pressure, in patients with HF, as demonstrated in sub-studies from the EMPEROR-reduced and EMPEROR-preserved trials (165,166). Blood pressure reduction is also observed in normotensive non-diabetic subjects. Although the precise mechanism(s) behind the antihypertensive effects of SGLT2 inhibitors are not fully understood, they seem to be mediated by osmotic diuretic effects resulting from the inhibition of sodium reabsorption in the proximal tubules of the kidney (206).

Inflammation

Empagliflozin treatment exhibits anti-inflammatory effects by reducing the expression of pro-inflammatory cytokines, including TNF- α , IL-6, and IL-1 β , as well as CRP and MCP-1 (167–169,171–173) (**Table 2**). It also prevents the accumulation of inflammatory M1 macrophages and promotes their polarization toward the anti-inflammatory M2 phenotype (175,176). Additionally, empagliflozin decreases oxidative products such as MDA and lipid peroxidation, while restoring antioxidant enzyme levels like superoxide dismutase (SOD) (171,177,178). The anti-inflammatory effects of SGLT2 inhibitors are attributed to various mechanisms. A key pathway involves the activation of AMPK, which regulates cellular energy balance and suppresses inflammation by inhibiting pro-inflammatory pathways, reducing inflammatory mediators, inducing autophagy, and modulating glucose and lipid metabolism (207). This leads to a decreased production of pro-inflammatory cytokines such as TNF- α , IL-6, and IL-1 β by inhibiting Nuclear

factor kappa B (NF- κ B) activity. The activation of AMPK by empagliflozin has been confirmed in numerous studies (175,208). In addition to AMPK activation, SGLT2 inhibitors suppresses the activation of nucleotide binding domain leucin rich repeat and pyrin domain containing 3 (NLRP3) inflammasome, a key driver of inflammation that releases pro-inflammatory cytokines like IL-1 β and IL-18. By inhibiting the activation of inflammasome, SGLT2 inhibitors reduces inflammatory processes, contributing to its cardioprotective effects. This effect of empagliflozin on suppressing inflammasome has been reported in numerous preclinical (171,174) and clinical (162,170) studies.

Cardiac metabolism

In a failing heart, there is a metabolic shift from using free fatty acids (FFA), the preferred energy source in a healthy heart, to glucose, which is a less energetically efficient substrate. Empagliflozin treatment has been shown to reverse this shift, improving cardiac metabolism and energy efficiency. In a small study involving patients with HF and T2DM, 12 weeks of empagliflozin treatment significantly improved the myocardial phosphocreatine-to-ATP (PCr/ATP) ratio, an indicator of cellular energetics (179) (**Table 2**). Additionally, in T2DM patients, empagliflozin increased circulating levels of FFA and ketone bodies (KBs), which are recognized as highly efficient fuels for the heart (180,181). Zannad and colleagues identified differential protein expression associated with improved myocardial mitochondrial health in serum samples from the EMPEROR-Reduced and EMPEROR-Preserved trials (209). However, the results were not consistent across all studies (181,210). For instance, the EMPA-VISION trial, which included patients with HFrEF and

HFpEF, found no significant impact of empagliflozin on the myocardial PCr/ATP ratio or circulating KB levels (210). Many of these clinical studies have involved a limited number of patients, indicating the need of larger patient cohorts. Preclinical studies generally supports the metabolic shift hypothesis. In a swine model of MI, empagliflozin reduced myocardial glucose uptake and increased utilization of FFA and KB, resulting in a higher myocardial ATP levels (182). Similar findings of improved myocardial energetics have been reported in rodent models of MI (183–185), diabetes (181), and cardiotoxicity (211). The proposed mechanisms underlying these effects include the activation of the AMPK and SIRT1/PGC-1 α /FGF21 pathways (212).

Fibrosis

The effects of SGLT2 inhibitors on myocardial fibrosis has not been extensively studied in patients, requiring further research. A sub-study of the EMPEROR-Reduced and EMPEROR-Preserved trials examined the impact of empagliflozin on serum markers of collagen turnover. Empagliflozin reduced procollagen type I carboxy-terminal propeptide (PICP) and the fragment of N-terminal type III collagen (PRO-C3) compared to placebo over time. However, it had no effect on other fibrotic markers, including procollagen type I amino-terminal peptide (PINP), fragment of C-terminal type VIa3 collagen (PRO-C6), fragment of type I collagen (C1M), and fragment of type III collagen (C3M) (186) (**Table 2**). In contrast, other clinical studies involving T2DM patients, with or without coronary artery disease (CAD), found no significant impact of empagliflozin on fibrotic markers such as sST2 or MMP-2. However, these were small studies with limited sample sizes (188,213). In another study that

involved patients with HFrEF, empagliflozin reduced interstitial fibrosis, as assessed through T1 mapping with CMR (187). Similar findings were observed in patients with T2DM and CAD (188). Nevertheless, these improvements in myocardial diffuse fibrosis were not replicated in the study by Jung-Chi Hsu et. al., which also involved T2DM patients (214), suggesting inconsistent and controversial results. In preclinical models, empagliflozin has consistently shown efficacy in reducing myocardial fibrosis in HF (183,189,190), MI (184,191), diabetes (192,215), and cardiotoxicity (171,216) models. Empagliflozin has also been reported to decrease the expression of pro-fibrotic markers such as MMP9, TGF- β 1, Col I and Col III (189,191,192). Several mechanisms of action have been proposed including activation of AMPK pathway (215) and improved energy metabolic efficiency (183). However, the primary mechanism reported is the inhibition of the TGF- β 1/Smad3 signalling pathway (189–192).

Cardiac function

Several clinical studies have examined the effects of empagliflozin on cardiac function. Omar and co-workers (193) recently demonstrated that, compared to placebo, empagliflozin treatment had a modest yet significant positive effect on LV volumes and mass in patients with HFrEF and T2DM, by reducing indexed LVESV, indexed LVEDV, and indexed LV Mass, without affecting LVEF (**Table 2**). Similar findings were observed in the SUGAR-DM-HF trial, where Lee and colleagues reported that empagliflozin reduced LV volumes in patients with HFrEF and T2DM (194). A greater impact on cardiac volumes was documented in the EMPA-TROPISM trial, which involved non-diabetic patients with HFrEF (197). In this study, empagliflozin, compared to placebo,

significantly reduced LVEDV, LVESV, and LVMass, while improving LVEF after 6 months of treatment. Furthermore, the results of two meta-analysis that evaluated the effects of SGLT2 inhibitors on cardiac remodelling parameters in patients with T2DM and/or HF concluded that SGLT2 inhibitors improved LVEF, LV volumes and mass, specifically in HFrEF patients, regardless of the glycaemic status (195,196). Empagliflozin also shown a significant positive effect on LV reverse remodelling in pre-clinical studies of HF models, including those conducted on pigs (182,189) and rodents (183,217,218). In the context of MI, the EMMY trial, which included 476 patients with AMI, found that empagliflozin treatment was associated with improved echocardiographic outcomes, including LV volumes and LVEF (198).

Arrhythmias

To date, limited research has explored the impact of SGLT2 inhibitors on arrhythmia susceptibility. Among the available studies, three meta-analysis involving patients with T2DM, HF and CKD concurred on the ability of SGLT2 inhibitors to reduce the risk of atrial arrhythmias, including atrial fibrillation (AF) and AF/atrial flutter, without significantly affecting VAs (199–201) (**Table 2**). Furthermore, empagliflozin has demonstrated effectiveness in reducing atrial tachyarrhythmias in patients with cardiac implantable electronic devices (202). In the context of MI, Genlong Xue et al. found that empagliflozin treatment reduced premature ventricular beats (PVBs) and VF in a mouse MI model (203). Similarly, in another study led by Zhaoyang Hu, et al. empagliflozin treatment reduced the vulnerability to sudden death and ischaemia-reperfusion-injury arrhythmias in a rat model (204). Overall, these

findings suggest that empagliflozin exerts anti-arrhythmic effects, primarily on atrial arrhythmias.

4.3. Safety and Synergistic Effects of ARNi and SGLT2 Inhibitors

Since the introduction of ARNi and SGLT2 inhibitors therapies for HFrEF, several studies have evaluated the safety and the potential synergistic effects of their co-administration.

In terms of safety, co-treatment with sacubitril/valsartan and SGLT2 inhibitors has been shown to be generally well-tolerated in most patients with HFrEF (165,219–221), including elderly patients (222). Regarding efficacy, subgroup analyses from clinical trials revealed that patients who initiated empagliflozin treatment while already receiving sacubitril/valsartan experienced improvements in health indicators, such as lower systolic blood pressure, heart rate, and NT-proBNP levels, compared to those not treated with sacubitril/valsartan. However, despite these positive effects, co-treatment with sacubitril/valsartan and empagliflozin did not result in a statistically significant reduction in CV death or HF hospitalizations (223). Similarly, the DAPA-HF trial found no significant differences in the benefits of dapagliflozin when comparing patients taking sacubitril/valsartan with those who were not, with respect to CV death or worsening HF outcomes (221). Furthermore, findings from the EMPIRE-HF trial indicated that the effects of empagliflozin on cardiac structure and function were not influenced by concomitant sacubitril/valsartan treatment (224). Despite these unexpected findings, the proportion of patients receiving both medications in these trials

was considerably smaller than those receiving SGLT2 inhibitors alone, highlighting the need for larger-scale studies. Regardless of the limitation of studies, some preclinical evidence suggests that combining dapagliflozin and sacubitril/valsartan may offer superior protection against ischemia-reperfusion injury compared to either drug administered alone (225).

4.4. Early Initiation of Sacubitril/Valsartan and Empagliflozin After MI

In recent years, the introduction of ARNi and SGLT2 inhibitor therapies has significantly improved the prognosis of patients with HF, with notable reductions in mortality from CV causes and HF hospitalizations. However, the potential role of these pharmacological therapies in AMI patients remains uncertain.

Sacubitril/valsartan in AMI

Early initiation of sacubitril/valsartan following MI has shown benefits in preclinical and clinical studies, including reductions in inflammation (116) and fibrosis (112), improvements in cardiac function (126), and decreases in VAs incidence (132). In the clinical setting, the primary trial investigating this therapy in the context of MI is the PARADISE-MI, which aimed to determine whether sacubitril/valsartan is superior to ramipril (ACEi) in improving outcomes for AMI patients. The trial included 5661 patients who had experienced an AMI within seven days, complicated by LV systolic dysfunction ($LVEF \leq 40\%$), pulmonary congestion, or both. Participants were randomized to receive either ramipril (n=2831) or sacubitril/valsartan (n=2830) and were followed for a median of 22 months (recruitment

occurred between December 2016 and March 2020). The primary endpoint was the composite of CV death and HF episodes (226). Results showed that sacubitril/valsartan was safe and well-tolerated for AMI patients. However, although it led to a 10% risk reduction in the primary endpoint, this result did not reach statistical significance. Regarding the secondary outcomes, there were no significant differences between the two groups in all-cause mortality, CV mortality, or the incidence of new heart attacks and strokes. However, sacubitril/valsartan was significantly more effective than ramipril in reducing recurrences of HF episodes (227,228).

Empagliflozin in AMI

Regarding empagliflozin treatment, limited studies have evaluated the effects of its early initiation following MI. Some preclinical studies have demonstrated benefits, including reductions in inflammation (169) and fibrosis (184), enhancements in cardiac function (198), improvements in cardiac metabolism (182), and decreased inducibility of VAs (203). Clinically, the results from the EMPACT-MI trial (229) were recently published, in which the effects of early initiation of empagliflozin following MI were evaluated. This trial included 6522 patients hospitalized for AMI who were at high risk for HF (LVEF < 45% or signs or symptoms of congestion). Patients were randomized to receive empagliflozin or placebo within 14 days of admission and were followed for a median of 17.9 months (recruitment occurred between December 2020 and March 2023). The primary endpoint of the study was a composite of hospitalization for HF and all-cause of death. Although the percentage of events was lower in the empagliflozin group compared to the placebo group, this difference did not result in a statistically significant reduction in the risk of the primary endpoint. However,

empagliflozin significantly reduced the risk of time to first hospitalization for HF by 23% and the total number of hospitalizations for HF by 33%, compared to placebo (230).

Although the outcomes of these studies have been less impactful as anticipated, both sacubitril/valsartan and empagliflozin have demonstrated beneficial effects in the context of MI. Therefore, further research is necessary to reach more definitive conclusions and identify potential subgroups of AMI patients who may benefit from the early initiation of these therapies.

Chapter Two

Hypothesis & Objectives

The heterogeneity of the post-infarction myocardial scar, partially caused by the inflammatory cascade, establishes the substrate for the initiation of adverse structural and electrical cardiac remodelling, thereby promoting the development of HF and fatal VAs. Additionally, metabolic remodelling in a failing heart further exacerbates HF progression. Empagliflozin and sacubitril/valsartan, two novel drugs for HF, have demonstrated significant improvements on clinical outcomes in HF patients by exerting beneficial effects on inflammation, fibrosis, cardiac metabolism, electrophysiological properties, and/or cardiac function. Although the roles of empagliflozin and sacubitril/valsartan in HF management are well established, their efficacy in the post-acute MI context remains largely unexplored.

The working hypothesis of this thesis is:

Early administration of empagliflozin and/or sacubitril/valsartan may exert cardioprotective effects against post-ischemic injury by attenuating inflammation at both myocardial and systemic levels, enhancing myocardial metabolism, and mitigating adverse post-MI structural and electrophysiological remodelling. The combination of these drugs could be safe and may offer synergistic therapeutic effects.

In order to address this hypothesis, we evaluated the following objectives:

Objective 1: To develop a pre-clinical translational porcine model of MI.

Objective 2: To evaluate the effects of early initiation of empagliflozin and/or sacubitril/valsartan in a translational porcine model of MI, in terms of inflammation, myocardial metabolism, and structural and electrophysiological remodelling.

Objective 3: To assess the safety and potential synergistic therapeutic effects of combining empagliflozin and sacubitril/valsartan.

Chapter Three

Material, Methods & Results

ARTICLE 1

Myocardial Infarction by Percutaneous Embolization Coil Deployment in a Swine Model

Martínez-Falguera D, Fadeuilhe E, Teis A, Aranyó J, Adeliño R, Bisbal F, Rodríguez-Leor O, Gálvez-Montón C.

Published in the *Journal of Visualized Experiments* 2021 Nov 4;(177). doi: 10.3791/63172.

Impact factor (Journal Citation Reports): **1.424**

Quartil (Journal Citation Reports): **Q3** MULTIDISCIPLINARY SICENCES

Objective: This article is related to objective 1. The study aimed to describe the procedure for developing a translational pre-clinical porcine model of MI using the permanent coil deployment technique.

Highlights: This approach was feasible, highly reproducible, and accurately emulated the pathophysiology of human non-revascularized MI, while avoiding traditional open-chest surgery and its associated postoperative inflammation.

Myocardial Infarction by Percutaneous Embolization Coil Deployment in a Swine Model

Daina Martínez-Falguera^{*,1,2}, Edgar Fadeuilhe^{*,3}, Albert Teis³, Julia Aranyo³, Raquel Adeliño^{1,3}, Felipe Bisbal^{3,4}, Oriol Rodríguez-Leor^{3,4}, Carolina Gálvez-Montón^{1,3,4}

¹ICREC Research Program, Germans Trias i Pujol Health Research Institute (IGTP) ²Faculty of Medicine, University of Barcelona (UB) ³Heart Institute (ICOR), Germans Trias i Pujol University Hospital ⁴CIBER Cardiovascular, Instituto de Salud Carlos III

*These authors contributed equally

Corresponding Author

Carolina Gálvez-Montón
cgalvez@igt.p.cat

Citation

Martínez-Falguera, D., Fadeuilhe, E., Teis, A., Aranyo, J., Adeliño, R., Bisbal, F., Rodríguez-Leor, O., Gálvez-Montón, C. Myocardial Infarction by Percutaneous Embolization Coil Deployment in a Swine Model. *J. Vis. Exp.* (177), e63172, doi:10.3791/63172 (2021).

Date Published

November 4, 2021

DOI

10.3791/63172

URL

jove.com/video/63172

Abstract

Myocardial infarction (MI) is the leading cause of mortality worldwide. Despite the use of evidence-based treatments, including coronary revascularization and cardiovascular drugs, a significant proportion of patients develop pathological left-ventricular remodeling and progressive heart failure following MI. Therefore, new therapeutic options, such as cellular and gene therapies, among others, have been developed to repair and regenerate injured myocardium. In this context, animal models of MI are crucial in exploring the safety and efficacy of these experimental therapies before clinical translation. Large animal models such as swine are preferred over smaller ones due to the high similarity of swine and human hearts in terms of coronary artery anatomy, cardiac kinetics, and the post-MI healing process. Here, we aimed to describe an MI model in pig by permanent coil deployment. Briefly, it comprises a percutaneous selective coronary artery cannulation through retrograde femoral access. Following coronary angiography, the coil is deployed at the target branch under fluoroscopic guidance. Finally, complete occlusion is confirmed by repeated coronary angiography. This approach is feasible, highly reproducible, and emulates the pathogenesis of human non-revascularized MI, avoiding the traditional open-chest surgery and the subsequent postoperative inflammation. Depending on the time of follow-up, the technique is suitable for acute, sub-acute, or chronic MI models.

Introduction

Myocardial infarction (MI) is the most prevalent cause of mortality, morbidity, and disability worldwide¹. Despite current therapeutic advances, a significant proportion of patients develop adverse ventricular remodeling and

progressive heart failure following MI, resulting in poor prognosis due to ventricular dysfunction and sudden death^{2,3,4}. New therapeutic options to repair and/or regenerate injured myocardium are thus under scrutiny, and

translational MI animal models are crucial in testing their safety and efficacy. Although several models have been used for cardiovascular research, including rats^{5,6}, mice^{7,8}, dogs⁹, and sheep¹⁰, pigs are one of the best choices for modeling cardiac ischemia studies because of their high similarity to humans in terms of heart size, coronary artery anatomy, cardiac kinetics, physiology, metabolism, and the post-MI healing process^{11,12,13,14,15}.

In this context, many different open-surgical and percutaneous approaches are available to develop MI swine models. The open-chest approach involves a left lateral thoracotomy procedure and is useful in performing surgical coronary artery ligation^{16,17}, myocardial cryo-injury, cauterization¹², and coronary artery placement of a hydraulic occlude¹⁸ or an ameroid constrictor¹⁹, among others. Surgical coronary occlusion has been extensively used to test new therapeutic options such as cardiac tissue engineering and cell therapy, as it allows wide access and visual assessment of the heart; however, in contrast to human MI, it can result in surgical adhesions, adjacent scarring, and postoperative inflammation¹⁷. Myocardial cryo-injury and cauterization are easily reproducible techniques but do not reproduce the pathophysiological MI progression observed in humans¹². On the other hand, several percutaneous techniques have been developed to produce temporary or permanent coronary blocking. These comprise transcatheter or intracoronary ethanol ablation^{20,21}, occlusion by balloon angioplasty²², or delivery of thrombogenic materials such as agarose gel beads²³, fibrinogen mixtures⁹, or coil embolization^{17,24}. While balloon angioplasty is better suited for ischemia/reperfusion studies, coronary coil deployment is one of the best choices for modeling non-revascularized MI. This percutaneous approach is feasible, consistently reproducible, and avoids open-chest surgery. It allows

precise control of the infarct location and results in pathophysiology similar to that of a human non-reperfused MI. Moreover, coil embolization is suitable for modeling acute, sub-acute, or chronic MI; chronic congestive heart failure; or valvular disease¹⁷.

The present protocol aims to describe how to develop an MI swine model by permanent coil deployment. Briefly, it comprises a percutaneous selective coronary artery cannulation through retrograde femoral access. Following coronary angiography, a coil is deployed at the target branch artery under fluoroscopic guidance. Finally, complete occlusion is confirmed by repeated coronary angiography.

Protocol

This study was approved by the Animal Experimentation Unit Ethical Committee of the Germans Trias i Pujol Health Research Institute (IGTP) and Government Authorities (Generalitat de Catalunya; Code: 10558 and 11208), and complies with all guidelines concerning the use of animals in research and teaching as defined by the Guide for the Care and Use of Laboratory Animals²⁵.

1. Preprocedural preparation of animals

1. Use crossbred Landrace X Large White pigs (30-35 kg) of either sex.
2. Keep the animals in a fasting state for 12 h prior to the procedure.

2. Sedation, anesthesia, and analgesia

1. Sedate the animal with an intramuscular (IM) injection of ketamine (3 mg/kg), midazolam (0.3 mg/kg), and dexmedetomidine (0.03 mg/kg). Wait for approximately 10-15 min.

2. Once the pig is sedated, ventilate it with an oxygen (90-100%)-isoflurane (1-2%) mixture and a face mask to ensure optimal sedation.
3. Place vet ointment on the pig's eyes to prevent dryness.
NOTE: Repeat every 20 min.
4. Place intravenously (IV) a 20 G catheter in a lateral ear vein. Administer propofol (1-2 mg/kg) to induce anesthesia.
5. Once the pig has no swallowing reflex, intubate the animal using an endotracheal tube (size 6.5-7.0 for 30-35 kg).
NOTE: Adjust the size of the endotracheal tube according to the size of the pig. Intubation should be carried out rapidly to prevent a deeper anesthetic plane and prolonged apnea.
6. Administer IV buprenorphine (0.01 mg/kg) for intra-surgical analgesia. Use a fentanyl transdermal patch (100 µg/h) for post-operative analgesia.
NOTE: The fentanyl patch is applied to the inguinal skin, and it is active for 72 h to limit postoperative pain. Its pharmacological effect does not start immediately after delivery, thus apply it before starting the procedure.
7. Perform airway mask bag unit-ventilation (20 inflations/min) during the transport of the pig to the vascular interventional radiology (VIR) room.
8. Connect the endotracheal tube to the anesthesia machine equipped with an airway sensor and capnography recording.
9. Start mechanical positive pressure ventilation with FiO₂ 0.50, using a tidal volume of 10 mL/kg and a frequency of 16-20 breaths/min. Maintain the anesthesia with isoflurane (1-3%).

NOTE: To confirm the correct surgical anesthetic plane, the animal should not be respiring spontaneously nor have corneal or pupillary light reflexes.

3. Hemodynamic monitoring and preparation of the surgical area

1. Place the animal on the operating table in the supine position and fix the limbs to the table with tape or bandage.
2. Place electrocardiogram (ECG) probes subcutaneously in the animal's extremities for recording changes in ST-segment, T-waves, and heart rate during the experimental procedure.
3. Place a pulse oximeter on the tongue or a corner of the lip of the animal and the non-invasive pressure cuff on the forelimb.
4. Measure the rectal/esophageal temperature with a probe.
5. Clean the right femoral area with surgical soap and antiseptic povidone-iodine solution under sterile conditions.
6. Ensure that the surgeon performs surgical handwashing and wears a sterile gown and sterile gloves.
7. Cover the animal with a sterile surgical drape.
8. Prepare and flush with heparinized saline solution the needle, a 6F vascular sheath, a 0.035-inch J-tipped wire, a 6F JR4 90-cm guiding catheter, a 0.014-inch 200-cm guidewire, a 150-cm length/0.017-inch inner diameter microcatheter, and the contrast medium injection manifold kit.

4. Vascular access

1. Puncture the right femoral artery via a percutaneous approach with ultrasound-guided puncture. Locate the bifurcation between the superficial femoral artery and the deep femoral artery.
2. Position the transducer 2-3 cm proximal to the bifurcation, in the common femoral artery, and align the center of the transducer with the common femoral artery.
3. Position the needle in the center of the transducer and puncture the artery at an angulation of approximately 45°. Subsequently, insert a 6F vascular sheath using the modified Seldinger technique²⁶.

NOTE: In case of significant spasm or hematoma, crossover to the contralateral femoral artery.

4. Flush the catheters with heparinized saline solution. (5000 IU unfractionated heparin/1000 mL of 0.9% NaCL).
5. Administer heparin through the sheath (300 IU/kg).

5. Coronary angiography

1. Insert the J-tip wire into the JR4 guide catheter and advance the wire through the sheath into the ascending aorta, and then place the catheter up over the valvular surface.
2. Remove the wire and connect the catheter to the injection manifold system. Purge the entire system.
3. Under fluoroscopy, engage the catheter into the left main coronary artery and inject 10 mL of iodinated contrast medium to visualize the left coronary system (**Figure 1A, C**).

NOTE: It is important to ensure that the arterial pressure waveform is not damped before injecting to avoid the risk of coronary dissection.

4. Perform angiograms in two orthogonal views: left anterior oblique 40° and right anterior oblique 30° projections.
5. Advance a 0.014-inch guidewire pre-assembled on the microcatheter to the middle left anterior descending (LAD) or distal left circumflex (LCX) coronary artery under fluoroscopic guidance.

6. Coil implantation

1. Under fluoroscopic guidance, advance the microcatheter through the wire to the desired location where the coil implant should be deployed. In the case of LAD occlusion, place the coil distal to the first diagonal branch, and for LCX, place the coil distal to the first marginal branch.

NOTE: Proximal approaches (before the first diagonal or first marginal branches) have very low survival rates.

2. Remove the wire and select the coil.

NOTE: It is important to select the optimal coil size and length. A small or short coil may not position well in the vessel lumen and has a very high risk of distal migration due to contrast injections or spontaneous, resulting in smaller infarct size. A large or long coil may prolapse proximal to the vessel and produce a larger infarct than desired. The choice of the correct coil is especially important if non-detectable coils are used, as they cannot be removed. The optimal size is 1-2 mm larger than the lumen of the vessel to be embolized, and the length between 20-60 mm is usually adequate for 30-40-kg pigs.

3. Deliver the coil via microcatheter and slowly inject 5 mL of iodinated contrast medium under fluoroscopy to visualize the correct position of the coil.
4. Remove the microcatheter inside the guide catheter and place the guide in a side branch to perform control injections and to ensure access to the artery in case a second coil needs to be implanted.
5. Wait for the coil to thrombose and occlude the artery.
NOTE: When the artery is occluded, changes in the electrocardiogram can be observed. Another way to check complete arterial occlusion is to perform slow injections of iodinated contrast every 10 min (**Figure 1B, D**). If the artery does not occlude within 20-30 min, another coil implant may be required.

7. End of procedure

1. Once the artery is occluded, administer a continuous IV infusion of lidocaine (50-100 µg/kg/min) for at least 1 h to prevent arrhythmic episodes.
2. Perform an angiogram to ensure that there is no flow distal to the occlusion.
3. Remove the wire, microcatheter, and guiding catheter.
4. Remove the sheath and perform manual compression for 20 min.

8. Postoperative procedure and animal recovery

1. Monitor the animal until it is fully recovered, using ECG, rectal temperature, pulse oximetry, and capnography.
NOTE: In case of ventricular arrhythmias, administer a bolus of lidocaine (1.5-3.5 mg/kg).
2. Administer an IM injection of tulathromycin (2.5 mg/kg) as prophylactic postoperative antibiotic therapy. For

post-surgical analgesia, a transdermal fentanyl patch is administered before the surgical procedure (step 2.6).

3. Turn off the isoflurane and maintain mechanical ventilation until the animal begins to breathe spontaneously.
4. When the pig recovers the swallowing reflex, remove the endotracheal tube.**NOTE:** Check if the animal has a good SpO₂ (more than 95%) before and after extubation.
5. Transport the animal to an individual cage. Position the animal over a hot water blanket and cover it with a thermal drape to avoid post-surgical hypothermia.
NOTE: Do not return the pig to the company of other animals until it has fully recovered.
6. Monitor the animal until it has regained sufficient consciousness to maintain sternal recumbency.

9. Euthanasia method

1. Under previous sedation and anesthesia, as previously described, administer an IV sodium thiopental overdose (200 mg/kg).
2. Confirm cardiorespiratory arrest and death by monitoring vital signs (electrocardiogram, blood pressure, capnography).

Representative Results

MI survival rates and location

Fifty-seven pigs underwent coronary coil implantation in the LCX marginal branch (n = 25; 12 females and 13 males) or in the LAD between the first and the second diagonal branches (n = 32; 16 females and 16 males) of the coronary artery and were followed up for 30 days. The survival rate of animals submitted to an MI at the LCX marginal branch was 80% (n = 20). Three pigs died as a result of fatal complications

related to atrioventricular (AV) block and asystole before coil deployment, and 2 pigs died after ventricular fibrillation (VF) related to transmural MI after coil placement. The survival rate of animals submitted to MI at LAD was 72% (n = 23): 1 pig died due to an AV block and asystole after coil deployment and 8 animals after VF (5 after coil deployment, 2 at 12-48 h post-MI, and one 26 days post-MI). The survival rates differed between the LCX marginal branch (2-2.5 mm in diameter) and middle LAD (2.5-3 mm in diameter) MI, probably due to the larger infarct extension in the LAD model.

Magnetic resonance imaging (MRI) analysis was performed in all animals 30 days post-MI. **Figure 2** illustrates late gadolinium-enhanced MRI images of the LCX marginal branch (**Figure 2A,C**) and distal LAD (**Figure 2B,D**) infarct models. As depicted, coil deployment in the LCX marginal coronary artery affects the LV lateral wall, while the interventricular septum is the most affected area in distal LAD placement. These results were also confirmed after heart sectioning (**Figure 2E,F**).

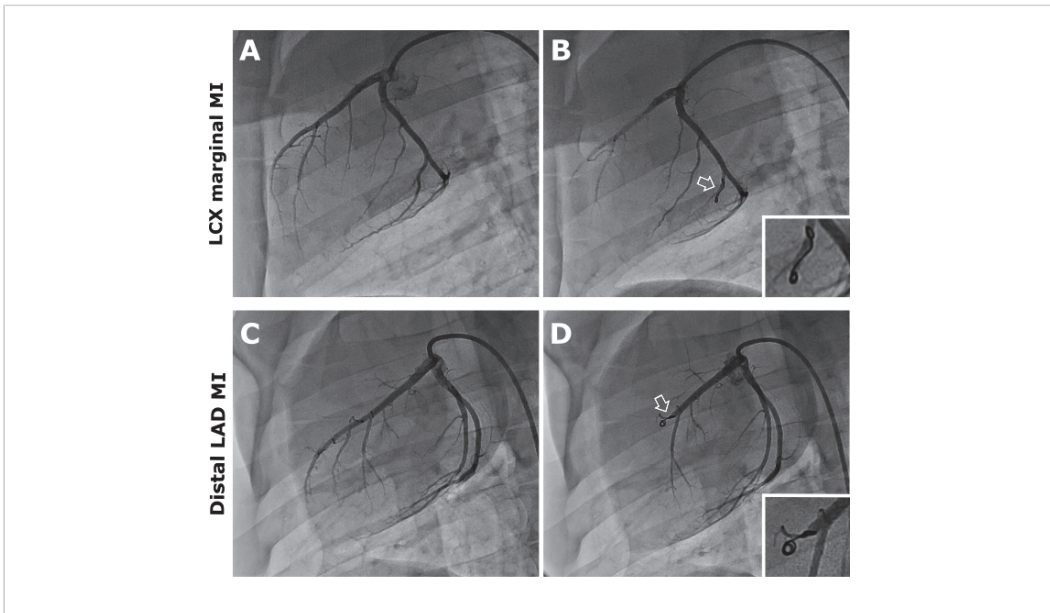


Figure 1: Coronary angiography, anteroposterior projection. Representative images of pre- (A,B) and post-coil (white arrows) deployment (C,D) in the LCX marginal branch and distal LAD coronary artery. [Please click here to view a larger version of this figure.](#)

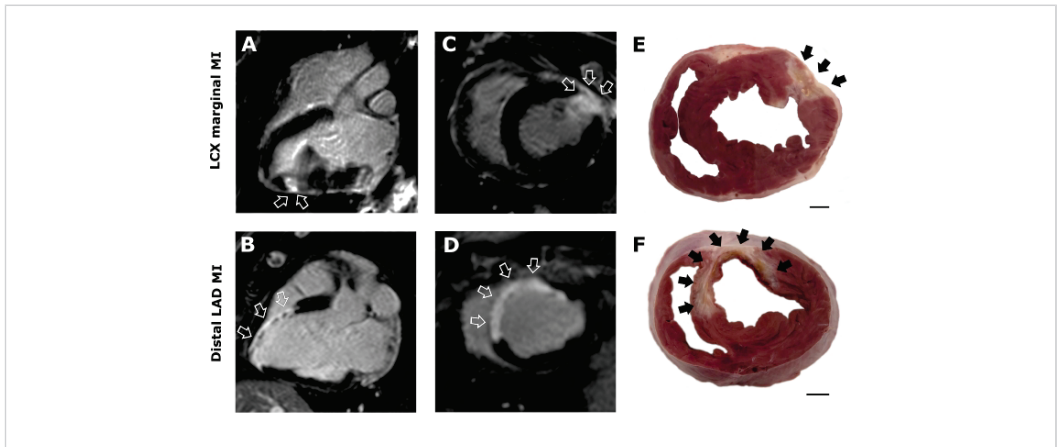


Figure 2: Magnetic resonance imaging and cardiac tissue sections. Representative T1 3-chamber (A,B) and short-axis (C,D) delayed enhancement images for LCX marginal and distal LAD infarction. Images reveal healthy (black) and infarcted (white) myocardium. Photographs of heart sections after LCX marginal (E) and distal LAD MI (F). Arrows indicate the location and extension of the infarcted area. Scale bar = 1 cm [Please click here to view a larger version of this figure.](#)

Discussion

A coil deployed in a coronary artery provides a reproducible and consistent pre-clinical non-reperused MI model in swine that can be used to develop and test new cardiovascular therapeutic strategies.

In our hands, mortality at follow-up was 19% related to complications of MI, mostly within the first 24 h of the procedure. All these deaths are related to the natural history of the non-reperused MI and were the primary outcomes of the study. One of the most critical steps in this protocol relies on the entry of the microcatheter into the coronary arteries. In some cases, microcatheter advancement caused a vagal reaction leading to severe hypotension, AV block, and finally asystole. Nevertheless, this can be avoided by administering an IV bolus of adrenaline (0.001 mg/kg) before advancing

the microcatheter. Another complication is the occurrence of malignant arrhythmias that can lead to VF. These episodes usually occur 30 min after MI instauration. We recommend delivering a bolus of lidocaine (1.5-3.5 mg/kg), atropine for bradycardia (0.01 mg/kg), noradrenaline perfusion (0.05-3 µg/kg/min) for mild or moderate hypotension, and adrenaline (0.03 mg/kg) for severe hypotension, electromechanical dissociation, AV block, or asystole. However, when a VF occurs, a 320J ventricular defibrillation has to be applied with a monophasic cardiac defibrillator and repeated until the animal recovers its cardiac rhythm. When several ventricular defibrillations are needed or asystole occurs, perform manual chest compressions (80-90 compressions/min), depressing the ribcage 4 inches, and connect the animal to the mechanical ventilator under 100% O₂.

Many other occlusion models have been described to simulate MI based on cessation of coronary flow by arterial ligation, an ameroid constrictor, or balloon inflation. However, a deployed coil sets off the coagulation cascade with thrombus formation that occludes the coronary artery. This mechanism simulates as closely as possible the pathophysiology of human MI, compared with other non-invasive techniques like balloon occlusion. Despite the fact that non-reperfused MI results in more extensive scarring, less viable myocardium, and a greater reduction in terms of cardiac function than ischemia-reperfusion models²⁷, it is more suitable for screening anti-inflammatory therapies, reverse cardiac remodeling, and gene or stem cell therapy for the treatment of cardiovascular disease²⁸.

Disclosures

The authors have nothing to disclose

Acknowledgments

We express our gratitude to the Center of Comparative Medicine and Bioimaging of Catalonia (CMCiB) and staff for their contribution to the animal model execution. This work was supported by the Instituto de Salud Carlos III (PI18/01227, PI18/00256, INT20/00052), the Sociedad Española de Cardiología, and the Generalitat de Catalunya [2017-SGR-483]. This work was also funded by the Red de Terapia Celular - TerCel [RD16/0011/0006] and CIBER Cardiovascular [CB16/11/00403] projects, as part of the Plan Nacional de I+D+I, and cofunded by the ISCIII-Subdirección General de Evaluación y el Fondo Europeo de Desarrollo Regional (FEDER). Dr. Fadeuilhe was supported by a grant from the Spanish Society of Cardiology (Madrid, Spain).

References

1. Khan, M. et al. Global epidemiology of ischemic heart disease: Results from the global burden of disease study. *Cureus*. **12** (7),e9349 (2020).
2. Bhatt, A. S., Ambrosy, A. P., Velazquez, E. J. Adverse remodeling and reverse remodeling after myocardial infarction. *Current Cardiology Reports*. **19** (8), 71 (2017).
3. Verma, A. et al. Prognostic implications of left ventricular mass and geometry following myocardial infarction: The VALIANT (VALsartan In Acute myocardial iNfarcTion) echocardiographic study. *JACC: Cardiovascular Imaging*. **1** (5), 582-591 (2008).
4. Konstam, M., Kramer, D., Patel, A., Maron, M., Udelson, J. Left ventricular remodeling in heart failure: current concepts in clinical significance and assessment. *JACC: Cardiovascular Imaging*. **4** (1), 98-108 (2011).
5. Srikanth, G., Prakash, P., Tripathy, N., Dikshit, M., Nityanand, S. Establishment of a rat model of myocardial infarction with a high survival rate: A suitable model for evaluation of efficacy of stem cell therapy. *Journal of Stem Cells and Regenerative Medicine*. **5** (1), 30 (2009).
6. Wu, Y., Yin, X., Wijaya, C., Huang, M. -H., McConnell, B. K. Acute myocardial infarction in rats. *Journal of Visualized Experiments: JoVE*. (48), e2464 (2011).
7. Takagawa, J. et al. Myocardial infarct size measurement in the mouse chronic infarction model: comparison of area- and length-based approaches. *Journal of Applied Physiology (Bethesda, MD.: 1985)*. **102** (6), 2104-2111 (2007).
8. Yang, F. et al. Myocardial infarction and cardiac remodelling in mice. *Experimental Physiology*. **87** (5), 547-555 (2002).

9. Suzuki, M., Asano, H., Tanaka, H., Usuda, S. Development and evaluation of a new canine myocardial infarction model using a closed-chest injection of thrombogenic material. *Japanese Circulation Journal*. **63** (11), 900-905 (1999).
10. Rienzo, M. et al. A total closed chest sheep model of cardiogenic shock by percutaneous intracoronary ethanol injection. *Scientific Reports*. **10** (1), 12417 (2020).
11. Spannbaauer, A. et al. Large animal models of heart failure with reduced ejection fraction (HFrEF). *Frontiers in Cardiovascular Medicine*. **6**, 117 (2019).
12. Liu, J., Li, X. Novel porcine models of myocardial ischemia/infarction - Technical progress, modified electrocardiograms validating, and future application. *Advances in Electrocardiograms - Clinical Applications*. 175-190, In Tech, Shanghai, China (2012).
13. Hughes, G. C., Post, M., Simons, M., Annex, B. Translational physiology: porcine models of human coronary artery disease: implications for pre-clinical trials of therapeutic angiogenesis. *Journal of Applied Physiology (Bethesda, MD. : 1985)*. **94** (5), 1689-1701 (2003).
14. Tsang, H. G. et al. Large animal models of cardiovascular disease. *Cell Biochemistry and Function*. **34** (3), 113 (2016).
15. Dixon, J. A., Spinale, F. G. Large animal models of heart failure. *Circulation: Heart Failure*. **2** (3), 262-271 (2009).
16. Gálvez-Montón, C. et al. Transposition of a pericardial-derived vascular adipose flap for myocardial salvage after infarct. *Cardiovascular Research*. **91** (4), 659-667 (2011).
17. Gálvez-Montón, C. et al. Comparison of two pre-clinical myocardial infarct models: coronary coil deployment versus surgical ligation. *Journal of Translational Medicine*. **12**, 137 (2014).
18. Domkowski, P. W., Hughes, G. C., Lowe, J. E. Ameroid constrictor versus hydraulic occluder: creation of hibernating myocardium. *The Annals of Thoracic Surgery*. **69** (6), 1984 (2000).
19. Tuzun, E. et al. Correlation of ischemic area and coronary flow with ameroid size in a porcine model. *Journal of Surgical Research*. **164** (1), 38-42 (2010).
20. Weismüller, P., Mayer, U., Richter, P., Heieck, F., Kochs, M., Hombach, V. Chemical ablation by subendocardial injection of ethanol via catheter - preliminary results in the pig heart. *European Heart Journal*. **12** (11), 1234-1239 (1991).
21. Haines, D., Verow, A., Sinusas, A., Whayne, J., DiMarco, J. Intracoronary ethanol ablation in swine: characterization of myocardial injury in target and remote vascular beds. *Journal of Cardiovascular Electrophysiology*. **5** (1), 41-49 (1994).
22. Li, K., Wagner, L., Moctezuma-Ramirez, A., Vela, D., Perin, E. A robust percutaneous myocardial infarction model in pigs and its effect on left ventricular function. *Journal of Cardiovascular Translational Research*. (2021).
23. Eldar, M., Ohad, D., Bor, A., Varda-Bloom, N., Swanson, D., Battler, A. A closed-chest pig model of sustained ventricular tachycardia. *Pacing and Clinical Electrophysiology: PACE*. **17** (10), 1603-1609 (1994).
24. Dib, N., Diethrich, E. B., Campbell, A., Gahremanpour, A., McGarry, M., Opie, S. R. A percutaneous swine model

- of myocardial infarction. *Journal of Pharmacological and Toxicological Methods*. **53** (3), 256-263 (2006).
25. National Research Council (US) Committee for the Update of the Guide for the Care and Use of Laboratory Animals. *Guide for the Care and Use of Laboratory Animals*. 8th ed. National Academies Press, Washington (DC), US (2011).
26. Carter, C., Girod, D., Hurwitz, R. Percutaneous cardiac catheterization of the neonate. *Pediatrics*. **55** (5), 662-665 (1975).
27. Koudstaal, S. et al. Myocardial infarction and functional outcome assessment in pigs. *Journal of Visualized Experiments : JoVE*. (86), e51269 (2014).
28. Kumar, M. et al. Animal models of myocardial infarction: Mainstay in clinical translation. *Regulatory Toxicology And Pharmacology : RTP*. **76**, 221-230 (2016).

ARTICLE 2

Antiarrhythmic and Anti-Inflammatory Effects of Sacubitril/Valsartan on Post-Myocardial Infarction Scar

Martínez-Falguera D, Aranyó J, Teis A, Ferrer-Curriu G, Monguió-Tortajada M, Fadeuilhe E, Rodríguez-Leor O, Díaz-Güemes I, Roura S, Villuendas R, Sarrias A, Bazan V, Delgado V, Bayes-Genis A, Bisbal F, Gálvez-Montón C.

Published in the *Circulation: Arrhythmia and Electrophysiology*. 2024 May;17(5):e012517. doi: 10.1161/CIRCEP.123.012517. Epub 2024 Apr 26. PMID: 38666379.

Impact factor (Journal Citation Reports): **9.1**

Quartil (Journal Citation Reports): **Q1 (D1)** CARDIAC& CARDIOVASCULAR SYSTEMS

Objective: This article is related to objective 2. This study aimed to evaluate the effects of early initiation of sacubitril/valsartan following MI on inflammation, fibrosis, and structural and electrophysiological myocardial properties in a translational porcine model of MI.

Highlights: Early initiation of sacubitril/valsartan after MI decreased acute systemic inflammatory response and promoted favourable scar remodelling by reducing Col I content in the scar, as well as decreasing total scar mass and border zone (BZ) mass, and the number and mass of BZ corridors. These effects contributed to a reduced risk of VT inducibility 30 days post-MI.

Circulation: Arrhythmia and Electrophysiology

ORIGINAL ARTICLE



Antiarrhythmic and Anti-Inflammatory Effects of Sacubitril/Valsartan on Post-Myocardial Infarction Scar

Daina Martínez-Falguera¹, MSc*; Júlia Aranyó¹, MD*; Albert Teis¹, MD, PhD; Gemma Ferrer-Curriu, MSc, PhD; Marta Monguío-Tortajada¹, MSc, PhD; Edgar Fadeuilhe¹, MD; Oriol Rodríguez-Leor¹, MD, PhD; Idoia Díaz-Güemes, DVM, PhD; Santiago Roura, MSc, PhD; Roger Villuendas¹, MD, PhD; Axel Sarrias¹, MD; Victor Bazan¹, MD, PhD; Victoria Delgado¹, MD, PhD; Antoni Bayes-Genis¹, Prof., MD, PhD; Felipe Bisbal¹, MD, PhD†; Carolina Gálvez-Montón¹, DVM, MSc, PhD†

BACKGROUND: Sacubitril/valsartan (Sac/Val) is superior to angiotensin-converting enzyme inhibitors in reducing the risk of heart failure hospitalization and cardiovascular death, but its mechanistic data on myocardial scar after myocardial infarction (MI) are lacking. The objective of this work was to assess the effects of Sac/Val on inflammation, fibrosis, electrophysiological properties, and ventricular tachycardia inducibility in post-MI scar remodeling in swine.

METHODS: After MI, 22 pigs were randomized to receive β -blocker (BB; control, n=8) or BB+Sac/Val (Sac/Val, n=9). The systemic immune response was monitored. Cardiac magnetic resonance data were acquired at 2-day and 29-day post MI to assess ventricular remodeling. Programmed electrical stimulation and high-density mapping were performed at 30-day post MI to assess ventricular tachycardia inducibility. Myocardial samples were collected for histological analysis.

RESULTS: Compared with BB, BB+Sac/Val reduced acute circulating leukocytes ($P=0.009$) and interleukin-12 levels ($P=0.024$) at 2-day post MI, decreased C-C chemokine receptor type 2 expression in monocytes ($P=0.047$) at 15-day post MI, and reduced scar mass ($P=0.046$) and border zone mass ($P=0.043$). It also lowered the number and mass of border zone corridors ($P=0.009$ and $P=0.026$, respectively), scar collagen I content ($P=0.049$), and collagen I/III ratio ($P=0.040$). Sac/Val reduced ventricular tachycardia inducibility ($P=0.034$) and the number of deceleration zones ($P=0.016$).

CONCLUSIONS: After MI, compared with BB, BB+Sac/Val was associated with reduced acute systemic inflammatory markers, reduced total scar and border zone mass on late gadolinium-enhanced magnetic resonance imaging, and lower ventricular tachycardia inducibility.

GRAPHIC ABSTRACT: A graphic abstract is available for this article.

Key Words: arrhythmias ■ cardiac ■ fibrosis ■ inflammation ■ myocardial infarction ■ sacubitril ■ valsartan

Coronary artery disease is the leading cause of heart failure (HF).¹ After myocardial infarction (MI), an intense inflammatory reaction is activated to remove dead cells and activate the replacement of necrotic tissue by a collagen-based scar.² Reparative fibrosis after

MI produces adverse cardiac remodeling and electrical disturbances within the scar, including conduction heterogeneity.³ This structural and electrical remodeling occurring in ischemic cardiomyopathy, together with neurohormonal, inflammatory, and electrolyte abnormalities

Correspondence to: Felipe Bisbal, MD, PhD, Germans Trias i Pujol University Hospital, Carretera del Canyet s/n, 08916 Badalona, Spain, Email f.bisbalvb@gmail.com; or Carolina Gálvez-Montón, DVM, MSc, PhD, Germans Trias i Pujol Research Institute, Camí de les Escoles s/n, 08916 Badalona, Spain, Email cgalvez@igtp.cat

*D. Martínez-Falguera and J. Aranyó contributed equally and are joint first authors.

†F. Bisbal and C. Gálvez-Montón are joint senior authors.

Supplemental Material is available at <https://www.ahajournals.org/doi/suppl/10.1161/CIRCEP.123.012517>.

For Sources of Funding and Disclosures, see page 301.

© 2024 American Heart Association, Inc.

Circulation: Arrhythmia and Electrophysiology is available at www.ahajournals.org/journal/circep

WHAT IS KNOWN?

- Sacubitril/valsartan is superior to angiotensin-converting enzyme inhibitors in reducing the risk of heart failure hospitalization and cardiovascular death; however, its effects on myocardial scar after myocardial infarction are lacking.
- The structural and electrical cardiac remodeling occurring in the post-myocardial infarction scenario are considered triggers of ventricular arrhythmias. Treatment targeting inflammatory pathways and tissue remodeling may have the potential to reduce ventricular arrhythmias and improve patient life expectancy.

WHAT THE STUDY ADDS

- The study highlights the benefits of early initiation of sacubitril/valsartan after myocardial infarction, which were associated with reduced acute systemic inflammatory markers, modified scar composition, total scar and border zone mass reduction, lower border zone corridor number and mass, and a 55% reduction in ventricular tachycardia inducibility.

Nonstandard Abbreviations and Acronyms

BZ	border zone
CMR	cardiac magnetic resonance
Col I	collagen I
Col III	collagen III
DZ	deceleration zone
HDM	high-density electroanatomic mapping
HF	heart failure
LGE	late gadolinium
LV	left ventricle
MI	myocardial infarction
RV	right ventricle
Sac/Val	sacubitril/valsartan
VA	ventricular arrhythmia

are considered an arrhythmogenic substrate of ventricular arrhythmias (VA). Treatment targeting tissue remodeling and neurohormonal/inflammatory pathways may have the potential to reduce VA and improve patient life expectancy.⁴

Sacubitril/valsartan (Sac/Val) is an inhibitor of neprilysin and the angiotensin II type-1 receptor and has been demonstrated to be superior to conventional angiotensin-converting enzyme (ACE) inhibitors in reducing the risk of HF hospitalization and cardiovascular death, including sudden cardiac death.^{5,6} The mechanism by which Sac/Val reduces mortality seems to be multifactorial and includes a reduction in left ventricular (LV) remodeling and myocardial fibrosis.^{7–9} Furthermore, previous studies

have suggested a possible antiarrhythmic effect of Sac/Val based on its association with decreased incidence of atrial fibrillation, appropriate shocks in patients with implantable cardioverter defibrillators, and sudden cardiac death.^{10–12}

The mechanisms by which Sac/Val modulates cardiac arrhythmias are unclear, and multiple mechanisms have been proposed. Sac/Val has been suggested to modulate cardiomyocyte electrophysiology at a molecular level, leading to increased conduction velocity, reduced effective refractory period, and suppressed ectopic activity.^{13–15} Reduced VA burden may also be driven by reduced LV remodeling and neurohormonal activity associated with Sac/Val.^{16,17} Specifically, post-MI modulation of the immune response that promotes the resolution of the acute inflammatory stage is a decisive step in managing fibrosis, limiting adverse cardiac remodeling, and, likely, reducing the incidence of VA.^{18,19}

The aim of the present study was to assess the effects of Sac/Val in a translational porcine model of nonvascularized MI by evaluating scar remodeling in terms of inflammation, fibrosis, electrophysiological properties, and inducibility to VA.

METHODS

The authors declare that all supporting data are available within the article and its online supplementary files.

Study Design

This was a randomized, double-blinded, controlled study including 22 crossbreed Landrace × Large White pigs (30–35 kg, 50% females) with nonrevascularized MI. After MI, animals were randomly allocated to receive treatment with β -blocker (BB) and Sac/Val (Sac/Val group) or BB only (control group) for 30 days. A diagram of the study design is shown in Figure 1. Medications were administered orally from 1 day post MI until the end of the study (30 days post MI) as follows: bisoprolol 0.04 mg/kg daily and Sac/Val 49/51 mg twice a day.

Bisoprolol is a highly selective beta-1 adrenergic receptor blocker, devoid of intrinsic sympathomimetic activity and having no relevant membrane-stabilizing effect. Bisoprolol has a bioavailability of \approx 90% after oral administration, of which 50% is transformed in the liver and the other 50% is eliminated directly by the kidneys. Sac/Val exhibits the mechanism of action of an angiotensin receptor neprilysin inhibitor by simultaneously inhibiting neprilysin (neutral endopeptidase 24.11) via LBQ657 and by blocking the angiotensin II type-1 receptor via valsartan. Sacubitril was predominantly excreted in feces in mice, rats, and dogs, whereas urinary excretion was minor. In monkeys and humans, sacubitril- or Sac/Val is excreted to a greater extent in urine.

Swine MI Model

Animals underwent a nonreperfused anterior MI procedure as previously described.²⁰ MI was induced by percutaneous

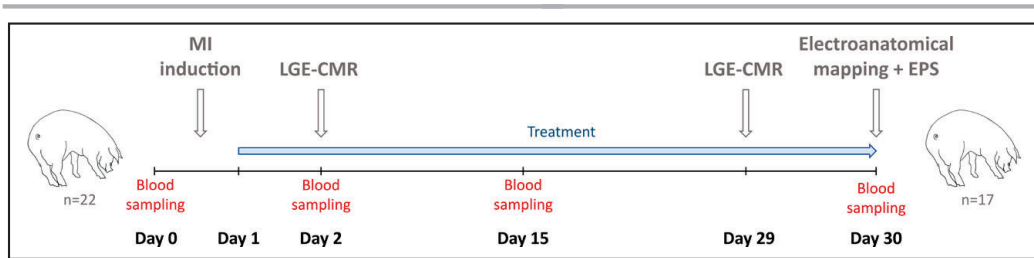


Figure 1. Chronogram and workflow of the study.

EPS indicates electrophysiologic study; LGE-CMR, late gadolinium-enhanced cardiac magnetic resonance; and MI, myocardial infarction.

selective coil embolization (VortX-18 Diamond 3-mm/3.3-mm coil; Boston Scientific/Target, Natick, MA) of the left anterior descending coronary artery after the first diagonal branch, under general anesthesia. Complete thrombotic occlusion was confirmed by persistent ST-segment elevation on the ECG and by repeating the coronary angiography 10 minutes after coil implantation (Thrombolysis in Myocardial Infarction flow score of 0). Serum cardiac troponin I levels were analyzed at baseline and 2 hours after MI induction to evaluate acute myocardial damage. Animals recovered and survived for 1 month following the MI induction procedure.

Systemic Immune Response

To study the evolution of the systemic immune response after MI, blood samples were collected at baseline, 2 (the first peak of inflammation), 15, and 30 days post MI. Aliquots (100 μ L) were stained with CD172a-PE (1:100, clone 74-22-15; Southern Biotech) for monocyte detection and CCR2/CD192-PE-Vio770 (1:20, clone REA624; Miltenyi Biotech), CD163 (1:100, clone EDHu-1; Novus Biologicals) and CD73 (1:100, polyclonal; Novus Biologicals) to distinguish different populations of activated monocytes, with fluorescein isothiocyanate and Cy5 (1:500; Jackson ImmunoResearch) as secondary antibodies. In parallel, lymphocyte, monocyte, and neutrophil absolute numbers were quantified in 100 μ L of unstained whole blood mixed with 20 μ L of Perfect Count Microspheres (Cytognos). Samples were acquired in an LSR Fortessa flow cytometer (BD Biosciences) and analyzed using FlowJo (v10.8.1, BD). The gating strategy is detailed in Figure S1. For circulating inflammatory cytokine response analysis, serum levels of granulocyte-macrophage colony-stimulating factor, interferon- γ , interleukin (IL)-1 α , IL-1 β , IL-1ra, IL-2, IL-4, IL-6, IL-8, IL-10, IL-12, IL-18, and TNF- α (tumor necrosis factor- α) were measured using the Milliplex MAP Porcine Cytokine/Chemokine Magnetic Bead Kit (PCYTMG-23K-13PX; Millipore) in a Luminex 200 instrument (Luminex Corporation).

Noninvasive Tissue Characterization

Two late gadolinium-enhanced cardiac magnetic resonance (LGE-CMR) scans were performed in all animals at 2 and 29 days post MI. Cine and LGE-CMR data were acquired with a 3T MRI scanner (Canon Vantage Galan 3T, Canon Medical Systems) under general anesthesia, apnea, and continuous electrocardiographic gating. The image acquisition protocol is summarized in the Supplemental Methods. LV ejection

fraction, LV end-diastolic volume, LV end-systolic volume, LV stroke volume, LV mass, right ventricular (RV) ejection fraction, RV end-diastolic volume, RV end-systolic volume, and RV stroke volume were measured. Indexed volumes were also analyzed. Scar analysis was performed offline using the ADAS 3-dimensional software (Galgo Medical S.L.). The standard pixel intensity thresholds (>60%, 40%–60%, and <40% of the maximum pixel intensity) were used to define dense, heterogeneous/border zone (BZ), and healthy tissue, respectively. LV scar mass, BZ corridors, and scar transmuralities were automatically measured using LGE data. As described elsewhere, a BZ corridor was defined as a corridor of BZ connecting 2 areas of healthy myocardium and surrounded by dense scars (Figure S2).²¹ The number and mass of LGE-CMR-detected BZ corridors were quantified. An LV transmural study was performed using an automatic analysis in which total, dense, and BZ endocardial and epicardial scars (mean of total, dense, and BZ scar in layers 10%–50% and 50% to 90%, respectively) were displayed (Figure S3). LGE-CMR analysis was performed by an expert investigator blinded to the randomization.

Invasive Tissue Characterization

Animals underwent invasive endocardial and epicardial high-density electroanatomic mapping (HDM) at 30 days post MI using the Rhythmia HDx 3-dimensional mapping system and a 64-pole basket catheter (Intellimap Orion, Boston Scientific, MA). Retrograde aortic and sub-xiphoid accesses were used for endocardial and epicardial mapping, respectively. HDM was performed at a paced cycle length of 400 ms with 1 extra stimulus 20 ms above the ventricular effective refractory period. The filling threshold was ≤ 2 mm in regions of low bipolar voltage and ≤ 10 mm elsewhere; interpolation between points ≤ 2 mm apart was required in all cases. Bipolar electrograms were recorded with band-pass filters of 30 to 300 Hz.

All electroanatomic maps were analyzed offline. Standard peak-to-peak bipolar voltage thresholds were used (0.5 and 1.5 mV) to define infarct core, BZ, and healthy tissue. Infarct core and BZ voltage regions were quantified using the Rhythmia mapping system's surface area measurement tool. The Lumipoint module (Rhythmia, Boston Scientific) was used to highlight and re-annotate slow and delayed conduction, including the number of deceleration zones (DZs), as previously described.²² Local abnormal ventricular activities and late potentials, defined based on activation timing with respect to the QRS complex, were considered pathological electrograms and were annotated.

VT Burden and Inducibility

At 30 days post MI, after HDM, induction of VT was attempted. Standard ventricular extra-stimulation at a paced cycle length of 400 to 500 ms with 1 to 5 extrastimuli down to the ventricular effective refractory period was performed. Up to S5 were allowed to increase the likelihood of VT induction based on previous studies.²³ Positive electrophysiologic study was considered with the induction of sustained monomorphic VTs (considered scar-related reentrant tachycardias). Polymorphic VT and ventricular fibrillation, as well as noninducibility, were considered negative electrophysiologic study.

In addition, following MI induction, continuous ECG-Holter monitoring was performed for 2 weeks in a subgroup of 10 animals (5 per group).

Myocardial Tissue Collection

Animals were euthanized with an overdose of pentobarbital sodium (200 mg/kg, IV; Dolethal, Vetoquinol E.V.S.A.) after 30 days of follow-up. After mid-sternotomy, hearts were excised and washed in buffered saline solution, then sliced transversely into three 1 to 1.5 cm sections from the coil location to the apex and digitally photographed. Next, tissue transverse samples from the scar (infarct core) and the septum noninfarcted wall (remote zone) of each section were obtained, fixed in 10% buffered formalin, and embedded in paraffin; or frozen in an optimal cutting temperature compound; or snap-frozen in liquid nitrogen for histopathologic, immunohistochemical, and transcriptomic evaluation, respectively.

Histopathologic Analysis

Masson's trichrome and modified Movat's pentachrome were used to stain 4- μ m-thick paraffin sections of infarct core samples. Picrosirius red staining of the infarct core and the remote zone was used to quantify the collagen volume fraction, collagen I (Col I), collagen III (Col III), and the Col I/III ratio. At least 4 random fields per sample section were captured under polarized light with a DMI6000B microscopy (Leica) and analyzed using Image-Pro Plus software (v.6.2.1; Media Cybernetics, Inc).

Immunohistochemical Analysis

Vascular density in the infarct core was assessed by staining 10- μ m optimal cutting temperature-embedded tissue cryosections with biotinylated *Griffonia simplicifolia* Lectin I IsolectinB4 (IsoB4, 1:25; Vector Labs) and Streptavidin-Alexa568 (1:500; Invitrogen). Immune infiltration in the infarct core was analyzed by staining for CD3 (1:100, clone CD3-12; BioRad), CD25 (1:100, clone K231.3B2; BioRad), for total and activated lymphocytes, respectively, and CD163 (1:100; polyclonal, Bioss) for macrophage detection. Alexa Fluor 488, 647, and Cy3 (1:500; Jackson ImmunoResearch) were used as secondary antibodies, and DAPI (4',6-diamidino-2-phenylindole) was used to counterstain nuclei. Four representative fields per section were acquired with an Axio-Observer Z1 confocal microscope (Zeiss). Vascular density was measured by measuring the IsoB4+ area with Image-Pro Plus software. Total CD3+, CD25+, CD25+/CD3+,

and CD163+ cell quantification was performed by 2 independent investigators.

Transcriptomic Evaluation

Frozen tissue samples from the infarct core (78.21 \pm 15.92 mg) and remote area (77.00 \pm 11.28 mg) were mechanically homogenized using a TissueRuptor (Qiagen) in a cold TriPure Isolation reagent (Merck) to isolate RNA, DNA, and protein fractions. After analyzing the concentration and quality of RNA, 10 μ g of RNA were retrotranscribed to cDNA using the High-Capacity cDNA Reverse Transcription Kit (Applied Biosystems). The expression levels of *IL-10*, *TNF- α* , *CCL2*, *TGF- β 1*, *TGF- β 3*, *LRP1*, *MMP2*, *MMP9*, *TIMP1*, and *PGK1* were analyzed starting from 2 μ L of cDNA using the TaqMan Fast Advances Master Mix (Thermo Fisher Scientific) and the corresponding porcine TaqMan FAM-MGB probes (Table S1). Data were evaluated with a LightCycler 480 real-time polymerase chain reaction system (Roche). The expression of all genes was determined using the 2^{- Δ Ct} method²⁴ and normalized to endogenous *PGK1* gene expression.

Sex Differences

All the above-mentioned analyses were also evaluated based on the sex of the animals to discern if males and females differed. All information about sex differences is reported in the Supplemental Results.

Ethical Implications

This study was approved by the Animal Experimentation Unit Ethical Committee of the Germans Trias i Pujol Health Research Institute and Government Authorities (Generalitat de Catalunya; Code: 11208) and complies with all guidelines concerning the use of animals in research and teaching as defined by the Guide for the Care and Use of Laboratory Animals.

Statistical Analysis

Statistical analyses were performed with SPSS (v.19.0.1; SPSS, Inc, Chicago, IL) and Graphpad Prism (v.9.3.1) software. The appropriate statistical test for each dataset is summarized in the Supplemental Methods. Values of $P < 0.05$ were considered significant.

RESULTS

Study Population and MI Induction

Twenty-two animals (34.2 \pm 2.3 kg, 50% females) underwent MI induction, with an acute survival rate of 77% (n=17; 9 females and 8 males). The causes of death included atrioventricular block and asystole after coil deployment (n=1) and ventricular fibrillation (n=4; 3 immediately after coil deployment and one 12 hours post MI). The surviving animals were allocated to the control (n=8) or Sac/Val group (n=9). Myocardial damage according to circulating serum cardiac troponin I levels were similar in both groups (control group: +821.1 \pm 1314 pg/mL versus Sac/Val group: +3821 \pm 7998 pg/mL; $P=0.743$; Mann-Whitney *U* test).

Systemic and Myocardial Immune Response

Sac/Val animals, compared with controls, showed less systemic immune response after MI by (1) a reduction in circulating leukocytes at 2 days post MI (Sac/Val group baseline: 13818.97±2596.56 cells/μL versus 2d: 10897.20±2531.50 cells/μL; control group baseline: 12722.10±2818.73 cells/μL versus 2d: 12355.58±5478.23 cells/μL; *P*=0.009) mainly through a decrease in neutrophil count (Sac/Val group baseline: 6543.70±2134.75 cells/μL versus 2d: 3990.80±1363.24 cells/μL; control group baseline: 5582.78±1950.30 cells/μL versus 2d: 4972.16±3471.32 cells/μL; *P*=0.014) with no acute increase in neutrophil-recruitment interleukins (IL-6 and IL-8; Figure 2A; Figure S4); (2) reducing the expression of the mobilizing receptor CCR2 in circulating monocytes at 15 days post MI (Sac/Val group baseline: 57.51±34.80 MFI (Mean Fluorescence Intensity) versus 15d: 31.81±25.91 MFI; control group baseline: 46.07±20.47 MFI versus 15d: 4316±3386 MFI; *P*=0.047; Figure 2A); and (3) decreasing IL-12 pro-inflammatory cytokine levels at 2 days post MI (Sac/Val group baseline: 718.84±241.98 pg/mL versus 2d: 470.63±93.74 pg/mL; control group baseline: 672.51±124.11 pg/mL versus 2d: 579.14±174.60 pg/mL; *P*=0.024; Figure 2B). Notably, Sac/Val treatment

maintained the anti-inflammatory *IL-10* levels that decreased over time in the control group (Sac/Val group 2d: 73.61±70.00 pg/mL versus 30d: 108.27±152.85 pg/mL; control group 2d: 262.97±203.49 pg/mL versus 30d: 52.23±21.17 pg/mL; *P*=0.072; Figure 2B). Of note, no differences were found in the monocyte expression of *CD73* or *CD163* (data not shown). Gene expression levels of *IL-10*, *TNF-α*, and *CCL2* were similar in the 2 groups at 30 days post MI (Table S2).

At the tissue level, no differences in infarct core T lymphocyte (CD3⁺), activated T lymphocyte (CD25⁺/CD3⁺), or macrophage counts were detected.

Cardiac Magnetic Resonance Imaging

LGE-CMR was performed in 100% (control n=8; Sac/Val n=9) and 94% (control n=7; Sac/Val n=9) of animals 2 and 29 days post MI, respectively.

An extensive scar was detected in all animals at the 2-day LGE-CMR, without significant differences in total scar mass, BZ, or core between groups. No baseline differences were found regarding indexed LV end-diastolic volume, indexed LV end-systolic volume, indexed LV mass, indexed RV end-diastolic volume, indexed RV end-systolic volume, LV ejection fraction, and RV ejection fraction, or in the number and mass of the BZ corridors (Table 1).

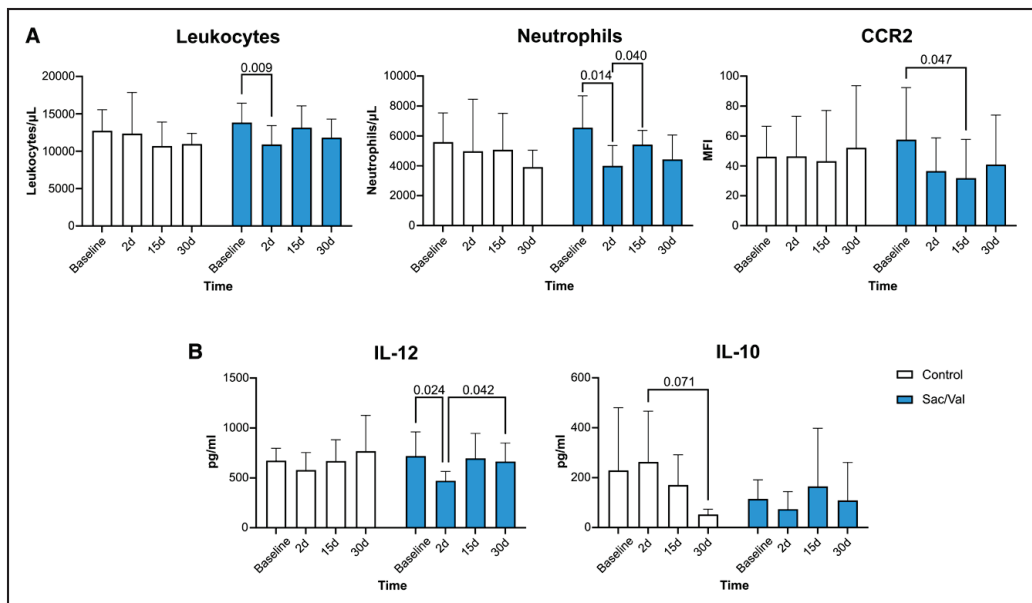


Figure 2. Systemic immune response analyses.

A, Total number of leukocytes, neutrophils, and CCR2 expression of monocytes (CD172a⁺) at baseline and at 2, 15, and 30 days of follow-up. **B**, Serum levels of IL (interleukin)-12 and IL-10 at baseline and at 2, 15, and 30 days post myocardial infarction. Data are presented as mean±SD. Statistical significance indicated according to modified Tukey post hoc test from a repeated-measures ANOVA. MFI, meal fluorescence intensity; and Sac/Val, sacubitril/valsartan.

Downloaded from <http://ahajournals.org> by on May 22, 2024

Table 1. Cardiac Late Gadolinium-Enhanced Cardiac Magnetic Resonance Imaging Data

	Control		Sac/Val		P value
	Baseline, n=8	Follow-up, n=7	Baseline, n=9	Follow-up, n=9	
LVEF, %	33.6±5.3	36.2±8.1	35.7±11.7	42.2±8.0	0.487
iLVEDV, mL/m ²	134.1±23.5	124.0±26.5	135.5±21.8	131.9±22.4	0.523
iLVESV, mL/m ²	88.4±13.9	79.5±20.1	87.4±23.3	76.3±16.1	0.781
iLV mass, g/m ²	84.2±4.9	82.1±5.7	91.2±10.9	82.0±8.8	0.219
RVEF, %	40.5±7.5	50.1±8.2	47.8±7.7	57.0±7.6	0.949
iRVEDV, mL/m ²	104.6±17.3	83.2±15.0	102.2±20.6	93.4±21.4	0.175
iRVESV, mL/m ²	62.2±13.0	41.1±7.6	54.6±18.5	40.3±11.8	0.326
Total scar mass, g	9.9 [4.1–12.5]	10.1 [7.8–14.0]	10.8 [9.4–15.5]	6.6 [3.5–9.1]	0.046*
Dense scar mass, g	4.0 [2.0–6.7]	4.1 [0.5–5.6]	6.6 [4.5–7.9]	5.2 [3.5–5.9]	0.210
BZ scar mass, g	4.1 [2.1–6.7]	4.8 [3.7–6.7]	4.2 [2.3–6.4]	2.8 [1.4–3.7]	0.043*
No. of corridors	1 [0–2]	2 [2–3]	2 [1–3]	0 [0–2]	0.009*
Mass of corridors, g	1.1 [0.3–2.3]	1.5 [0.9–2.8]	1.1 [0.8–1.3]	0.4 [0–1.2]	0.026*
Total epicardial scar, cm ²	26.2 [18.2–33.1]	28.8 [18.8–36.1]	25.9 [11.3–32.6]	19.7 [6.7–32.0]	0.007*
Epicardial dense scar, cm ²	14.3 [5.8–16.1]	16.9 [11.6–20.3]	13.6 [2.7–16.2]	11.1 [3.0–17.5]	0.093
Epicardial BZ scar, cm ²	13.3 [7.5–18.8]	8.1 [4.9–8.9]	11.4 [6.6–16.8]	4.3 [3.7–6.2]	0.043*

Late gadolinium-enhanced cardiac magnetic resonance data at baseline (2 days post myocardial infarction) and follow-up (29 days post myocardial infarction) for control and Sac/Val animals. Statistical significance indicated according to repeated-measures ANOVA. Data are presented as mean±SD or median [Q25–Q75] as appropriate. BZ indicates border zone; iLV mass, indexed left ventricular mass; iLVEDV, indexed left ventricular end-diastolic volume; iLVESV, indexed left ventricular end-systolic volume; iRVEDV, indexed right ventricular end-diastolic volume; iRVESV, indexed right ventricular end-systolic volume; LVEF, left ventricular ejection fraction; RVEF, right ventricular ejection fraction; and Sac/Val, sacubitril/valsartan.

*Indicates significant P values (<0.05).

At 29-day follow-up, the Sac/Val group in comparison with the controls showed a significant reduction in total scar and BZ mass on LGE-CMR (6.6 [3.5–9.1] versus 10.1 [7.8–14.0] g, $P=0.046$, and 2.8 [1.4–3.7] versus 4.8 [3.7–6.7] g, respectively, $P=0.043$), without differences in dense scar mass. Animals treated with Sac/Val exhibited fewer and smaller BZ corridors as compared with controls (number of corridors 0 [0–2] versus 2 [2–3], $P=0.009$; corridor mass 0.4 [0–1.2] versus 1.5 [0.9–2.8] g, respectively, $P=0.026$; Figure 3), and a significant reduction in the number and mass of BZ corridors over time (differences between baseline and follow-up LGE-CMR for the Sac/Val group and control group: -1 [-2 to 0] versus 1 [0 – 2] corridors, respectively, $P=0.020$, and -0.9 [-1.3 to -0.2] versus 0.4 [0 – 0.8] g, respectively, $P=0.050$), whereas the control group remained unchanged. At follow-up, no differences were found in LV ejection fraction, RV ejection fraction, indexed LV end-diastolic volume, indexed LV end-systolic volume, or indexed LV mass. However, the control group showed larger transmural thickness of the scar as compared with the Sac/Val animals, with a larger total epicardial scar (28.8 [18.8–36.1] versus 19.7 [6.7–32.0] cm², respectively; $P=0.007$) and a larger epicardial BZ scar mass (8.1 [4.9–8.9] versus 4.3 [3.7–6.2] cm², respectively; $P=0.043$) without differences in epicardial dense scar mass (16.9 [11.6–20.3] versus 11.1 [3.0–17.5] cm², respectively; $P=0.093$).

Spontaneous and Induced VT

No sustained VT was detected during the 15-day post-MI monitoring period, with similar nonsustained VT episodes and mean heart rate among control and Sac/Val animals (117.6±6.7 versus 117.0±7.9 bpm, respectively; $P=0.928$). One sudden death occurred in the control group at 26 days post MI, probably due to malignant arrhythmia, not monitored.

VT induction with programmed electrical stimulation was significantly lower in the Sac/Val group than in the controls (44% [$n=4$] versus 100% [$n=7$], respectively; $P=0.034$), representing a relative risk reduction of 55%.

Regardless of the assigned group, induction of VT was associated with LGE-CMR-detected BZ scar mass (odds ratio, 2.5 [95% CI, 1.1–5.6]; $P=0.04$) and number of BZ corridors (odds ratio, 5.1 [95% CI, 1.5–16.9]; $P=0.008$), as well as with the presence of DZ in high-density activation mapping (odds ratio, 3.0 [95% CI, 1.1–8.4]; $P=0.035$).

Electroanatomic High-Density Mapping

Sixteen animals (94%) completed the 30-day survival period and underwent HDM mapping. HDM was performed endocardially in 16 animals (2177±561 data points) and epicardially in 13 animals (control: $n=5$, and Sac/Val: $n=8$; 5098±1431 points). Table 2 summarizes the HDM data. There were no differences between groups about the sizes of the total endocardial scar, core,

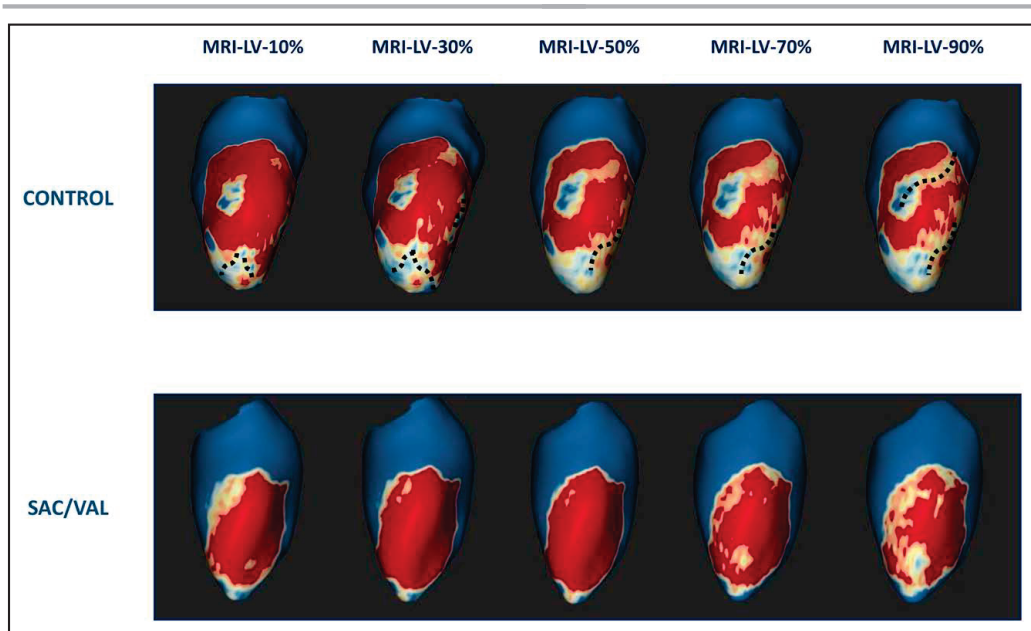


Figure 3. Noninvasive tissue characterization.

Late gadolinium-enhanced cardiac magnetic resonance at 29 days post myocardial infarction of Sac/Val (**bottom**) and control (**top**) animals. Extent of myocardial scar in successive layers of myocardial wall thickness from the endocardium (LV 10%) to the epicardium (LV 90%). The animal receiving Sac/Val exhibited extensive homogeneous scarring with a predominant dense (core) component without BZ corridors. The animal in the control group showed a similarly extensive anterior scar, but with larger heterogeneous/BZ components and multiple BZ corridors. BZ indicates border zone; LV, left ventricle; MRI, magnetic resonance imaging; and Sac/Val, sacubitril/valsartan.

BZ areas, or epicardial scar. All animals (94%) exhibited local abnormal ventricular electrograms in the endocardium without differences between groups. However, the Sac/Val group compared with controls exhibited a trend toward fewer pathological abnormal epicardial electrograms (50% versus 100% of the animals, respectively; $P=0.068$) and fewer DZs (1 [0–1] versus 3 [2–3] DZ per animal, respectively; $P=0.016$; Figure 4).

Myocardial Fibrosis and Vascular Density

Macroscopically, myocardial scars in the controls appeared more fibrotic and denser than those in the Sac/Val group. Myocardial calcium deposits were detected in all control animals but only in 44% ($n=4$) of the Sac/Val animals ($P=0.026$, Fisher's exact test; Figure 5A). Masson's trichrome (Figure 5B and 5C, left) and modified Movat's pentachrome (Figure 5C, right) staining displayed more dense fibrotic deposition in the infarct core of controls as compared with the Sac/Val group. Picosirius red analysis revealed that the Sac/Val group in comparison with the controls had significant reductions in both Col I content ($5.54\pm 4.92\%$ versus $15.01\pm 9.85\%$, respectively; $P=0.049$) and Col I/III ratio in the infarct core (0.28 ± 0.18 versus 0.94 ± 0.66 ,

respectively; $P=0.040$), with no differences in collagen volume fraction or Col III (Figure 5D and 5E). Collagen volume fraction, Col I, Col III, and the Col I/III ratio in the remote zone were similar between groups.

Sac/Val-treated animals did not differ from controls in their expression levels of the fibrotic marker genes *TGF- β 1*, *TGF- β 3*, *LRP1*, *MMP2*, *MMP9*, and *TIMP1* in the infarct and remote zones (Table S2). Vascular density at the infarct core was similar in both groups.

DISCUSSION

The main findings of the study were that Sac/Val (1) decreased the acute systemic inflammatory response post MI, (2) promoted favorable scar remodeling, reducing the total scar and BZ mass as well as the number and mass of BZ corridors, (3) reduced the risk of VT inducibility 30 days post MI, and (4) modulated the composition of the fibrotic scar.

Inflammatory Response Modulation

Cardiac repair after MI is initiated by a severe inflammatory response and immune cell infiltration, followed by a reparative phase with resolution of inflammation, scar formation,

Table 2. Invasive High-Density Mapping and VT Inducibility Parameters

	Control, n=7	Sac/Val, n=9	P value
Endocardial area ≤ 1.5 mV, cm ²	22.3 [10.7–24.4]	20.2 [7.6–25.8]	0.815
Endocardial area ≤ 0.5 mV, cm ²	18.9 [14.7–19.8]	13.5 [5.1–20.5]	0.427
Endocardial area 0.5–1.5 mV, cm ²	3.9 [3.5–5.9]	2.2 [1.9–5.8]	0.185
Endocardial abnormal EGMs, n (%)	7 (100)	8 (89)	0.861
Epicardial area ≤ 0.5 mV, cm ²	8.3 [6.6–8.7]	6.1 [0.9–8.3]	0.173
Epicardial abnormal EGMs, n (%)	5 (100)	4 (50)	0.068
DZ (median [IQR])	3 [2–3]	1 [0–1]	0.016*
VT inducibility, n (%)	7 (100)	4 (44)	0.034*
VT inducibility+CV death, n (%)	8 (100)	4 (44)	0.015*

Statistical significance indicated according to Mann-Whitney *U* test and Fisher's exact test for numerical and categorical variables, respectively. Data are presented as median [Q25–Q75]. CV indicates cardiovascular; DZ, deceleration zone; EGMs, electrograms; IQR, interquartile range; Sac/Val, sacubitril/valsartan; and VT, ventricular tachycardia.

*Indicates significant *P* values (<0.05).

and collagen deposition. The inflammatory response and subsequent ventricular remodeling are directly involved in the development of post-MI VA.²⁵ In our study, the early increase of inflammatory markers early after MI evolution was not observed in the control group; the anti-inflammatory effects of bisoprolol in this group might have driven this attenuation.²⁶ However, compared with BB treatment alone, the combination of BB+Sac/Val reduced the post-MI acute inflammatory systemic response by decreasing the number of circulating leukocytes, specifically neutrophils. In the first post-MI hours, neutrophils are recruited into the myocardium to clear up dead cells and cellular debris.¹⁸ During this process, an inflammatory peak is generated, which leads to an increase in the recruitment of several types of immune cells. These include circulating activated CCR2⁺ monocytes, which have been associated with adverse remodeling and cardiac dysfunction.^{27,28} Notably, Sac/Val treatment reduced CCR2 expression in circulating monocytes at 15 days post MI, indicating that fewer activated monocytes would be recruited to the heart. We also observed a reduction in IL-12, a proinflammatory interleukin involved in macrophage activation.^{18,29} Finally, the sustained circulating levels of anti-inflammatory IL-10 in contrast to their decline in controls suggest that macrophage/monocyte activation was inhibited in Sac/Val animals.³⁰

Arrhythmic Risk

In this study, early treatment with Sac/Val reduced the risk of induced VA 30 days post MI by 55%. This finding is consistent with previous studies in patients with

HF with implantable cardioverter defibrillator which have shown that Sac/Val reduces cardiovascular mortality, sudden cardiac death, and VA.¹² The mechanisms underlying this effect have been attributed to reverse remodeling but remain mostly unclear. Our findings suggest that a reduced risk of VA may be driven by favorable tissue and electrophysiological remodeling caused by an improved inflammatory profile after MI.

Favorable Scar Remodeling

Treatment with Sac/Val promoted favorable scar remodeling, reducing the total scar and BZ mass assessed by LGE-CMR as well as the number and mass of BZ corridors.

The mass of the BZ and the amount and mass of BZ corridors have been strongly associated with VA and were reduced in the Sac/Val group.^{31,32} In fact, efforts are being made to integrate these variables into prognostic algorithms.^{33–35} In our study, the observed reductions in BZ mass and corridors in the Sac/Val group could potentially explain the reduction in inducible VT, as animals with inducible VT had greater BZ mass and BZ corridor numbers, regardless of the treatment received. Reduction of BZ mass was only observed in LGE-CMR, not in electroanatomic mapping. The use of standard voltage thresholds (1.5 and 0.5 mV) to define the BZ/core area could potentially explain the discordance.

There is evidence that scar composition and scar transmural depth may determine the electrophysiological properties of the scar. We found that Sac/Val modulated scar composition by reducing total scar mass, transmural depth, and heterogeneity (BZ mass), which is known to be an independent predictor of VA and mortality.^{34,35} In terms of electrophysiological properties, Sac/Val animals had fewer conduction abnormalities, as evidenced by having fewer DZs and abnormal epicardial electrograms compared with controls.

LV remodeling occurring after MI is characterized by progressive dilatation and contractile dysfunction and is an important determinant of poor outcomes, including VA and cardiovascular death.³⁶ The effect of Sac/Val on the remodeling process may potentially affect the arrhythmic profile. Previous clinical studies showed a possible effect of Sac/Val on LV reverse remodeling when assessed by echocardiographic parameters (LV ejection fraction, LV volumes, and E/E' ratio) and N-terminal pro-B-type natriuretic peptide quantification.^{8,9} Interestingly, patients with HF who manifested more LV reverse remodeling under Sac/Val treatment had a more pronounced reduction in VA in terms of premature ventricular contraction burden and nonsustained VT episodes in comparison with those without reverse remodeling.³⁷ However, recent work designed to determine whether Sac/Val is superior to ACE inhibitors in the postacute MI scenario challenged these

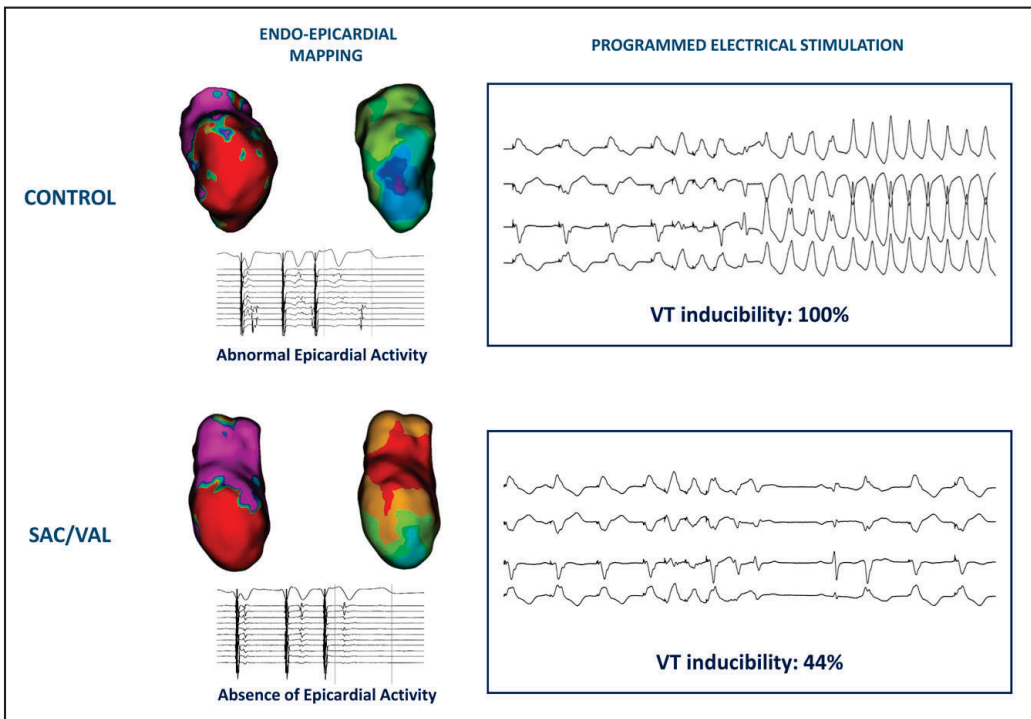


Figure 4. Electrophysiological substrate 30 days post myocardial infarction.

High-density mapping showed extensive low voltage areas in both groups. However, the Sac/Val group exhibited smaller deceleration zone and less abnormal epicardial electrograms than did the controls, with a reduced risk of VT inducibility. Sac/Val indicates sacubitril/valsartan; and VT, ventricular tachycardia.

observations, showing no benefit in terms of cardiovascular outcomes (cardiovascular death or HF episodes) and echocardiographic remodeling parameters.³⁸ In our study, we observed no between-group differences in LV remodeling as assessed by LGE-CMR. We hypothesize that treatment with Sac/Val did not affect LV volumes and ejection fraction at short follow-up, likely due to the extensive, nonrevascularized scars at baseline. In contrast, Sac/Val showed beneficial effects in reducing the heterogeneous tissue component of the scar, which led to lesser and smaller corridors. Although we did not find differences in cardiovascular outcomes at short-term follow-up, we observed a significant reduction in the propensity for VT induction. Programmed electrical stimulation shortly after MI could unmask potential clinical arrhythmic events, which otherwise would require long-term follow-up to be detected. However, the clinical benefit of Sac/Val in terms of arrhythmic events in the long term needs to be further investigated.

At the histological level, Sac/Val animals displayed less Col I deposition in the myocardial scar, resulting in a lower Col I/III ratio, consistent with other preclinical studies.³⁹ Post-MI ventricular remodeling involves several

factors including changes in the composition of the cardiac extracellular matrix due to the secretion of Col I and Col III and an imbalance of the collagen ratio in the infarcted and BZ areas. These modifications can eventually develop into HF, VA, and death.⁴⁰ Thus, the limited scar fibrosis found in Sac/Val-treated animals could be partially responsible for the observed attenuation of ventricular remodeling.

Taken together, these results suggest that BB+Sac/Val, compared with BB only, modulates the systemic inflammatory response after MI, attenuates ventricular remodeling, reduces collagen deposition, and improves the electrophysiological properties of the myocardial scar.

Limitations

Animals received only BB as a baseline HF treatment. Whether the addition of other HF medications would have influenced the results is unknown and requires further investigation. The lack of PK/PD data for Sac/Val applicable to the porcine model is a significant limitation and should be considered when interpreting the

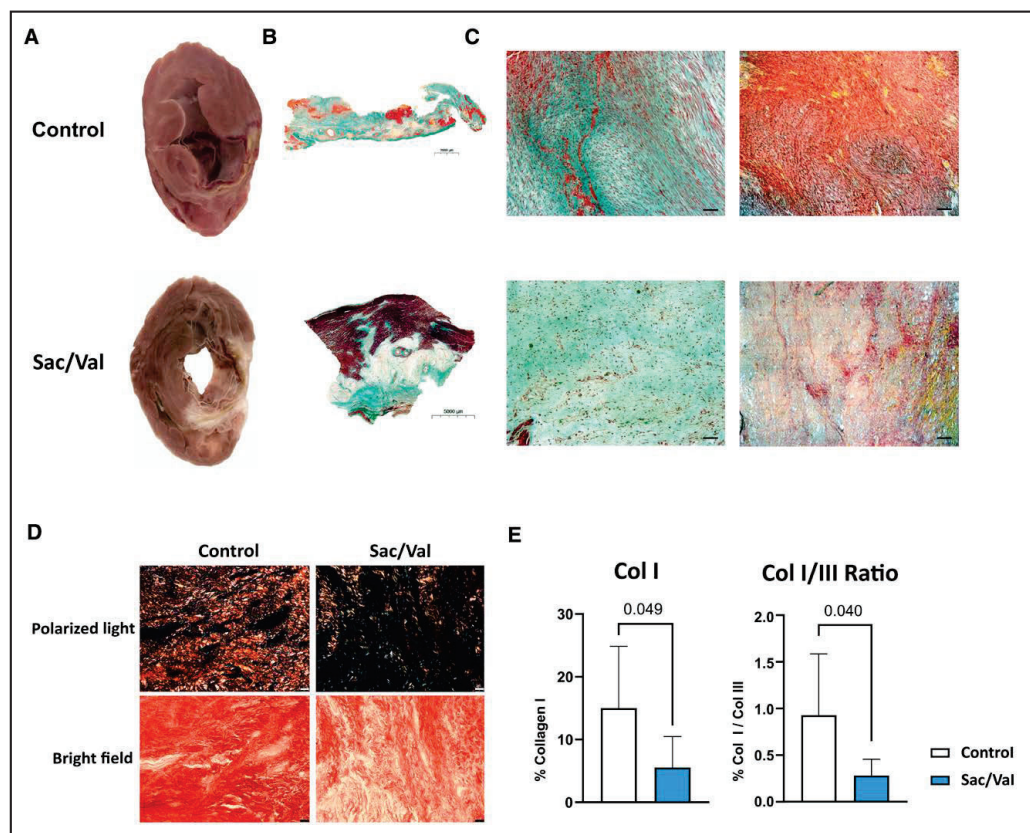


Figure 5. Descriptive anatomopathological analysis and myocardial fibrosis. **A**, Representative photographs of heart sections from control and Sac/Val-treated animals. **B**, Masson's trichrome staining of cardiac slices showing the infarct area with fibrosis (light green), myocardium/inflammatory infiltration (pink), and their respective zoomed images (**C**, left). **C** (right), Photomicrographs after modified Movat's pentachrome staining revealing dense fibrosis (red; scale bar = 50 μ m). **D** (top), Representative picrosirius red staining images under polarized light microscopy showing fibrils of collagen (Col) I (red/yellow) and Col III (green) in the infarct core. **D** (bottom), Same sections under bright field distinguishing collagen (red) and cardiac muscle (yellow; scale bar = 25 μ m). **E**, Col I in percentage and Col I/III ratio in the infarct zone as measured from polarized light images. Statistical significance was calculated with a Welch *t* test. Sac/Val indicates sacubitril/valsartan.

measurements on inflammatory state on day 2. The follow-up was rather short and might have underestimated the occurrence of spontaneous VT or sudden death. Reduction of the BZ scar mass was only observed in LGE-CMR, not in the electroanatomic mapping.

Conclusions

After MI, treatment with BB+Sac/Val, compared with BB, reduced the propensity for VT induction and the acute inflammatory response and modulated the scar tissue composition. Sac/Val treatment was associated with decreased total scar mass, BZ mass and corridor numbers, collagen content, scar transmural, and improved conduction properties.

ARTICLE INFORMATION

Received October 2, 2023; accepted February 23, 2024.

Affiliations

ICREC Research Program, Germans Trias i Pujol Research Institute, Barcelona, Spain (D.M.-F., G.F.-C., M.M.-T., I.D.-G., S.R., A.B.-G., C.G.-M.). Faculty of Medicine, University of Barcelona, Spain (D.M.-F.). Heart Institute (ICOR), Germans Trias i Pujol University Hospital, Barcelona, Spain (J.A., A.T., E.F., O.R.-L., S.R., R.V., A.S., V.B., V.D., A.B.-G., F.B., C.G.-M.). Department of Medicine, Autonomous University of Barcelona, Spain (J.A., A.B.-G.). Department of Immunobiology, University of Lausanne, Epalinges, Vaud, Switzerland (M.M.-T.). CIBER Cardiovascular, Instituto de Salud Carlos III, Madrid, Spain (O.R.-L., S.R., R.V., A.B.-G., F.B., C.G.-M.). Faculty of Medicine, University of Vic-Central University of Catalonia, Barcelona, Spain (S.R.).

Acknowledgments

This study was possible thanks to the core facilities of the Germans Trias i Pujol Research Institute, with special thanks to the Flow Cytometry and Microscopy units, and the Comparative Medicine and Biomechanics Center of Catalonia.

Sources of Funding

This study was supported in part by grants from the Spanish Ministry of Science and Innovation-MICIN (PID2021-1247030B-I00), and the Instituto de Salud Carlos III under Grants CIBERCY (CB16/11/00403) and Red RICORS-TERAV (RD21/0017/0022) as a part of the Plan Nacional de I+D+i, and was co-funded by ISCIII-Subdirección General de Evaluación y el Fondo Europeo de Desarrollo Regional (FEDER), AGAUR Generalitat de Catalunya (2021-SGR-01437), JMC Legacy Research Fund of Germans Trias i Pujol University Hospital (2021_45), and Institut Català de Salut.

Disclosures

Victoria Delgado received speaker fees from Abbott Vascular, Edwards Lifesciences, GE Healthcare, Medtronic, Novartis, JenaValve and Philips and consulting fees from Edwards Lifesciences, MSD and Novo Nordisk.

Antoni Bayes-Genis has lectured and/or participated in ad boards for Abbott, AstraZeneca, Bayer, Boehringer Ingelheim, Medtronic, Novartis, Novo Nordisk, Roche Diagnostics, Vifor.

Supplemental Material

Supplemental Methods

Supplemental Results

Figures S1–S5

Tables S1–S3

Reference 41

REFERENCES

- Ziaeian B, Fonarow GC. Epidemiology and aetiology of heart failure. *Nat Rev Cardiol*. 2016;13:368–378. doi: 10.1038/nrcardio.2016.25
- Prabhu SD, Frangogiannis NG. The biological basis for cardiac repair after myocardial infarction: from inflammation to fibrosis. *Circ Res*. 2016;119:91–112. doi: 10.1161/CIRCRESAHA.116.303577
- Tomaselli GF, Zipes DP. What causes sudden death in heart failure? *Circ Res*. 2004;95:754–763. doi: 10.1161/01.RES.0000145047.14691.db
- Masarone D, Limongelli G, Rubino M, Valente F, Vastarella R, Ammendola E, Gravino R, Verrengia M, Salerno G, Pacifico G. Management of arrhythmias in heart failure. *J Cardiovasc Dev Dis*. 2017;4:3. doi: 10.3390/jcdd4010003
- Mogensen UM, Gong J, Jhund PS, Shen L, Køber L, Desai AS, Lefkowitz MP, Packer M, Rouleau JL, Solomon SD, et al. Effect of sacubitril/valsartan on recurrent events in the prospective comparison of ARNI with ACEI to determine impact on global mortality and morbidity in heart failure trial (PARADIGM-HF). *Eur J Heart Fail*. 2018;20:760–768. doi: 10.1002/ehf.1139
- Docherty KF, Vaduganathan M, Solomon SD, McMurray JJV. Sacubitril/Valsartan: neprilysin inhibition 5 years after PARADIGM-HF. *JACC Heart Fail*. 2020;8:800–810. doi: 10.1016/j.jchf.2020.06.020
- Guerra F, Ammendola E, Ziacchi M, Aspromonte V, Pellegrino PL, Del Giorno G, Dell'Era G, Pimpini L, Santoro F, Floris R, et al. Effect of sacubitril/valsartan on left ventricular ejection fraction and on the potential indication for implantable cardioverter defibrillator in primary prevention: the SAVE-ICD study. *Eur J Clin Pharmacol*. 2021;77:1835–1842. doi: 10.1007/s00228-021-03189-8
- Almufleh A, Marbach J, Chih S, Stadnick E, Davies R, Liu P, Mielniczuk L. Ejection fraction improvement and reverse remodeling achieved with sacubitril/valsartan in heart failure with reduced ejection fraction patients. *Am J Cardiovasc Dis*. 2017;7:108–113. <https://pubmed.ncbi.nlm.nih.gov/29348971/>
- Januzzi JL, Prescott MF, Butler J, Felker GM, Maisel AS, McCague K, Camacho A, Pinã IL, Rocha RA, Shah AM, et al; PROVE-HF Investigators. Association of change in n-terminal pro-b-type natriuretic peptide following initiation of sacubitril-valsartan treatment with cardiac structure and function in patients with heart failure with reduced ejection fraction. *JAMA*. 2019;322:1085–1095. doi: 10.1001/jama.2019.12821
- Curtain JP, Jackson AM, Shen L, Jhund PS, Docherty KF, Petrie MC, Castagno D, Desai AS, Rohde LE, Lefkowitz MP, et al. Effect of sacubitril/valsartan on investigator-reported ventricular arrhythmias in PARADIGM-HF. *Eur J Heart Fail*. 2022;24:551–561. doi: 10.1002/ehf.2419
- Guerra F, Pimpini L, Flori M, Contadini D, Stronati G, Gioacchini F, Massara MF, Gennaro F, Antonicelli R, Busacca P, et al. Sacubitril/valsartan reduces atrial fibrillation and supraventricular arrhythmias in patients with HFrEF and remote monitoring: preliminary data from the SAVE THE RHYTHM. *Eur Heart J*. 2020;41(Supplement_2):ehaa946.0926. doi: 10.1093/ehjci/ehaa946.0926
- de Diego C, González-Torres L, Núñez JM, Centurión Inda R, Martín-Langerwerf DA, Sangio AD, Chochowski P, Casanovas P, Blazquez JC, Almendra J. Effects of angiotensin-neprilysin inhibition compared to angiotensin inhibition on ventricular arrhythmias in reduced ejection fraction patients under continuous remote monitoring of implantable defibrillator devices. *Heart Rhythm*. 2018;15:395–402. doi: 10.1016/j.hrthm.2017.11.012
- Chang PC, Wo HT, Lee HL, Lin SF, Chu Y, Wen MS, Chou CC. Sacubitril/valsartan therapy ameliorates ventricular tachyarrhythmia inducibility in a rabbit myocardial infarction model. *J Card Fail*. 2020;26:527–537. doi: 10.1016/j.cardfail.2020.03.007
- Tsai YN, Cheng WH, Chang YT, Hsiao YW, Chang TY, Hsieh YC, Lin YJ, Lo LW, Chao TF, Kuo MJ, et al. Mechanism of angiotensin receptor-neprilysin inhibitor in suppression of ventricular arrhythmia. *J Cardiol*. 2021;78:275–284. doi: 10.1016/j.jjcc.2021.04.011
- Jun-Yu H, Wan-Ying J, Chen C, Chen R, Tian-Tian G, Chang Q, Zhu L, Geng J, Zhi-Xin J, Qi-Jun S. Effects of angiotensin receptor neprilysin inhibitors on inducibility of ventricular arrhythmias in rats with ischemic cardiomyopathy. *Int Heart J*. 2019;60:1168–1175. doi: 10.1536/ihj.19-065
- Martens P, Belien H, Dupont M, Vandervoort P, Mullens W. The reverse remodeling response to sacubitril/valsartan therapy in heart failure with reduced ejection fraction. *Cardiovasc Ther*. 2018;36:e12435. doi: 10.1111/1755-5922.12435
- Wang Y, Zhou R, Lu C, Chen Q, Xu T, Li D. Effects of the angiotensin-receptor neprilysin inhibitor on cardiac reverse remodeling: meta-analysis. *J Am Heart Assoc*. 2019;8:e012272. doi: 10.1161/JAHA.119.012272
- Frangogiannis NG, Smith CW, Entman ML. The inflammatory response in myocardial infarction. *Cardiovasc Res*. 2002;53:31–47. doi: 10.1016/s0008-6363(01)00434-5
- Kologrivova I, Shtatolkina M, Suslova T, Ryabov V. Cells of the immune system in cardiac remodeling: main players in resolution of inflammation and repair after myocardial infarction. *Front Immunol*. 2021;12:664457. doi: 10.3389/fimmu.2021.664457
- Martínez-Falguera D, Fadeuilhe E, Teis A, Aranyo J, Adeliño R, Bisbal F, Rodríguez-Leor O, Gálvez-Montón C. Myocardial infarction by percutaneous embolization coil deployment in a swine model. *J Vis Exp*. 2021. doi: 10.3791/63172
- Perez-David E, Arenal A, Rubio-Guervain JL, Del Castillo R, Atea L, Arbelo E, Caballero E, Celorrio V, Datino T, Gonzalez-Torrecilla E, et al. Non-invasive identification of ventricular tachycardia-related conducting channels using contrast-enhanced magnetic resonance imaging in patients with chronic myocardial infarction: comparison of signal intensity scar mapping and endocardial voltage mapping. *J Am Coll Cardiol*. 2011;57:184–194. doi: 10.1016/j.jacc.2010.07.043
- Raiman M, Tung R. Automated isochronal late activation mapping to identify deceleration zones: Rationale and methodology of a practical electro-anatomic mapping approach for ventricular tachycardia ablation. *Comput Biol Med*. 2018;102:336–340. doi: 10.1016/j.combiomed.2018.07.012
- Eldar M, Ohad D, Bor A, Varda-Bloom N, Swanson DK, Battler A. A closed-chest pig model of sustained ventricular tachycardia. *Pacing Clin Electrophysiol*. 1994;17:1603–1609. doi: 10.1111/j.1540-8159.1994.tb02353.x
- Livak KJ, Schmittgen TD. Analysis of relative gene expression data using real-time quantitative PCR and the 2^{-delta delta} (CT) method. *Methods*. 2001;25:402–408. doi: 10.1006/meth.2001.1262
- Wei Z, Fei Y, Wang Q, Hou J, Cai X, Yang Y, Chen T, Xu Q, Wang Y, Li YG. Loss of Camk2n1 aggravates cardiac remodeling and malignant ventricular arrhythmia after myocardial infarction in mice via NLRP3 inflammasome activation. *Free Radic Biol Med*. 2021;167:243–257. doi: 10.1016/j.freeradbiomed.2021.03.014
- Panahi M, Vадgama N, Kuganesan M, Ng FS, Sattler S. Immunopharmacology of post-myocardial infarction and heart failure medications. *J Clin Med*. 2018;7:403. doi: 10.3390/jcm7110403
- França CN, Izar MCO, Hortêncio MNS, do Amaral JB, Ferreira CES, Tuleta ID, Fonseca FAH. Monocyte subtypes and the CCR2 chemokine receptor in cardiovascular disease. *Clin Sci (Lond)*. 2017;131:1215–1224. doi: 10.1042/CS20170009
- Bajpai G, Schneider C, Wong N, Bredemeyer A, Hulsmans M, Narendorf M, Epelman S, Kreisel D, Liu Y, Itoh A, et al. The human heart contains distinct macrophage subsets with divergent origins and functions. *Nat Med*. 2018;24:1234–1245. doi: 10.1038/s41591-018-0059-x
- Balasubramanian D, Goodlett BL, Mitchell BM. Is IL-12 pro-inflammatory or anti-inflammatory? Depends on the blood pressure. *Cardiovasc Res*. 2019;115:998–999. doi: 10.1093/cvr/cvz028
- O'Farrell AM, Liu Y, Moore KW, Mui ALF. IL-10 inhibits macrophage activation and proliferation by distinct signaling mechanisms: for

- Stat3-dependent and -independent pathways. *EMBO J*. 1998;17:1006–1018. doi: 10.1093/emboj/17.4.1006
31. Yan AT, Shayne AJ, Brown KA, Gupta SN, Chan CW, Luu TM, Di Carli MF, Reynolds HG, Stevenson WG, Kwong RY. Characterization of the peri-infarct zone by contrast-enhanced cardiac magnetic resonance imaging is a powerful predictor of post-myocardial infarction mortality. *Circulation*. 2006;114:32–39. doi: 10.1161/CIRCULATIONAHA.106.613414
 32. Thomsen AF, Bertelsen L, Jøns C, Jabbari R, Lønberg J, Kyhl K, Göransson C, Nepper-Christensen L, Atharovski K, Ekström K, et al. Scar border zone mass and presence of border zone channels assessed with cardiac magnetic resonance imaging are associated with ventricular arrhythmia in patients with ST-segment elevation myocardial infarction. *Europace*. 2023;25:978–988. doi: 10.1093/europace/euac256
 33. Roes SD, Borleffs CJW, Van Der Geest RJ, Westenberg JJM, Marsan NA, Kaandorp TAM, Reiber JHC, Zeppenfeld K, Lamb HJ, De Roos A, et al. Infarct tissue heterogeneity assessed with contrast-enhanced MRI predicts spontaneous ventricular arrhythmia in patients with ischemic cardiomyopathy and implantable cardioverter-defibrillator. *Circ Cardiovasc Imaging*. 2009;2:183–190. doi: 10.1161/CIRCIMAGING.108.826529
 34. Fernández-Armenta J, Berruzo A, Mont L, Sitges M, Andreu D, Silva E, Ortiz-Pérez JT, Tolosana JM, De Caralt TM, Perea RJ, et al. Use of myocardial scar characterization to predict ventricular arrhythmia in cardiac resynchronization therapy. *Europace*. 2012;14:1578–1586. doi: 10.1093/europace/eus104
 35. Ortiz Pérez JT, Armenta JF, Berruzo A, Silva E, Andreu D, Calvo N, Prat S, Girbau LM, Brugada J. Myocardial scar sizing and characterization predicts ventricular arrhythmia in cardiac resynchronization therapy candidates. *J Cardiovasc Magn Reson*. 2011;13:P247. doi: 10.1186/1532-429X-13-S1-P247
 36. White HD, Norris RM, Brown MA, Brandt PW, Whitlock RM, Wild CJ. Left ventricular end-systolic volume as the major determinant of survival after recovery from myocardial infarction. *Circulation*. 1987;76:44–51. doi: 10.1161/01.cir.76.1.44
 37. Martens P, Nuyens D, Rivero-Ayerza M, Van Herendael H, Vercaemmen J, Ceysens W, Luwel E, Dupont M, Mullens W. Sacubitril/valsartan reduces ventricular arrhythmias in parallel with left ventricular reverse remodeling in heart failure with reduced ejection fraction. *Clin Res Cardiol*. 2019;108:1074–1082. doi: 10.1007/s00392-019-01440-y
 38. Mehran R, Steg PG, Pfeffer MA, Jering K, Claggett B, Lewis EF, Granger C, Køber L, Maggioni A, Mann DL, et al. The effects of angiotensin receptor-neprilysin inhibition on major coronary events in patients with acute myocardial infarction: insights from the PARADISE-MI trial. *Circulation*. 2022;146:1749–1757. doi: 10.1161/CIRCULATIONAHA.122.060841
 39. Wu M, Guo Y, Wu Y, Xu K, Lin L. Protective Effects of sacubitril/valsartan on cardiac fibrosis and function in rats with experimental myocardial infarction involves inhibition of collagen synthesis by myocardial fibroblasts through downregulating TGF- β 1/Smads pathway. *Front Pharmacol*. 2021;12:696472. doi: 10.3389/fphar.2021.696472
 40. Li X, Xiang N, Wang Z. Ginsenoside Rg2 attenuates myocardial fibrosis and improves cardiac function after myocardial infarction via AKT signaling pathway. *Biosci Biotechnol Biochem*. 2020;84:2199–2206. doi: 10.1080/09168451.2020.1793292
 41. Kelley KW, Curtis SE, Marzan GT, Karara HM, Anderson CR. Body surface area of female swine. *J Anim Sci*. 1973;36:927–930. doi: 10.2527/jas1973.365927x

SUPPLEMENTAL MATERIAL

Supplemental Methods

Sedation and anesthesia

Myocardial infarction (MI) induction and late gadolinium-enhanced cardiac magnetic resonance (LGE-CMR) analyses were carried out under general anesthesia and endotracheal intubation.

Animals were pre-anesthetized with an intramuscular (IM) injection of dexmedetomidine (0.03 mg/kg; Dexdor, Orion Pharma, Espoo, Finland), midazolam (0.3 mg/kg; Laboratorios Normon, Barcelona, Spain), and butorphanol (0.3 mg/kg; Butomidor, Richter Pharma AG, Wels, Austria).

Anesthetic induction was then performed with an intravenous (IV) bolus of propofol (1-2 mg/kg; Propovet, Zoetis, Barcelona, Spain). Animals underwent endotracheal intubation, and anesthesia was maintained by 2-2.5% isoflurane (IsoVet, BBraun) inhalation. Fentanyl (0.075 mg/kg/45 minutes, IV; Fentadon, Dechra, Bladel, the Netherlands) was used as intra-operative analgesia.

Finally, a tulathromycin IM injection (2.5 mg/kg, IM; Draxxin, Pfizer Animal Health) was administered as antibiotic therapy, and a transdermal fentanyl patch was delivered to allow analgesic postoperative care (Fentanilo Matrix STADA, STADA).

Noninvasive cardiac magnetic resonance imaging

All images were performed in a 3T state-of-the-art imaging system (Vantage Galan 3T, Canon Medical Systems) with all animals in prone position using a 16-element phased array coil (Atlas SPEEDER Body Coil) placed over the chest. Images were acquired during breath-holds with electrocardiographic gating. We used a segmented k-space steady state precession (SSFP) cine sequence (typically TR/TE 3.0/1.5 ms; 65° flip angle; 291 × 265 mm field of view (FOV); 352 × 320 pixel matrix, 8-mm slice thickness, 1302 Hz/pixel bandwidth) at 2, 3, and 4 chamber views

and short axis from base to apex with no gap. Phase-contrast sequences (typically TR/TE 5.4/2.6 ms; 10° flip angle; 350 × 350 mm FOV; 8-mm slice thickness; 130-200 cm/sec VENC) were performed at the sinotubular junction to calculate the aortic forward flow. Delayed enhancement images were acquired 10 to 20 min after IV injection of gadolinium-based contrast (Gd-DTPA; 0.2 mmol/kg) using a phase-sensitive inversion recovery sequence (TR/TE 8.9/3.4 ms; 20° flip angle; 180-250 ms inversion time; 340 × 340 mm FOV; 572 × 448 pixel matrix; 8-mm slice thickness, 140 Hz/pixel bandwidth) matching cine images positions. Inversion time was optimized to null the normal myocardium.

All images were reviewed and analyzed off-line using CMR dedicated analysis software (Medis) by a level 3 CMR expert blinded to the clinical data. Left and right ventricular (LV and RV, respectively) endocardial borders (papillary muscles were excluded) were manually traced in all short-axis cine images at the end-diastolic and end-systolic frames to determine end-diastolic and end-systolic volumes (EDV and ESV), respectively, using QMass (Medis). LV mass was calculated by subtracting the endocardial volume from the epicardial volume at end diastole and then multiplying by tissue density (1.05 g/mL). Left and right ejection fraction (LVEF and RVEF, respectively) were calculated. Calculation of forward aortic volume was performed using QFlow (Medis) tracing ROIs at the aorta in phase-contrast sequences. Background noise correction was performed on all images. The endocardial and epicardial contours on delayed enhancement images were also outlined manually. ROIs were then manually traced in the hyperenhanced area at the place of maximum signal intensity and in the normal-appearing remote myocardium. As previously described, the areas of hyperenhanced myocardium were then automatically segmented by using a full-width at half-maximum (FWHM) algorithm with QMass. Two corrections were required for all automated ROIs. First, microvascular obstruction (defined as

hypointensity within a hyperintense region in subjects with infarctions) was adjusted to be included as LGE if present. Second, any obvious blood pool or pericardial partial volume and artifacts were further removed. Scar volume for each slice was calculated as scar area \times slice thickness. The scar mass was expressed as total scar volume \times 1.05 g. Scar size was also expressed as a percentage of the total myocardial volume: (scar volume / myocardium volume) \times 100.

The height, weight, and heart rate of each pig were recorded at every LGE-CMR scan. Body surface area (BSA) was calculated as previously described.⁴¹ Cardiac index was calculated as (forward aortic volume \times heart rate)/ BSA.

Statistical analysis

The appropriate statistical test for each dataset was applied after exploring the normal distribution of continuous data with QQ plots. Continuous variables are expressed as mean \pm standard deviation or median with interquartile range, as appropriate; categorical variables are expressed as numbers and percentages. Continuous variables were compared with a paired Student t-test or nonparametric test, as appropriate; categorical variables were compared using the chi-square or Fisher exact test, as needed. Repeated measures analysis of variance (RM-ANOVA) with the Greenhouse-Geisser correction and Tukey's post hoc test were used to assess changes in a continuous variable across time and within subjects. Univariate logistic regression was used to evaluate potential associations between scar properties and VT inducibility.

Supplemental Results

Sex differences

Statistical differences according to modified Tukey post-hoc test from repeated-measures ANOVA showed a significant decrease in monocyte count 2 days post MI in the Sac/Val group only in females (baseline: $577.65 \pm 182.57\%$ vs. 2 days post MI: $346.43 \pm 141.34\%$; $p = 0.029$) while this decrease was not detected in males (baseline: 884.46 ± 617.74 vs. 2 days post MI: 806.00 ± 202.76) (*Supplementary Figure 5*). No sex-related effect was observed in the rest of the studied variables.

Supplemental Table 1. TaqMan probes (Thermo Fisher) used in RT-PCR analysis.

Gene transcript	TaqMan Probe	Amplicon Length	Exon boundary
<i>IL10</i>	Ss03382372_u1	87	3-3
<i>TNF</i>	Ss03391318_g1	73	3-4
<i>CCL2/MCP-1</i>	Ss03394377_m1	58	1-2
<i>TGFB1</i>	Ss04955543_m1	57	5-6
<i>TGFB3</i>	Ss03394351_m1	104	-
<i>LRP1</i>	Ss06917026_m1	57	4-5
<i>MMP2</i>	Ss03394318_m1	77	4-5
<i>MMP9</i>	Ss03392100_m1	58	12-13
<i>TIMP1</i>	Ss03381944_u1	105	5-5
<i>PGK1</i>	Ss03389144_m1	66	4-5

IL10 = interleukin 10; *TNF* = tumor necrosis factor alpha; *CCL2/MCP1* = chemokine (C-C motif) ligand 2 or monocyte chemoattractant protein 1; *TGFB1/3* = transforming growth factor beta 1/3; *LRP1* = LDL receptor-related protein 1; *MMP2/9* = matrix metalloproteinase 2/9; *TIMP1* = tissue inhibitor of metalloproteinase-1; *PGK1* = phosphoglycerate kinase 1.

Supplemental Table 2. Gene expression levels of fibrotic and inflammatory drivers in infarct and remote zone. Gene expression was calculated using the $\Delta\Delta C_t$ method relative to the endogenous gene *PGK1*. Differences between the control and Sac/Val groups were calculated with a Student t-test (+) or Mann-Whitney U test (#), as appropriate.

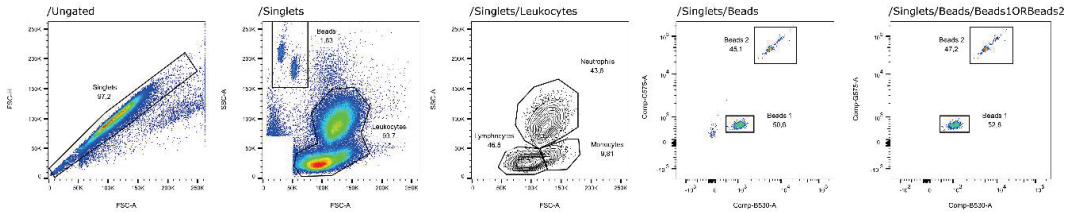
INFARCT ZONE	CONTROL (n = 5)	SAC/VAL (n = 7)	P value
<i>TGFB1</i>	0.49±0.21	0.48±0.18	0.885+
<i>TGFB3</i>	0.68±0.49	0.69±0.36	0.940+
<i>LRP1</i>	1.07±0.55	1.06±0.47	0.970+
<i>MMP2</i>	12.15±8.85	10.42±5.33	0.680+
<i>MMP9</i>	0.03±0.05	0.60±0.92	>0.999#
<i>TIMP1</i>	5.46±5.48	1.84±1.55	0.218+
<i>IL10</i>	0.01±0.007	0.009±0.005	0.742+
<i>TNF</i>	0.002±0.001	0.004±0.001	0.063+
<i>CCL2/MCP-1</i>	3.49±1.03	3.43±2.61	0.968+
REMOTE ZONE	CONTROL (n = 5)	SAC/VAL (n = 7)	P value
<i>TGFB1</i>	0.14±0.026	0.14±0.03	0.859+
<i>TGFB3</i>	0.027±0.01	0.025±0.01	0.639#
<i>LRP1</i>	0.10±0.03	0.12±0.03	0.345+
<i>MMP2</i>	0.72±0.24	0.63±0.14	0.460+
<i>MMP9</i>	0.0005±0.0002	0.0007±0.0003	0.189+
<i>TIMP1</i>	0.11±0.08	0.07±0.02	0.347+
<i>IL10</i>	0.0014±0.001	0.0014±0.0004	0.432#
<i>TNF</i>	0.0008±0.0003	0.0013±0.007	0.180+
<i>CCL2/MCP-1</i>	0.22±0.05	0.20±0.11	0.850+

Supplemental Table 3. Invasive blood pressure. Blood pressure data (mmHg) at baseline (at the beginning of MI procedure) and follow-up (30 days post MI; before starting mapping procedure) for control and Sac/Val animals. P values according to repeated-measures ANOVA.

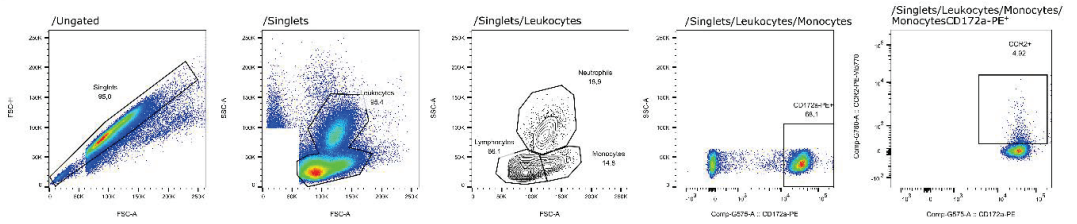
	<i>Control</i>		<i>SAC/VAL</i>		<i>P value</i>
	<i>Baseline</i>	<i>Follow-up</i>	<i>Baseline</i>	<i>Follow-up</i>	
<i>ISBP</i>	105.1 ± 10.47	86.25 ± 1.77	98.33 ± 11.14	88.75 ± 8.02	<i>0.343</i>
<i>IDBP</i>	78.75 ± 19.45	51.25 ± 5.30	74.17 ± 15.06	53.33 ± 5.63	<i>0.582</i>

Supplemental Figure 1. Cytometry gating strategy. (A) Singlets were gated according to FSC-A/FSC-H. Monocytes, leukocytes, and neutrophils were gated according to their complexity and size from the singlet/leukocyte population. For cell absolute number quantification, Perfect Count Microspheres beads (Cytognos) were used. They were gated as a Boolean “OR” gate of the two bead populations defined by their FITC (B530-A channel) and PE (G575-A channel) signal, and a 50:50 ratio (45:55 maximum difference) was ensured in every assay, according to the manufacturer’s instructions. (B) Monocytes were gated according to their distinctive FSC-A/SSC-A appearance from the singlet/leukocyte population. Then, the different percentages of cells expressing each marker and the median fluorescence intensity (MFI) in each channel were calculated.

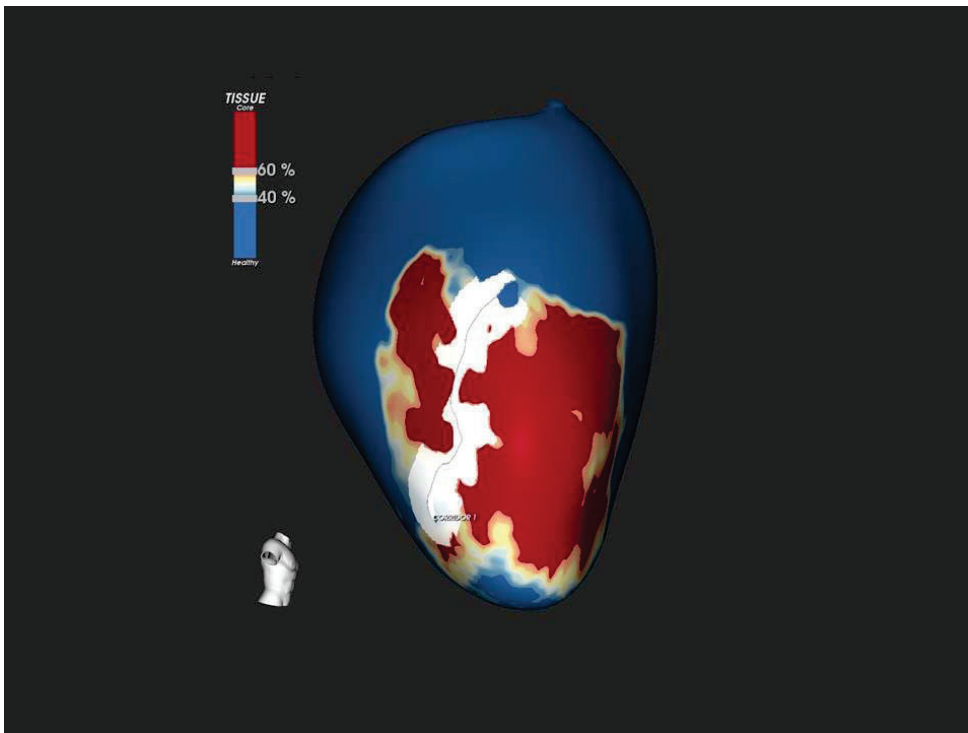
A



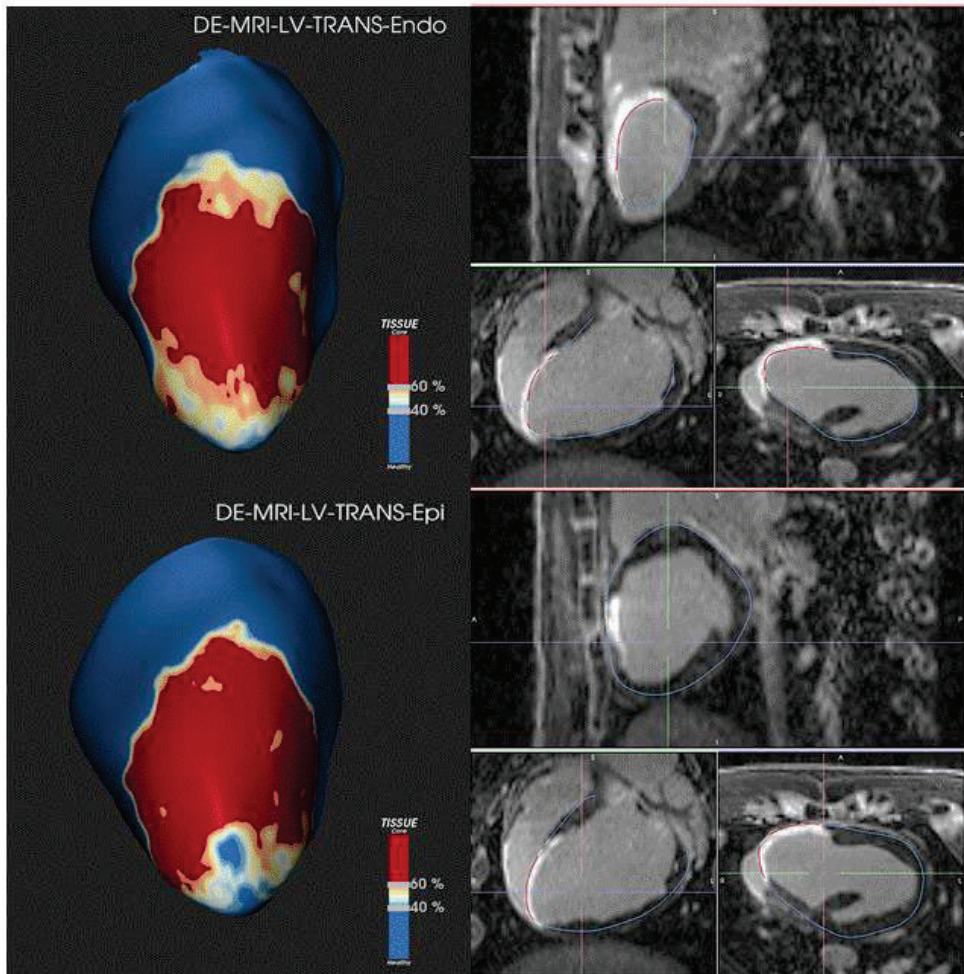
B



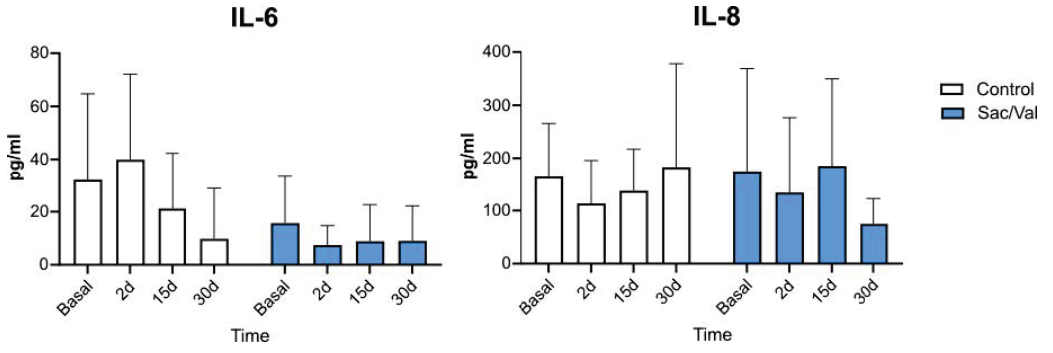
Supplemental Figure 2. LGE-CMR and BZ corridor detection. In vivo high-resolution LGE-CMR and 3D LV volume reconstruction with automatic detection of arrhythmic substrate (ADAS) 3D software is shown. Three-dimensional LV scar reconstruction using the standard pixel intensity cut-offs (>60%, 40-60%, and <40%) to define dense (red), BZ (yellow), and healthy tissue (blue) is shown. Note the large anterior endocardial (layer 30%) MI, with large dense and BZ scar. A BZ central corridor (white) is defined as a BZ region connecting two areas of healthy myocardium and protected by the core scar region.



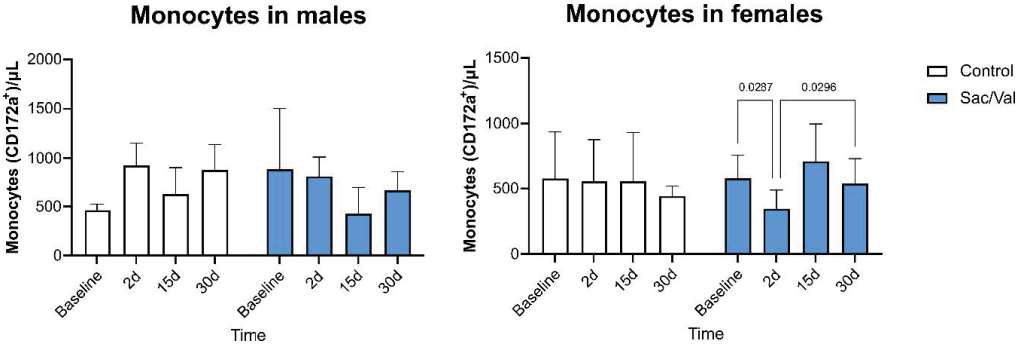
Supplemental Figure 3. LGE-CMR of LV scar transmuralty. LV transmuralty analysis was performed using the automatic tool of the software ADAS-3D. Total, dense, and BZ endocardial and epicardial scar were automatically reconstructed, calculated, and annotated.



Supplemental Figure 4. Cytokine profile. Serum levels of IL-6 and IL-8 at baseline and at 2, 15, and 30 days post MI. Data are presented as mean \pm SD.



Supplemental Figure 5. Sex differences in systemic inflammation. Histogram representing differences in total number of monocytes at baseline and at 2, 15, and 30 days of follow-up: males on the left (control: n = 2; Sac/Val: n = 5) and females on the right (control n = 6; Sac/Val: n = 4). Statistical significance indicated according to modified Tukey post-hoc test from a repeated-measures ANOVA.



ARTICLE 3

Initiating Empagliflozin and Sacubitril/Valsartan Early Post-Acute Myocardial Infarction: Mechanistic Study

Martínez-Falguera D, Aranyó J, Ferrer-Curriu G, Teis A, Revuelta-López E, Díaz-Güemes I, Monguió-Tortajada M, Fadeuilhe E, Rodríguez-Leor O, Poblador F, Montejo B, Roura S, Villuendas R, Sarrias A, Bazan V, Jorge E, Delgado V, Jimenez Trinidad FR, Rigol M, Martinez-Micaelo N, Amigó N, Bayes-Genis A, Bisbal F, Gálvez-Montón C.

Status: Under review

Objective: This article is related to objectives 2 and 3. This study aimed to assess the effects of early initiation of empagliflozin, with or without sacubitril/valsartan, after MI on inflammation, oxidative stress, metabolism, fibrosis, and the structural and electrophysiological properties of the myocardium in a translational porcine model of MI.

Highlights: Early initiation of empagliflozin after MI reduced acute systemic inflammatory response, modulated nitride oxide (NO) bioavailability, altered scar collagen composition, and elevated levels of cardioprotective liver lipid. When combined with sacubitril/valsartan, it promoted favourable scar remodelling by decreasing Col I deposition in the scar and reducing the number of BZ corridors and deceleration zones (DZs), which led to improved LV compliance and a reduced risk of VT inducibility.

Initiating Empagliflozin and Sacubitril/Valsartan

Early Post-Acute Myocardial Infarction:

Mechanistic Study

Daina Martínez-Falguera^{a,b*}, Júlia Aranyó^{c*}, Gemma Ferrer-Curriu^{a,c}, Albert Teis^c, Elena Revuelta-Lopez^{a,c,d}, Idoia Diaz-Güemes^a, Marta Monguió-Tortajada^{a,c,e}, Edgar Fadeuilhe^c, Oriol Rodríguez-Leor^{c,d}, Francesc Poblador^a, Borja Montejo^a, Santiago Roura^{a,c,d,f}, Roger Villuendas^{c,d}, Axel Sarrias^c, Victor Bazan^c, Esther Jorge^{a,g}, Victoria Delgado^{c,h}, Francisco Rafael Jimenez Trinidad^{l,j}, Montserrat Rigol^{l,j}, Neus Martinez-Micaelo^k, Núria Amigó^k, Antoni Bayes-Genis^{a,c,d,l}, Felipe Bisbal^{c,d,†}, Carolina Gálvez-Montón^{a,c,d,†}

^aICREC Research Program, Germans Trias i Pujol Research Institute (IGTP), Badalona, Barcelona, Spain.

^bFaculty of Medicine, University of Barcelona (UB), Spain.

^cHeart Institute (iCOR), Germans Trias i Pujol University Hospital, Badalona, Barcelona, Spain

^dCIBER Cardiovascular, Instituto de Salud Carlos III, Madrid, Spain.

^eDepartment of Immunobiology, University of Lausanne, Epalinges, Vaud, Switzerland.

^fFaculty of Medicine, University of Vic-Central University of Catalonia (UVic-UCC), Vic, Barcelona, Spain.

^gDepartment of Basic Sciences, Faculty of Health Sciences at Manresa, University of Vic – Central University of Catalonia (UVic-UCC), Manresa, Spain.

^hCentre of Comparative Medicine and Bioimaging, Badalona, Spain

ⁱCardiology Department, Institut Clinic Cardiovascular (ICCV), Hospital Clinic de Barcelona, 08036 Barcelona, Spain.

^jInstitute d'Investigacions Biomèdiques August Pi i Sunyer (IDIBAPS), 08036 Barcelona, Spain.

^kBiosfer Teslab, Reus, Tarragona, Spain

^lDepartment of Medicine, Campus Can Ruti, Autonomous University of Barcelona, Spain

*Both authors contributed equally

† Dr Gálvez-Montón and Dr Bisbal share senior authorship.

Abstract

Aims: The benefits of empagliflozin and sacubitril/valsartan (sac/val) in managing heart failure are well-established, but their effects on post-acute myocardial infarction (MI) are not as well understood. Given the limited evidence on relevant mechanisms, we evaluated how early initiation of empagliflozin with or without sac/val affects inflammation, oxidative stress, metabolism, fibrosis, cardiac function, electrophysiological and histological scar properties, and ventricular tachycardia (VT) inducibility in an acute MI pig model.

Methods and Results: Twenty-four pigs with MI were randomly assigned to receive beta-blocker treatment alone (as control), beta-blocker+empagliflozin, or beta-blocker+empagliflozin+sac/val. Immune response, metabolomic profile, and cardiac function were monitored. At 30 days post-MI, programmed electrical stimulation and high-density mapping were performed to assess VT inducibility. Tissue samples were collected for cardiac inflammatory, oxidative stress, and metabolomic analyses. With empagliflozin, acute circulating leukocytes decreased at 2 and 15 days post-MI ($P = 0.010$, $P = 0.050$, respectively), and CCR2⁺ activated monocytes also declined at 15 days post-MI ($P = 0.049$). Nitric oxide bioavailability increased in the remote myocardium ($P = 0.059$), as did cardioprotective omega lipid levels in the liver and collagen (Col) III content in the myocardial scar ($P = 0.023$). No effect on cardiac function or VT inducibility was observed at 30 days. With empagliflozin+sac/val treatment, at one month post-MI, scar Col I deposition decreased ($P = 0.082$), left ventricular compliance increased ($P = 0.044$), electrophysiological remodelling improved (reduced border-zone corridors and deceleration zones; $P = 0.008$ and $P = 0.006$, respectively), and VT inducibility decreased ($P = 0.025$).

Conclusion: In this pig model, early post-MI empagliflozin initiation reduced inflammation and oxidative stress, increased cardioprotective liver lipids, and altered scar collagen without affecting cardiac function or VT inducibility. With empagliflozin and sac/val combined, scar Col I and VT inducibility declined and LV remodelling was enhanced.

Short Title: Empagliflozin and Sac/Val for Myocardial Infarction

Key words: empagliflozin, sacubitril/valsartan, myocardial infarction, inflammation, oxidative stress, metabolism, fibrosis, cardiac function, ventricular arrhythmia

Introduction

Despite improvements in reperfusion strategies and pharmacological advancements, morbidity and mortality remain significant after myocardial infarction (MI). Mortality during the chronic phase of MI is primarily associated with left ventricular (LV) adverse remodelling and the development of heart failure (HF) and ventricular arrhythmias (VAs).^{1,2}

Post-MI cardiac remodelling is a complex process. Following MI, the injured myocardium triggers an acute inflammatory reaction, characterized by the release of pro-inflammatory cytokines and the subsequent infiltration of leukocytes into the myocardium.³ The first inflammatory peak evolves into a reparatory phase characterized by collagen deposition and scar formation. Although the scar maintains cardiac structural integrity, it also leads to adverse structural and electrical cardiac remodelling, contributing to cardiac dysfunction and VA.⁴

Recently, the introduction of new drugs such as sacubitril/valsartan (sac/val) and empagliflozin has markedly improved clinical outcomes in patients with HF.⁵ Sac/val inhibits the renin–angiotensin–aldosterone system and preserves endogenous natriuretic peptides from degradation, modulating systemic inflammation and enhancing favourable LV remodelling and myocardial fibrosis.^{6–8} Empagliflozin is a sodium/glucose co-transporter inhibitor (SGLT2i) and has demonstrated cardiovascular (CV) benefits, including reductions in CV death and recurrent HF hospitalizations in patients with HF.^{9,10} These effects are attributed to modulating inflammation, reducing oxidative stress, altering cardiac metabolism, and improving LV remodelling.^{11,12}

Both drugs have the potential to prevent arrhythmic events, with a reduction in sudden cardiac death and VA burden with sac/val^{13,14} and in atrial

fibrillation with the SGLT2i.¹⁵ The role of empagliflozin and sac/val in HF thus is already established, but their efficacy in post-acute MI remains largely unexplored. Recently published results of the EMPACT-MI trial indicate that compared to placebo, empagliflozin after MI decreased the risk of first and total hospitalizations for HF, although it did not reduce the combined primary endpoint of HF hospitalization and all-cause mortality.^{16,17} Furthermore, the mechanism of action of empagliflozin following MI is understudied, and its potential synergistic effect with sac/val remains unknown.

The aim of this post-MI model study was to evaluate the impact of early administration of empagliflozin, with or without sac/val, on inflammation, oxidative stress, metabolic changes, cardiac structural and electrical remodelling, and the likelihood of VA.

Methods

Experimental animal design

The design for inclusion of study animals is shown in **Figure 1**. Thirty crossbreed Landrace X Large White pigs (50% females) underwent a non-revascularized MI and were then randomized to receive treatment with beta-blocker (BB) as control (bisoprolol, 0.04 mg/kg daily) or with BB+empagliflozin (empagliflozin, 0.27 mg/kg daily) or BB+empagliflozin+sac/val (sac/val, 1.25/1.30 mg/kg twice per day) during 30 days after MI.

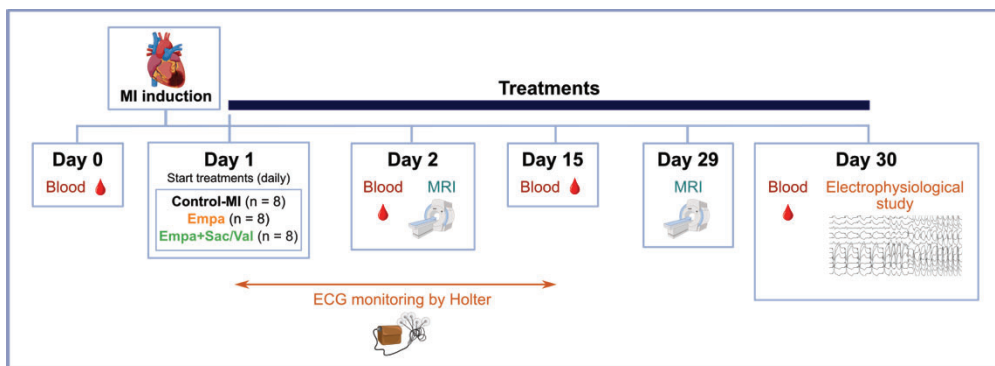


Figure 1. Chronogram and workflow of the animal study. MRI, magnetic resonance imaging; ECG, electrocardiogram.

MI porcine model

All experimental animal protocols were approved by the Animal Experimentation Ethical Committee Unit of the Germans Trias i Pujol Health Research Institute and Government Authorities (Generalitat de Catalunya; Code: 11208), in accordance with the guidelines outlined in the *Guide for the Care and Use of Laboratory Animals*¹⁸ and Directive 2010/63/EU of the European Parliament on the protection of animals used for scientific purposes, as well as the NIH Guide for the Care and Use of Laboratory Animals.

As previously described,¹⁹ the left anterior descending coronary artery of the animals was permanently occluded by percutaneous deployment of 1–3 coils (VortX-18 Diamond 3-4-5 mm/3.3 mm coil, Boston Scientific, Marlborough, Massachusetts, USA). Complete occlusion (TIMI flow score = 0) was confirmed by repeated coronary angiography. Acute myocardial damage was evaluated by analysing serum cardiac troponin I at baseline and 2 h after MI induction. Finally, animals were randomized to the control, empagliflozin, or empagliflozin+sac/val groups and followed up for 30 days.

Cardiac magnetic resonance imaging

Late gadolinium-enhanced (LGE) cardiac magnetic resonance (CMR) imaging was performed at 2 and 30 days post-MI in a 3T imaging system (Vantage Galan 3T, Canon Medical Systems, Otawara, Tochigi, Japan). Cardiac structure and function data were analysed with Medis Medical Imaging software (Leiden, Netherlands), including LV ejection fraction (LVEF), LV stroke volume (LVSV), indexed LV (iLV) end-diastolic volume (iLVEDV), iLV end-systolic volume (iLVESV), iLV mass, right ventricular (RV) ejection fraction, RV stroke volume, indexed RV end-diastolic volume, indexed RV end-systolic volume, and cardiac index parameters.

LGE images were post-processed using ADAS software (Galgo Medical S.L, Barcelona, Spain).^{20,21} Standard pixel intensity thresholds were used to define dense (>60% of the maximum pixel intensity), border-zone (BZ; 40%–60%), and healthy tissue (<40%). Mass (grams) of total, dense, and BZ scar were quantified. Percentage of fibrosis was calculated as the scar area divided by total LV mass. The number of BZ corridors was identified automatically by the software and quantified. A BZ corridor was defined as a channel of BZ tissue connecting two areas of healthy myocardium and surrounded by core areas

on both sides or by a core area on one side and a valve annulus on the other.²² LV transmural analysis was also performed, and total, dense, and BZ epicardial scar values were calculated and annotated.

Sedation and anaesthesia

MI induction and CMR analyses were carried out with animals under general anaesthesia and endotracheal intubation. Animals were pre-anesthetized with an intramuscular (IM) injection of dexmedetomidine (0.03 mg/kg; Dexdor[®], Orion Pharma, Espoo, Finland), midazolam (0.3 mg/kg; Laboratorios Normon, Barcelona, Spain), and butorphanol (0.3 mg/kg; Butomidor[®], Richter Pharma AG, Wels, Austria). Anaesthetic induction was then performed with an intravenous (IV) bolus of propofol (1-2 mg/kg; Propovet[®], Zoetis, Barcelona, Spain). Animals underwent endotracheal intubation, and anaesthesia was maintained with 2%–2.5% isoflurane (IsoVet[®], BBraun, Melsungen, Germany) inhalation. Fentanyl (0.075 mg/kg/45 min, IV; Fentadon[®], Dechra, Bladel, The Netherlands) was used as intra-operative analgesia. Finally, a tulathromycin injection (2.5 mg/kg, IM; Draxxin[®], Pfizer Animal Health) was administered as anti-biotherapy, and a transdermal fentanyl patch was delivered to allow for analgesic post-operative care (Fentanilo Matrix STADA[®], STADA, Bad Vilbel, Germany).

Electroanatomic high-density mapping

Invasive endo-epicardial LV high-density mapping (HDM) was performed 30 days post-MI via retrograde aortic access for the endocardium and sub-xiphoid puncture for the epicardium, using the Rhythmia HDx 3D Mapping System (Boston Scientific, Marlborough, Massachusetts, USA) and a 64-pole

basket catheter (INTELLAMAP ORION, Boston Scientific, Marlborough, Massachusetts, USA). HDM was performed at a paced cycle length of 400 ms with 1 extrastimuli 20 ms above the ventricular effective refractory period. Filling threshold was ≤ 2 mm in regions of low bipolar voltage and ≤ 10 mm elsewhere; interpolation between points ≤ 2 mm was required in all cases. Bandpass filters were set at 30 to 300 Hz for bipolar signals and 1 to 300 Hz for unipolar signals.

Voltage and activation maps were analysed off-line with the Rhythmia system. Conventional voltage cut-offs were used (0.5 and 1.5 mV) to define core, BZ, and healthy tissue. Core and BZ voltage regions were quantified using the mapping system's surface area measurement utility. The LUMIPOINT™ module was used to determine areas of slow and delayed conduction, including the number of deceleration zones (DZs, defined as >3 isochrones within 1 cm out of 8 isochrones comprising the entire ventricular activation window) and pathologic activation (local abnormal ventricular activities or late potentials).

Ventricular tachycardia inducibility

Following HDM, inducibility of ventricular tachycardia (VT) was tested by programmed ventricular stimulation from the RV. LV stimulation was attempted in case of non-inducibility from the RV. Ventricular extra-stimulation at a paced cycle length of 400, 350, and 300 ms with 1 to 5 extrastimuli down to the ventricular refractory period was performed.

Electrocardiography monitoring

Following MI, continuous heart rhythm monitoring using a 15-day Holter monitor was conducted in 5 animals/group. The number and length of sustained and non-sustained VT episodes were quantified.

CV deaths

Deaths in the first 96 h after MI induction were considered related to the MI. After this period, deaths were associated with chronic ischemic cardiomyopathy and were considered for the survival analysis. We measured a composite endpoint of CV death or VT induction.

Systemic immune response

Whole blood samples were collected at baseline and at 2, 15, and 30 days after MI. Samples were stained with monocyte marker CD172a-PE (1:100; Southern Biotech, Birmingham, Alabama, USA). and the activated monocyte markers CCR2/CD192-PE-Vio770 (1:20; Miltenyi Biotech, Bergisch Gladbach, Germany), CD163 (1:100; Novus Biologicals, Centennial, Colorado, USA), and CD73 (1:100; Novus Biologicals, Centennial, Colorado, USA), with FITC and Cy5 as secondary antibodies (1:500; Jackson ImmunoResearch, West Grove, PA and Cambridge, U.K.). Unstained samples were left for absolute number quantification of lymphocytes, monocytes, and neutrophils. Samples were acquired in an LSRFortessa cytometer (BD Biosciences, Franklin Lakes, New Jersey, USA) and analysed with FlowJo software (v10.8.1, BD Biosciences, Franklin Lakes, New Jersey, USA). The gate strategy is detailed in **Supplementary Figure 1**. Serum levels of circulating cytokines, i.e., granulocyte macrophage colony-stimulating factor, interferon- γ , interleukin (IL)-1 α , IL-1 β , IL-1ra, IL-2, IL-4, IL-6, IL-8, IL-10, IL-12, IL-18, and tumour

necrosis factor (TNF)- α , were analysed using the MILLIPLEX MAP Porcine Cytokine/Chemokine Magnetic Bead Kit (PCYTMG-23K-13PX; Millipore, Burlington, Massachusetts, USA) in a Luminex 200 instrument (Luminex Corporation, Austin, Texas, USA).

Histopathological and immunohistochemical analysis

Thirty days post-MI, animals were euthanized with an overdose of pentobarbital sodium (200 mg/kg, IV; Dolethal[®], Vetoquinol E.V.S.A.). Infarct core and remote myocardial samples were collected. To characterize the myocardial scar, histopathological evaluations were conducted using Masson's trichrome staining. Collagen (Col) types I and III, Col I/III ratio, and Col volume fraction (CVF) in the infarcted and remote myocardium were assessed using Picrosirius Red staining. Vessel density in the infarct was assessed using biotinylated *Griffonia simplicifolia* Lectin I IsolectinB4 (1:25; Vector Labs, Newark, California, USA) and Streptavidin-Alexa 568 (1:500; Invitrogen, Waltham, Massachusetts, USA). Immune infiltration into the infarct core was quantified via immunofluorescence staining for CD3 (for total lymphocytes, 1:100; Bio-Rad, Hercules, California, USA), CD25 (for activated lymphocytes, 1:100; Bio-Rad, Hercules, California, USA), and CD163 (for macrophages, 1:100; Bioss, Woburn, Massachusetts, USA). Mitochondrial activity in the preserved myocardium within the infarct zone was assessed by immunofluorescence expression of translocase of outer mitochondrial membrane 20 (Tom20; 1:200; Proteintech, Rosemont, Illinois, USA) and sarcoplasmic/endoplasmic reticulum Ca²⁺-ATPase (SERCA2, 1:50; Santa Cruz, Dallas, Texas, USA). Details of quantification are provided in the **Supplementary Methods**.

Myocardial oxidative stress analyses

As markers of oxidative stress, we used the following: malondialdehyde (MDA) protein levels, evaluated using a commercial enzyme-linked immunosorbent assay in tissue homogenates from the infarct and remote zones (Abbexa, Cambridge, UK) and in serum samples taken at baseline, 15 and 30 days post-MI (OxiSelect™ MDA Adduct Competitive ELISA Kit, Cell Biolabs, San Diego, California, USA); nitric oxide (NO) levels, evaluated with a colorimetric assay kit (Cayman, Ann Arbor, Michigan, USA) in myocardial homogenates and in serum samples; and expression of inducible NO synthase (iNOS), endothelial NOS (eNOS), and activated phosphorylated eNOS (peNOS), evaluated by western blot. Detailed information on these assays is provided in the **Supplementary Methods**.

Gene expression analyses for myocardial inflammation, oxidative stress, metabolism, and fibrosis

Expression levels of genes associated with inflammation (*IL-10*, *TNF- α* , *CCL2*), antioxidants (*NOS2*, *NOS3*, *SOD2*, *PRDX2*, *NOX4*), metabolism (*GLUT4*, *PDK4*), and fibrosis (*TGF- β 1*, *TGF- β 3*, *LRP1*, *MMP2*, *MMP9*, *TIMP1*) were analysed from 2 μ L of cDNA of the infarcted and remote myocardium tissue collected at follow-up, using the TaqMan® Fast Advanced Master Mix (Thermo Fisher Scientific, Waltham, Massachusetts, USA) and the corresponding porcine TaqMan® FAM-MGB probes (**Supplementary Table 1**). Detailed information is provided in the **Supplementary Methods**.

Metabolism assessment

Protein levels of Sirtuin 1 (SIRT1), peroxisome proliferator-activated receptor γ co-activator 1 α (PGC1 α), and fibroblast growth factor 21 (FGF21) from the

infarct and remote zones were evaluated by western blot. The lipoprotein, glycoprotein, lipid, and low-molecular-weight metabolite profiles of the animals were analysed by proton nuclear magnetic resonance spectroscopy technology in serum samples collected at baseline and at 2, 15, and 30 days post-MI and in tissue samples from the infarcted myocardium and liver, collected at follow-up. Detailed procedural information is provided in the **Supplementary Methods**.

***In vitro* H₂O₂ model: reactive oxygen species and cell viability studies**

A model of oxidative stress induced by hydrogen peroxide (H₂O₂) was developed using the cardiomyocyte cell line AC16. Oxidative stress injury was prompted with 300 µM of H₂O₂ (Sigma Aldrich, Burlington, Massachusetts, USA).²³ Cells not subjected to H₂O₂ were used as negative control. Before or after H₂O₂ injury, cells were treated for 20 h (T1, T4) or 1 h (T2, T3) with empagliflozin (low dose: 0.5 µM; or high dose: 1 µM) or empagliflozin + LBQ657 (the active metabolite of sacubitril) + valsartan (low dose: 0.5 µM, 20 µM, and 20 µM; or high dose: 1 µM, 40 µM, and 40 µM, respectively). Determination of reactive oxygen species (ROS) was performed immediately after H₂O₂ treatment for 1 h via measuring intracellular ROS, including H₂O₂, hydroxyl radical (OH), and intracellular superoxide radical anion (O₂^{•-}) levels. Cell viability was assessed at 24 h post-H₂O₂ treatment with the alamarBlue Assay (Thermo Fisher Scientific, Waltham, Massachusetts, USA). More information is detailed in **Supplementary Methods**.

Statistical analysis

Data were described using mean and standard deviation or median and interquartile range, as appropriate. Normality was assessed using quantile

plots, and a logarithmic transformation was carried out needed. The appropriate statistical test for each dataset was applied. Continuous variables among the three groups were compared using analysis of variance (ANOVA) with a Tukey post-hoc test or the non-parametric Kruskal Wallis test with Dunn's post-hoc test, as appropriate. Pairwise group comparisons were also performed in some cases and are noted in the text. In these cases, either Student's t test or the appropriate non-parametric test was used; Categorical variables were compared using the chi-square or Fisher's exact test, as needed. Repeated-measures analysis of variance (RM-ANOVA) with the Greenhouse-Geisser correction or a modified Tukey post hoc test was used to assess changes in continuous variables over time and within subjects. Univariate logistic regression was used to evaluate potential associations between CV death and VT inducibility. Sub-analyses based on the sex of the animals were also performed to discern if males and females differed. Statistical analyses were performed using GraphPad Prism (version 9.5.1), SPSS (version 21.0.0.0, SPSS, Inc.), and R Bioconductor (version 4.1.1) software. Statistical significance was inferred when $P < 0.05$.

Results

MI swine model

A total of 30 animals (34.8 ± 6.8 kg) underwent MI induction. Six animals (5 males) died from ventricular fibrillation during MI induction. The 24 surviving pigs (14 female and 10 male) completed 35 ± 7 days of follow-up. Then, animals were randomized to the control ($n = 8$; 75% females), empagliflozin ($n = 8$; 50% females), and empagliflozin+sac/val ($n = 8$; 50% females) groups. One animal died at day 26 of follow-up (control group, female) and was excluded from LGE-CMR and HDM analyses. No significant differences in circulating cardiac troponin I levels were found between groups, indicating that the magnitude of acute myocardial injury was similar among them ($P = 0.547$; **Supplementary Table 2**).

Systemic and tissue immune inflammatory response

Compared with the other groups, the empagliflozin group exhibited a reduced inflammatory systemic response after MI (**Figure 2A**), with a block of the acute surge of circulating leukocytes at 2 days ($P = 0.010$) and 15 days post-MI ($P = 0.050$) compared to baseline; a reduced presence of CCR2⁺ activated monocytes at 15 days post-MI compared to baseline ($P = 0.049$); and a trend towards reduced CCR2 expression on the monocyte surface at 15 days compared to baseline ($P = 0.072$). The empagliflozin group also had nonsignificant trends towards decreased levels of IL-1 β and IL-18 and increased levels of IL-1ra, which are associated with inflammasome activation (**Supplementary Figure 2**). With combined treatment, circulating monocyte counts increased at 30 days post-MI compared to values at 15 days ($P = 0.003$), but CCR2⁺ monocyte count did not increase (**Figure 2A**).

Immunohistochemical (CD3, CD25, and CD25/CD3) and gene expression (*IL-10*, *TNF- α* , and *CCL2*) analyses of the infarcted and remote myocardium tissue collected at follow-up indicated that all groups showed a similar tissue inflammatory response (**Supplementary Table 3**).

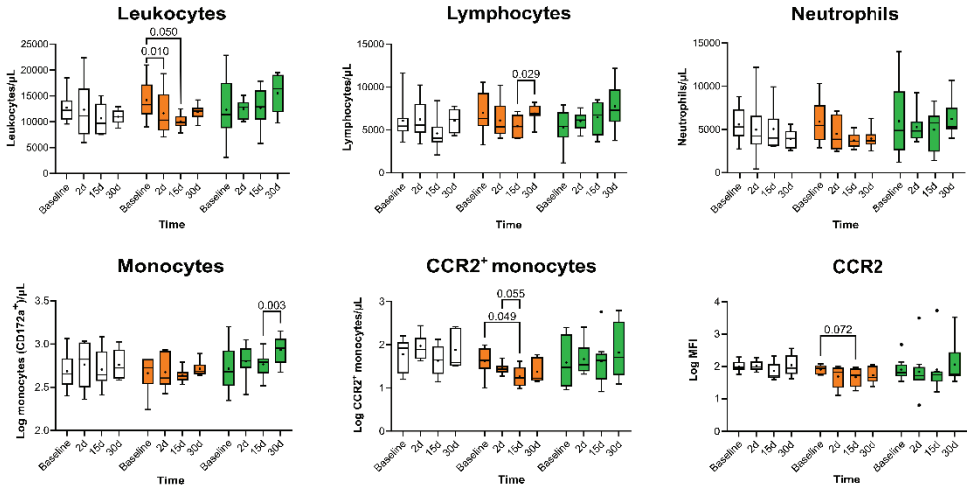
Myocardial oxidative stress

In infarct samples, MDA, NO, eNOS, phosphorylated eNOS, and iNOS levels were similar among the groups. In the remote zone, the empagliflozin group showed a trend towards increased total NO levels compared to the control ($P = 0.084$) and empagliflozin+sac/val groups ($P = 0.059$). Additionally, empagliflozin animals had increased levels of eNOS compared to controls ($P = 0.013$) and elevated peNOS concentrations compared to controls ($P = 0.026$) and to the empagliflozin+sac/val group ($P = 0.044$; **Figure 2B**; **Supplementary Figure 3A**; **Supplementary Table 4**). No significant differences in iNOS and MDA concentrations were observed among groups (**Supplementary Figure 4A**). In both the empagliflozin and empagliflozin+sac/val groups, eNOS levels were diminished in the infarct compared to respective remote myocardium ($P = 0.001$ and $P = 0.039$, respectively; **Figure 2B**). Expression of *NOS2*, *NOS3*, *SOD2*, *PRDX2*, and *NOX4* in the infarct core and remote zones was similar among the three groups (**Supplementary Table 3**).

Mitochondrial analysis

Immunohistochemical analysis showed no changes among groups in the quantification of mitochondrial activity proteins Tom20 and SERCA2 within the infarct zone of preserved myocardium taken at 30 days post-MI (**Supplementary Figure 3B**).

A



B

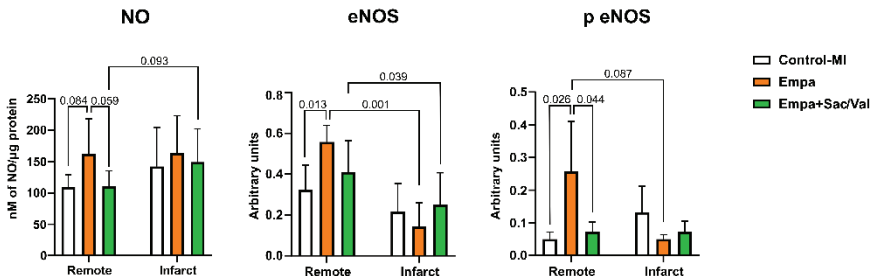


Figure 2. Systemic immune response and NO analysis. (A) Histograms representing total number of leukocytes, lymphocytes, neutrophils, monocytes, CCR2⁺ monocytes, and expression of CCR2 (mean fluorescence intensity; MFI), at baseline and at 2, 15, and 30 days of follow-up of animals from control (Control-MI; n=8), empagliflozin (Empa; n=8), and Empa+Sac/Val (n=8) groups. Statistical differences according to the modified Tukey post-hoc test from repeated-measures ANOVA. (B) Histograms showing NO availability and quantification of eNOS and phosphorylated eNOS in remote and infarct zones of animals from the control (Control-MI; n=7), empagliflozin (Empa; n=8), and Empa+Sac/Val (n=8) groups. Statistical differences according to Tukey post-hoc test from ANOVA or paired t-test, as appropriate.

Metabolic analysis

In the infarct zone, the empagliflozin group had significantly increased levels of SIRT1 protein compared to control animals ($P = 0.042$; **Figure 3A**; **Supplementary Figure 3B**), but PGC1 α and FGF21 protein expression was similar among the groups (data not shown). SIRT1, PGC1 α , and FGF21 protein

levels in the remote zone also did not differ among groups. The empagliflozin group showed no differences in serum content evolution compared to the other groups or in the expression of metabolic genes related to substrate use (*GLUT4*, *PDK4*), either in the infarct or in the remote zones (**Supplementary Table 3**). From baseline to 30 days post-MI, however, empagliflozin+sac/val animals had progressively increasing total triglyceride values ($P < 0.001$) and values for triglycerides transported by lipoproteins (**Figure 3B**). These increases in triglyceride metabolism were not associated with an increase in inflammatory (glycoprotein) profile (data not shown). Compared with controls, in the infarcted myocardial tissue, empagliflozin-only or empagliflozin+sac/val animals showed a significant decrease in free cholesterol (empagliflozin+sac/val group: $P = 0.042$), phosphatidylcholine (empagliflozin group: $P = 0.041$; empagliflozin+sac/val group: $P = 0.029$), saturated fatty acids (empagliflozin+sac/val group: $P = 0.049$), and arachidonic acid + eicosapentaenoic acid (ARA + EPA) (empagliflozin group: $P = 0.038$) (**Figure 3C**). In the liver, the empagliflozin group in comparison to controls had significantly increased levels of glycerophospholipids ($P = 0.012$), phosphatidylcholine ($P = 0.009$), phosphatidylethanolamine ($P = 0.019$), polyunsaturated fatty acids ($P = 0.020$), the omega (w)3 ($P = 0.042$), w6 + w7 ($P = 0.045$), and w9 ($P = 0.011$) fatty acids, docosahexaenoic acid (DHA) ($P = 0.032$), ARA + EPA ($P = 0.016$), and plasmalogen ($P = 0.012$) (**Figure 3D**).

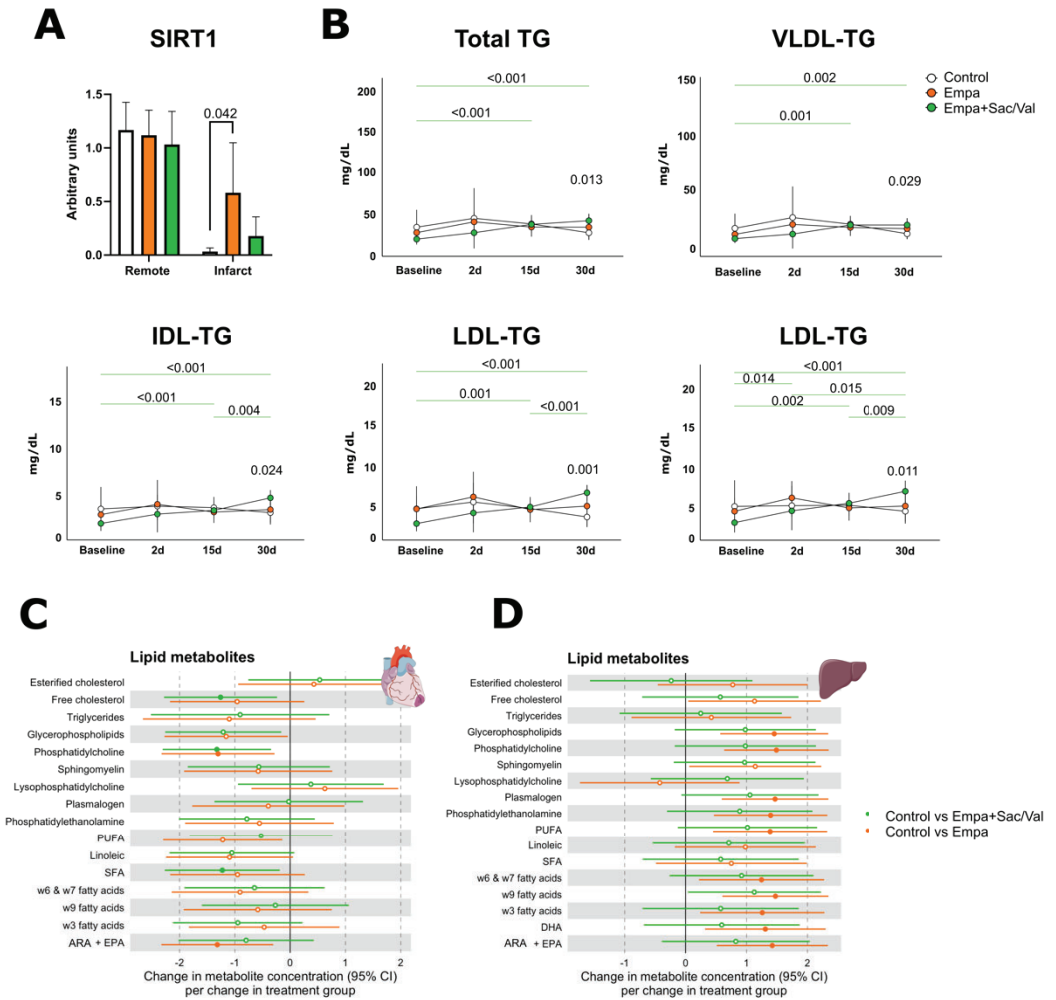


Figure 3. Metabolomic analysis. (A) SIRT1 quantification in remote and infarct zones. Statistical differences according to Tukey post-hoc test from ANOVA. Control-MI, controls (n=7); Empa, empagliflozin (n=8); Empa+Sac/Val (n=8). (B) Lipoprotein profile of animals at baseline and at 2, 15, and 30 days post-MI. Statistical differences according to modified Tukey post-hoc test from repeated-measures ANOVA. TG, triglycerides; VLDL, very low-density lipoprotein; IDL, intermediate-density lipoprotein; LDL, low-density lipoprotein; HDL, high-density lipoprotein. (C and D) Association analyses of odds ratios (ORs) from comparing controls (Control-MI) vs. empagliflozin (Empa) and controls vs. Empa+Sac/Val in the infarct myocardium and liver tissue, respectively. Variables with a filled circle indicate $P < 0.05$. PUFA, polyunsaturated fatty acids; SFA, saturated fatty acids; ARA+EPA, arachidonic acid + eicosapentaenoic acid; DHA, docosahexaenoic acid; CI, confidence interval. Control-MI, controls (n=8); Empa, empagliflozin (n=8); Empa+Sac/Val (n=8).

Myocardial fibrosis and vascular density

Masson's trichrome staining revealed qualitative differences in MI scar composition, with controls displaying higher levels of fibrosis deposition compared to the other groups (**Figure 4A, top**). In line with this finding, analysis of Picrosirius Red-stained infarct samples (**Figure 4A, bottom**) revealed a significant increase in Col III content in the empagliflozin group compared with controls ($20.5\% \pm 3.5\%$ vs. $16.5\% \pm 2.3\%$, $P = 0.023$) and empagliflozin+sac/val animals ($20.5\% \pm 3.5\%$ vs. $16.5\% \pm 4.1\%$, $P = 0.054$), along with a tendency to a reduced Col I/III ratio compared with control animals (0.5 ± 0.3 vs. 0.9 ± 0.7 ; $P = 0.095$) (**Figure 4B**). In addition, the empagliflozin+sac/val group, compared with controls, displayed a tendency towards reduced Col I content ($7.1\% \pm 3.9\%$ vs. $15.0\% \pm 9.8\%$; $P = 0.082$), Col I/III ratio (0.4 ± 0.2 vs. $0.9\% \pm 0.7\%$; $P = 0.085$), and CVF ($23.5\% \pm 7.3\%$ vs. $31.5\% \pm 9.6\%$; $P = 0.092$) (**Figure 4B**). No differences in CVF, Col I, Col III, or Col I/III ratio were observed in the remote zone among groups. The expression of fibrotic genes (*TGF- β 1*, *TGF- β 3*, *LRP1*, *MMP2*, *MMP9*, *TIMP1*) in either the infarct or remote zones was similar between the groups (**Supplementary Table 3**). Immunohistochemical analysis of IsoB4 revealed a similar vascular density in the infarct core among the three groups (data not shown).

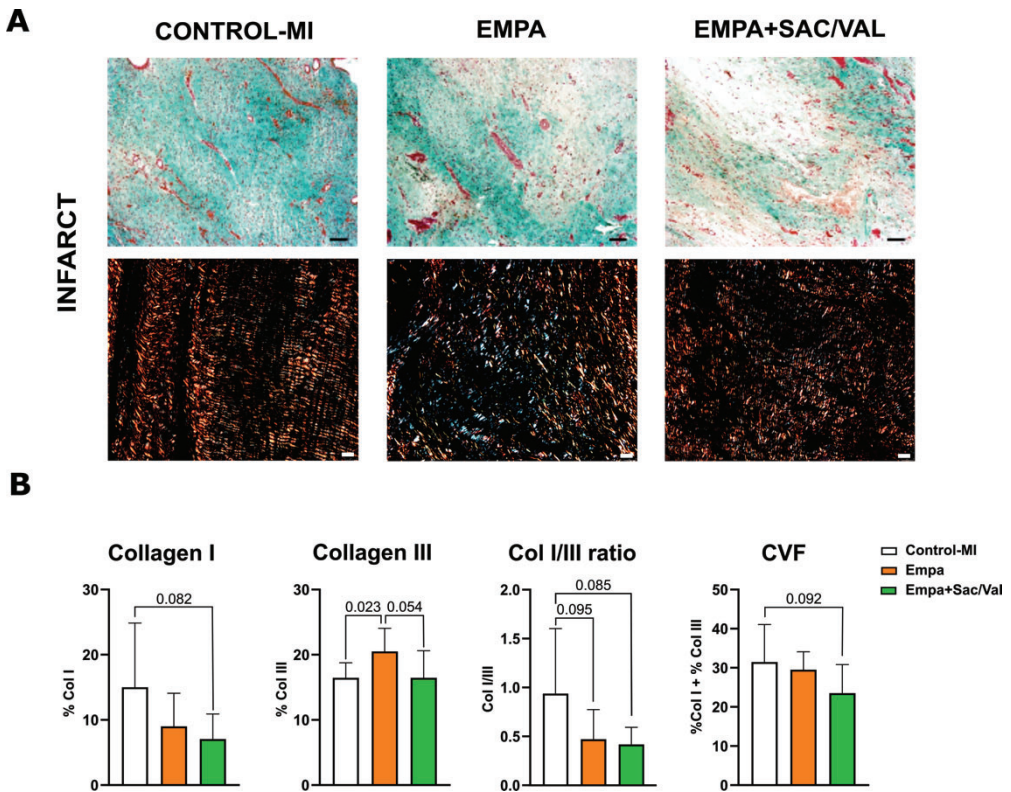


Figure 4. Fibrosis analysis. (A) Top: microphotographs of Masson's trichrome staining from the infarct core; collagen, light green; muscle, dark pink; cytoplasm, pink; nuclei, black (scale bar = 100 μ m). Bottom: polarized light microscopy images of Picrosirius Red staining in infarct core samples, showing Col fibrils type I (red/yellow) and type III (green) (scale bar = 25 μ m). Control-MI, controls (n=8); Empa, empagliflozin (n=8); Empa+Sac/Val (n=7). (B) Percentage of Col I and Col III, Col I/Col III ratio, and CVF in the infarct core. Statistical differences according to Welch t-test or t-test, as appropriate.

Cardiac function and myocardial scar analysis

Cardiac function parameters are summarized in **Table 1**. At 2 days post-MI, CMR data were similar among the groups. At the end of the study (30 ± 6 days post-MI) compared with 2 days post-MI, the empagliflozin group showed no changes in any cardiac function parameters. In contrast, the empagliflozin+sac/val group, compared with control animals, had increases in LV compliance with no changes in iLVESV, along with increased iLVEDV (*P*

= 0.029) and LVSV ($P = 0.044$). Although LVEF increased the most in the empagliflozin+sac/val group compared with the other groups, this change did not reach statistical significance (**Table 1**). LGE-CMR analyses 2 days post-MI and at follow-up showed similar scar mass across groups (**Table 1**). The empagliflozin and empagliflozin+sac/val groups had fewer BZ corridors at follow-up (30 days post-MI) compared with 2 days post-MI CMR and compared with controls, that showed an increase in median [interquartile range] counts between 2 and 30 days post-MI (2 days vs. follow-up; controls: 1 [0–2] vs. 2 [2–3]; empagliflozin: 2 [2–3] vs. 2 [1–2], $P = 0.063$; empagliflozin+sac/val: 2 [2–3] vs. 1 [0–2], $P = 0.006$; **Table 1**).

Table 1. CMR imaging data at baseline (2 days post-MI) and 30 days of follow-up

	Control (n=7)		Empagliflozin (n=8)		<i>P</i>	Empagliflozin+sac/val (n=8)		<i>P</i>
	Post-MI	Follow-up	Post-MI	Follow-up		Post-MI	Follow-up	
LVEF (%)	33.6 ± 5.3	36.2 ± 8.1	33.1 ± 9.8	36.9 ± 6.8	0.831	27.2 ± 6.3	38.0 ± 6.1	0.104
LVSV (mL)	34.6 ± 10.6	40.7 ± 10.3	33.3 ± 11.4	43.4 ± 9.7	0.654	25.0 ± 6.1	45.9 ± 10.1	0.044*
iLVEDV (mL/m ²)	134.1 ± 23.5	124.0 ± 26.5	130.5 ± 17.3	126.5 ± 16.7	0.638	123.6 ± 15.8	138.8 ± 20.5	0.029*
iLVESV (mL/m ²)	88.4 ± 13.9	79.5 ± 20.1	86.9 ± 14.2	79.6 ± 12.5	0.776	90.3 ± 17.2	86.0 ± 14.0	0.570
iLV mass (g/m ²)	84.2 ± 4.9	82.2 ± 5.7	86.9 ± 9.6	80.0 ± 10.1	0.358	82.6 ± 9.2	77.1 ± 10.1	0.564
RVEF (%)	40.5 ± 7.5	50.1 ± 8.1	43.8 ± 8.3	44.4 ± 6.4	0.131	39.8 ± 1.7	46.4 ± 10.1	0.608
RVSV (mL)	32.0 ± 8.4	38.3 ± 8.9	30.7 ± 7.8	34.1 ± 6.9	0.650	28.0 ± 11.8	42.5 ± 10.1	0.304
iRVEDV (mL/m ²)	104.6 ± 17.3	83.2 ± 15.0	92.8 ± 21.5	82.3 ± 8.9	0.323	95.2 ± 40.9	101.7 ± 15.5	0.123
iRVESV (mL/m ²)	62.2 ± 13.0	41.1 ± 7.6	52.7 ± 16.1	45.5 ± 4.9	0.067	57.3 ± 24.6	53.0 ± 13.0	0.131

Cardiac index (L*min/m²)	4.0 ± 1.0	4.6 ± 1.1	4.1 ± 1.2	4.3 ± 0.8	0.700	3.4 ± 0.7	4.6 ± 0.9	0.470
LGE (%)	24.3 ± 7.4	13.2 ± 2.9	27.7 ± 8.9	13.9 ± 3.4	0.454	23.2 ± 7.4	12.5 ± 3.3	0.911
Total scar mass (g)	9.9 [4.1–12.5]	10.1 [7.8–14.0]	13.5 [12.2–14.8]	7.9 [6.3–10.0]	0.069	10.3 [7.7–11.5]	7.8 [6.3–8.1]	0.217
Dense scar mass (g)	4.0 [2.0–6.7]	4.1 [0.5–5.6]	6.0 [5.5–7.6]	5.1 [3.1–5.4]	0.126	5.4 [2.5–6.5]	4.6 [2.6–5.3]	0.231
BZ scar mass (g)	4.1 [2.1–6.7]	4.8 [3.7–6.7]	6.5 [5.0–8.1]	3.2 [2.6–5.3]	0.077	4.9 [4.1–5.4]	3.2 [2.9–4.0]	0.246
Number of corridors	1 [0–2]	2 [2–3]	2 [2–3]	2 [1–2]	0.06	2 [2–3]	1 [0–2]	0.006*

Data are presented as mean ± standard deviation or median [interquartile range] as appropriate. P value according to repeated-ANOVA test with Green-house Geisser correction.

Abbreviations: LVEF, left ventricular ejection fraction; LVSV, left ventricular stroke volume; iLVEDV, indexed left ventricular end-diastolic volume; iLVESV, indexed left ventricular end-systolic volume; iLV mass, indexed left ventricular mass; RVEF, right ventricular ejection fraction; RVSV, right ventricular stroke volume; iRVEDV, indexed right ventricular end-diastolic volume; iRVESV, indexed right ventricular end-systolic volume; LGE, late-gadolinium enhancement (full width at half maximum); BZ, border zone.

Invasive tissue characterization and programmed ventricular stimulation

Endocardial HDM was performed in 23 animals (controls = 7, empagliflozin = 8, empagliflozin+sac/val = 8; 2605 ± 526 points) and epicardial HDM in 18 animals (controls = 5, empagliflozin = 6, empagliflozin+sac/val = 7; 5312 ± 1816 points). In all pigs, left anterior descending occlusion resulted in an anterior wall infarction with an extensive area of low endocardial (≤ 1.5 mV median area: $22.1 [16.7-28.4]$ cm² and ≤ 0.5 mV median area: $18.4 [14.2-21.7]$ cm²) and epicardial (≤ 0.5 mV median area: $22.1 [16.6-28.4]$ cm²) bipolar voltage. The controls and empagliflozin-treated animals did not differ in size of total endocardial scar, core, or BZ, or in the size of the epicardial scar (**Supplementary Table 5**). Almost all animals had pathological electrograms in the endocardium and epicardium, with no differences among groups. A total of 30 DZs were found in 19 animals (median 1 [0-2]), with a lower proportion in the empagliflozin+sac/val group compared to controls (1 [0-1] vs. 3 [2-3]; $P = 0.008$; **Supplementary Table 5**).

Arrhythmia burden

Controls had a higher median value for non-sustained VT compared to the two treatment groups (5 [3-124] vs. 0 [0-3] for empagliflozin [$P = 0.019$] and vs. 2 [0-19] for empagliflozin+sac/val [$P = 0.046$]). No sustained VT was detected.

The composite endpoint of CV death or VT induction occurred in 100% (8/8 animals) in the control group, 75% (6/8 animals) in the empagliflozin group (not significant vs. controls), and 50% (4/8 animals) in the empagliflozin+sac/val group ($P = 0.025$ vs. to controls).

Sex differences

No sex-dependent difference was detected for any studied parameters.

***In vitro* H₂O₂ model: ROS generation and cell viability analyses**

To investigate whether treatment with empagliflozin or empagliflozin+sac/val could offer protective effects against tissue damage, we used a model of oxidative stress induced by H₂O₂ with the human AC16 cardiomyocyte cell line. ROS levels (H₂O₂ and OH) significantly increased under the pretreatment 20-h condition with low doses of empagliflozin+sac/val, in comparison to the equivalent untreated control cells ($P = 0.023$) (**Supplementary Figure 5A, left**). O₂^{•-} levels significantly increased under the pretreatment 1-h condition with low and high doses of empagliflozin ($P = 0.012$ and $P = 0.023$, respectively) (**Supplementary Figure 5A, right**). Cell viability was preserved under the pre- and post-treatment 20-h condition with low doses of empagliflozin+sac/val compared with control cells (pretreatment: $P = 0.004$; post-treatment: $P = 0.011$) (**Supplementary Figure 5B**).

Discussion

The main findings of the present study are that empagliflozin reduced the immune inflammatory response, increased NO bioavailability after MI, raised cardioprotective lipid levels in the liver, and modified collagen composition of the scar without affecting cardiac function and VT inducibility; and that empagliflozin+sac/val decreased scar Col I deposition, improved LV compliance, promoted favourable electrical scar remodelling, and reduced the composite endpoint of CV death or VT inducibility at 30 days post-MI.

Anti-inflammatory effect of empagliflozin

In the present study, empagliflozin modulated the immune inflammatory response after MI by reducing the total number of circulating leukocytes and CCR2⁺ activated monocytes. Following MI, danger signals released by dead cells trigger an intense immune reaction aimed at clearing cellular and matrix debris and initiating tissue repair and scar formation. Initially, injured myocardium releases pro-inflammatory cytokines such as IL-1, IL-6, IL-8, TNF, and CCL2, which promote the recruitment of neutrophils and monocytes into the myocardium. Monocyte infiltration is crucial for both the inflammatory and reparative phases. However, excessive inflammation can adversely affect LV remodelling, potentially leading to HF.²⁴ CCR2⁺ monocytes are activated monocytes that abound during the first inflammatory peak after MI. They are recruited by the heart, where they differentiate into pro-inflammatory CCR2⁺ macrophages that resemble classically M1 macrophages²⁵ and promote pathogenic adverse cardiac remodelling and dysfunction post-MI.^{26,27} Our study is the first to suggest that empagliflozin could decrease circulating inflammatory CCR2⁺ monocytes after MI, potentially leading to a better prognosis regarding its progression. In line with this inference, previous

studies have shown that empagliflozin decreases expression of the CCR2 ligand (monocyte-chemotactic protein-1/CCL2),^{28,29} as well as reducing the presence of pro-inflammatory M1 macrophages and promoting a shift to the anti-inflammatory M2 phenotype in white adipose tissue in a mouse model of obesity and in a macrophage cell line.^{30,31}

Inflammasomes are large multiprotein cytoplasmic complexes that play a crucial role in the acute MI inflammation process, activating release of pro-inflammatory cytokines such as IL-1 β and IL-18, which are involved in IL-1 receptor activation. IL-1 receptor activation is linked to inflammation and results in cardiomyocyte apoptosis via caspase-1–dependent death (pyroptosis), contributing to adverse cardiac remodelling and post-MI HF development.³² The IL-1 pathway represents a potential target for interventions to modulate the post-MI inflammatory response. Different recombinant IL-1 receptor antagonists have been developed that yield improvements in post-MI healing and prevent adverse remodelling, as well as HF progression.³³ Our results suggest that empagliflozin could attenuate inflammasome activation, with a remarkable trend towards reduced IL-1 β and IL-18 and increased secretion of an antagonist of IL-1R (IL-1Ra). This effect also has been reported in other preclinical^{34,35} and clinical³⁶ studies, in HF and cardiotoxicity scenarios, constituting one of the proposed mechanisms of action of empagliflozin in inflammatory pathways. Although we did not observe further immunomodulatory effects in our swine experimental model, other studies have shown additional anti-inflammatory effects of empagliflozin, including the reduction of inflammatory C-reactive protein, IL-6, TNF- α , monocyte-chemotactic protein-1, and interferon- γ expression.^{28,37}

The reason for the lack of these anti-inflammatory effects in the combined treatment group (empagliflozin+sac/val) is unclear. In a previous study,¹⁴ we found that sac/val exerted an acute anti-inflammatory response after MI, and we thus predicted a more powerful anti-inflammatory effect in the combined group. Given that empagliflozin and sac/val target different pathways, a negative synergistic effect between them seems unlikely. Future studies are needed to elucidate this finding.

Empagliflozin and cardiac oxidative stress

Empagliflozin is postulated to have antioxidant actions. Different sources give rise to NO, including iNOS, which is controlled by inflammatory mediators and cytokines, has pro-inflammatory properties, and plays an important role in chronic inflammatory diseases. Another NO source is eNOS, which is constitutively expressed in endothelium and preserves homeostasis between the endothelium and immune cells. Several studies have shown that NO derived from eNOS plays a protective role in MI, possibly by promoting angiogenesis, together with inhibiting inflammatory pathways.³⁸ In our study, compared to controls, the empagliflozin group showed reduced systemic inflammation, increased levels of NO, and increased expression of the activated form of eNOS (phosphorylated eNOS). The increased eNOS levels in the myocardium with empagliflozin could be partially related to the reduced leukocyte diapedesis,³⁹ leading to lower circulating leukocytes in these animals.

Empagliflozin and sac/val effects on cardiometabolism

Empagliflozin is suggested to influence cardiac metabolism by activating nutrient deprivation pathways such as gluconeogenesis and ketogenesis.⁴⁰ In energy surplus conditions, such as type 2 diabetes mellitus and chronic HF, nutrient deprivation sensors are typically suppressed. SGLT2is stimulate them via the SIRT1/PGC-1 α /FGF21 signalling pathway, showing significant cardioprotective effects across different experimental models.⁴¹ Their actions are linked to a reduction in oxidative stress and promotion of autophagy, a process that eliminates dysfunctional organelles, thereby mitigating cellular damage. In our study, empagliflozin-treated animals showed increased levels of SIRT1 protein in the infarct zone. However, there was no subsequent increase in the downstream mediators PGC1 α and FGF21, indicating that the SIRT1/PGC-1 α /FGF21 metabolic pathway was not activated. SIRT1 not only control genes and proteins involved in metabolism but also serves as a master regulator for numerous genes, including in inflammatory pathways. In addition, SIRT1 has been associated with anti-inflammatory actions in macrophages⁴² via suppression of the NF- κ B signalling pathway in MI-injured hearts,⁴³ as well as with inflammasome activation in ischemic stroke.⁴⁴ The fact that the empagliflozin group exhibited more SIRT1 in the infarct core could be partially associated with the reduced inflammation in this group. Empagliflozin is also postulated to normalize myocardial substrate metabolism from the pathological use of glucose to the normal use of free fatty acids.¹² In contrast to these findings, our study showed no effect of empagliflozin with or without sac/val on systemic free fatty acid or ketone body levels, as assessed by proton nuclear magnetic resonance. Additionally, we did not detect any changes in the

expression of genes associated with substrate use, including GLUT4 and PDK4, in either the infarcted or remote heart zones.

In the present study, though, empagliflozin-treated animals presented increased cardioprotective lipid levels in the liver, including omega w3 and w6+w7, DHA, and ARA+EPA. The liver regulates energy metabolism and serves as a central hub for metabolic interactions with different tissues.⁴⁵ Omega lipids have been linked to anti-inflammatory, anti-fibrotic, and anti-arrhythmic properties.⁴⁶ In particular, several studies have shown that w3 suppresses inflammasome activation.⁴⁷ EPA and DHA, different types of w3 lipids, are associated with anti-fibrotic properties and seem to enhance the production of beneficial NO from eNOS.⁴⁸ At the systemic level, we observed a clear effect of empagliflozin+sac/val treatment on modulating triglyceride metabolism, which progressively increased in terms of total triglycerides and triglycerides transported by lipoproteins. Although elevated triglyceride levels are often linked to an increased CV risk, they can be a sign of a greater dietary intake. Our study involved animals in the growth stage (3 months of age) and, furthermore, the increased triglyceride metabolism was not associated with a rise in the inflammatory (glycoprotein) profile of the animals that typically is present in the atherosclerotic condition. For these reasons, at least in part, we attribute the observed triglyceride increase to improved dietary intake, so that it could have been a positive indicator of animal well-being and quality of life.

Empagliflozin and sac/val effects on fibrosis, cardiac function, VT substrate, and arrhythmic risk

In contrast to previous studies,⁴⁹ we found no significant improvements in cardiac function parameters in the empagliflozin group, as assessed by CMR. However, in the combined treatment group, we observed improved LV compliance properties (iLVEDV and LVSV), which may be linked to the reduced fibrotic response in this group (lower Col I and Col I/III ratio). Although LVEF improved the most in this group, the increase was not statistically significant, suggesting the need for a larger sample size.

Imaging has a key role in arrhythmic risk stratification. Factors such as scar size, BZ mass, and BZ corridors (representing heterogeneous scarring with dissimilar conduction and excitability, promoting re-entry) have been associated with an increased incidence of VA.^{50,51} Invasive mapping provides relevant information regarding arrhythmic risk, and BZ area and the presence of pathological electrograms and DZ have been associated with VA. Our study showed no impact of empagliflozin in any of these parameters, with no modification of 30-day induced VA risk after MI. In contrast, clinical studies have shown a trend towards reduced incident VA in HF patients treated with SGLT2is.⁵² It seems plausible that empagliflozin could modulate the arrhythmogenic substrate through its anti-inflammatory properties, and larger studies are needed to confirm this hypothesis.

The combination of empagliflozin with sac/val reduced the composite endpoint of CV death or VT inducibility at 30 days post-MI. Multiple factors may underlie this finding, including favourable electrical scar remodelling with fewer conduction abnormalities (fewer CMR-BZ corridors and DZ) and

less myocardial fibrosis (less Col I, lower Col I/III ratio and CVF). These findings were not reproduced in the empagliflozin group, suggesting that the effects are attributable to the sac/val treatment. In a previous pre-clinical study with a porcine model of MI, we found that sac/val reduced VT induction after MI, total scar mass, BZ corridors, and DZs, suggesting that this drug may have powerful anti-arrhythmic properties.¹⁴ These findings were ascribed to multiple mechanisms, including reduced acute systemic inflammation and lower collagen deposition.

The scar formation process and collagen composition are important in modulating LV remodelling. Previous data suggest that an increased Col I/III ratio promotes reduced elasticity of the LV wall ratio and contributes to LV adverse remodelling, affecting cardiac function.⁵³ Our results are consistent with several clinical studies demonstrating an effect of sac/val on reverse cardiac remodelling, VA events, and implantable cardioverter defibrillator shocks in HF patients despite no impact on LVEF.¹³ Other studies have shown improved cardiac function parameters with sac/val treatment in a post-MI scenario.⁵⁴ Given these mixed findings, further studies are needed.

Our results from the *in vitro* sub-study suggest that combined treatment with empagliflozin and sac/val, administered both before and after H₂O₂ injury, preserves cell viability. These findings open the door to further research into whether these medications could have a protective effect when administered before and after an ischemic event.

In summary, we found that empagliflozin played an important role in modulating the acute inflammatory response post-MI, NO bioavailability,

metabolomic content in the liver, and changes in collagen composition of the scar, but not sufficiently to improve cardiac function and reduce the propensity to VA at 30 days post-MI. However, the combination of empagliflozin treatment with sac/val showed greater therapeutic potential, resulting in improvements in myocardial fibrosis, LV remodelling, and reduced VA inducibility.

Conclusions

Early initiation of empagliflozin after MI exerts an acute immunomodulatory effect, modulates NO bioavailability and collagen composition of the scar, and increases cardioprotective lipid levels in the liver, without affecting cardiac function and VA inducibility. Combined treatment with empagliflozin and sac/val promotes a reduction in Col I and the Col I/III ratio in the scar, stimulates favourable electrical and structural remodelling, and leads to reduced VT inducibility post-MI.

Study limitations

Animals received only BB as the baseline HF treatment. Whether the addition of other HF medication would have affected the results is unclear and requires further investigation. The sex subgroup analysis was limited by the total number of the animals per group.

Funding

This work was supported in part by grants from the Spanish Ministry of Economy and Competitiveness-MICIU (PID2021-124703OB-I00) and the Instituto de Salud Carlos III under Grants CIBERCV (CB16/11/00403) and Red

RICORS (PI21/01703) as a part of the Plan Nacional de I+D+I, and was co-funded by ISCIII-Subdirección General de Evaluación y el Fondo Europeo de Desarrollo Regional (FEDER), AGAUR Generalitat de Catalunya (2021-SGR-01437), and Institut Català de Salut. This work also was supported by a grant from the JMC Legacy Research Fund of Germans Trias i Pujol University Hospital (2021_45) and by Boehringer Ingelheim España, S.A.

Acknowledgements

This work was possible thanks to the core facilities of the Germans Trias i Pujol Research Institute, with special thanks to the Flow Cytometry and Microscopy units, and the Comparative Medicine and Bioimage Center of Catalonia (CMCiB). The AC16 cardiomyocyte cell line was generously donated by Dr. Josep Julve, Department of Endocrinology & Nutrition, Institut de Recerca SANT PAU, Barcelona, for strictly scientific purposes and under nonprofit conditions.

Disclosures

This work was partially funded by Boehringer Ingelheim through an unrestricted grant with Germans Trias i Pujol Health Science Research Institute Foundation. Boehringer Ingelheim (BI) was given the opportunity to review the manuscript for medical and scientific accuracy as well as intellectual property considerations in relation to potential mention of BI substances.

Victoria Delgado has received speaker fees from Abbott Vascular, Edwards Lifesciences, GE Healthcare, Medtronic, Novartis, JenaValve, and Philips and consulting fees from Edwards Lifesciences, MSD, and Novo Nordisk.

Antoni Bayes-Genis has lectured and/or participated in ad boards for Abbott, AstraZeneca, Bayer, Boehringer Ingelheim, Medtronic, Novartis, Novo Nordisk, Roche Diagnostics, and Vifor. Felipe Bisbal has received speaker fees from Abbott, Biosense Webster, and Biotronik and consulting fees from Abbott. Gemma Ferrer-Curriu has received fees from Boehringer Ingelheim.

References

1. Lippi G, Sanchis-Gomar F. Global epidemiology and future trends of heart failure. *AME Medical Journal*. 2020;5(0). doi:10.21037/amj.2020.03.03
2. Gerber Y, Weston SA, Enriquez-Sarano M, et al. Mortality Associated With Heart Failure After Myocardial Infarction: A Contemporary Community Perspective. *Circ Heart Fail*. 2016;9(1):e002460. doi:10.1161/CIRCHEARTFAILURE.115.002460
3. Zhang Q, Wang L, Wang S, et al. Signaling pathways and targeted therapy for myocardial infarction. *Signal Transduct Target Ther*. 2022;7:78. doi:10.1038/s41392-022-00925-z
4. Azevedo PS, Polegato BF, Minicucci MF, Paiva SAR, Zornoff LAM. Cardiac Remodeling: Concepts, Clinical Impact, Pathophysiological Mechanisms and Pharmacologic Treatment. *Arq Bras Cardiol*. 2016;106(1):62-69. doi:10.5935/abc.20160005
5. Bauersachs J. Heart failure drug treatment: the fantastic four. *Eur Heart J*. 2021;42(6):681-683. doi:10.1093/eurheartj/ehaa1012
6. Bunsawat K, Ratchford SM, Alpenglow JK, et al. Sacubitril-valsartan improves conduit vessel function and functional capacity and reduces inflammation in heart failure with reduced ejection fraction. *J Appl Physiol (1985)*. 2021;130(1):256-268. doi:10.1152/jappphysiol.00454.2020
7. Liu LW, Wu PC, Chiu MY, Tu PF, Fang CC. Sacubitril/Valsartan Improves Left Ventricular Ejection Fraction and Reverses Cardiac Remodeling in Taiwanese Patients with Heart Failure and Reduced Ejection Fraction. *Acta Cardiologica Sinica*. 2020;36(2):125. doi:10.6515/ACS.202003_36(2).20190812A
8. von Lueder TG, Wang BH, Kompa AR, et al. Angiotensin receptor neprilysin inhibitor LCZ696 attenuates cardiac remodeling and dysfunction after myocardial infarction by reducing cardiac fibrosis and hypertrophy. *Circ Heart Fail*. 2015;8(1):71-78. doi:10.1161/CIRCHEARTFAILURE.114.001785
9. Packer M, Anker SD, Butler J, et al. Cardiovascular and Renal Outcomes with Empagliflozin in Heart Failure. *N Engl J Med*. 2020;383(15):1413-1424. doi:10.1056/NEJMoa2022190
10. Anker SD, Butler J, Filippatos G, et al. Empagliflozin in Heart Failure with a Preserved Ejection Fraction. *N Engl J Med*. 2021;385(16):1451-1461. doi:10.1056/NEJMoa2107038
11. Myasoedova VA, Bozzi M, Valerio V, et al. Anti-Inflammation and Anti-Oxidation: The Key to Unlocking the Cardiovascular Potential of SGLT2 Inhibitors and GLP1 Receptor Agonists. *Antioxidants*. 2024;13(1):16. doi:10.3390/antiox13010016
12. Santos-Gallego CG, Requena-Ibanez JA, San Antonio R, et al. Empagliflozin Ameliorates Adverse Left Ventricular Remodeling in Nondiabetic Heart Failure by Enhancing Myocardial Energetics. *J Am Coll Cardiol*. 2019;73(15):1931-1944. doi:10.1016/j.jacc.2019.01.056
13. de Diego C, González-Torres L, Núñez JM, et al. Effects of angiotensin-neprilysin inhibition compared to angiotensin inhibition on ventricular arrhythmias in reduced ejection fraction patients under continuous remote monitoring of

- implantable defibrillator devices. *Heart Rhythm*. 2018;15(3):395-402. doi:10.1016/j.hrthm.2017.11.012
14. Martínez-Falguera D, Aranyó J, Teis A, et al. Antiarrhythmic and Anti-Inflammatory Effects of Sacubitril/Valsartan on Post-Myocardial Infarction Scar. *Circ Arrhythm Electrophysiol*. 2024;17(5):e012517. doi:10.1161/CIRCEP.123.012517
15. Sfairopoulos D, Liu T, Zhang N, et al. Association between sodium-glucose cotransporter-2 inhibitors and incident atrial fibrillation/atrial flutter in heart failure patients with reduced ejection fraction: a meta-analysis of randomized controlled trials. *Heart Fail Rev*. 2023;28(4):925-936. doi:10.1007/s10741-022-10281-3
16. Butler J, Jones WS, Udell JA, et al. Empagliflozin after Acute Myocardial Infarction. *N Engl J Med*. 2024;390(16):1455-1466. doi:10.1056/NEJMoa2314051
17. Hernandez AF, Udell JA, Jones WS, et al. Effect of Empagliflozin on Heart Failure Outcomes After Acute Myocardial Infarction: Insights From the EMPACT-MI Trial. *Circulation*. 2024;149(21):1627-1638. doi:10.1161/CIRCULATIONAHA.124.069217
18. *Guide for the Care and Use of Laboratory Animals: Eighth Edition*. National Academies Press; 2011. doi:10.17226/12910
19. Martínez-Falguera D, Fadeuilhe E, Teis A, et al. Myocardial Infarction by Percutaneous Embolization Coil Deployment in a Swine Model. *J Vis Exp*. 2021;(177). doi:10.3791/63172
20. Fernández-Armenta J, Berruezo A, Andreu D, et al. Three-dimensional architecture of scar and conducting channels based on high resolution ce-CMR: insights for ventricular tachycardia ablation. *Circ Arrhythm Electrophysiol*. 2013;6(3):528-537. doi:10.1161/CIRCEP.113.000264
21. Soto-Iglesias D, Penela D, Jáuregui B, et al. Cardiac Magnetic Resonance-Guided Ventricular Tachycardia Substrate Ablation. *JACC Clin Electrophysiol*. 2020;6(4):436-447. doi:10.1016/j.jacep.2019.11.004
22. Perez-David E, Arenal A, Rubio-Guivernau JL, et al. Noninvasive identification of ventricular tachycardia-related conducting channels using contrast-enhanced magnetic resonance imaging in patients with chronic myocardial infarction: comparison of signal intensity scar mapping and endocardial voltage mapping. *J Am Coll Cardiol*. 2011;57(2):184-194. doi:10.1016/j.jacc.2010.07.043
23. Jimenez Trinidad FR, Arrieta Ruiz M, Solanes Batlló N, et al. Linking In Vitro Models of Endothelial Dysfunction with Cell Senescence. *Life (Basel)*. 2021;11(12):1323. doi:10.3390/life11121323
24. Frangogiannis NG. Regulation of the inflammatory response in cardiac repair. *Circ Res*. 2012;110(1):159-173. doi:10.1161/CIRCRESAHA.111.243162
25. Li L, Cao J, Li S, et al. M2 Macrophage-Derived sEV Regulate Pro-Inflammatory CCR2+ Macrophage Subpopulations to Favor Post-AMI Cardiac Repair. *Adv Sci (Weinh)*. 2023;10(14):2202964. doi:10.1002/advs.202202964
26. Bajpai G, Schneider C, Wong N, et al. The human heart contains distinct macrophage subsets with divergent origins and functions. *Nat Med*. 2018;24(8):1234-1245. doi:10.1038/s41591-018-0059-x
27. Yerra VG, Advani A. Role of CCR2-Positive Macrophages in Pathological

- Ventricular Remodelling. *Biomedicines*. 2022;10(3):661. doi:10.3390/biomedicines10030661
28. Theofilis P, Sagris M, Oikonomou E, et al. The impact of SGLT2 inhibitors on inflammation: A systematic review and meta-analysis of studies in rodents. *Int Immunopharmacol*. 2022;111:109080. doi:10.1016/j.intimp.2022.109080
29. Aragón-Herrera A, Feijóo-Bandín S, Otero Santiago M, et al. Empagliflozin reduces the levels of CD36 and cardiotoxic lipids while improving autophagy in the hearts of Zucker diabetic fatty rats. *Biochem Pharmacol*. 2019;170:113677. doi:10.1016/j.bcp.2019.113677
30. Xu L, Nagata N, Nagashimada M, et al. SGLT2 Inhibition by Empagliflozin Promotes Fat Utilization and Browning and Attenuates Inflammation and Insulin Resistance by Polarizing M2 Macrophages in Diet-induced Obese Mice. *EBioMedicine*. 2017;20:137-149. doi:10.1016/j.ebiom.2017.05.028
31. Lee N, Heo YJ, Choi SE, et al. Anti-inflammatory Effects of Empagliflozin and Gemigliptin on LPS-Stimulated Macrophage via the IKK/NF- κ B, MKK7/JNK, and JAK2/STAT1 Signalling Pathways. *J Immunol Res*. 2021;2021:9944880. doi:10.1155/2021/9944880
32. Ong SB, Hernández-Reséndiz S, Crespo-Avilan GE, et al. Inflammation following acute myocardial infarction: Multiple players, dynamic roles, and novel therapeutic opportunities. *Pharmacol Ther*. 2018;186:73-87. doi:10.1016/j.pharmthera.2018.01.001
33. Abbate A, Salloum FN, Vecile E, et al. Anakinra, a recombinant human interleukin-1 receptor antagonist, inhibits apoptosis in experimental acute myocardial infarction. *Circulation*. 2008;117(20):2670-2683. doi:10.1161/CIRCULATIONAHA.107.740233
34. Quagliariello V, De Laurentiis M, Rea D, et al. The SGLT-2 inhibitor empagliflozin improves myocardial strain, reduces cardiac fibrosis and pro-inflammatory cytokines in non-diabetic mice treated with doxorubicin. *Cardiovasc Diabetol*. 2021;20(1):150. doi:10.1186/s12933-021-01346-y
35. Byrne NJ, Matsumura N, Maayah ZH, et al. Empagliflozin Blunts Worsening Cardiac Dysfunction Associated With Reduced NLRP3 (Nucleotide-Binding Domain-Like Receptor Protein 3) Inflammasome Activation in Heart Failure. *Circ Heart Fail*. 2020;13(1):e006277. doi:10.1161/CIRCHEARTFAILURE.119.006277
36. Kim SR, Lee SG, Kim SH, et al. SGLT2 inhibition modulates NLRP3 inflammasome activity via ketones and insulin in diabetes with cardiovascular disease. *Nat Commun*. 2020;11(1):2127. doi:10.1038/s41467-020-15983-6
37. Gohari S, Reshadmanesh T, Khodabandehloo H, et al. The effect of EMPAgliflozin on markers of inflammation in patients with concomitant type 2 diabetes mellitus and Coronary ARtery Disease: the EMPA-CARD randomized controlled trial. *Diabetol Metab Syndr*. 2022;14(1):170. doi:10.1186/s13098-022-00951-5
38. Gentile C, Kesteven S, Wu J, et al. 16 - Endothelial nitric oxide synthase plays a protective role against myocardial infarction. *Free Radical Biology and Medicine*. 2018;128:S26. doi:10.1016/j.freeradbiomed.2018.10.018

39. Cirino G, Fiorucci S, Sessa WC. Endothelial nitric oxide synthase: the Cinderella of inflammation? *Trends in Pharmacological Sciences*. 2003;24(2):91-95. doi:10.1016/S0165-6147(02)00049-4
40. Trang NN, Chung CC, Lee TW, et al. Empagliflozin and Liraglutide Differentially Modulate Cardiac Metabolism in Diabetic Cardiomyopathy in Rats. *Int J Mol Sci*. 2021;22(3):1177. doi:10.3390/ijms22031177
41. Packer M. Cardioprotective Effects of Sirtuin-1 and Its Downstream Effectors: Potential Role in Mediating the Heart Failure Benefits of SGLT2 (Sodium-Glucose Cotransporter 2) Inhibitors. *Circ Heart Fail*. 2020;13(9):e007197. doi:10.1161/CIRCHEARTFAILURE.120.007197
42. Yoshizaki T, Schenk S, Imamura T, et al. SIRT1 inhibits inflammatory pathways in macrophages and modulates insulin sensitivity. *Am J Physiol Endocrinol Metab*. 2010;298(3):E419-428. doi:10.1152/ajpendo.00417.2009
43. Wei N, Zhang C, He H, et al. Protective effect of saponins extract from *Panax japonicus* on myocardial infarction: involvement of NF- κ B, Sirt1 and mitogen-activated protein kinase signalling pathways and inhibition of inflammation. *J Pharm Pharmacol*. 2014;66(11):1641-1651. doi:10.1111/jphp.12291
44. Zhang S, Jiang L, Che F, Lu Y, Xie Z, Wang H. Arctigenin attenuates ischemic stroke via SIRT1-dependent inhibition of NLRP3 inflammasome. *Biochem Biophys Res Commun*. 2017;493(1):821-826. doi:10.1016/j.bbrc.2017.08.062
45. Rui L. Energy metabolism in the liver. *Compr Physiol*. 2014;4(1):177-197. doi:10.1002/cphy.c130024
46. Endo J, Arita M. Cardioprotective mechanism of omega-3 polyunsaturated fatty acids. *J Cardiol*. 2016;67(1):22-27. doi:10.1016/j.jjcc.2015.08.002
47. Yan Y, Jiang W, Spinetti T, et al. Omega-3 fatty acids prevent inflammation and metabolic disorder through inhibition of NLRP3 inflammasome activation. *Immunity*. 2013;38(6):1154-1163. doi:10.1016/j.immuni.2013.05.015
48. Chen J, Shearer GC, Chen Q, et al. Omega-3 fatty acids prevent pressure overload-induced cardiac fibrosis through activation of cyclic GMP/protein kinase G signaling in cardiac fibroblasts. *Circulation*. 2011;123(6):584-593. doi:10.1161/CIRCULATIONAHA.110.971853
49. Omar M, Jensen J, Ali M, et al. Associations of Empagliflozin With Left Ventricular Volumes, Mass, and Function in Patients With Heart Failure and Reduced Ejection Fraction: A Substudy of the Empire HF Randomized Clinical Trial. *JAMA Cardiol*. 2021;6(7):836-840. doi:10.1001/jamacardio.2020.6827
50. Schmidt A, Azevedo CF, Cheng A, et al. Infarct tissue heterogeneity by magnetic resonance imaging identifies enhanced cardiac arrhythmia susceptibility in patients with left ventricular dysfunction. *Circulation*. 2007;115(15):2006-2014. doi:10.1161/CIRCULATIONAHA.106.653568
51. Jáuregui B, Soto-Iglesias D, Penela D, et al. Cardiovascular magnetic resonance determinants of ventricular arrhythmic events after myocardial infarction. *Europace*. 2022;24(6):938-947. doi:10.1093/europace/euab275
52. Fernandes GC, Fernandes A, Cardoso R, et al. Association of SGLT2 inhibitors with arrhythmias and sudden cardiac death in patients with type 2 diabetes or heart

failure: A meta-analysis of 34 randomized controlled trials. *Heart Rhythm*. 2021;18(7):1098-1105. doi:10.1016/j.hrthm.2021.03.028

53. Uchinaka A, Yoshida M, Tanaka K, et al. Overexpression of collagen type III in injured myocardium prevents cardiac systolic dysfunction by changing the balance of collagen distribution. *J Thorac Cardiovasc Surg*. 2018;156(1):217-226.e3. doi:10.1016/j.jtcvs.2018.01.097

54. Zhang D, Wu H, Liu D, et al. Clinical efficacy of sacubitril-valsartan combined with acute ST-segment elevation myocardial infarction after reperfusion: A systematic review and meta-analysis. *Front Cardiovasc Med*. 2022;9:1036151. doi:10.3389/fcvm.2022.1036151

Supplementary material

METHODS

Histopathological and immunohistochemical analysis

Olympus CKX41, Leica DMI6000B, and Axio-Observer Z1 confocal (Zeiss, Oberkochen, Baden-Württemberg, Germany) microscopes were used for anatomopathological, histological, and immunofluorescence analyses, respectively. Interstitial collagen, vascular density, and TOM20- and SERCA2-positive areas were quantified using Image-Pro Plus software (Media Cybernetics, Rockville, Maryland, United States). CD3+, CD25+/CD3+, and CD163+ cell quantification was performed manually by two independent investigators.

Myocardial oxidative stress analyses

For western blot analysis, 50 µg of protein from the infarct and remote zones was electrophorized in 7.5% gels and transferred to nitrocellulose membranes (Amersham). Membranes were incubated with the following antibodies: anti-inducible NOS (iNOS) (NOS2, 1:1000, Novus Biologicals, Centennial, Colorado, USA), anti-endothelial NOS (eNOS) (NOS3, 1:1000; Cell Signalling, Danvers, Massachusetts, USA), activated phosphorylated eNOS (S1177,1:1000; Cell Signalling, Danvers, Massachusetts, USA), anti- Sirt1 (1:1000; Proteintech, Rosemont, Illinois, USA), anti-PGC1α (1:10000; Proteintech, Rosemont, Illinois, USA), anti-FGF21 (1:500; Abyntek, Zamudio, Bizkaia, Spain), and anti α-tubulin (1:1000; Sigma Aldrich, Burlington, Massachusetts, USA). Images were acquired with a LI-COR Odyssey (Li-Cor

Biosciences, Lincoln, Nebraska, USA) and analysed with Image J software, using α -tubulin as endogenous reference.

Gene expression analyses of myocardial inflammation, oxidative stress, metabolism, and fibrosis

Myocardial frozen tissue samples from the infarct core (74.67 ± 14.96 mg) and remote area (75.82 ± 14.25 mg) were mechanically homogenized using the TissueRuptor (Qiagen, Venlo, The Netherlands) in cold TriPure Isolation reagent (Merck, Rahway, New Jersey, USA). One microgram of RNA was then retrotranscribed to cDNA using the High-Capacity cDNA Reverse Transcription kit (Applied Biosystems, Waltham, Massachusetts, USA). Data were evaluated in a LightCycler[®] 480 Real-Time PCR System (Roche, Basel, Switzerland). Gene expression levels were determined using the $2^{-\Delta Ct}$ method,¹ normalizing to *PGK1* (TaqMan[®] FAM-MGB probes; Thermo Fisher Scientific, Waltham, Massachusetts, USA) as the endogenous gene.

¹H-NMR Metabolomic characterization of pig serum samples

Frozen pig serum samples were shipped on dry ice to Biosfer Teslab (Reus, Spain) for the proton nuclear magnetic resonance (¹H-[NMR]) spectrometry analysis. Briefly, 50 μ L of each serum sample was added to a standardized 150 μ L humanized serum buffer and diluted with 50 μ L deuterated water (D₂O) and 300 μ L of 50 mM phosphate-buffered saline (PBS) at pH 7.4 into a 5-mm \emptyset NMR glass tube. ¹H-NMR spectra were recorded at 306 K on an Avance III-500 Bruker spectrometer (Bruker BioSciences Española S.A., Rivas Vaciamadrid, Madrid, Spain) operating at a proton frequency of 500.13 MHz (11.7 T).

Lipoprotein analysis by NMR spectroscopy (advanced lipoprotein profile)

The lipoprotein profile was analysed using the NMR-based Liposcale[®] test. The lipid concentrations (i.e., triglycerides and cholesterol), size, and particle number of the four main classes of lipoproteins (intermediate-density lipoprotein [IDL], very low-density lipoprotein [VLDL], low-density lipoprotein [LDL], high-density lipoprotein [HDL]), as well as the particle number of nine subclasses (large, medium, and small VLDL, LDL, and HDL) were determined as previously reported.² Each subclass particle concentration was calculated by dividing the lipid volume by the particle volume of a given class. Lipid volumes were determined using common conversion factors to convert concentration units into volume units.³ Finally, weighted average VLDL, LDL, and HDL particle sizes were calculated from various subclass concentrations by summing the known diameter of each subclass multiplied by its relative percentage of subclass particle number.

Glycoprotein profiling by using ¹H-NMR spectroscopy

The glycoprotein profile was determined by analysing the region of the ¹H-NMR spectrum where the glycoproteins resonated (2.15–1.90 ppm) using several analytical functions according to a previously published procedure.⁴ H/W ratios of GlycA and GlycB were also reported as parameters associated with the aggregation state of the sugar–protein bonds.⁵ Height was calculated as the difference from baseline to maximum of the corresponding NMR peaks, and the width value corresponds to the peak width at half height.

Low-molecular-weight metabolites analysis

Low-molecular-weight metabolites (LMWMs) were identified and quantified in the 1D Carr-Purcell-Meiboom-Gill spectra using an adaptation of Dolphin.⁶

Each metabolite was identified by checking for all its resonances along the spectra, and then quantified using line–shape fitting methods on one of its signals.⁷

Lipid extraction

After ¹H-NMR metabolomic characterization, the diluted pig serum samples were lyophilized and then diluted with 100 μL of 50 mM PBS at pH 7.4 before lipid extraction using the BUME⁸ method with slight modifications. BUME was optimized for each batch of extractions with di-isopropyl ether replacing heptane as the organic solvent. This procedure was performed with a BRAVO liquid handling robot with the capacity to extract 96 samples at once. The upper lipophilic phase was completely dried in a Speedvac until evaporation of organic solvents and frozen at -80 °C until NMR analysis. Lipid extracts were reconstituted in a solution of CDCl₃:CD₃OD:D₂O (16:7:1, v/v/v) containing tetramethylsilane at 1.18 mM as a chemical shift reference and transferred into 5-mm Ø NMR glass tubes. ¹H-NMR spectra were recorded at 286 K operating at a proton frequency of 600.20 MHz using an Avance III-600 Bruker spectrometer. A 90° pulse with a water pre-saturation sequence was used. Quantification of lipid signals in the ¹H-NMR spectra was carried out with LipSpin,⁹ an in-house software based on MATLAB. Resonance assignments were done on the basis of literature values.¹⁰

¹H-NMR characterization of pig liver and heart tissues

Aqueous and lipid extracts were obtained from pig liver or heart tissues using the Folch method with slight modifications.¹¹ Briefly, 950 μL of dichloromethane:methanol (2:1, v/v) was added to 20 mg of previously lyophilized tissue followed by three 5-min sonication steps with one shaking

step in between. Next, 395 μL of ultrapure water was added, mixed and centrifuged at 25,100 g during 5 min at 4 °C. Aqueous and lipid extracts were recovered and completely dried in a Speedvac to achieve solvent evaporation and frozen at -80 °C until ^1H -NMR analysis.

Aqueous extracts were reconstituted in a solution of 45 mM PBS containing 2.32 mM of trimethylsilylpropanoic acid (as a chemical shift reference) and transferred into 5-mm \emptyset NMR glass tubes. ^1H -NMR spectra were recorded at 300 K operating at a proton frequency of 600.20 MHz using an Avance III-600 Bruker spectrometer. LMWMs were identified and quantified in the 1D nuclear Overhauser effect spectroscopy with presaturation (NOESYPR1D). Resonance assignments were done on the basis of literature values.¹⁰

Lipid extracts were reconstituted in a solution of $\text{CDCl}_3:\text{CD}_3\text{OD}:\text{D}_2\text{O}$ (16:7:1, v/v/v) containing tetramethylsilane and transferred into 5-mm \emptyset NMR glass tubes. Quantification of lipid signals was performed as described above for pig serum samples.

Non-invasive CMR imaging

All imaging was performed in a 3T state-of-the-art imaging system (Vantage Galan 3T, Canon Medical Systems, Otawara, Tochigi, Japan) with all animals in prone position using a 16-element phased array coil (Atlas SPEEDER Body Coil) placed over the chest. Images were acquired during breath-holds with electrocardiographic gating. We used a segmented k-space steady state precession cine sequence (typically TR/TE 3.0/1.5 ms, 65° flip angle, field of view (FOV) 291 \times 265 mm, pixel matrix 352 \times 320, slice thickness 8 mm, 1302 Hz/pixel bandwidth) at 2, 3, and 4 chamber views and short axis from base to apex with no gap. Phase-contrast sequences (typically TR/TE 5.4/2.6 ms, 10°

flip angle, FOV 350 × 350 mm, slice thickness 8 mm, 130–200 cm/s VENC) were performed at the sino-tubular junction to calculate the aortic forward flow. Delayed enhancement images were acquired 10 to 20 min after IV injection of gadolinium-based contrast (Gd-DTPA; 0.2 mmol/kg) using a phase-sensitive inversion recovery sequence (TR/TE 8.9/3.4 ms, 20° flip angle, inversion time 180–250 ms, FOV 340 × 340 mm, pixel matrix 572 × 448, slice thickness 8 mm, 140 Hz/pixel bandwidth) matching cine image positions. Inversion time was optimized to null the normal myocardium.

All images were reviewed and analysed off-line using the CMR imaging (cMRI) dedicated analysis software (Medis) by a level 3 cMRI expert blinded to the clinical data. Left ventricular (LV) and right ventricular (RV) endocardial borders (papillary muscles excluded) were manually traced in all short-axis cine images at the end-diastolic and end-systolic frames to determine end-diastolic and end-systolic volumes (EDV and ESV, respectively), using QMass (Medis). LV mass was calculated by subtracting the endocardial volume from the epicardial volume at end diastole and then multiplying by tissue density (1.05 g/mL). Left and right ventricular ejection fractions (LVEF and RVEF, respectively) were calculated. Background noise correction was performed on all images. The endocardial and epicardial contours on delayed enhancement images were also outlined manually. Regions of interest were then manually traced in the hyperenhanced area at the place of maximum signal intensity and in the normal-appearing remote myocardium. As previously described, the areas of hyperenhanced myocardium were then automatically segmented by using a full-width at half-maximum algorithm with QMass. Two corrections were required for all automated regions of interest. First, microvascular obstruction (defined as hypointensity within a hyperintense region in subjects with infarctions) was adjusted to be included

as late gadolinium enhancement (LGE) if present. Second, any obvious blood pool or pericardial partial voluming and artefacts were further removed. Scar volume for each slice was calculated as scar area \times slice thickness.

Height, weight, and heart rate of the pigs was recorded at every cMRI scan. Volumes and mass were indexed by body surface area (BSA) of the animals calculated as previously described.¹² The cardiac index was calculated as (forward aortic volume \times heart rate)/BSA.

Cell culture, H₂O₂ model, ROS, and cell viability studies

AC16 cardiomyocytes were cultured in Dulbecco's Modified Eagle's Medium (DMEM)/Nutrient F-12 Ham (Thermo Fisher Scientific, Waltham, Massachusetts, USA) supplemented with 12% foetal bovine serum (FBS; Thermo Fisher Scientific, Waltham, Massachusetts, USA) and 100 U/mL penicillin/100 mg/mL streptomycin (Thermo Fisher Scientific, Waltham, Massachusetts, USA) in a humidified incubator at 37 °C with 21% O₂ and 5% CO₂. To induce oxidative stress, cells were treated for 1 h with 300 μ M hydrogen peroxide (H₂O₂, Sigma Aldrich, Burlington, Massachusetts, USA) diluted in DMEM/F-12 without phenol red (Thermo Fisher Scientific, Waltham, Massachusetts, USA) and without FBS.

ROS production was evaluated using fluorescent probes: 2,7-dichlorofluorescein diacetate (DCFHDA) for measuring intracellular ROS, including H₂O₂ and OH, and dihydroethidium (DHE) for detecting intracellular superoxide radical anion (O₂^{•-}). Immediately after H₂O₂ treatment, cells were washed twice with PBS and incubated with DCFHDA (50 μ M; Sigma-Aldrich, Burlington, Massachusetts, USA), DHE (50 μ M; Thermo Fisher Scientific, Waltham, Massachusetts, USA), and Hoechst (0.03 nM; Thermo Fisher Scientific, Waltham, Massachusetts, USA), diluted in fresh supplemented

DMEM/F12 with 0.04% FBS without phenol red, for 1 h in the dark. Fluorescence signals were measured using a Varioska™ Flash microplate reader (Thermo Fisher Scientific, Waltham, Massachusetts, USA) at the following excitation/emission wavelengths: 495/520 nm for DCFHDA, 518/606 nm for DHE, and 350/461 nm for Hoechst. The fluorescence signals of DCFHDA and DHE were standardized by Hoechst fluorescence, and the results were presented as fold change of fluorescence compared to control (untreated cells). For cell viability analysis, following the manufacturer's instructions, cells were incubated in alamarBlue reagent diluted 1:10 in DMEM/F12 supplemented with 0.04% FBS without phenol red, for 2 h at 37 °C in the dark. Fluorescence signal was then read at 560 nm with a Varioskan™ Flash microplate reader (Thermo Fisher Scientific, Waltham, Massachusetts, USA). Data were presented as fold change of fluorescence intensity relative to the negative control (non-treated cells).

Supplementary Tables

Supplementary Table 1. TaqMan probes (Thermo Fisher Scientific, Waltham, Massachusetts, USA) used in RT-PCR analysis

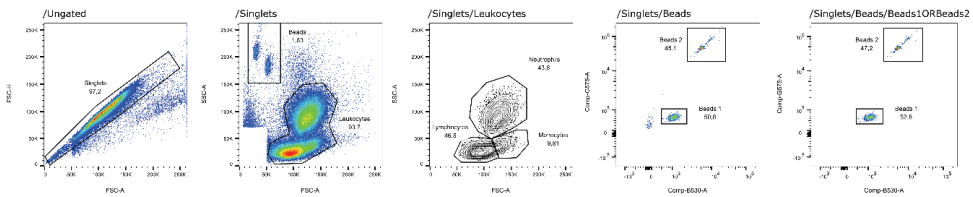
Gene transcript	TaqMan Probe	Amplicon Length	Exon boundary
IL-10	Ss03382372_u1	87	3-3
TNF- α	Ss03391318_g1	73	3-4
CCL2/MCP-1	Ss03394377_m1	58	1-2
NOS2	Ss03374608_u1	65	9-10
NOS3	Ss03383840_u1	77	-
SOD2	Ss03374828_m1	56	2-3
PRDX2	Ss04327514_g1	85	4-5
NOX4	Ss06909549_m1	79	-
GLUT4	Ss03373325_g1	75	-
PDK4	Ss03822089_s1	103	-
TGF- β 1	Ss04955543_m1	57	5-6
TGF- β 3	Ss03394351_m1	104	-
LRP1	Ss06917026_m1	57	4-5
MMP2	Ss03394318_m1	77	4-5
MMP9	Ss03392100_m1	58	12-13
TIMP1	Ss03381944_u1	105	5-5
PGK1	Ss03389144_m1	66	4-5

Abbreviations: IL-10, interleukin 10; TNF- α , tumour necrosis factor alpha; CCL2/MCP-1, chemokine (C-C motif) ligand 2 or monocyte chemoattractant protein 1; NOS2, nitric oxide synthase 2; NOS3, nitric oxide synthase 3; SOD2, superoxide dismutase 2; PRDX2, peroxiredoxin 2; NOX4, NADPH oxidase 4; GLUT4, glucose transporter 4; PDK4, pyruvate dehydrogenase kinase 4; TGF- β 1, transforming growth factor beta 1; TGF- β 3, transforming growth factor beta 3; LRP1, LDL receptor-related protein 1; MMP2, matrix metalloproteinase 2; MMP9, matrix metalloproteinase 9; TIMP1, tissue inhibitor of metalloproteinase 1; PGK1, phosphoglycerate kinase 1.

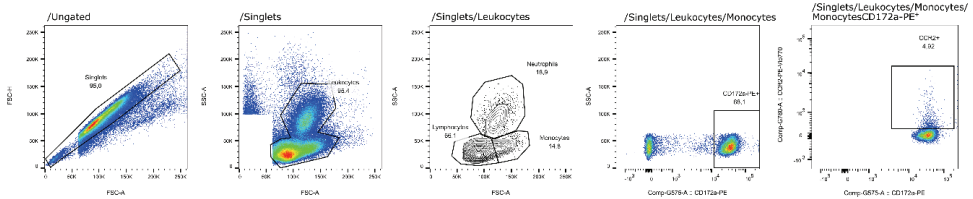
Supplementary Figures

Supplementary Figure 1. Cytometry gating strategy. (A) Singlets were gated according to FSC-A/FSC-H. Monocytes, leukocytes, and neutrophils were gated according to their complexity and size from the singlet/leukocyte population. For absolute cell number quantification, we used Perfect Count Microspheres beads (Cytognos, Santa Marta de Tormes, Salamanca, Spain). Cells were gated as a Boolean “OR” gate of the two beads populations defined by their FITC (B530-A channel) and phycoerythrin (G575-A channel) signal. A 50:50 ratio (45:55 maximum difference) was ensured in every assay, according to the manufacturer’s instructions. (B) Monocytes were gated according to their distinctive FSC-A/SSC-A appearance from the singlet/leukocyte population. Subsequently, the percentages of cells expressing each marker and the median fluorescence intensity in each channel were computed.

A



B



RESULTS

Supplementary Tables

Supplementary Table 2. Serum cardiac troponin I levels (pg/mL) in animals at baseline and 2 h after MI induction. Data are presented as mean \pm standard deviation. Statistical differences according to Kruskal–Wallis test of differential (2 h post-MI value – baseline value).

Group	Baseline	2 h post-MI	Differential	<i>P</i>
Control (n=8)	39.28 \pm	860.4 \pm	821.1 \pm	0.547
	45.86	1309	1314	
Empagliflozin (n=8)	33.51 \pm	2317 \pm	2284 \pm 5072	
	35.25	5067		
Empagliflozin+sac/val (n=8)	31.49 \pm	1177 \pm	1146 \pm 2518	
	26.18	2517		

Supplementary Table 3. Gene expression levels of fibrotic and inflammatory drivers and oxidative markers in the infarct and remote zones. Gene expression was calculated using the $\Delta\Delta C_t$ method relative to the endogenous gene *PGK1*. Differences between groups were calculated with a one-way ANOVA with Tukey post-hoc or Kruskal–Wallis with Dunn’s post-hoc, as appropriate. In the table, *P* values correspond to the *P* value from the ANOVA (+) or Kruskal–Wallis (#) test.

Infarct zone	Control (n=7)	Empagliflozin (n=8)	Empagliflozin+ sac/val (n=8)	<i>P</i>
TGF- β 1	0.49 \pm 0.21	0.58 \pm 0.20	0.61 \pm 0.23	0.664 ⁺
TGF- β 3	0.68 \pm 0.49	0.76 \pm 0.32	0.84 \pm 0.40	0.785 ⁺
LRP1	1.07 \pm 0.55	1.59 \pm 0.89	1.46 \pm 0.60	0.463 ⁺
MMP2	12.15 \pm 8.85	14.65 \pm 6.87	12.87 \pm 5.55	0.812 ⁺
MMP9	0.03 \pm 0.05	0.83 \pm 1.05	0.12 \pm 0.21	0.835 [#]
TIMP1	5.46 \pm 5.48	2.29 \pm 0.96	1.89 \pm 0.73	0.928 [#]
IL10	0.01 \pm 0.007	0.01 \pm 0.004	0.01 \pm 0.005	0.851 ⁺
TNF α	0.002 \pm 0.001	0.005 \pm 0.003	0.004 \pm 0.001	0.164 ⁺
CCL2/MCP-1	3.49 \pm 1.03	3.54 \pm 1.55	3.20 \pm 1.69	0.907 ⁺
CPT1A	0.24 \pm 0.15	0.20 \pm 0.78	0.33 \pm 0.14	0.161 ⁺
mTOR	0.20 \pm 0.08	0.19 \pm 0.09	0.24 \pm 0.08	0.589 [#]
PRKAA2	0.17 \pm 0.13	0.18 \pm 0.18	0.19 \pm 0.11	0.985 ⁺
GLUT4	0.18 \pm 0.04	0.20 \pm 0.04	0.23 \pm 0.08	0.350 ⁺
PDK4	3.14 \pm 2.37	2.30 \pm 1.46	2.46 \pm 2.62	0.794 ⁺
NOS2	0.046 \pm 0.02	0.057 \pm 0.02	0.05 \pm 0.01	0.505 ⁺
NOS3	0.19 \pm 0.09	0.18 \pm 0.06	0.20 \pm 0.1	0.860 ⁺
SOD2	1.02 \pm 0.46	0.91 \pm 0.45	0.76 \pm 0.41	0.613 ⁺
PRDX2	1.20 \pm 0.28	1.24 \pm 0.26	1.34 \pm 0.24	0.603 ⁺
NOX4	0.17 \pm 0.13	0.14 \pm 0.07	0.18 \pm 0.070	0.700 ⁺

Remote zone	Control (n=7)	Empagliflozin (n=8)	Empagliflozin+ sac/val (n=8)	<i>P</i>
TGF- β 1	0.14 \pm 0.03	0.15 \pm 0.03	0.17 \pm 0.04	0.221 [#]
TGF- β 3	0.03 \pm 0.01	0.03 \pm 0.01	0.04 \pm 0.02	0.434 ⁺
LRP1	0.10 \pm 0.03	0.12 \pm 0.02	0.15 \pm 0.08	0.242 ⁺

Material, Methods & Results

MMP2	0.72 ± 0.24	0.87 ± 0.23	0.73 ± 0.22	0.439 ⁺
MMP9	0.001 ± 0.0002	0.001 ± 0.0003	0.001 ± 0.001	0.765 [#]
TIMP1	0.11 ± 0.08	0.11 ± 0.05	0.12 ± 0.09	0.724 [#]
IL10	0.001 ± 0.001	0.001 ± 0.001	0.002 ± 0.001	0.335 [#]
TNF α	0.001 ± 0.0003	0.001 ± 0.001	0.001 ± 0.0002	0.888 [#]
CCL2/MCP-1	0.22 ± 0.054	0.64 ± 0.84	0.43 ± 0.51	0.736 [#]
CPT1A	0.05 ± 0.01	0.05 ± 0.01	0.07 ± 0.03	0.149 ⁺
mTOR	0.13 ± 0.05	0.11 ± 0.04	0.14 ± 0.04	0.387 ⁺
PRKAA2	0.38 ± 0.089	0.38 ± 0.10	0.39 ± 0.08	0.980 ⁺
GLUT4	0.08 ± 0.02	0.10 ± 0.01	0.10 ± 0.01	0.182 ⁺
PDK4	3.68 ± 1.32	3.00 ± 1.73	3.24 ± 1.90	0.794 ⁺
NOS2	0.042 ± 0.019	0.047 ± 0.014	0.042 ± 0.009	0.711 [#]
NOS3	0.07 ± 0.01	0.08 ± 0.005	0.09 ± 0.04	0.552 [#]
SOD2	1.65 ± 0.62	1.47 ± 0.16	1.30 ± 0.55	0.462 ⁺
PRDX2	1.09 ± 0.13	1.12 ± 0.14	1.29 ± 0.21	0.116 ⁺
NOX4	0.052 ± 0.01	0.051 ± 0.01	0.057 ± 0.02	0.955 [#]

Data are presented as mean ± standard deviation.

Abbreviations: TGF- β 1, transforming growth factor beta 1; TGF- β 3, transforming growth factor beta 3; LRP1, LDL receptor-related protein 1; MMP2, matrix metalloproteinase 2; MMP9, matrix metalloproteinase 9; TIMP1, tissue inhibitor of metalloproteinase 1; IL-10, interleukin 10; TNF- α , tumour necrosis factor alpha; CCL2/MCP-1, chemokine (C-C motif) ligand 2 or monocyte chemoattractant protein 1; NOS2, nitric oxide synthase 2; NOS3, nitric oxide synthase 3; SOD2, superoxide dismutase 2; PRDX2, peroxiredoxin 2; NOX4, NADPH oxidase 4.

Supplementary Table 4. Cardiac oxidative stress analysis at 30 days of follow-up.

Remote zone	Control (n=7)	Empagliflozin (n=8)	Empagliflozin +sac/val (n=8)	<i>P</i>
NO	109.8 ± 19.49	162.1 ± 56.04	110.4 ± 24.91	0.08 * 0.99 \$ 0.05 #
eNOS	0.32 ± 0.12	0.55 ± 0.08	0.41 ± 0.15	0.01 * 0.46 \$ 0.09 #
Phosphorylated eNOS	0.05 ± 0.02	0.25 ± 0.15	0.07 ± 0.02	0.02 * 0.93 \$ 0.04 #

Data are presented as mean ± standard deviation. Statistical differences according to one-way ANOVA with Tukey post-hoc.

*Control vs. empagliflozin

\$Control vs. empagliflozin+sac/val

#Empagliflozin vs. empagliflozin+sac/val

NO, nitric oxide; eNOS, endothelial nitric oxide.

Supplementary Table 5. Invasive high-density mapping parameters.

	Control (n=7)	Empagliflozin (n=8)	Empagliflozin+sac/Val (n=8)	p value
Endocardial area ≤ 1.5mV, cm ²	22.3 [10.7-24.4]	19.4 [9.2-22.7]	22.5 [17.1-30.2]	0.382* 0.431 [§]
Endocardial area ≤ 0.5mV, cm ²	18.9 [14.7-19.8]	13.5 [5.1-20.5]	18.1 [13.0-23.2]	0.867* 0.817 [§]
Endocardial area 0.5-1.5mV, cm ²	3.9 [3.5-5.9]	2.9 [1.6-3.9]	3.9 [3.3-4.8]	0.152* 0.907 [§]
Epicardial area ≤ 0.5mV, cm ²	8.3 [6.6-8.7]	9.9 [6.6-14.1]	9.5 [8.8-11.6]	0.762* 0.665 [§]
DZ (median [IQR])	3 [2-3]	1 [0-2]	1 [0-1]	0.073* 0.008[§]

Data are presented as median [interquartile range]. Statistical differences according to one-way ANOVA with Tukey post-hoc.

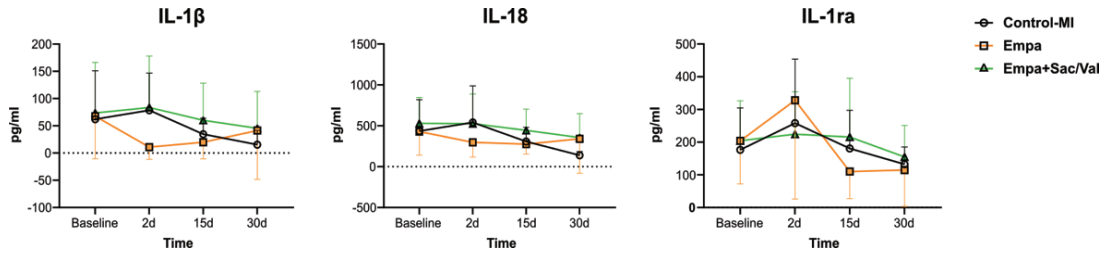
*Control vs. empagliflozin

[§]Control vs. empagliflozin+sac/val

DZ: Deceleration zones

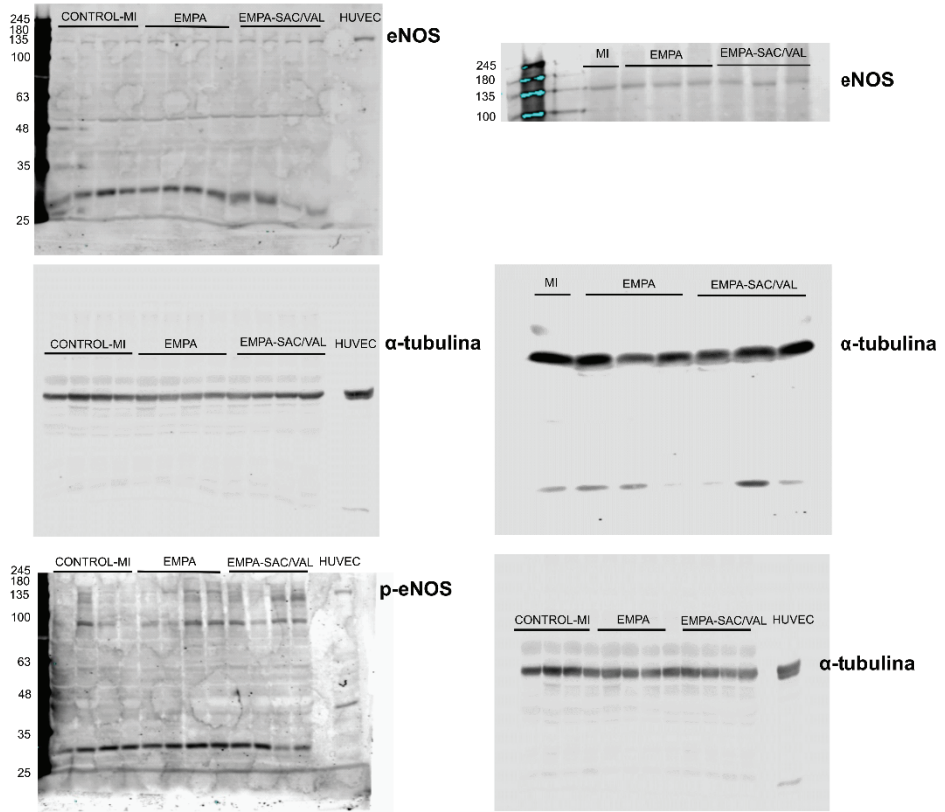
Supplementary Figures

Supplementary Figure 2. Cytokine evaluation. (B) Evolution of IL-1 β , IL-18, and IL-1Ra at baseline and 2, 15, and 30 days of follow-up. Control-MI, controls (n=8); Empa, empagliflozin (n=8); Empa+Sac/Val (n=8).

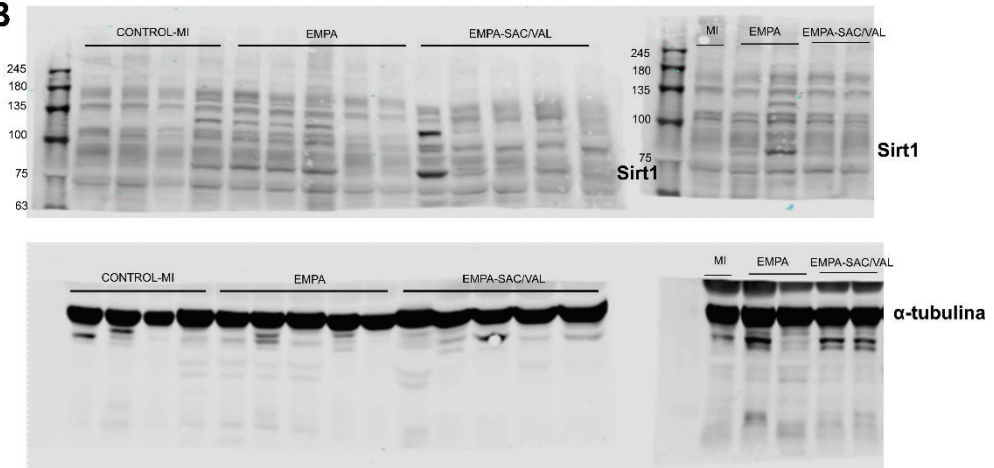


Supplementary Figure 3. Western blot analysis. (A) Membrane images of eNOS and phosphorylated eNOS protein levels in the remote zone at 30 days post-MI control (Control-MI; n=7), empagliflozin (Empa; n=8), and Empa+Sac/Val (n=8) animals. Human umbilical vein endothelial cells (HUVEC) were used as a positive control for eNOS expression. (B) Membrane images of SIRT1 protein levels in infarct zone at 30 days post-MI in treated animals. α -tubulin was used as a loading control.

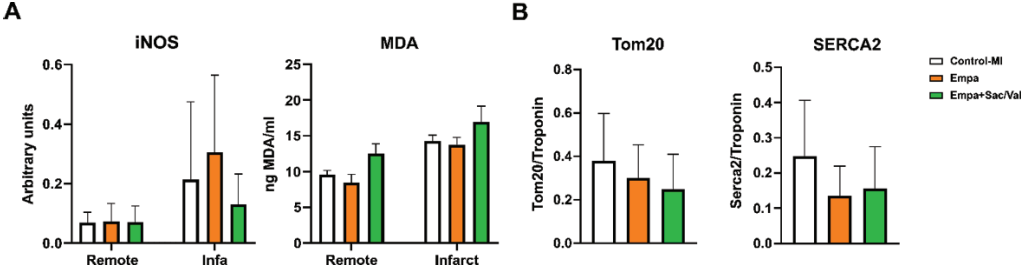
A



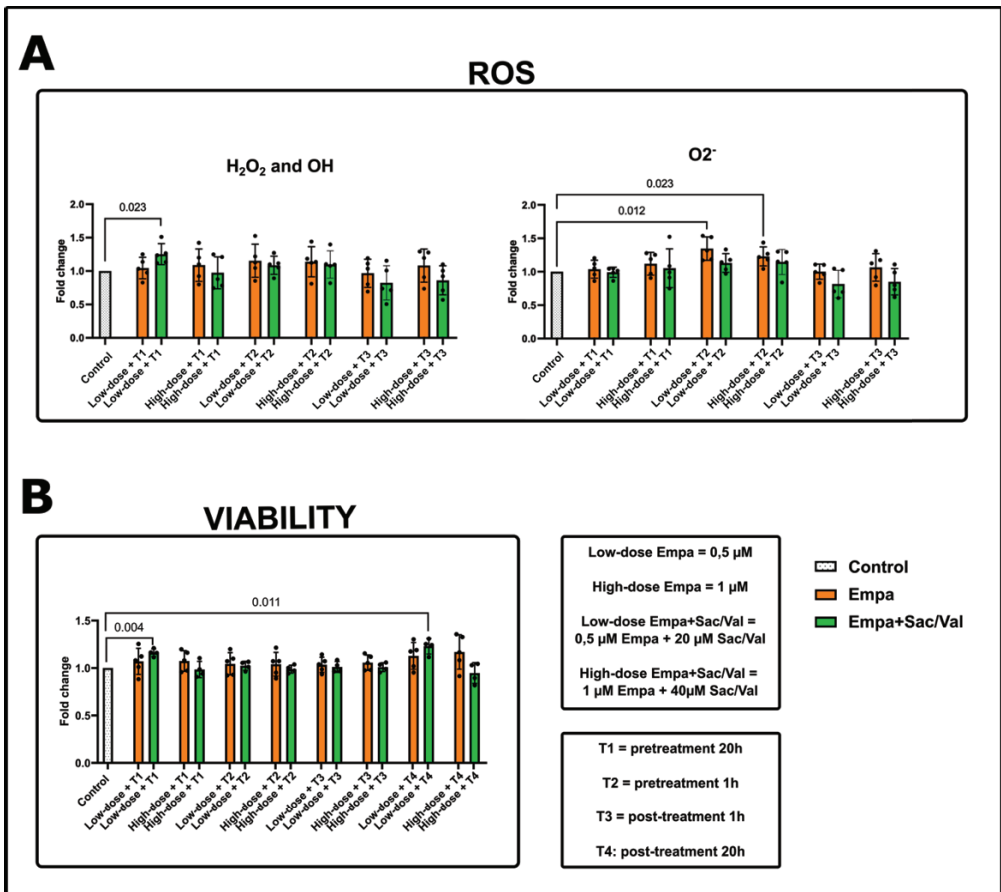
B



Supplementary Figure 4. Oxidative stress and mitochondrial analysis. (A) Histograms showing the iNOS and MDA quantification in remote and infarct zone of control (Control-MI; n=7), empagliflozin (Empa; n=8), and Empa+Sac/Val animals (n=8). (B) TOM20 and SERCA2 quantification in the preserved myocardium within the infarct core of control (Control-MI; n=8), empagliflozin (Empa; n=8), and Empa+Sac/Val animals (n=8).



Supplementary Figure 5. ROS and cell viability analyses. (A) ROS levels. Histograms presenting intracellular ROS levels (determined by DCFHDA fluorescence) and intracellular $O_2^{\cdot-}$ levels (determined by DHE fluorescence) in the 300 μM H_2O_2 model, under different conditions of low or high doses of empagliflozin (Empa; orange) or Empa+Sac/Val (green); T1: pretreatment 20 h; T2: pretreatment 1 h; T3: post-treatment 1 h. Data are presented as fold change of fluorescence compared to control cells not treated with the drugs. **(B) Cellular viability.** Histograms showing cell viability (determined by alamarBlue assay) in the 300 μM H_2O_2 model, under different conditions of low or high doses of (Empa; orange) or Empa+Sac/Val (green); T1: pretreatment 20 h; T2: pretreatment 1 h; T3: post-treatment 1 h; T4: post-treatment 20 h. Data are presented as fold change of fluorescence compared to control cells not treated with the drugs. Statistical differences according to one-sample t-test comparing with value 1 (control). n=5 experiments; n=3 technical replicates.



References

1. Livak KJ, Schmittgen TD. Analysis of relative gene expression data using real-time quantitative PCR and the 2(-Delta Delta C(T)) Method. *Methods*. 2001;25(4):402-408. doi:10.1006/meth.2001.1262
2. Mallol R, Amigó N, Rodríguez MA, et al. Liposcale: a novel advanced lipoprotein test based on 2D diffusion-ordered 1H NMR spectroscopy. *J Lipid Res*. 2015;56(3):737-746. doi:10.1194/jlr.D050120
3. Jeyarajah EJ, Cromwell WC, Otvos JD. Lipoprotein particle analysis by nuclear magnetic resonance spectroscopy. *Clin Lab Med*. 2006;26(4):847-870. doi:10.1016/j.cll.2006.07.006
4. Fuertes-Martín R, Taverner D, Vallvé JC, et al. Characterization of 1H NMR Plasma Glycoproteins as a New Strategy To Identify Inflammatory Patterns in Rheumatoid Arthritis. *J Proteome Res*. 2018;17(11):3730-3739. doi:10.1021/acs.jproteome.8b00411
5. Fuertes-Martín R, Moncayo S, Insenser M, et al. Glycoprotein A and B Height-to-Width Ratios as Obesity-Independent Novel Biomarkers of Low-Grade Chronic Inflammation in Women with Polycystic Ovary Syndrome (PCOS). *J Proteome Res*. 2019;18(11):4038-4045. doi:10.1021/acs.jproteome.9b00528
6. Gómez J, Brezmes J, Mallol R, et al. Dolphin: a tool for automatic targeted metabolite profiling using 1D and 2D (1)H-NMR data. *Anal Bioanal Chem*. 2014;406(30):7967-7976. doi:10.1007/s00216-014-8225-6
7. Wishart DS, Feunang YD, Marcu A, et al. HMDB 4.0: the human metabolome database for 2018. *Nucleic Acids Res*. 2018;46(D1):D608-D617. doi:10.1093/nar/gkx1089
8. Löfgren L, Ståhlman M, Forsberg GB, Saarinen S, Nilsson R, Hansson GI. The BUME method: a novel automated chloroform-free 96-well total lipid extraction method for blood plasma. *J Lipid Res*. 2012;53(8):1690-1700. doi:10.1194/jlr.D023036
9. Barrilero R, Gil M, Amigó N, et al. LipSpin: A New Bioinformatics Tool for Quantitative 1H NMR Lipid Profiling. *Anal Chem*. 2018;90(3):2031-2040. doi:10.1021/acs.analchem.7b04148
10. Vinaixa M, Rodríguez MA, Rull A, et al. Metabolomic assessment of the effect of dietary cholesterol in the progressive development of fatty liver disease. *J Proteome Res*. 2010;9(5):2527-2538. doi:10.1021/pr901203w
11. Folch J, Lees M, Sloane Stanley GH. A simple method for the isolation and purification of total lipides from animal tissues. *J Biol Chem*. 1957;226(1):497-509.
12. Kelley KW, Curtis SE, Marzan GT, Karara HM, Anderson CR. Body surface area of female swine. *J Anim Sci*. 1973;36(5):927-930. doi:10.2527/jas1973.365927x

Chapter Four

Discussion

Animal models of MI constitute a highly valuable experimental resource for the assessment and development of novel therapeutic strategies. These models provide critical insights into drug efficacy, mechanisms of action, and safety, often serving as the foundational steps in the translational research process.

In translational CV research, pigs are one of the preferred animal models due to the remarkable similarity of their CV system to that of humans, in terms of anatomical, physiological, and metabolic properties (231).

In the present thesis, we developed a porcine model of MI using the coil deployment technique. This model offers the advantages of a closed-chest approach, including high reproducibility, minimal trauma and infection risks, low mortality, cost- and time- efficiency, and strong clinical relevance (232,233). Compared to the balloon occlusion model, the coil deployment method more accurately simulates the pathophysiology of a human MI, as the coil interferes with blood flow, thereby initiating the coagulation cascade and the subsequent thrombus formation (234). However, this approach models a non-reperfused MI, whereas current clinical practice prioritizes the rapid restoration of blood flow in the affected artery as the primary treatment for MI. Although this divergence represents a significant limitation, non-reperfused MI models yield a more stable, permanent myocardial scar with consistent and reproducible infarct area, as they avoid the variability introduced by occlusion duration, reperfusion timing, and reperfusion injury. As reperfusion injury is not a component of the coil-deployment procedure, the focus of this research is directed toward the primary tissue injury response (235,236). These consistent scars make non-reperfusion models particularly suitable for studying myocardial tissue injury, wound healing, long-term adverse cardiac remodelling, and the subsequent pathologies,

including the development of VAs and the progression to HF (237). One of the primary endpoints of our study was to assess the long-term effects of the drugs on fibrosis, cardiac function, and VAs. Consequently, we developed a permanent coronary occlusion model in swine and shared the protocol with the scientific community to provide a reproducible and robust model for future research.

Despite advancements in the management of MI, morbidity and mortality remain significant. The primary causes of death during the chronic phase of MI are attributed to adverse LV remodelling, which leads to HF and VAs. The post-MI inflammatory response plays a crucial role in subsequent cardiac repair and remodelling. Furthermore, metabolic remodelling occurring in a failing heart further contributes to HF progression.

Over the past few years, several therapies effective for chronic HF, such as BBs, MRAs, and RAAS inhibitors, have also demonstrated benefits for patients with LV systolic dysfunction, pulmonary congestion, or both following an AMI (238). The recent introduction of novel HF drugs, such as ARNi and SGLT2 inhibitors, has opened the door for exploring their potential effectiveness in the MI setting. These drugs have shown beneficial effects by modulating inflammation, reducing oxidative stress, improving cardiac metabolism, and/or enhancing LV remodelling across various cardiac pathologies. However, the recently published results of the PARADISE-MI and EMPACT-MI trials have not been as impactful as anticipated. Although early initiation of sacubitril/valsartan and empagliflozin after MI reduced the incidence of CV death/all-cause of death and HF hospitalizations, these reductions did not achieve statistical significance. Nonetheless, it is important to note that these studies may have been influenced by potential design bias, such as the assessment of all-cause death during the COVID-19 pandemic period.

Consequently, further research is required to reach more definitive conclusions and determine whether specific subgroups of AMI patients may benefit from the early initiation of these treatments. To address these gaps, the present thesis evaluates the effects of early initiation of empagliflozin and/or sacubitril/valsartan, as well as their potential synergistic effects, in a translational porcine model of non-reperfused MI. The following section discusses the main findings.

Inflammation

In response to MI, the heart undergoes a complex repair process beginning with a robust inflammatory response and immune cell infiltration into the ischemic myocardium. This is followed by a reparative phase characterized by the resolution of inflammation, scar tissue formation, and collagen deposition. The initial inflammatory response is critical in the subsequent structural and electrical remodelling of the ventricles, significantly contributing to the development of HF and VAs (17). Proper resolution of this inflammatory response after an MI may protect against adverse cardiac remodelling.

In our study, all animal groups were treated with bisoprolol, a BB recommended for long-term treatment in AMI patients with impaired LV function (56). Our objective was to assess whether empagliflozin and/or sacubitril/valsartan could provide superior therapeutic effects compared to bisoprolol alone.

The control group in our study did not exhibit the typical early increase in inflammatory markers post-MI. This attenuation can likely be attributed to bisoprolol treatment, which is known to have anti-inflammatory properties (239). However, sacubitril/valsartan treatment demonstrated superior anti-

inflammatory effects compared to BB treatment alone. This was evidenced by a reduction in circulating leukocytes, particularly neutrophils, during the acute phase post-MI, decreased CCR2 expression on monocytes, reduced secretion of the pro-inflammatory IL-12, and sustained levels of the anti-inflammatory IL-10 over time compared to controls.

To profile monocytes following MI, we excluded the classical evaluation of CD14 and CD16 markers, as previous studies reported no significant expression of these markers in porcine blood (240). Instead, we focused on alternative markers of monocyte activation, specifically CCR2 and CD163. CCR2⁺ monocytes are activated monocytes that predominate during the initial peak of inflammation after MI. These cells are recruited to the myocardium in response to the cytokine MCP-1/CCL2, which is rapidly upregulated in the infarcted tissue following an MI. Upon arrival in the heart, CCR2⁺ monocytes differentiate into pro-inflammatory macrophages that closely resemble the classical M1 phenotype (241), and enhance leukocyte recruitment, thereby intensifying the inflammatory response. Notably, an increase presence of CCR2⁺ macrophages has been associated with adverse cardiac remodelling and impaired cardiac function following MI (25,242).

In our study, the Sac/Val group exhibited reduced CCR2 expression on the surface of circulating monocytes 15 days after MI, suggesting decreased monocyte activation. However, the overall number of circulating CCR2⁺ monocytes did not significantly decline over time in this group. Previous studies have demonstrated the anti-inflammatory properties of sacubitril/valsartan, primarily through the reduction of pro-inflammatory cytokines in conditions such as HF and MI (99,101,103,104,116). In contrast, in our study, we did not observe reductions in cytokines associated with inflammasome activation, such as IL-1 β and IL-18, or in other pro-

inflammatory cytokines like IL-6 or TNF- α , either systemically or within myocardial tissue. Nonetheless, a notable reduction in the pro-inflammatory cytokine IL-12 was observed. IL-12 family cytokines play a critical role in regulating inflammatory disorders, including rheumatoid arthritis, multiple sclerosis, as well as CVDs (243). Specifically, IL-12 promotes inflammation by stimulating Th1 cell differentiation (244). The decreased IL-12 levels observed in the Sac/Val group suggest a mitigated inflammatory response following MI. Additionally, animals in the Sac/Val group consistently maintained elevated levels of the anti-inflammatory cytokine IL-10, which is known to play a key role in the transition from inflammation to tissue repair. IL-10 promotes the shift from the pro-inflammatory M1 macrophage phenotype to the reparative M2 phenotype and modulates fibroblast activity by reducing the Col I/III ratio, thereby enhancing tissue elasticity, and improving myocardial function (18,34). The effect of sacubitril/valsartan on maintaining IL-10 levels has also been confirmed in previous studies (105,106).

The Empa group also exhibited anti-inflammatory effects. Similar to sacubitril/valsartan, empagliflozin attenuated the typical inflammatory peak following MI, as evidenced by a reduction in leukocyte count 2 days post-MI. Empagliflozin also reduced the number of circulating CCR2⁺ monocytes and decreased their surface expression. To the best of our knowledge, this is the first study to suggest that empagliflozin could reduce circulating CCR2⁺ monocytes after MI, potentially leading to better MI outcomes. These findings align with previous research in which empagliflozin reduced CCR2 ligand secretion (MCP-1/CCL2) (172,173), limited the accumulation of pro-inflammatory M1 macrophages, and promoted a shift toward the anti-inflammatory M2 macrophage phenotype (175,176). On the other hand, one of the primary reported effects of SGLT2 inhibitors in inflammation is the

attenuation of NLRP3 inflammasome activation (162,170). Our results support this, as they suggest that empagliflozin could attenuate inflammasome activation after MI, with a remarkable trend toward reduced IL-1 β and IL-18, alongside increased secretion of the IL-1R antagonist (IL-1Ra). Although we did not observe additional immunomodulatory effects, other studies have reported further anti-inflammatory actions of empagliflozin, such as reductions in inflammatory markers like CRP, IL-6, TNF α , and IFN- γ expression (169,172). These effects may be more pronounced in the myocardial tissue during the early inflammatory phase, which occurs in the days immediately following MI. However, as our samples were collected at the end of the study (30 days post-MI), our analysis reflects the resolution phase rather than the peak inflammatory response.

On the other hand, it is well established that empagliflozin decreases cardiac oxidative products such as MDA and lipid peroxidation, while restoring antioxidant enzyme levels like SOD in the heart (171,177,178). Consistent with this, in our study, we observed an increase in endogenous nitric oxide levels (NO) derived from the activation of endothelial nitric oxide synthase (eNOS) activity in the non-infarcted tissue of the Empa group. This form of NO has beneficial effects, including promoting angiogenesis, inhibiting inflammatory pathways, maintaining endothelial function, reducing oxidative stress, inducing vasodilatation, and exerting anti-apoptotic effects (245).

Unexpectedly, the combination of empagliflozin and sacubitril/valsartan did not exhibit any anti-inflammatory effects. Instead, animals in the combined group showed an increase in the number of monocytes at 30 days post-MI, although there was no corresponding increase in CCR2⁺ monocytes. This inflammatory response of the combination therapy has not been reported in previous studies. The absence of anti-inflammatory effects from the

individual drugs in the combined group remains unexplained, and a negative synergistic interaction between the two drugs seems unlikely, given that they act through distinct pathways. Importantly, this observed mild inflammatory response does not appear to adversely impact fibrosis, cardiac function, or arrhythmogenic risk in the post-MI progression. In fact, the combination group demonstrated reduced Col I levels, smaller scar mass, and improved anti-arrhythmic properties. Nonetheless, further studies with larger sample sizes are needed to determine whether this effect is reproducible and to clarify its potential clinical implications.

Cardiac metabolism

In a failing heart, there is a metabolic shift from using FFA to glucose, which is a less energetically efficient substrate, contributing to the progression of HF. Empagliflozin has been shown to reverse this shift, improving cardiac metabolism and energy efficiency, particularly in the context of metabolic disorders such as T2DM (180,181). However, results in non-metabolic scenarios, such as HF, are mixed (210), suggesting that the effects of empagliflozin may vary depending on the metabolic status of the patient. Nonetheless, some preclinical studies in non-diabetic MI models support this metabolic hypothesis, showing reduced glucose uptake and increased FFA and KB utilization following empagliflozin treatment, leading to elevated myocardial ATP levels (182,185). In our study, however, we did not observe an impact of empagliflozin, with or without sacubitril/valsartan, on systemic FFA or KB levels, as evaluated by NMR. Additionally, we found no changes in the expression of genes related to substrate utilization, such as glucose transporter type 4 (GLUT4) and pyruvate dehydrogenase kinase 4 (PDK4), in

either the infarcted or remote myocardium. Overall, these findings suggest that improved metabolic status was not observed in our study.

On the other hand, empagliflozin appears to offer other cardiac benefits by reducing oxidative stress and promoting autophagy, thereby enhancing cardiac cell functionality. One of the pathways underlying these effects is the SIRT1/PGC-1 α /FGF21 pathway (212). In our study, we observed increased levels of SIRT1 protein in the infarct zone but did not detect increases in the downstream mediators PGC1 α and FGF21, suggesting that this pathway was not activated. However, SIRT1 is also known to regulate genes involved in inflammatory pathways, exerting anti-inflammatory effects by suppressing the NF- κ B signalling pathway and inhibiting inflammasome activation (246,247). Therefore, the elevated SIRT1 levels in empagliflozin-treated animals might be associated with reduced inflammation in this group.

We also assessed the impact of empagliflozin and/or sacubitril/valsartan on metabolite profiles in the liver, infarct core, and serum of the animals. Empagliflozin-treated animals exhibited increased levels of cardioprotective lipids, such as omega-3, omega-6 and -7, docosahexaenoic acid (DHA), and arachidonic acid + eicosapentaenoic acid (ARA+EPA) in the liver. These omega fatty acids are known to have anti-inflammatory, anti-fibrotic, and anti-arrhythmic properties (248). However, no corresponding increases in these cardioprotective lipid levels were observed in the serum or infarcted tissue. Considering the liver's essential role in energy regulation and its central involvement in metabolic interactions across tissues, it is plausible to suggest that hepatic lipid modulation may have significant cardiac implications. This effect could be particularly relevant to the non-infarcted myocardium, the viable region of the heart that remains responsive to metabolic adaptation.

Fibrosis

Sacubitril/valsartan has demonstrated anti-fibrotic properties in multiple studies. Patients with HFrEF and HFpEF who were treated with sacubitril/valsartan exhibited significant reductions in plasma pro-fibrotic biomarkers (108,109). Additionally, in various preclinical models, including MI, sacubitril/valsartan effectively reduced fibrosis area and downregulated pro-fibrotic markers such as Col I, Col III, and α -SMA (112–117). Our findings are consistent with the published studies, as we observed a reduction in Col I and Col I/III ratio in the infarct core of Sac/Val animals. However, we did not observe significant differences in total collagen volume fraction (CVF) or Col III levels.

The structural cardiac remodelling occurring after MI also involves changes in the composition of collagen matrix. Col I and Col III are the primary ECM structural proteins in the CV system, crucial for maintaining the balance between elasticity, resilience, and rigidity that is necessary for normal cardiac function. In pathological CV conditions, the ratios of these ECM proteins are often altered, impacting the mechanical and structural functionality of the heart (249). Col I fibrils are stiff and provide structural rigidity and strength, whereas Col III fibrils are thinner, offering less tensile strength but greater elasticity, which enhances tissue resilience (249). After MI, scar formation and its collagen composition play an important role in modulating the LV remodelling process. For instance, an increased Col I/III ratio reduces wall elasticity, contributing to adverse remodelling, impaired cardiac function, and the potential development of HF, VAs, and death (250,251). In our study, Sac/Val-treated animals displayed reduced Col I deposition within the myocardial scar, resulting in a lower Col I/III ratio and consequently limiting scar fibrosis. Furthermore, we observed reductions in total scar mass and scar

transmurality, as evaluated by late gadolinium enhancement cardiac magnetic resonance (LGE-CMR). However, despite these beneficial anti-fibrotic effects, cardiac function did not significantly improve in this group. Previous studies suggest that the anti-fibrotic effects of sacubitril/valsartan are mediated through the inhibition of the TGF- β 1/Smad3 and Wnt/ β -catenin signalling pathways (114,115,118). However, we did not observe significant changes in the expression levels of fibrotic genes such as TGF- β 1, TGF- β 3, LRP1, MMP2, MMP9, and TIMP1 in either infarct or remote zones at 30 days post-MI. It is possible that these effects may be more pronounced in myocardial tissue during the inflammatory-reparative phases that occur within the first week after MI. Our analysis focused on tissue samples collected at the end of the study, 30 days post-MI, suggesting that shorter-term studies may provide a more accurate assessment of these molecular pathways as they manifest during the acute post-MI phase.

Regarding empagliflozin treatment, some studies have suggested anti-fibrotic effects of this drug in various CV conditions such as HF and MI (184,186,187,189), although results have been inconsistent. In our study, no differences were detected in CVF or Col I levels. However, we observed an increase in Col III in the myocardial scar, along with a trend toward a decreased Col I/III ratio, suggesting a potentially more flexible scar. These anti-fibrotic effects could be attributed to the reduced inflammatory response observed in the Empa group post-MI. On the other hand, empagliflozin has been shown to reduce the expression of pro-fibrotic markers, including MMP9, TGF- β 1, Col I, and Col III (171,189,192). However, in our study, we did not find differential expression levels of fibrotic genes in this group, which may be attributed to the timing of our analysis (30 days post-MI).

The combined treatment group showed similar results to the Sac/Val group, including a reduction in Col I levels and the Col I/III ratio. This suggests that the anti-fibrotic effect of sacubitril/valsartan operates independently of any anti-inflammatory action, as no anti-inflammatory response was observed in the combined group. Previous studies indicate that the anti-fibrotic effects of sacubitril/valsartan are likely linked to the inhibition of TGF- β 1/Smad3 and Wnt/ β -catenin signalling pathways. Shorter follow-up studies would be more appropriate to confirm whether these pathways are indeed involved in the anti-fibrotic action of sacubitril/valsartan in the early stages following MI. In the non-infarcted zone, no differences were observed between groups in terms of Col I, Col III, CVF and Col I/III. While it is reasonable to expect that these treatments could improve overall heart remodelling, including in the remote zone, such changes typically occur later in the post-MI progression. Therefore, a longer study duration may be more appropriate to examine these potential long-term remodelling effects.

Cardiac function

In the context of HF, sacubitril/valsartan has demonstrated beneficial results in reversing adverse LV remodelling, including improvements in ventricular volumes (LVEDV and LVESV), which lead to enhanced LVEF, among other parameters (119,120). Regarding AMI patients, despite the limited number of studies, sacubitril/valsartan initiation has also been associated with improvements in cardiac function, albeit with mixed outcomes. Rezq and colleagues reported higher LVEF values and improved LV remodelling (LVEDV and LVESV) after 6 months of sacubitril/valsartan treatment compared to enalapril (ACEi) (126). However, in the PARADISE-MI trial, sacubitril/valsartan did not significantly improve LVEF compared to ramipril (ACEi) after 8

months, although it did result in a smaller increase in LVEDV and a greater decline in LV mass (127). It is reasonable to suggest that sacubitril/valsartan could improve cardiac function after MI due to its anti-fibrotic properties. However, we did not observe a superior effect on cardiac function compared to the control group treated with BBs alone.

Regarding empagliflozin treatment, previous studies involving HF patients with or without T2DM have shown improvements in LVEDV, LVESV, and LV mass, following the initiation of the treatment (193). The effects were more pronounced, particularly in improving LVEF, when baseline cardiac function was impaired (197). Additionally, in the context of AMI, empagliflozin has been shown to improve echocardiographic parameters (198). In our study, we found no significant improvements in cardiac function in the Sac/Val and Empa groups, as assessed by LGE-CMR. Despite these groups exhibiting beneficial effects on the inflammatory response after MI and enhanced fibrotic characteristics of the myocardial scar, these improvements appeared insufficient to significantly improve cardiac function parameters.

Nevertheless, in the combined treatment group, we observed improved LV compliance, as evidenced by an increase in indexed LVEDV, which led to a greater LVSV – the volume of blood pumped out in each systolic cardiac contraction. However, the observed improvement in LVEF did not reach statistical significance. This outcome should be linked to the results regarding fibrosis in this group (lower Col I and Col I/III ratio), mainly attributed to sacubitril/valsartan treatment, as they reproduced the findings observed in the Sac/Val group. It remains unclear why the cardiac function benefits observed in the combined treatment group were not evident in the Sac/Val group. One possible explanation could be the limited sample size of our study. Alternatively, the addition of empagliflozin may have provided an

additional therapeutic effect, potentially influencing other fibrotic and remodelling pathways. For instance, the observed Col III increment in the myocardial scar could contribute to improve cardiac compliance. However, this hypothesis requires further validation through additional research.

Arrhythmias

Non-invasive and invasive techniques are crucial for arrhythmic risk stratification. LGE-CMR imaging facilitates the assessment of factors such as scar size, BZ mass, and the number and mass of BZ corridors—channels of BZ tissue connecting healthy myocardium and surrounded by non-excitabile areas such as dense scar (252). These factors reflect heterogeneous scar areas with diverse conduction and excitability properties, which are favourable for re-entry circuits, thereby increasing the incidence of VAs (253,254). Invasive electroanatomical mapping provides additional insights, enabling the characterization of BZ and scar tissue, pathological electrograms, and deceleration zones (DZs), all of which are associated with VAs.

In our study, the Sac/Val group exhibited favourable electrophysiological properties of the scar, as indicated by reductions in total scar mass, BZ mass, and the number and mass of BZ corridors. As a result, there was a significant 55% reduction in the relative risk of VT inducibility at 30 days post-MI compared to the control group, which received BB treatment alone—a treatment recognized for its anti-arrhythmic effects (255). This suggests that sacubitril/valsartan may provide an important additional anti-arrhythmic benefit beyond what BB treatment provides, in the post-MI context. These results align with prior studies, where sacubitril/valsartan has demonstrated potential in preventing severe ventricular arrhythmic events in HF patients,

including reductions in the number of ICD shocks, episodes of VF and VT, PVCs, and the incidence of cardiac arrest or sudden cardiac death (87,128–131). In the context of MI, besides our study, sacubitril/valsartan has also demonstrated anti-arrhythmic effects in two primary preclinical studies by reducing VA inducibility (132,133). The mechanisms behind this anti-arrhythmic effects are largely attributed to the reversal or prevention of adverse cardiac remodelling, although further investigation is necessary. Our findings suggest that the decreased risk of VAs is likely mediated by improved post-MI fibrosis and the associated electrophysiological remodelling. Despite these promising results, there is limited evidence on the specific arrhythmic effects of early sacubitril/valsartan administration in AMI patients. The only relevant clinical trial, involving 131 AMI patients receiving sacubitril/valsartan or enalapril (ACEi) after PCI, reported a reduction in the secondary endpoint of combined adverse events, including malignant arrhythmias (256). While the sacubitril/valsartan group experienced fewer malignant arrhythmias, the small sample size underscores the need for larger clinical trials to confirm these findings.

Regarding the Empa group, we found no impact of empagliflozin in any of the evaluated electrophysiological parameters, resulting in no modification of the risk of VT inducibility 30 days post-MI compared to controls. Research on the effects of SGLT2 inhibitors on VAs susceptibility remains limited. Among these studies, three meta-analyses involving patients with T2DM, HF, and CKD concurred on the ability of SGLT2 inhibitors to reduce the risk of atrial arrhythmias (199–201), but no impact on VAs was reported. However, a recent study involving 150 patients with T2DM treated with an ICDs showed that empagliflozin reduced the number of VAs episodes compared to placebo (257). In preclinical studies of MI, empagliflozin has been shown to reduce

premature ventricular beats (PVBs), VF (203), and sudden death (204). It is reasonable to suggest that empagliflozin might influence the arrhythmogenic substrate due to its anti-inflammatory and anti-fibrotic properties. Nonetheless, more extensive studies are required to validate this hypothesis. The combined treatment group (Empa+Sac/Val) also exhibited a reduced risk of VT inducibility 30 days post-MI. This reduction may be attributed to several factors observed in this group, including beneficial electrical scar remodelling, characterized by fewer conduction abnormalities (fewer BZ corridors and DZs), and reduced myocardial fibrosis, evidenced by lower levels of Col I, Col I/III ratio, and CVF. Notably, these effects were absent in the Empa-only group, suggesting that they are primarily driven by the anti-fibrotic properties of sacubitril/valsartan.

Empagliflozin and sacubitril/valsartan safe and synergistic effects

Previous studies have demonstrated that the combination of ARNi and SGLT2 inhibitors is safe and well-tolerated in HF patients, including older populations (222,223). Although specific data on the safety of this combination following MI are lacking, our study showed that it was well-tolerated in pigs, with no observed adverse effects.

Regarding the efficacy of the co-treatment, previous sub-studies evaluating the potential synergistic effects of these two drugs did not show a significant reduction in the risk of CV death or hospitalization for HF in the combination group compared to the group treated with empagliflozin alone. However, patients receiving both medications exhibited improvements in several clinical indicators such as systolic pressure, heart rates, and NT-proBNP levels (223), compared to those patients that were treated with empagliflozin alone. It is important to note that the number of patients receiving both

medications in these studies was considerably smaller than those receiving only SGLT2 inhibitors. The results of our MI study suggest that co-treatment with empagliflozin and sacubitril/valsartan did not provide significant additional therapeutic benefits. Surprisingly, this combined group did not exhibit the anti-inflammatory effects observed when the drugs were administered individually in the Empa and Sac/Val groups. However, similar to the Sac/Val group, the Empa+Sac/Val group showed reduced fibrosis, as evidenced by lower Col I levels and a reduced Col I/III ratio. This reduction in fibrosis translated into significant anti-arrhythmic effects, such as fewer BZ corridors and DZs, which contributed to a notable reduction in VT inducibility 30 days post-MI. Although the exact mechanisms underlying these anti-arrhythmic benefits remain unclear, the anti-fibrotic effect appears to be a crucial factor in reducing arrhythmogenic risk in both the Sac/Val and Empa+Sac/Val groups. In contrast, while a moderate anti-fibrotic effect was observed in the Empa group, it did not result in any anti-arrhythmic benefit. The primary advantage of the combined treatment seems to lie in improved LV compliance, as evidenced by an increased LVSV. The fibrosis-related characteristics of the combined treatment group closely resembled those of the Sac/Val group, with lower Col I levels and a reduced Col I/III ratio. Taken together, these findings suggest that sacubitril/valsartan exerts a more pronounced effect on reducing fibrosis and arrhythmias compared to empagliflozin.

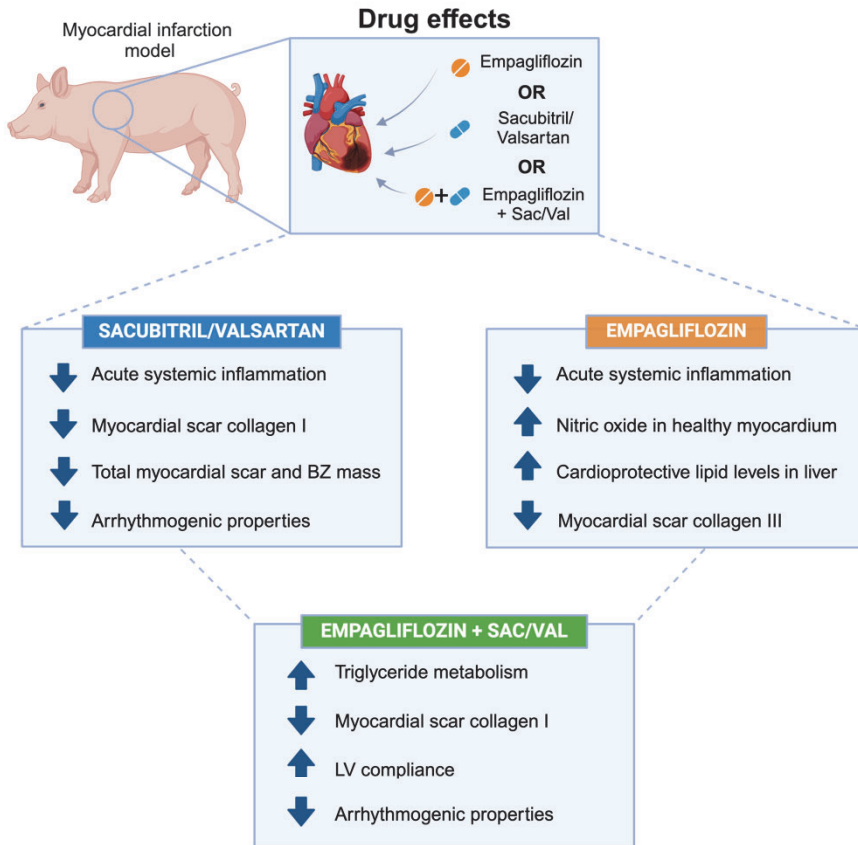


Figure 14. Graphical summary of results: effects of early initiation of sacubitril/valsartan and/or empagliflozin after MI. Sacubitril/valsartan reduced systemic inflammation and promoted favourable scar remodelling by reducing Col I content in the scar, total scar mass, BZ mass, and the number and mass of BZ corridors, leading to a reduced risk of VT inducibility. Empagliflozin reduced systemic inflammation, improved cardiac oxidative stress, modified the collagen composition of the scar, and increased cardioprotective lipid levels in the liver. The combination of empagliflozin and sacubitril/valsartan decreased Col I in the scar, increased triglyceride metabolism (intake), and promoted favourable structural and electrical remodelling, leading to an improved LV compliance and a reduced risk of VT inducibility. *Original figure created with Biorender.com.*

Chapter Five

Conclusions

The conclusions derived from this thesis project are:

1. The coil deployment method in swine successfully provided a highly reproducible, consistent, and translational pre-clinical MI model suitable for testing new CV therapeutic strategies.
2. Early initiation of sacubitril/valsartan after MI decreased the acute systemic inflammatory response, Col I content in the scar, total scar and border zone mass, the number and mass of border zone corridors, as well as the number of deceleration zones. These effects led to a reduced risk of ventricular tachycardia inducibility 30 days post-MI, without significantly affecting cardiac function.
3. Early initiation of empagliflozin after MI reduced the acute systemic inflammatory response, modulated NO bioavailability, altered scar collagen composition, and increased cardioprotective liver lipid levels. However, empagliflozin showed no impact on electrophysiological properties, ventricular tachycardia inducibility, or cardiac function.
4. Early initiation of combined empagliflozin and sacubitril/valsartan treatments after MI promoted favourable scar remodelling by decreasing Col I deposition in the scar and the number of border zone corridors and deceleration zones. These effects contributed to a lower risk of ventricular tachycardia inducibility 30 days post-MI and improved left ventricular compliance.

5. Co-treatment with empagliflozin and sacubitril/valsartan after MI was safe but did not provide significant additional therapeutic benefits compared to individual treatments.

References

1. Cardiovascular diseases (CVDs) [Internet]. [cited 2023 Aug 8]. Available from: [https://www.who.int/news-room/fact-sheets/detail/cardiovascular-diseases-\(cvds\)](https://www.who.int/news-room/fact-sheets/detail/cardiovascular-diseases-(cvds))
2. Roth GA, Mensah GA, Johnson CO, Addolorato G, Ammirati E, Baddour LM, et al. Global Burden of Cardiovascular Diseases and Risk Factors, 1990-2019: Update From the GBD 2019 Study. *J Am Coll Cardiol*. 2020 Dec 22;76(25):2982–3021.
3. Mensah GA, Roth GA, Fuster V. The Global Burden of Cardiovascular Diseases and Risk Factors: 2020 and Beyond. *J Am Coll Cardiol*. 2019 Nov 19;74(20):2529–32.
4. The top 10 causes of death [Internet]. [cited 2023 Aug 8]. Available from: <https://www.who.int/news-room/fact-sheets/detail/the-top-10-causes-of-death>
5. Townsend N, Kazakiewicz D, Lucy Wright F, Timmis A, Huculeci R, Torbica A, et al. Epidemiology of cardiovascular disease in Europe. *Nat Rev Cardiol*. 2022 Feb;19(2):133–43.
6. Criteria I of M (US) C on SSCD. Ischemic Heart Disease. In: *Cardiovascular Disability: Updating the Social Security Listings* [Internet]. National Academies Press (US); 2010 [cited 2023 Aug 8]. Available from: <https://www.ncbi.nlm.nih.gov/books/NBK209964/>
7. Davies MJ, Thomas A. Thrombosis and acute coronary-artery lesions in sudden cardiac ischemic death. *N Engl J Med*. 1984 May 3;310(18):1137–40.
8. Regmi M, Siccardi MA. Coronary Artery Disease Prevention. In: *StatPearls* [Internet]. Treasure Island (FL): StatPearls Publishing; 2023 [cited 2023 Aug 8]. Available from: <http://www.ncbi.nlm.nih.gov/books/NBK547760/>
9. Gray G, Toor I, Castellan R, Crisan M, Meloni M. Resident cells of the myocardium: more than spectators in cardiac injury, repair and regeneration. *Curr Opin Physiol*. 2018 Feb;1:46–51.
10. Frangiannis NG. Regulation of the inflammatory response in cardiac repair. *Circ Res*. 2012 Jan 6;110(1):159–73.
11. Mendonca Costa C, Plank G, Rinaldi CA, Niederer SA, Bishop MJ. Modeling the Electrophysiological Properties of the Infarct Border Zone. *Front Physiol*. 2018;9:356.
12. Ojha N, Dhamoon AS. Myocardial Infarction. In: *StatPearls* [Internet]. Treasure Island (FL): StatPearls Publishing; 2023 [cited 2023 Aug 8]. Available from: <http://www.ncbi.nlm.nih.gov/books/NBK537076/>

13. Lu L, Liu M, Sun R, Zheng Y, Zhang P. Myocardial Infarction: Symptoms and Treatments. *Cell Biochem Biophys*. 2015 Jul;72(3):865–7.
14. Bauersachs J. Heart failure drug treatment: the fantastic four. *Eur Heart J*. 2021 Feb 11;42(6):681–3.
15. Frangogiannis NG. The inflammatory response in myocardial injury, repair, and remodelling. *Nat Rev Cardiol*. 2014 May;11(5):255–65.
16. Prabhu SD, Frangogiannis NG. The Biological Basis for Cardiac Repair After Myocardial Infarction: From Inflammation to Fibrosis. *Circ Res*. 2016 Jun 24;119(1):91–112.
17. Francis Stuart SD, De Jesus NM, Lindsey ML, Ripplinger CM. The crossroads of inflammation, fibrosis, and arrhythmia following myocardial infarction. *J Mol Cell Cardiol*. 2016 Feb;91:114–22.
18. Scalise RFM, De Sarro R, Caracciolo A, Lauro R, Squadrito F, Carerj S, et al. Fibrosis after Myocardial Infarction: An Overview on Cellular Processes, Molecular Pathways, Clinical Evaluation and Prognostic Value. *Med Sci*. 2021 Mar 1;9(1):16.
19. Chan JK, Roth J, Oppenheim JJ, Tracey KJ, Vogl T, Feldmann M, et al. Alarmins: awaiting a clinical response. *J Clin Invest*. 2012 Aug;122(8):2711–9.
20. Takahashi M. Cell-Specific Roles of NLRP3 Inflammasome in Myocardial Infarction. *J Cardiovasc Pharmacol*. 2019 Sep;74(3):188.
21. Ong SB, Hernández-Reséndiz S, Crespo-Avilan GE, Mukhametshina RT, Kwek XY, Cabrera-Fuentes HA, et al. Inflammation following acute myocardial infarction: Multiple players, dynamic roles, and novel therapeutic opportunities. *Pharmacol Ther*. 2018 Jun;186:73–87.
22. Nahrendorf M, Pittet MJ, Swirski FK. Monocytes: protagonists of infarct inflammation and repair after myocardial infarction. *Circulation*. 2010 Jun 8;121(22):2437–45.
23. Lambert JM, Lopez EF, Lindsey ML. Macrophage Roles Following Myocardial Infarction. *Int J Cardiol*. 2008 Nov 12;130(2):147–58.
24. Dewald O, Zymek P, Winkelmann K, Koerting A, Ren G, Abou-Khamis T, et al. CCL2/Monocyte Chemoattractant Protein-1 regulates inflammatory responses critical to healing myocardial infarcts. *Circ Res*. 2005 Apr 29;96(8):881–9.

25. Bajpai G, Bredemeyer A, Li W, Zaitsev K, Koenig AL, Lokshina I, et al. Tissue Resident CCR2⁻ and CCR2⁺ Cardiac Macrophages Differentially Orchestrate Monocyte Recruitment and Fate Specification Following Myocardial Injury. *Circ Res*. 2019 Jan 18;124(2):263–78.
26. Kubota A, Frangogiannis NG. Macrophages in myocardial infarction. *Am J Physiol - Cell Physiol*. 2022 Oct 1;323(4):C1304–24.
27. Tsujioka H, Imanishi T, Ikejima H, Kuroi A, Takarada S, Tanimoto T, et al. Impact of heterogeneity of human peripheral blood monocyte subsets on myocardial salvage in patients with primary acute myocardial infarction. *J Am Coll Cardiol*. 2009 Jul 7;54(2):130–8.
28. Bansal SS, Ismahil MA, Goel M, Patel B, Hamid T, Rokosh G, et al. Activated T-Lymphocytes are Essential Drivers of Pathological Remodeling in Ischemic Heart Failure. *Circ Heart Fail*. 2017 Mar;10(3):e003688.
29. Shinde AV, Frangogiannis NG. Fibroblasts in myocardial infarction: a role in inflammation and repair. *J Mol Cell Cardiol*. 2014 May;0:74–82.
30. van den Borne SWM, Diez J, Blankesteyn WM, Verjans J, Hofstra L, Narula J. Myocardial remodeling after infarction: the role of myofibroblasts. *Nat Rev Cardiol*. 2010 Jan;7(1):30–7.
31. Talman V, Ruskoaho H. Cardiac fibrosis in myocardial infarction—from repair and remodeling to regeneration. *Cell Tissue Res*. 2016 Sep;365(3):563–81.
32. Frangogiannis NG. Matricellular proteins in cardiac adaptation and disease. *Physiol Rev*. 2012 Apr;92(2):635–88.
33. Bujak M, Frangogiannis NG. The role of TGF- β Signaling in Myocardial Infarction and Cardiac Remodeling. *Cardiovasc Res*. 2007 May 1;74(2):184–95.
34. Ulloa L, Doody J, Massagué J. Inhibition of transforming growth factor-beta/SMAD signalling by the interferon-gamma/STAT pathway. *Nature*. 1999 Feb 25;397(6721):710–3.
35. Bansal SS, Ismahil MA, Goel M, Zhou G, Rokosh G, Hamid T, et al. DYSFUNCTIONAL AND PRO-INFLAMMATORY REGULATORY T-LYMPHOCYTES ARE ESSENTIAL FOR ADVERSE CARDIAC REMODELING IN ISCHEMIC CARDIOMYOPATHY. *Circulation*. 2019 Jan 8;139(2):206–21.
36. Van Linthout S, Miteva K, Tschöpe C. Crosstalk between fibroblasts and inflammatory cells. *Cardiovasc Res*. 2014 May 1;102(2):258–69.

37. Crome SQ, Clive B, Wang AY, Kang CY, Chow V, Yu J, et al. Inflammatory effects of ex vivo human Th17 cells are suppressed by regulatory T cells. *J Immunol Baltim Md* 1950. 2010 Sep 15;185(6):3199–208.
38. Weirather J, Hofmann UD, Beyersdorf N, Ramos GC, Vogel B, Frey A, et al. Foxp3+ CD4+ T cells improve healing after myocardial infarction by modulating monocyte/macrophage differentiation. *Circ Res*. 2014 Jun 20;115(1):55–67.
39. Ilatovskaya DV, Pitts C, Clayton J, Domondon M, Troncoso M, Pippin S, et al. CD8+ T-cells negatively regulate inflammation post-myocardial infarction. *Am J Physiol Heart Circ Physiol*. 2019 Sep 1;317(3):H581–96.
40. Weber KT, Sun Y, Bhattacharya SK, Ahokas RA, Gerling IC. Myofibroblast-mediated mechanisms of pathological remodelling of the heart. *Nat Rev Cardiol*. 2013 Jan;10(1):15–26.
41. Weber KT. Cardiac interstitium in health and disease: the fibrillar collagen network. *J Am Coll Cardiol*. 1989 Jun;13(7):1637–52.
42. Wei S, Chow LT, Shum IO, Qin L, Sanderson JE. Left and right ventricular collagen type I/III ratios and remodeling post-myocardial infarction. *J Card Fail*. 1999 Jun;5(2):117–26.
43. Caulfield JB, Borg TK. The collagen network of the heart. *Lab Investig J Tech Methods Pathol*. 1979 Mar;40(3):364–72.
44. Schimmel K, Ichimura K, Reddy S, Haddad F, Spiekerkoetter E. Cardiac Fibrosis in the Pressure Overloaded Left and Right Ventricle as a Therapeutic Target. *Front Cardiovasc Med*. 2022;9:886553.
45. Khan R, Sheppard R. Fibrosis in heart disease: understanding the role of transforming growth factor-beta in cardiomyopathy, valvular disease and arrhythmia. *Immunology*. 2006 May;118(1):10–24.
46. Nguyen MN, Kiriazis H, Gao XM, Du XJ. Cardiac Fibrosis and Arrhythmogenesis. *Compr Physiol*. 2017 Jun 18;7(3):1009–49.
47. Disertori M, Masè M, Ravelli F. Myocardial fibrosis predicts ventricular tachyarrhythmias. *Trends Cardiovasc Med*. 2017 Jul;27(5):363–72.
48. Cm R, Q L, W L, J H, Ir E. Panoramic imaging reveals basic mechanisms of induction and termination of ventricular tachycardia in rabbit heart with chronic infarction: implications for low-voltage cardioversion. *Heart Rhythm [Internet]*. 2009 Jan [cited 2024 Jun 30];6(1). Available from: <https://pubmed.ncbi.nlm.nih.gov/18996057/>

49. Nikolic G. Definition of ventricular tachycardia. *Am J Cardiol.* 1982 Nov;50(5):1197–8.
50. Nguyen TP, Qu Z, Weiss JN. Cardiac fibrosis and arrhythmogenesis: the road to repair is paved with perils. *J Mol Cell Cardiol.* 2014 May;70:83–91.
51. Pinto JM, Boyden PA. Electrical remodeling in ischemia and infarction. *Cardiovasc Res.* 1999 May;42(2):284–97.
52. Peters NS, Coromilas J, Severs NJ, Wit AL. Disturbed connexin43 gap junction distribution correlates with the location of reentrant circuits in the epicardial border zone of healing canine infarcts that cause ventricular tachycardia. *Circulation.* 1997 Feb 18;95(4):988–96.
53. Dun W, ter Keurs H, Boyden PA. The Role of Intracellular Ca²⁺ in Arrhythmias in the Postmyocardial Infarction Heart. In: Tripathi ON, Ravens U, Sanguinetti MC, editors. *Heart Rate and Rhythm: Molecular Basis, Pharmacological Modulation and Clinical Implications* [Internet]. Berlin, Heidelberg: Springer; 2011 [cited 2024 Jul 1]. p. 305–22. Available from: https://doi.org/10.1007/978-3-642-17575-6_16
54. Streitner F, Kuschyk J, Veltmann C, Brueckmann M, Streitner I, Brade J, et al. Prospective study of interleukin-6 and the risk of malignant ventricular tachyarrhythmia in ICD-recipients--a pilot study. *Cytokine.* 2007 Oct;40(1):30–4.
55. Maradit-Kremers H, Crowson CS, Nicola PJ, Ballman KV, Roger VL, Jacobsen SJ, et al. Increased unrecognized coronary heart disease and sudden deaths in rheumatoid arthritis: a population-based cohort study. *Arthritis Rheum.* 2005 Feb;52(2):402–11.
56. Byrne RA, Rossello X, Coughlan JJ, Barbato E, Berry C, Chieffo A, et al. 2023 ESC Guidelines for the management of acute coronary syndromes: Developed by the task force on the management of acute coronary syndromes of the European Society of Cardiology (ESC). *Eur Heart J.* 2023 Oct 7;44(38):3720–826.
57. Thygesen K, Alpert JS, Jaffe AS, Chaitman BR, Bax JJ, Morrow DA, et al. Fourth universal definition of myocardial infarction (2018). *Eur Heart J.* 2019 Jan 14;40(3):237–69.
58. Thygesen K, Alpert JS, Jaffe AS, Simoons ML, Chaitman BR, White HD, et al. Third universal definition of myocardial infarction. *Eur Heart J.* 2012 Oct;33(20):2551–67.
59. Diercks DB, Peacock WF, Hiestand BC, Chen AY, Pollack CV, Kirk JD, et al. Frequency and consequences of recording an electrocardiogram >10 minutes after arrival in an

emergency room in non-ST-segment elevation acute coronary syndromes (from the CRUSADE Initiative). *Am J Cardiol*. 2006 Feb 15;97(4):437–42.

60. Ibanez B, James S, Agewall S, Antunes MJ, Bucciarelli-Ducci C, Bueno H, et al. 2017 ESC Guidelines for the management of acute myocardial infarction in patients presenting with ST-segment elevation: The Task Force for the management of acute myocardial infarction in patients presenting with ST-segment elevation of the European Society of Cardiology (ESC). *Eur Heart J*. 2018 Jan 7;39(2):119–77.

61. Thygesen K, Mair J, Katus H, Plebani M, Venge P, Collinson P, et al. Recommendations for the use of cardiac troponin measurement in acute cardiac care. *Eur Heart J*. 2010 Sep;31(18):2197–204.

62. Thygesen K, Mair J, Giannitsis E, Mueller C, Lindahl B, Blankenberg S, et al. How to use high-sensitivity cardiac troponins in acute cardiac care. *Eur Heart J*. 2012 Sep;33(18):2252–7.

63. Mueller C. Biomarkers and acute coronary syndromes: an update. *Eur Heart J*. 2014 Mar;35(9):552–6.

64. Goodman SG, Steg PG, Eagle KA, Fox KAA, López-Sendón J, Montalescot G, et al. The diagnostic and prognostic impact of the redefinition of acute myocardial infarction: lessons from the Global Registry of Acute Coronary Events (GRACE). *Am Heart J*. 2006 Mar;151(3):654–60.

65. Fox KAA, FitzGerald G, Puymirat E, Huang W, Carruthers K, Simon T, et al. Should patients with acute coronary disease be stratified for management according to their risk? Derivation, external validation and outcomes using the updated GRACE risk score. *BMJ Open*. 2014 Feb 1;4(2):e004425.

66. Martínez-González B, Reyes-Hernández CG, Quiroga-Garza A, Rodríguez-Rodríguez VE, Esparza-Hernández CN, Elizondo-Omaña RE, et al. Conduits Used in Coronary Artery Bypass Grafting: A Review of Morphological Studies. *Ann Thorac Cardiovasc Surg*. 2017;23(2):55–65.

67. Baig MU, Bodle J. Thrombolytic Therapy. In: StatPearls [Internet]. Treasure Island (FL): StatPearls Publishing; 2024 [cited 2024 Jan 28]. Available from: <http://www.ncbi.nlm.nih.gov/books/NBK557411/>

68. Boersma E, Maas AC, Deckers JW, Simoons ML. Early thrombolytic treatment in acute myocardial infarction: reappraisal of the golden hour. *Lancet Lond Engl*. 1996 Sep 21;348(9030):771–5.
69. Morrison LJ, Verbeek PR, McDonald AC, Sawadsky BV, Cook DJ. Mortality and prehospital thrombolysis for acute myocardial infarction: A meta-analysis. *JAMA*. 2000 May 24;283(20):2686–92.
70. Zeymer U, Gitt A, Jünger C, Bauer T, Heer T, Koeth O, et al. Clopidogrel in addition to aspirin reduces in-hospital major cardiac and cerebrovascular events in unselected patients with acute ST segment elevation myocardial. *Thromb Haemost*. 2008 Jan;99(1):155–60.
71. Wallentin L, Becker RC, Budaj A, Cannon CP, Emanuelsson H, Held C, et al. Ticagrelor versus Clopidogrel in Patients with Acute Coronary Syndromes. *N Engl J Med*. 2009 Sep 10;361(11):1045–57.
72. Wiviott SD, Braunwald E, McCabe CH, Montalescot G, Ruzyllo W, Gottlieb S, et al. Prasugrel versus Clopidogrel in Patients with Acute Coronary Syndromes. *N Engl J Med*. 2007 Nov 15;357(20):2001–15.
73. Ambrosetti M, Abreu A, Corrà U, Davos CH, Hansen D, Frederix I, et al. Secondary prevention through comprehensive cardiovascular rehabilitation: From knowledge to implementation. 2020 update. A position paper from the Secondary Prevention and Rehabilitation Section of the European Association of Preventive Cardiology. *Eur J Prev Cardiol*. 2021 May 14;28(5):460–95.
74. Salzwedel A, Jensen K, Rauch B, Doherty P, Metzendorf MI, Hackbusch M, et al. Effectiveness of comprehensive cardiac rehabilitation in coronary artery disease patients treated according to contemporary evidence based medicine: Update of the Cardiac Rehabilitation Outcome Study (CROS-II). *Eur J Prev Cardiol*. 2020 Nov;27(16):1756–74.
75. Dibben G, Faulkner J, Oldridge N, Rees K, Thompson DR, Zwisler AD, et al. Exercise-based cardiac rehabilitation for coronary heart disease. *Cochrane Database Syst Rev*. 2021 Nov 6;11(11):CD001800.
76. Critchley JA, Capewell S. Mortality risk reduction associated with smoking cessation in patients with coronary heart disease: a systematic review. *JAMA*. 2003 Jul 2;290(1):86–97.
77. Delgado-Lista J, Alcalá-Díaz JF, Torres-Peña JD, Quintana-Navarro GM, Fuentes F, García-Ríos A, et al. Long-term secondary prevention of cardiovascular disease with a

Mediterranean diet and a low-fat diet (CORDIOPREV): a randomised controlled trial. *Lancet Lond Engl*. 2022 May 14;399(10338):1876–85.

78. Visseren FLJ, Mach F, Smulders YM, Carballo D, Koskinas KC, Bäck M, et al. 2021 ESC Guidelines on cardiovascular disease prevention in clinical practice. *Eur Heart J*. 2021 Sep 7;42(34):3227–337.

79. Bull FC, Al-Ansari SS, Biddle S, Borodulin K, Buman MP, Cardon G, et al. World Health Organization 2020 guidelines on physical activity and sedentary behaviour. *Br J Sports Med*. 2020 Dec 1;54(24):1451–62.

80. Dahl Aarvik M, Sandven I, Dondo TB, Gale CP, Ruddox V, Munkhaugen J, et al. Effect of oral β -blocker treatment on mortality in contemporary post-myocardial infarction patients: a systematic review and meta-analysis. *Eur Heart J Cardiovasc Pharmacother*. 2019 Jan 1;5(1):12–20.

81. Dargie HJ. Effect of carvedilol on outcome after myocardial infarction in patients with left-ventricular dysfunction: the CAPRICORN randomised trial. *Lancet Lond Engl*. 2001 May 5;357(9266):1385–90.

82. Køber L, Torp-Pedersen C, Carlsen JE, Bagger H, Eliassen P, Lyngborg K, et al. A clinical trial of the angiotensin-converting-enzyme inhibitor trandolapril in patients with left ventricular dysfunction after myocardial infarction. Trandolapril Cardiac Evaluation (TRACE) Study Group. *N Engl J Med*. 1995 Dec 21;333(25):1670–6.

83. Fox KM, EUROpean trial On reduction of cardiac events with Perindopril in stable coronary Artery disease Investigators. Efficacy of perindopril in reduction of cardiovascular events among patients with stable coronary artery disease: randomised, double-blind, placebo-controlled, multicentre trial (the EUROPA study). *Lancet Lond Engl*. 2003 Sep 6;362(9386):782–8.

84. Heart Outcomes Prevention Evaluation Study Investigators, Yusuf S, Sleight P, Pogue J, Bosch J, Davies R, et al. Effects of an angiotensin-converting-enzyme inhibitor, ramipril, on cardiovascular events in high-risk patients. *N Engl J Med*. 2000 Jan 20;342(3):145–53.

85. Jenča D, Melenovský V, Stehlik J, Staněk V, Kettner J, Kautzner J, et al. Heart failure after myocardial infarction: incidence and predictors. *ESC Heart Fail*. 2021 Feb;8(1):222–37.

86. Gerber Y, Weston SA, Enriquez-Sarano M, Berardi C, Chamberlain AM, Manemann SM, et al. Mortality Associated With Heart Failure After Myocardial Infarction: A Contemporary Community Perspective. *Circ Heart Fail*. 2016 Jan;9(1):e002460.

87. McMurray JJV, Packer M, Desai AS, Gong J, Lefkowitz MP, Rizkala AR, et al. Angiotensin–Neprilysin Inhibition versus Enalapril in Heart Failure. *N Engl J Med*. 2014 Sep 11;371(11):993–1004.
88. Shaddy R, Canter C, Halnon N, Kochilas L, Rossano J, Bonnet D, et al. Design for the sacubitril/valsartan (LCZ696) compared with enalapril study of pediatric patients with heart failure due to systemic left ventricle systolic dysfunction (PANORAMA-HF study). *Am Heart J*. 2017 Nov;193:23–34.
89. Solomon SD, McMurray JJV, Anand IS, Ge J, Lam CSP, Maggioni AP, et al. Angiotensin–Neprilysin Inhibition in Heart Failure with Preserved Ejection Fraction. *N Engl J Med*. 2019 Oct 24;381(17):1609–20.
90. Fountain JH, Kaur J, Lappin SL. Physiology, Renin Angiotensin System. In: StatPearls [Internet]. Treasure Island (FL): StatPearls Publishing; 2024 [cited 2024 Feb 1]. Available from: <http://www.ncbi.nlm.nih.gov/books/NBK470410/>
91. Volpe M. Natriuretic peptides and cardio-renal disease. *Int J Cardiol*. 2014 Oct 20;176(3):630–9.
92. Mangiafico S, Costello-Boerrigter LC, Andersen IA, Cataliotti A, Burnett JC. Neutral endopeptidase inhibition and the natriuretic peptide system: an evolving strategy in cardiovascular therapeutics. *Eur Heart J*. 2013 Mar;34(12):886–893c.
93. Iborra-Egea O, Gálvez-Montón C, Roura S, Perea-Gil I, Prat-Vidal C, Soler-Botija C, et al. Mechanisms of action of sacubitril/valsartan on cardiac remodeling: a systems biology approach. *Npj Syst Biol Appl*. 2017 Apr 18;3(1):1–9.
94. Kario K, Sun N, Chiang FT, Supasyndh O, Baek SH, Inubushi-Molessa A, et al. Efficacy and Safety of LCZ696, a First-in-Class Angiotensin Receptor Neprilysin Inhibitor, in Asian Patients With Hypertension. *Hypertension*. 2014 Apr;63(4):698–705.
95. Kario K, Rakugi H, Yarimizu D, Morita Y, Eguchi S, Iekushi K. Twenty-Four-Hour Blood Pressure-Lowering Efficacy of Sacubitril/Valsartan Versus Olmesartan in Japanese Patients With Essential Hypertension Based on Nocturnal Blood Pressure Dipping Status: A Post Hoc Analysis of Data From a Randomized, Double-Blind Multicenter Study. *J Am Heart Assoc*. 2023 Apr 18;12(8):e027612.
96. De Vecchis R, Soreca S, Ariano C. Anti-Hypertensive Effect of Sacubitril/Valsartan: A Meta-Analysis of Randomized Controlled Trials. *Cardiol Res*. 2019 Feb;10(1):24–33.

97. Malik AH, Aronow WS. Efficacy of Sacubitril/Valsartan in Hypertension. *Am J Ther.* 2022 Jun 1;29(3):e322–33.
98. Geng Q, Yan R, Wang Z, Hou F. Effects of LCZ696 (Sacubitril/Valsartan) on Blood Pressure in Patients with Hypertension: A Meta-Analysis of Randomized Controlled Trials. *Cardiology.* 2020 Jul 29;145(9):589–98.
99. Valentim Goncalves A, Pereira-da-Silva T, Galrinho A, Rio P, Moura Branco L, Soares R, et al. C-reactive protein reduction with sacubitril-valsartan treatment in heart failure patients. *Am J Cardiovasc Dis.* 2020 Aug 15;10(3):174–81.
100. Pang Z, Pan C, Yao Z, Ren Y, Tian L, Cui J, et al. A study of the sequential treatment of acute heart failure with sacubitril/valsartan by recombinant human brain natriuretic peptide. *Medicine (Baltimore).* 2021 Apr 23;100(16):e25621.
101. Bunsawat K, Ratchford SM, Alpenglow JK, Park SH, Jarrett CL, Stehlik J, et al. Sacubitril-valsartan improves conduit vessel function and functional capacity and reduces inflammation in heart failure with reduced ejection fraction. *J Appl Physiol Bethesda Md* 1985. 2021 Jan 1;130(1):256–68.
102. Yu C, Li D, Li Z, Yu D, Zhai G. Effect of sacubitril/valsartan on inflammation and oxidative stress in doxorubicin-induced heart failure model in rabbits. *Acta Pharm Zagreb Croat.* 2021 Sep 1;71(3):473–84.
103. Shi YJ, Yang CG, Qiao WB, Liu YC, Liu SY, Dong GJ. Sacubitril/valsartan attenuates myocardial inflammation, hypertrophy, and fibrosis in rats with heart failure with preserved ejection fraction. *Eur J Pharmacol.* 2023 Dec 15;961:176170.
104. Ishii M, Kaikita K, Sato K, Sueta D, Fujisue K, Arima Y, et al. Cardioprotective Effects of LCZ696 (Sacubitril/Valsartan) After Experimental Acute Myocardial Infarction. *JACC Basic Transl Sci.* 2017 Dec;2(6):655–68.
105. Shen JF, Fan ZB, Wu CW, Qi GX, Cao QY, Xu F. Sacubitril Valsartan Enhances Cardiac Function and Alleviates Myocardial Infarction in Rats through a SUV39H1/SPP1 Axis. *Oxid Med Cell Longev.* 2022;2022:5009289.
106. Mohany M, Ahmed MM, Al-Rejaie SS. The Role of NF- κ B and Bax/Bcl-2/Caspase-3 Signaling Pathways in the Protective Effects of Sacubitril/Valsartan (Entresto) against HFD/STZ-Induced Diabetic Kidney Disease. *Biomedicines.* 2022 Nov 9;10(11):2863.

107. Imran M, Hassan MQ, Akhtar MS, Rahman O, Akhtar M, Najmi AK. Sacubitril and valsartan protect from experimental myocardial infarction by ameliorating oxidative damage in Wistar rats. *Clin Exp Hypertens N Y N* 1993. 2019;41(1):62–9.
108. Zile MR, O'Meara E, Claggett B, Prescott MF, Solomon SD, Swedberg K, et al. Effects of Sacubitril/Valsartan on Biomarkers of Extracellular Matrix Regulation in Patients With HFrEF. *J Am Coll Cardiol*. 2019 Feb 26;73(7):795–806.
109. Cunningham JW, Claggett BL, O'Meara E, Prescott MF, Pfeffer MA, Shah SJ, et al. Effect of Sacubitril/Valsartan on Biomarkers of Extracellular Matrix Regulation in Patients With HFpEF. *J Am Coll Cardiol*. 2020 Aug 4;76(5):503–14.
110. Maslov MY, Foianini S, Mayer D, Orlov MV, Lovich MA. Synergy between sacubitril and valsartan leads to hemodynamic, antifibrotic, and exercise tolerance benefits in rats with preexisting heart failure. *Am J Physiol Heart Circ Physiol*. 2019 Feb 1;316(2):H289–97.
111. Schauer A, Adams V, Augstein A, Jannasch A, Draskowski R, Kirchhoff V, et al. Sacubitril/Valsartan Improves Diastolic Function But Not Skeletal Muscle Function in a Rat Model of HFpEF. *Int J Mol Sci*. 2021 Mar 30;22(7):3570.
112. von Lueder TG, Wang BH, Kompa AR, Huang L, Webb R, Jordaan P, et al. Angiotensin receptor neprilysin inhibitor LCZ696 attenuates cardiac remodeling and dysfunction after myocardial infarction by reducing cardiac fibrosis and hypertrophy. *Circ Heart Fail*. 2015 Jan;8(1):71–8.
113. Trivedi RK, Polhemus DJ, Li Z, Yoo D, Koiwaya H, Scarborough A, et al. Combined Angiotensin Receptor–Neprilysin Inhibitors Improve Cardiac and Vascular Function Via Increased NO Bioavailability in Heart Failure. *J Am Heart Assoc Cardiovasc Cerebrovasc Dis*. 2018 Mar 3;7(5):e008268.
114. Wu M, Guo Y, Wu Y, Xu K, Lin L. Protective Effects of Sacubitril/Valsartan on Cardiac Fibrosis and Function in Rats With Experimental Myocardial Infarction Involves Inhibition of Collagen Synthesis by Myocardial Fibroblasts Through Downregulating TGF- β 1/Smads Pathway. *Front Pharmacol*. 2021;12:696472.
115. Liu J, Zheng X, Zhang C, Zhang C, Bu P. Lcz696 Alleviates Myocardial Fibrosis After Myocardial Infarction Through the sFRP-1/Wnt/ β -Catenin Signaling Pathway. *Front Pharmacol*. 2021;12:724147.

116. Shen J, Fan Z, Sun G, Qi G. Sacubitril/valsartan (LCZ696) reduces myocardial injury following myocardial infarction by inhibiting NLRP3-induced pyroptosis via the TAK1/JNK signaling pathway. *Mol Med Rep.* 2021 Sep;24(3):676.
117. Kompa AR, Lu J, Weller TJ, Kelly DJ, Krum H, von Lueder TG, et al. Angiotensin receptor neprilysin inhibition provides superior cardioprotection compared to angiotensin converting enzyme inhibition after experimental myocardial infarction. *Int J Cardiol.* 2018 May 1;258:192–8.
118. Suematsu Y, Miura S ichiro, Goto M, Matsuo Y, Arimura T, Kuwano T, et al. LCZ696, an angiotensin receptor–neprilysin inhibitor, improves cardiac function with the attenuation of fibrosis in heart failure with reduced ejection fraction in streptozotocin-induced diabetic mice. *Eur J Heart Fail.* 2016;18(4):386–93.
119. Januzzi JL, Prescott MF, Butler J, Felker GM, Maisel AS, McCague K, et al. Association of Change in N-Terminal Pro–B-Type Natriuretic Peptide Following Initiation of Sacubitril-Valsartan Treatment With Cardiac Structure and Function in Patients With Heart Failure With Reduced Ejection Fraction. *JAMA.* 2019 Sep 17;322(11):1085–95.
120. Gokhroo RK, Anushri K, Tarik MT, Kailash C, Rajesh N, Ashish K, et al. 1 year follow Up results of “ARTIM HF TRIAL” (angiotensin receptor neprilysin inhibitor effect on TEI index & left ventricular mass in heart failure). *Indian Heart J.* 2021;73(2):205–10.
121. Liu LW, Wu PC, Chiu MY, Tu PF, Fang CC. Sacubitril/Valsartan Improves Left Ventricular Ejection Fraction and Reverses Cardiac Remodeling in Taiwanese Patients with Heart Failure and Reduced Ejection Fraction. *Acta Cardiol Sin.* 2020 Mar;36(2):125.
122. Hu J, Wu Y, Zhou X, Wang X, Jiang W, Huo J, et al. Beneficial Effects of Sacubitril/Valsartan at Low Doses in an Asian Real-World Heart Failure Population. *J Cardiovasc Pharmacol.* 2020 Oct;76(4):445–51.
123. Bolla GB, Fedele A, Faggiano A, Sala C, Santangelo G, Carugo S. Effects of Sacubitril/Valsartan on biomarkers of fibrosis and inflammation in patients with heart failure with reduced ejection fraction. *BMC Cardiovasc Disord.* 2022 May 13;22(1):217.
124. Vitale G, Romano G, Di Franco A, Caccamo G, Nugara C, Ajello L, et al. Early Effects of Sacubitril/Valsartan on Exercise Tolerance in Patients with Heart Failure with Reduced Ejection Fraction. *J Clin Med.* 2019 Feb 20;8(2):262.

125. Fan G, Zhou C, Hou T, Li X, Wang L, Wang C. Effects of Sacubitril/Valsartan on cardiac function, blood biochemistry and clinical efficacy in early ventricular remodeling after acute myocardial infarction. *Biotechnol Genet Eng Rev*. 2023 Apr 12;1–16.
126. Rezaq A, Saad M, El Nozahi M. Comparison of the Efficacy and Safety of Sacubitril/Valsartan versus Ramipril in Patients With ST-Segment Elevation Myocardial Infarction. *Am J Cardiol*. 2021 Mar 15;143:7–13.
127. Shah AM, Claggett B, Prasad N, Li G, Volquez M, Jering K, et al. Impact of Sacubitril/Valsartan Compared With Ramipril on Cardiac Structure and Function After Acute Myocardial Infarction: The PARADISE-MI Echocardiographic Substudy. *Circulation*. 2022 Oct 4;146(14):1067–81.
128. Martens P, Nuyens D, Rivero-Ayerza M, Van Herendael H, Vercammen J, Ceysens W, et al. Sacubitril/valsartan reduces ventricular arrhythmias in parallel with left ventricular reverse remodeling in heart failure with reduced ejection fraction. *Clin Res Cardiol*. 2019 Oct 1;108(10):1074–82.
129. Medeiros P, Coelho C, Costa-Oliveira C, Rocha S. The Effect of Sacubitril-Valsartan on Ventricular Arrhythmia Burden in Patients With Heart Failure With Reduced Ejection Fraction. *Cureus*. 2023 Feb;15(2):e34508.
130. Diego C de, González-Torres L, Núñez JM, Inda RC, Martin-Langerwerf DA, Sangio AD, et al. Effects of angiotensin-neprilysin inhibition compared to angiotensin inhibition on ventricular arrhythmias in reduced ejection fraction patients under continuous remote monitoring of implantable defibrillator devices. *Heart Rhythm*. 2018 Mar 1;15(3):395–402.
131. Wang R, Ye H, Ma L, Wei J, Wang Y, Zhang X, et al. Effect of Sacubitril/Valsartan on Reducing the Risk of Arrhythmia: A Systematic Review and Meta-Analysis of Randomized Controlled Trials. *Front Cardiovasc Med*. 2022;9:890481.
132. Chang PC, Lin SF, Chu Y, Wo HT, Lee HL, Huang YC, et al. LCZ696 Therapy Reduces Ventricular Tachyarrhythmia Inducibility in a Myocardial Infarction-Induced Heart Failure Rat Model. *Cardiovasc Ther*. 2019;2019:6032631.
133. Chang PC, Wo HT, Lee HL, Lin SF, Chu Y, Wen MS, et al. Sacubitril/Valsartan Therapy Ameliorates Ventricular Tachyarrhythmia Inducibility in a Rabbit Myocardial Infarction Model. *J Card Fail*. 2020 Jun;26(6):527–37.

134. Jackson AM, Jhund PS, Anand IS, Düngen HD, Lam CSP, Lefkowitz MP, et al. Sacubitril–valsartan as a treatment for apparent resistant hypertension in patients with heart failure and preserved ejection fraction. *Eur Heart J*. 2021 Sep 21;42(36):3741–52.
135. Ge Q, Zhao L, Ren XM, Ye P, Hu ZY. Feature article: LCZ696, an angiotensin receptor-neprilysin inhibitor, ameliorates diabetic cardiomyopathy by inhibiting inflammation, oxidative stress and apoptosis. *Exp Biol Med*. 2019 Sep;244(12):1028–39.
136. Zhang H, Liu G, Zhou W, Zhang W, Wang K, Zhang J. Neprilysin Inhibitor-Angiotensin II Receptor Blocker Combination Therapy (Sacubitril/valsartan) Suppresses Atherosclerotic Plaque Formation and Inhibits Inflammation in Apolipoprotein E- Deficient Mice. *Sci Rep*. 2019 Apr 24;9(1):6509.
137. Wu Z, Chen H, Lin L, Lu J, Zhao Q, Dong Z, et al. Sacubitril/valsartan protects against arsenic trioxide induced cardiotoxicity in vivo and in vitro. *Toxicol Res*. 2022 Jun;11(3):451–9.
138. Dindaş F, Güngör H, Ekici M, Akokay P, Erhan F, Doğduş M, et al. Angiotensin receptor-neprilysin inhibition by sacubitril/valsartan attenuates doxorubicin-induced cardiotoxicity in a pretreatment mice model by interfering with oxidative stress, inflammation, and Caspase 3 apoptotic pathway. *Anatol J Cardiol*. 2021 Oct 19;25(11):821–8.
139. Shulzhenko LV, Pershukov IV, Batyraliev TA, Karben ZA, Gurovich OV, Fettser DV, et al. The Clinical Evolution of Diffuse Myocardial Fibrosis in Patients With Arterial Hypertension and Heart Failure With Mildly Reduced Ejection Fraction Treated by Olmesartan or Sacubitril / Valsartan. *Kardiologija*. 2023 Dec 26;63(12):31–8.
140. Liu Y, Zhong C, Si J, Chen S, Kang L, Xu B. The impact of Sacubitril/Valsartan on cardiac fibrosis early after myocardial infarction in hypertensive rats. *J Hypertens*. 2022 Sep 1;40(9):1822–30.
141. Li X, Braza J, Mende U, Choudhary G, Zhang P. Cardioprotective effects of early intervention with sacubitril/valsartan on pressure overloaded rat hearts. *Sci Rep*. 2021 Aug 16;11:16542.
142. Ai J, Liu J, Liu M. Data on effect of Sacubitril/valsartan on cardiac Remodelling in diabetic Cardiomyopathy rats. *Data Brief*. 2021 Apr;35:106963.

143. Vicent L, Méndez-Zurita F, Viñolas X, Alonso-Martín C, Arbòs CM, Pamies J, et al. Clinical characteristics of patients with sustained ventricular arrhythmias after sacubitril/valsartan initiation. *Heart Vessels*. 2020 Jan;35(1):136–42.
144. Vicent L, Juárez M, Bruña V, Devesa C, Sousa-Casasnovas I, Fernández-Avilés F, et al. Clinical Profile and Ventricular Arrhythmias after Sacubitril/Valsartan Initiation. *Cardiology*. 2019;142(1):26–7.
145. Okutucu S, Oto A. Electrical Storm after Initiating Sacubitril/Valsartan: Arrhythmic Paradox. *Cardiology*. 2019;142(1):24–5.
146. Zinman B, Wanner C, Lachin JM, Fitchett D, Bluhmki E, Hantel S, et al. Empagliflozin, Cardiovascular Outcomes, and Mortality in Type 2 Diabetes. *N Engl J Med*. 2015 Nov 26;373(22):2117–28.
147. Wiviott SD, Raz I, Bonaca MP, Mosenzon O, Kato ET, Cahn A, et al. Dapagliflozin and Cardiovascular Outcomes in Type 2 Diabetes. *N Engl J Med*. 2019 Jan 24;380(4):347–57.
148. Packer M, Anker SD, Butler J, Filippatos G, Pocock SJ, Carson P, et al. Cardiovascular and Renal Outcomes with Empagliflozin in Heart Failure. *N Engl J Med*. 2020 Oct 8;383(15):1413–24.
149. Anker SD, Butler J, Filippatos G, Ferreira JP, Bocchi E, Böhm M, et al. Empagliflozin in Heart Failure with a Preserved Ejection Fraction. *N Engl J Med*. 2021 Oct 14;385(16):1451–61.
150. McMurray JJV, Solomon SD, Inzucchi SE, Køber L, Kosiborod MN, Martinez FA, et al. Dapagliflozin in Patients with Heart Failure and Reduced Ejection Fraction. *N Engl J Med*. 2019 Nov 21;381(21):1995–2008.
151. Solomon SD, McMurray JJV, Claggett B, de Boer RA, DeMets D, Hernandez AF, et al. Dapagliflozin in Heart Failure with Mildly Reduced or Preserved Ejection Fraction. *N Engl J Med*. 2022 Sep 22;387(12):1089–98.
152. The EMPA-KIDNEY Collaborative Group, Herrington WG, Staplin N, Wanner C, Green JB, Hauske SJ, et al. Empagliflozin in Patients with Chronic Kidney Disease. *N Engl J Med*. 2023 Jan 12;388(2):117–27.
153. Heerspink HJL, Stefánsson BV, Correa-Rotter R, Chertow GM, Greene T, Hou FF, et al. Dapagliflozin in Patients with Chronic Kidney Disease. *N Engl J Med*. 2020 Oct 8;383(15):1436–46.

154. McDonagh TA, Metra M, Adamo M, Gardner RS, Baumbach A, Böhm M, et al. 2021 ESC Guidelines for the diagnosis and treatment of acute and chronic heart failure: Developed by the Task Force for the diagnosis and treatment of acute and chronic heart failure of the European Society of Cardiology (ESC) With the special contribution of the Heart Failure Association (HFA) of the ESC. *Eur Heart J*. 2021 Sep 21;42(36):3599–726.
155. McDonagh TA, Metra M, Adamo M, Gardner RS, Baumbach A, Böhm M, et al. 2023 Focused Update of the 2021 ESC Guidelines for the diagnosis and treatment of acute and chronic heart failure: Developed by the task force for the diagnosis and treatment of acute and chronic heart failure of the European Society of Cardiology (ESC) With the special contribution of the Heart Failure Association (HFA) of the ESC. *Eur Heart J*. 2023 Oct 1;44(37):3627–39.
156. Hediger MA, Rhoads DB. Molecular physiology of sodium-glucose cotransporters. *Physiol Rev*. 1994 Oct;74(4):993–1026.
157. Bakris GL, Fonseca VA, Sharma K, Wright EM. Renal sodium–glucose transport: role in diabetes mellitus and potential clinical implications. *Kidney Int*. 2009 Jun 2;75(12):1272–7.
158. List JF, Whaley JM. Glucose dynamics and mechanistic implications of SGLT2 inhibitors in animals and humans. *Kidney Int Suppl*. 2011 Mar;(120):S20-27.
159. Williams DM, Nawaz A, Evans M. Sodium-Glucose Co-Transporter 2 (SGLT2) Inhibitors: Are They All the Same? A Narrative Review of Cardiovascular Outcome Trials. *Diabetes Ther Res Treat Educ Diabetes Relat Disord*. 2021 Jan;12(1):55–70.
160. Lahnwong C, Chattipakorn SC, Chattipakorn N. Potential mechanisms responsible for cardioprotective effects of sodium-glucose co-transporter 2 inhibitors. *Cardiovasc Diabetol*. 2018 Jul 10;17(1):101.
161. Iborra-Egea O, Santiago-Vacas E, Yurista SR, Lupón J, Packer M, Heymans S, et al. Unraveling the Molecular Mechanism of Action of Empagliflozin in Heart Failure With Reduced Ejection Fraction With or Without Diabetes. *JACC Basic Transl Sci*. 2019 Nov;4(7):831–40.
162. Bayes-Genis A, Iborra-Egea O, Spitaleri G, Domingo M, Revuelta-López E, Codina P, et al. Decoding empagliflozin’s molecular mechanism of action in heart failure with preserved ejection fraction using artificial intelligence. *Sci Rep*. 2021 Jun 8;11:12025.

163. Chilton R, Tikkanen I, Cannon CP, Crowe S, Woerle HJ, Broedl UC, et al. Effects of empagliflozin on blood pressure and markers of arterial stiffness and vascular resistance in patients with type 2 diabetes. *Diabetes Obes Metab*. 2015;17(12):1180–93.
164. Tikkanen I, Narko K, Zeller C, Green A, Salsali A, Broedl UC, et al. Empagliflozin Reduces Blood Pressure in Patients With Type 2 Diabetes and Hypertension. *Diabetes Care*. 2014 Sep 30;38(3):420–8.
165. Packer M, Anker SD, Butler J, Filippatos G, Ferreira JP, Pocock SJ, et al. Influence of neprilysin inhibition on the efficacy and safety of empagliflozin in patients with chronic heart failure and a reduced ejection fraction: the EMPEROR-Reduced trial. *Eur Heart J*. 2021 Feb 11;42(6):671–80.
166. Packer M, Butler J, Zeller C, Pocock SJ, Brueckmann M, Ferreira JP, et al. Blinded Withdrawal of Long-Term Randomized Treatment With Empagliflozin or Placebo in Patients With Heart Failure. *Circulation*. 2023 Sep 26;148(13):1011–22.
167. Gotzmann M, Henk P, Stervbo U, Blázquez-Navarro A, Mügge A, Babel N, et al. Empagliflozin Reduces Interleukin-6 Levels in Patients with Heart Failure. *J Clin Med*. 2023 Jul 3;12(13):4458.
168. Koliijn D, Pabel S, Tian Y, Lódi M, Herwig M, Carrizzo A, et al. Empagliflozin improves endothelial and cardiomyocyte function in human heart failure with preserved ejection fraction via reduced pro-inflammatory-oxidative pathways and protein kinase G α oxidation. *Cardiovasc Res*. 2021 Jan 21;117(2):495–507.
169. Gohari S, Reshadmanesh T, Khodabandehloo H, Karbalaee-Hasani A, Ahangar H, Arsang-Jang S, et al. The effect of EMPAgliflozin on markers of inflammation in patients with concomitant type 2 diabetes mellitus and Coronary ARtery Disease: the EMPA-CARD randomized controlled trial. *Diabetol Metab Syndr*. 2022 Nov 17;14:170.
170. Kim SR, Lee SG, Kim SH, Kim JH, Choi E, Cho W, et al. SGLT2 inhibition modulates NLRP3 inflammasome activity via ketones and insulin in diabetes with cardiovascular disease. *Nat Commun*. 2020 May 1;11(1):2127.
171. Quagliariello V, De Laurentiis M, Rea D, Barbieri A, Monti MG, Carbone A, et al. The SGLT-2 inhibitor empagliflozin improves myocardial strain, reduces cardiac fibrosis and pro-inflammatory cytokines in non-diabetic mice treated with doxorubicin. *Cardiovasc Diabetol*. 2021 Jul 23;20(1):150.

172. Theofilis P, Sigris M, Oikonomou E, Antonopoulos AS, Siasos G, Tsioufis K, et al. The impact of SGLT2 inhibitors on inflammation: A systematic review and meta-analysis of studies in rodents. *Int Immunopharmacol*. 2022 Oct;111:109080.
173. Aragón-Herrera A, Feijóo-Bandín S, Otero Santiago M, Barral L, Campos-Toimil M, Gil-Longo J, et al. Empagliflozin reduces the levels of CD36 and cardiotoxic lipids while improving autophagy in the hearts of Zucker diabetic fatty rats. *Biochem Pharmacol*. 2019 Dec;170:113677.
174. Byrne NJ, Matsumura N, Maayah ZH, Ferdaoussi M, Takahara S, Darwesh AM, et al. Empagliflozin Blunts Worsening Cardiac Dysfunction Associated With Reduced NLRP3 (Nucleotide-Binding Domain-Like Receptor Protein 3) Inflammasome Activation in Heart Failure. *Circ Heart Fail*. 2020 Jan;13(1):e006277.
175. Xu L, Nagata N, Nagashimada M, Zhuge F, Ni Y, Chen G, et al. SGLT2 Inhibition by Empagliflozin Promotes Fat Utilization and Browning and Attenuates Inflammation and Insulin Resistance by Polarizing M2 Macrophages in Diet-induced Obese Mice. *EBioMedicine*. 2017 Jun;20:137–49.
176. Aragón-Herrera A, Moraña-Fernández S, Otero-Santiago M, Anido-Varela L, Campos-Toimil M, García-Seara J, et al. The lipidomic and inflammatory profiles of visceral and subcutaneous adipose tissues are distinctly regulated by the SGLT2 inhibitor empagliflozin in Zucker diabetic fatty rats. *Biomed Pharmacother Biomedecine Pharmacother*. 2023 May;161:114535.
177. Ashrafi Jigheh Z, Ghorbani Haghjo A, Argani H, Roshangar L, Rashtchizadeh N, Sanajou D, et al. Empagliflozin alleviates renal inflammation and oxidative stress in streptozotocin-induced diabetic rats partly by repressing HMGB1-TLR4 receptor axis. *Iran J Basic Med Sci*. 2019 Apr;22(4):384–90.
178. Wu X, Li H, Wan Z, Wang R, Liu J, Liu Q, et al. The combination of ursolic acid and empagliflozin relieves diabetic nephropathy by reducing inflammation, oxidative stress and renal fibrosis. *Biomed Pharmacother Biomedecine Pharmacother*. 2021 Dec;144:112267.
179. Thirunavukarasu S, Jex N, Chowdhary A, Hassan IU, Straw S, Craven TP, et al. Empagliflozin Treatment Is Associated With Improvements in Cardiac Energetics and Function and Reductions in Myocardial Cellular Volume in Patients With Type 2 Diabetes. *Diabetes*. 2021 Dec;70(12):2810–22.

180. Hiruma S, Shigiyama F, Hisatake S, Mizumura S, Shiraga N, Hori M, et al. A prospective randomized study comparing effects of empagliflozin to sitagliptin on cardiac fat accumulation, cardiac function, and cardiac metabolism in patients with early-stage type 2 diabetes: the ASSET study. *Cardiovasc Diabetol*. 2021 Feb 2;20(1):32.
181. Gaborit B, Ancel P, Abdullah AE, Maurice F, Abdesselam I, Calen A, et al. Effect of empagliflozin on ectopic fat stores and myocardial energetics in type 2 diabetes: the EMPACEF study. *Cardiovasc Diabetol*. 2021 Mar 1;20(1):57.
182. Santos-Gallego CG, Requena-Ibanez JA, San Antonio R, Ishikawa K, Watanabe S, Picatoste B, et al. Empagliflozin Ameliorates Adverse Left Ventricular Remodeling in Nondiabetic Heart Failure by Enhancing Myocardial Energetics. *J Am Coll Cardiol*. 2019 Apr 23;73(15):1931–44.
183. Lyu Y, Huo J, Jiang W, Yang W, Wang S, Zhang S, et al. Empagliflozin ameliorates cardiac dysfunction in heart failure mice via regulating mitochondrial dynamics. *Eur J Pharmacol*. 2023 Mar 5;942:175531.
184. Yurista SR, Silljé HHW, Oberdorf-Maass SU, Schouten EM, Pavez Giani MG, Hillebrands JL, et al. Sodium-glucose co-transporter 2 inhibition with empagliflozin improves cardiac function in non-diabetic rats with left ventricular dysfunction after myocardial infarction. *Eur J Heart Fail*. 2019 Jul;21(7):862–73.
185. Chase D, Eykyn TR, Shattock MJ, Chung YJ. Empagliflozin improves cardiac energetics during ischaemia/reperfusion by directly increasing cardiac ketone utilization. *Cardiovasc Res*. 2023 Dec 19;119(16):2672–80.
186. Ferreira JP, Butler J, Anker SD, Januzzi JL, Panova-Noeva M, Reese-Petersen AL, et al. Effects of empagliflozin on collagen biomarkers in patients with heart failure: Findings from the EMPEROR trials. *Eur J Heart Fail*. 2024 Feb;26(2):274–84.
187. Requena-Ibáñez JA, Santos-Gallego CG, Rodríguez-Cordero A, Vargas-Delgado AP, Mancini D, Sartori S, et al. Mechanistic Insights of Empagliflozin in Nondiabetic Patients With HFrEF: From the EMPA-TROPISM Study. *JACC Heart Fail*. 2021 Aug;9(8):578–89.
188. Mason T, Coelho-Filho OR, Verma S, Chowdhury B, Zuo F, Quan A, et al. Empagliflozin Reduces Myocardial Extracellular Volume in Patients With Type 2 Diabetes and Coronary Artery Disease. *JACC Cardiovasc Imaging*. 2021 Jun;14(6):1164–73.
189. Santos-Gallego CG, Requena-Ibanez JA, San Antonio R, Garcia-Roper A, Ishikawa K, Watanabe S, et al. Empagliflozin Ameliorates Diastolic Dysfunction and Left Ventricular

Fibrosis/Stiffness in Nondiabetic Heart Failure: A Multimodality Study. *JACC Cardiovasc Imaging*. 2021 Feb;14(2):393–407.

190. Elsayed M, Moustafa YM, Mehanna ET, Elrayess RA, El-Sayed NM, Hazem RM. Empagliflozin protects against isoprenaline-induced fibrosis in rat heart through modulation of TGF- β /SMAD pathway. *Life Sci*. 2024 Jan 15;337:122354.

191. Daud E, Ertracht O, Bandel N, Moady G, Shehadeh M, Reuveni T, et al. The impact of empagliflozin on cardiac physiology and fibrosis early after myocardial infarction in non-diabetic rats. *Cardiovasc Diabetol*. 2021 Jul 2;20(1):132.

192. Li C, Zhang J, Xue M, Li X, Han F, Liu X, et al. SGLT2 inhibition with empagliflozin attenuates myocardial oxidative stress and fibrosis in diabetic mice heart. *Cardiovasc Diabetol*. 2019 Feb 2;18(1):15.

193. Omar M, Jensen J, Ali M, Frederiksen PH, Kistorp C, Videbæk L, et al. Associations of Empagliflozin With Left Ventricular Volumes, Mass, and Function in Patients With Heart Failure and Reduced Ejection Fraction: A Substudy of the Empire HF Randomized Clinical Trial. *JAMA Cardiol*. 2021 Jul 1;6(7):836–40.

194. Lee MMY, Brooksbank KJM, Wetherall K, Mangion K, Roditi G, Campbell RT, et al. Effect of Empagliflozin on Left Ventricular Volumes in Patients With Type 2 Diabetes, or Prediabetes, and Heart Failure With Reduced Ejection Fraction (SUGAR-DM-HF). *Circulation*. 2021 Feb 9;143(6):516–25.

195. Zhang N, Wang Y, Tse G, Korantzopoulos P, Letsas KP, Zhang Q, et al. Effect of sodium-glucose cotransporter-2 inhibitors on cardiac remodelling: a systematic review and meta-analysis. *Eur J Prev Cardiol*. 2022 Feb 3;28(17):1961–73.

196. Shi FH, Li H, Shen L, Xu L, Ge H, Gu ZC, et al. Beneficial Effect of Sodium-Glucose Cotransporter 2 Inhibitors on Left Ventricular Function. *J Clin Endocrinol Metab*. 2022 Mar 24;107(4):1191–203.

197. Santos-Gallego CG, Vargas-Delgado AP, Requena-Ibanez JA, Garcia-Roperio A, Mancini D, Pinney S, et al. Randomized Trial of Empagliflozin in Nondiabetic Patients With Heart Failure and Reduced Ejection Fraction. *J Am Coll Cardiol*. 2021 Jan 26;77(3):243–55.

198. von Lewinski D, Kolesnik E, Tripolt NJ, Pferschy PN, Benedikt M, Wallner M, et al. Empagliflozin in acute myocardial infarction: the EMMY trial. *Eur Heart J*. 2022 Nov 1;43(41):4421–32.

199. Fernandes GC, Fernandes A, Cardoso R, Penalver J, Knijnik L, Mitrani RD, et al. Association of SGLT2 inhibitors with arrhythmias and sudden cardiac death in patients with type 2 diabetes or heart failure: A meta-analysis of 34 randomized controlled trials. *Heart Rhythm*. 2021 Jul;18(7):1098–105.
200. Sfairopoulos D, Liu T, Zhang N, Tse G, Bazoukis G, Letsas K, et al. Association between sodium-glucose cotransporter-2 inhibitors and incident atrial fibrillation/atrial flutter in heart failure patients with reduced ejection fraction: a meta-analysis of randomized controlled trials. *Heart Fail Rev*. 2023 Jul;28(4):925–36.
201. Zheng RJ, Wang Y, Tang JN, Duan JY, Yuan MY, Zhang JY. Association of SGLT2 Inhibitors With Risk of Atrial Fibrillation and Stroke in Patients With and Without Type 2 Diabetes: A Systemic Review and Meta-Analysis of Randomized Controlled Trials. *J Cardiovasc Pharmacol*. 2022 Feb 1;79(2):e145–52.
202. Younis A, Arous T, Klempfner R, Kharsa A, McNitt S, Schleede S, et al. Effect of sodium glucose cotransporter 2 inhibitors on atrial tachy-arrhythmia burden in patients with cardiac implantable electronic devices. *J Cardiovasc Electrophysiol*. 2023 Aug;34(8):1595–604.
203. Xue G, Yang X, Zhan G, Wang X, Gao J, Zhao Y, et al. Sodium-Glucose cotransporter 2 inhibitor empagliflozin decreases ventricular arrhythmia susceptibility by alleviating electrophysiological remodeling post-myocardial-infarction in mice. *Front Pharmacol*. 2022;13:988408.
204. Hu Z, Ju F, Du L, Abbott GW. Empagliflozin protects the heart against ischemia/reperfusion-induced sudden cardiac death. *Cardiovasc Diabetol*. 2021 Oct 4;20(1):199.
205. Mancia G, Cannon CP, Tikkanen I, Zeller C, Ley L, Woerle HJ, et al. Impact of Empagliflozin on Blood Pressure in Patients With Type 2 Diabetes Mellitus and Hypertension by Background Antihypertensive Medication. *Hypertension*. 2016 Dec;68(6):1355–64.
206. Reed JW. Impact of sodium-glucose cotransporter 2 inhibitors on blood pressure. *Vasc Health Risk Manag*. 2016;12:393–405.
207. Jeon SM. Regulation and function of AMPK in physiology and diseases. *Exp Mol Med*. 2016 Jul;48(7):e245.

208. Koyani CN, Plastira I, Sourij H, Hallström S, Schmidt A, Rainer PP, et al. Empagliflozin protects heart from inflammation and energy depletion via AMPK activation. *Pharmacol Res.* 2020 Aug;158:104870.
209. Zannad F, Ferreira JP, Butler J, Filippatos G, Januzzi JL, Sumin M, et al. Effect of empagliflozin on circulating proteomics in heart failure: mechanistic insights into the EMPEROR programme. *Eur Heart J.* 2022 Dec 21;43(48):4991–5002.
210. Hundertmark MJ, Adler A, Antoniadou C, Coleman R, Griffin JL, Holman RR, et al. Assessment of Cardiac Energy Metabolism, Function, and Physiology in Patients With Heart Failure Taking Empagliflozin: The Randomized, Controlled EMPA-VISION Trial. *Circulation.* 2023 May 30;147(22):1654–69.
211. Chen M. Empagliflozin attenuates doxorubicin-induced cardiotoxicity by activating AMPK/SIRT-1/PGC-1 α -mediated mitochondrial biogenesis. *Toxicol Res.* 2023 Apr;12(2):216–23.
212. Packer M. Role of Deranged Energy Deprivation Signaling in the Pathogenesis of Cardiac and Renal Disease in States of Perceived Nutrient Overabundance. *Circulation.* 2020 Jun 23;141(25):2095–105.
213. Cohen ND, Gutman SJ, Briganti EM, Taylor AJ. Effects of empagliflozin treatment on cardiac function and structure in patients with type 2 diabetes: a cardiac magnetic resonance study. *Intern Med J.* 2019 Aug;49(8):1006–10.
214. Hsu JC, Wang CY, Su MYM, Lin LY, Yang WS. Effect of Empagliflozin on Cardiac Function, Adiposity, and Diffuse Fibrosis in Patients with Type 2 Diabetes Mellitus. *Sci Rep.* 2019 Oct 25;9(1):15348.
215. Madonna R, Moscato S, Cufaro MC, Pieragostino D, Mattii L, Del Boccio P, et al. Empagliflozin inhibits excessive autophagy through the AMPK/GSK3 β signalling pathway in diabetic cardiomyopathy. *Cardiovasc Res.* 2023 May 22;119(5):1175–89.
216. Oh CM, Cho S, Jang JY, Kim H, Chun S, Choi M, et al. Cardioprotective Potential of an SGLT2 Inhibitor Against Doxorubicin-Induced Heart Failure. *Korean Circ J.* 2019 Dec;49(12):1183–95.
217. Chung CC, Lin YK, Chen YC, Kao YH, Yeh YH, Trang NN, et al. Empagliflozin suppressed cardiac fibrogenesis through sodium-hydrogen exchanger inhibition and modulation of the calcium homeostasis. *Cardiovasc Diabetol.* 2023 Feb 6;22(1):27.

218. Byrne NJ, Parajuli N, Levasseur JL, Boisvenue J, Beker DL, Masson G, et al. Empagliflozin Prevents Worsening of Cardiac Function in an Experimental Model of Pressure Overload-Induced Heart Failure. *JACC Basic Transl Sci.* 2017 Aug;2(4):347–54.
219. de la Espriella R, Bayés-Genís A, Morillas H, Bravo R, Vidal V, Núñez E, et al. Renal function dynamics following co-administration of sacubitril/valsartan and empagliflozin in patients with heart failure and type 2 diabetes. *ESC Heart Fail.* 2020 Dec;7(6):3792–800.
220. Seferovic PM, Polovina M, Milinkovic I, Anker S, Rosano G, Coats A. Expect the Unexpected in the Medical Treatment of Heart Failure with Reduced Ejection Fraction: between Scientific Evidence and Clinical Wisdom. *Int J Heart Fail.* 2021 Oct;3(4):205–18.
221. Solomon SD, Jhund PS, Claggett BL, Dewan P, Køber L, Kosiborod MN, et al. Effect of Dapagliflozin in Patients With HFrEF Treated With Sacubitril/Valsartan: The DAPA-HF Trial. *JACC Heart Fail.* 2020 Oct;8(10):811–8.
222. Adams J, Mosler C. Safety and efficacy considerations amongst the elderly population in the updated treatment of heart failure: a review. *Expert Rev Cardiovasc Ther.* 2022 Jul;20(7):529–41.
223. Packer M, Anker SD, Butler J, Filippatos G, Ferreira JP, Pocock SJ, et al. Influence of neprilysin inhibition on the efficacy and safety of empagliflozin in patients with chronic heart failure and a reduced ejection fraction: the EMPEROR-Reduced trial. *Eur Heart J.* 2021 Feb 11;42(6):671–80.
224. Larsen JH, Omar M, Jensen J, Andersen CF, Kistrup CM, Poulsen MK, et al. Influence of angiotensin receptor-neprilysin inhibition on the efficacy of Empagliflozin on cardiac structure and function in patients with chronic heart failure and a reduced ejection fraction: The Empire HF trial. *Am Heart J Plus Cardiol Res Pract.* 2023 Feb;26:100264.
225. Ko SF, Sung PH, Yang CC, Chiang JY, Yip HK. Combined therapy with dapagliflozin and entresto offers an additional benefit on improving the heart function in rat after ischemia-reperfusion injury. *Biomed J.* 2023 Jun;46(3):100546.
226. Jering KS, Claggett B, Pfeffer MA, Granger C, Køber L, Lewis EF, et al. Prospective ARNI vs. ACE inhibitor trial to Determine Superiority in reducing heart failure Events after Myocardial Infarction (PARADISE-MI): design and baseline characteristics. *Eur J Heart Fail.* 2021 Jun;23(6):1040–8.

227. Pfeffer MA, Claggett B, Lewis EF, Granger CB, Køber L, Maggioni AP, et al. Angiotensin Receptor-Neprilysin Inhibition in Acute Myocardial Infarction. *N Engl J Med*. 2021 Nov 11;385(20):1845–55.
228. Gatto L. Does sacubitril/valsartan work in acute myocardial infarction? The PARADISE-AMI study. *Eur Heart J Suppl J Eur Soc Cardiol*. 2021 Oct 8;23(Suppl E):E87–90.
229. Butler J, Jones WS, Udell JA, Anker SD, Petrie MC, Harrington J, et al. Empagliflozin after Acute Myocardial Infarction. *N Engl J Med*. 2024 Apr 25;390(16):1455–66.
230. Hernandez AF, Udell JA, Jones WS, Anker SD, Petrie MC, Harrington J, et al. Effect of Empagliflozin on Heart Failure Outcomes After Acute Myocardial Infarction: Insights From the EMPACT-MI Trial. *Circulation*. 2024 May 21;149(21):1627–38.
231. Osada H, Murata K, Masumoto H, Osada H, Murata K, Masumoto H. Large Animal Models in Cardiovascular Research. In: *Animal Models and Experimental Research in Medicine* [Internet]. IntechOpen; 2022 [cited 2024 Jul 4]. Available from: <https://www.intechopen.com/chapters/82464>
232. Crisóstomo V, Maestre J, Maynar M, Sun F, Báez-Díaz C, Usón J, et al. Development of a closed chest model of chronic myocardial infarction in Swine: magnetic resonance imaging and pathological evaluation. *ISRN Cardiol*. 2013;2013:781762.
233. Liu J, Li X, Liu J, Li X. Novel Porcine Models of Myocardial Ischemia/Infarction – Technical Progress, Modified Electrocardiograms Validating, and Future Application. In: *Advances in Electrocardiograms - Clinical Applications* [Internet]. IntechOpen; 2012 [cited 2024 Jul 4]. Available from: <https://www.intechopen.com/chapters/26829>
234. Xiao N, Lewandowski RJ. Embolic Agents: Coils. *Semin Interv Radiol*. 2022 Feb 18;39:113–8.
235. Hashmi S, Al-Salam S. Acute myocardial infarction and myocardial ischemia-reperfusion injury: a comparison. *Int J Clin Exp Pathol*. 2015 Aug 1;8(8):8786–96.
236. Martin TP, MacDonald EA, Elbassioni AAM, O’Toole D, Zaeri AAI, Nicklin SA, et al. Preclinical models of myocardial infarction: from mechanism to translation. *Br J Pharmacol*. 2022;179(5):770–91.
237. De Villiers C, Riley PR. Mouse models of myocardial infarction: comparing permanent ligation and ischaemia-reperfusion. *Dis Model Mech*. 2020 Nov 18;13(11):dmm046565.

238. Harrington J, Jones WS, Udell JA, Hannan K, Bhatt DL, Anker SD, et al. Acute Decompensated Heart Failure in the Setting of Acute Coronary Syndrome. *JACC Heart Fail.* 2022 Jun;10(6):404–14.
239. Panahi M, Vadgama N, Kuganesan M, Ng FS, Sattler S. Immunopharmacology of Post-Myocardial Infarction and Heart Failure Medications. *J Clin Med.* 2018 Oct 31;7(11):403.
240. Monguió-Tortajada M, Prat-Vidal C, Martínez-Falguera D, Teis A, Soler-Botija C, Courageux Y, et al. Acellular cardiac scaffolds enriched with MSC-derived extracellular vesicles limit ventricular remodelling and exert local and systemic immunomodulation in a myocardial infarction porcine model. *Theranostics.* 2022;12(10):4656–70.
241. Li L, Cao J, Li S, Cui T, Ni J, Zhang H, et al. M2 Macrophage-Derived sEV Regulate Pro-Inflammatory CCR2+ Macrophage Subpopulations to Favor Post-AMI Cardiac Repair. *Adv Sci.* 2023 Mar 22;10(14):2202964.
242. Yerra VG, Advani A. Role of CCR2-Positive Macrophages in Pathological Ventricular Remodelling. *Biomedicines.* 2022 Mar 12;10(3):661.
243. van der Heijden T, Bot I, Kuiper J. The IL-12 cytokine family in cardiovascular diseases. *Cytokine.* 2019 Oct 1;122:154188.
244. Manetti R, Parronchi P, Giudizi MG, Piccinni MP, Maggi E, Trinchieri G, et al. Natural killer cell stimulatory factor (interleukin 12 [IL-12]) induces T helper type 1 (Th1)-specific immune responses and inhibits the development of IL-4-producing Th cells. *J Exp Med.* 1993 Apr 1;177(4):1199–204.
245. Andrabi SM, Sharma NS, Karan A, Shahriar SMS, Cordon B, Ma B, et al. Nitric Oxide: Physiological Functions, Delivery, and Biomedical Applications. *Adv Sci Weinh Baden-Wurtt Ger.* 2023 Oct;10(30):e2303259.
246. Wei N, Zhang C, He H, Wang T, Liu Z, Liu G, et al. Protective effect of saponins extract from *Panax japonicus* on myocardial infarction: involvement of NF- κ B, Sirt1 and mitogen-activated protein kinase signalling pathways and inhibition of inflammation. *J Pharm Pharmacol.* 2014 Nov;66(11):1641–51.
247. Zhang S, Jiang L, Che F, Lu Y, Xie Z, Wang H. Arctigenin attenuates ischemic stroke via SIRT1-dependent inhibition of NLRP3 inflammasome. *Biochem Biophys Res Commun.* 2017 Nov 4;493(1):821–6.
248. Endo J, Arita M. Cardioprotective mechanism of omega-3 polyunsaturated fatty acids. *J Cardiol.* 2016 Jan;67(1):22–7.

249. Wittig C, Szulcek R. Extracellular Matrix Protein Ratios in the Human Heart and Vessels: How to Distinguish Pathological From Physiological Changes? *Front Physiol.* 2021 Aug 4;12:708656.
250. Uchinaka A, Yoshida M, Tanaka K, Hamada Y, Mori S, Maeno Y, et al. Overexpression of collagen type III in injured myocardium prevents cardiac systolic dysfunction by changing the balance of collagen distribution. *J Thorac Cardiovasc Surg.* 2018 Jul;156(1):217-226.e3.
251. Li X, Xiang N, Wang Z. Ginsenoside Rg2 attenuates myocardial fibrosis and improves cardiac function after myocardial infarction via AKT signaling pathway. *Biosci Biotechnol Biochem.* 2020 Nov;84(11):2199–206.
252. Perez-David E, Arenal A, Rubio-Guivernau JL, del Castillo R, Atea L, Arbelo E, et al. Noninvasive identification of ventricular tachycardia-related conducting channels using contrast-enhanced magnetic resonance imaging in patients with chronic myocardial infarction: comparison of signal intensity scar mapping and endocardial voltage mapping. *J Am Coll Cardiol.* 2011 Jan 11;57(2):184–94.
253. Schmidt A, Azevedo CF, Cheng A, Gupta SN, Bluemke DA, Foo TK, et al. Infarct tissue heterogeneity by magnetic resonance imaging identifies enhanced cardiac arrhythmia susceptibility in patients with left ventricular dysfunction. *Circulation.* 2007 Apr 17;115(15):2006–14.
254. Jáuregui B, Soto-Iglesias D, Penela D, Acosta J, Fernández-Armenta J, Linhart M, et al. Cardiovascular magnetic resonance determinants of ventricular arrhythmic events after myocardial infarction. *Eur Eur Pacing Arrhythm Card Electrophysiol J Work Groups Card Pacing Arrhythm Card Cell Electrophysiol Eur Soc Cardiol.* 2022 Jul 15;24(6):938–47.
255. Grandi E, Ripplinger CM. Antiarrhythmic mechanisms of beta blocker therapy. *Pharmacol Res.* 2019 Aug;146:104274.
256. Dong Y, Xu Y, Ding C, Yu Z, Yu Z, Xia X, et al. Comparing the efficacy of angiotensin receptor-neprilysin inhibitor and enalapril in acute anterior STEMI patients after primary percutaneous coronary intervention: a prospective randomized trial. *Cardiovasc Diagn Ther.* 2022 Feb;12(1):42–54.
257. Fujiki S, Iijima K, Nakagawa Y, Takahashi K, Okabe M, Kusano K, et al. Effect of empagliflozin on ventricular arrhythmias in patients with type 2 diabetes treated with an implantable cardioverter-defibrillator: the EMPA-ICD trial. *Cardiovasc Diabetol.* 2024 Jun 28;23:224.

